

Approaches to improve mixing in compression ignition engines

Citation for published version (APA):

Boot, M. D. (2010). *Approaches to improve mixing in compression ignition engines*. [Phd Thesis 1 (Research TU/e / Graduation TU/e), Mechanical Engineering]. Technische Universiteit Eindhoven. <https://doi.org/10.6100/IR669911>

DOI:

[10.6100/IR669911](https://doi.org/10.6100/IR669911)

Document status and date:

Published: 01/01/2010

Document Version:

Publisher's PDF, also known as Version of Record (includes final page, issue and volume numbers)

Please check the document version of this publication:

- A submitted manuscript is the version of the article upon submission and before peer-review. There can be important differences between the submitted version and the official published version of record. People interested in the research are advised to contact the author for the final version of the publication, or visit the DOI to the publisher's website.
- The final author version and the galley proof are versions of the publication after peer review.
- The final published version features the final layout of the paper including the volume, issue and page numbers.

[Link to publication](#)

General rights

Copyright and moral rights for the publications made accessible in the public portal are retained by the authors and/or other copyright owners and it is a condition of accessing publications that users recognise and abide by the legal requirements associated with these rights.

- Users may download and print one copy of any publication from the public portal for the purpose of private study or research.
- You may not further distribute the material or use it for any profit-making activity or commercial gain
- You may freely distribute the URL identifying the publication in the public portal.

If the publication is distributed under the terms of Article 25fa of the Dutch Copyright Act, indicated by the "Taverne" license above, please follow below link for the End User Agreement:

www.tue.nl/taverne

Take down policy

If you believe that this document breaches copyright please contact us at:

openaccess@tue.nl

providing details and we will investigate your claim.

Approaches to Improve Mixing in Compression Ignition Engines

Proefschrift

ter verkrijging van de graad van doctor aan de Technische Universiteit Eindhoven, op gezag van de rector magnificus, prof.dr.ir. C.J. van Duijn, voor een commissie aangewezen door het College voor Promoties in het openbaar te verdedigen op dinsdag 20 april 2010 om 16.00 uur

door

Michael Dirk Boot

geboren te Aurora, Verenigde Staten van Amerika

Dit proefschrift is goedgekeurd door de promotoren:

prof.dr.ir. R.S.G. Baert
en
prof.dr. L.P.H. de Goey

Copromotor:
dr.ir. C.C.M. Luijten

Dit proefschrift is mede tot stand gekomen door een financiële bijdrage van DAF TRUCKS NV.

Copyright©2010 by M.D. Boot

All rights reserved. No part of this publication may be reproduced, stored in a retrieval system, or transmitted, in any form, or by any means, electronic, mechanical, photocopying, recording, or otherwise, without the prior permission of the author.

Cover Design: M.D. Boot and Unit040

Cover: The cover "Gecko out of the box" symbolizes how creative ideas can help reshape the world. The gecko was chosen because of the Vanderwaals forces that enable it to stick to smooth surfaces. These same forces play a pivotal role in the soot formation process. The proposed fuel component in this thesis, cyclohexanone, was initially selected because it was believed to reduce the Vanderwaals forces in soot. This would be realized by creating curvature in the otherwise flat poly-aromatic hydrocarbons (primary building blocks of soot), thereby increasing the average distance between neighboring planes. Accordingly, lower Vanderwaals forces and, ultimately, a weaker (i.e. more readily combustible) soot nanostructure would prevail. In the end, however, other, more conventional, mechanisms were identified that could account for the low soot observed for cyclohexanone blends. Interestingly, the gecko uses the same curving technique to release its toes from the surface.

Printed by the Eindhoven University Press.

A catalogue record is available from the Technische Universiteit Eindhoven Library.

ISBN: 978-90-386-2203-3

To my family...

I Fuel Chemistry 15

1	Carbon Sequestration or Promotion of Curvature?	17
1.1	Introduction	19
1.2	Oxygenate fuel effects on soot production: a literature review	20
1.3	Multi-cylinder engine experiments	22
1.4	Optical engine experiments	40
1.5	Conclusions	44
2	Promotion of Curvature or Longer Ignition Delay?	49
2.1	Introduction	51
2.2	Experimental setup	51
2.3	Data acquisition and analysis	55
2.4	Discussion	63
2.5	Conclusions	70
3	Molecular Shape or Cetane Number?	75
3.1	Introduction	77
3.2	Impact of fuel reactivity on sooting tendency: a literature review	78
3.3	Impact of fuel oxygen on sooting tendency: a literature review	81
3.4	Experimental setup and test procedure	84
3.5	Fuel matrix	86
3.6	Results	87
3.7	Discussion	94
3.8	Conclusions	98
4	Longer Ignition Delay or Flame Lift-Off Length (Part A) ?	103
4.1	Introduction	105
4.2	Background	105
4.3	Fuel matrix	108
4.4	Experimental setup	109
4.5	Experimental results	111

4.6	Discussion	112
4.7	Conclusions	113
5	Longer Ignition Delay or Flame Lift-Off Length (Part B) ?	115
5.1	Introduction	117
5.2	Experiment	122
5.3	Analysis of the lift-off length	125
5.4	Luminosity	127
5.5	Results and Discussion	130
5.6	Conclusions	142

II Combustion Concept 149

6	Optimization of Operating Conditions in the Early Direct Injection Premixed Charge Compression Ignition Regime	151
6.1	Introduction	153
6.2	Experimental apparatus	154
6.3	Experimental procedure	158
6.4	Results & discussion: part 1 of 4	160
6.5	Results & discussion: part 2 of 4	168
6.6	Results & discussion: part 3 of 4	170
6.7	Results & discussion: part 4 of 4	172
6.8	Conclusions	173
7	Spray Impingement in the Early Direct Injection Premixed Charge Compression Ignition Regime	185
7.1	Introduction	187
7.2	Background	187
7.3	Modeling	188
7.4	Results and Discussion	194
7.5	Conclusions	201

III Engine Hardware 205

8	PFAMEN: Porous Fuel Air Mixing Enhancing Nozzle	207
8.1	Introduction	209
8.2	Preliminary work	210
8.3	Extended modeling of the porous injector	216
8.4	Experimental setup	220
8.5	Experimental results	223
8.6	Discussion	225
8.7	Conclusions	225

Approaches to Improve Mixing in Compression Ignition Engines

This thesis presents three approaches to suppress soot emissions in compression-ignition (CI) engines. First, a fuel chemistry approach is proposed. A particular class of fuels - cyclic oxygenates - is identified which is capable of significantly reducing engine-out soot emissions. By means of experiments in "closed" and optical engines, as well as on an industrial burner, two possible mechanisms are identified that could account for the observed reduction in soot: a) an extended ignition delay (ID) and b) a longer flame lift-off length (FLoL). Further analysis of the available data suggests that both mechanisms are related to the inherently low reactivity of the fuel class in question. These findings are largely in line with data found in literature.

In the second approach, it is attempted to reduce soot by adopting an alternative combustion concept: early direct injection premixed charge compression ignition (EDI PCCI). In this concept, fuel is injected relatively early in the compression stroke instead of conventional, close to top-dead-center (TDC), injection schemes. While the goal of soot reduction can indeed be achieved via this approach, an important drawback must be addressed before this concept can be considered practically viable. Due to the fact that combustion chamber temperature and pressure is relatively low early in the compression stroke, fuel impingement against the cylinder liner (wall-wetting) often occurs. Consequently, high levels of unburned hydrocarbons (UHC), oil dilution and poor efficiency are observed. Several strategies, combining a limited engine modification with dedicated air management and fueling settings, are investigated to tackle this drawback. All of these strategies, and especially their combination, resulted in significantly lower UHC emissions and improved fuel economy. Although UHC emissions are typically a tell-tale sign of wall-wetting, as mentioned earlier, the relation between these two has long been hypothetical. Therefore, computational fluid dynamics (CFD) calculations of the injection process are performed to confirm whether or not liquid fuel impingement on the combustion chamber walls is indeed reduced as a result of the aforementioned UHC reduction strategies. Combined model

and experimental results indicate that, for most strategies, the measured hydrocarbon emissions and predicted spray impingement are well correlated for a conventional DI injector nozzle, supporting the earlier assumption that wall-wetting is responsible for high hydrocarbon emissions in the investigated early injection timing approach.

Lastly, in the third approach, a new injector nozzle design is proposed to improve the mixing process; again with the aim of soot abatement. In conventional nozzles, fuel is injected through 5-10 holes with nominal diameters of 100-200 micrometer. From both literature and in-house experiments it is known that mixing can be improved by reducing the nozzle diameter. Unfortunately, in order to preserve the overall flow rate, the number of required holes quadratically increases with a reduction in hole diameter. Alternatively, it is proposed to not drill the holes, but to use a porous medium instead. The utilized medium is a sintered metal permeated by an interconnected network of (continuous) pores with nominal diameters of 10 micrometer. This material is machined into a nozzle like shape and subjected to atmospheric injection tests as well as to experiments in the Eindhoven High Pressure Cell. Macroscopic experimental data (e.g. shorter ignition delay, larger spray volume) suggests that mixing is indeed improved. However, more research is required, preferably in a(n) (optical) engine, to investigate the impact on (soot) emissions and overall engine performance. In addition, the issues of durability and fouling still have to be addressed.

Background of research

It is evident that soot emissions have a considerable impact on urban air quality. When inhaled, the carcinogenic aromatic fraction of the particles can lead to serious health risks. In addition, as the particles have become smaller and smaller over the years (as a result of legislation), the prevailing winds displace them further from the source. As a result, blackening of polar ice caps and glaciers has been observed, aggravating the global warming issue.

Conventional diesel combustion can best be paraphrased as diffusion combustion. Here, fuel and air are not well premixed prior to and during the combustion phase. Rather, they diffuse towards one another in a more or less fixed ratio, referred to as the stoichiometric ratio, in a thin peripheral area of the combusting fuel spray (figure 1). Locally, the fuel-to-air ratio varies from fuel-rich in the spray core to an approximately stoichiometric value near the high-temperature diffusion flame. Soot and

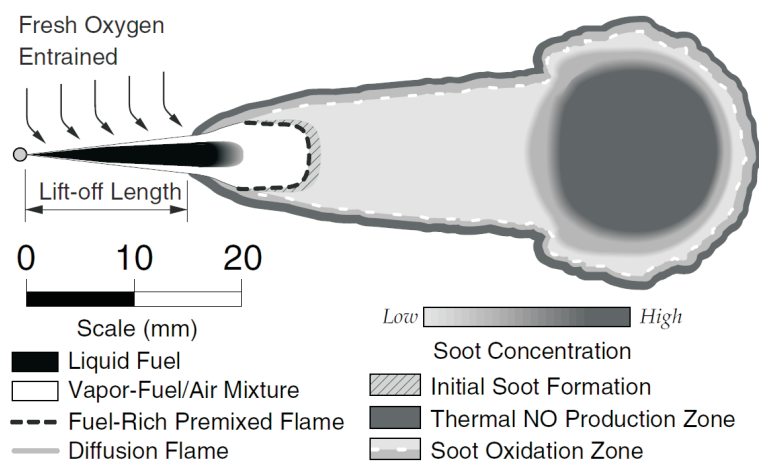


Figure 1: Visualization of the conceptual model for diffusion controlled CI diesel combustion (as proposed by John Dec, see chapter 1)

NO_x formation generally thrives under the former and latter conditions respectively. Nearly all formed PM oxidizes to "harmless" CO₂ in either the diffusion flame or the hot post-flame gasses. A minority of typically a few percent of the whole, however, will remain.

Reduction strategies geared at curbing soot emissions can be grouped into three distinct categories, each of which will be discussed in a dedicated part of this thesis:

- Reduction of soot through the use of alternative fuels with different chemical properties (part 1),
- by switching to an alternative combustion concept, different from conventional DI diesel combustion (part 2),
- and by utilization of new engine hardware (part 3).

At the moment, the most relied on approach is of a hardware nature, namely the application of exhaust gas aftertreatment. From both a practical and economical point of view, aftertreatment, which is designed to solve problems originating earlier in the chain, is not an attractive measure. This thesis will discuss strategies that represent a shift from the conventional approach and this for each of the three categories itemized above. Herein, each category will make up one of the three parts of this thesis. Each chapter in a given part is composed of one scientific publication, which is presented in its original published form with the exception of some basic editorial corrections.

Chapters 2, 4 and 5 of the thesis lean heavily on experiments, and associated diagnostics, performed and developed elsewhere. Herein, external parties were responsible for the experiments and design of the necessary (optical) diagnostics. In addition, the acquired results were interpreted in a joint effort. Such external measurements were necessary because optical access to the in-house engine was not possible (chapters 2 and 5) and a suitable diffusion burner (chapter 4) was not otherwise available. The main contribution of this part of the thesis is related to the development of measuring plans, selection of fuel matrices, analysis of the results and abstraction of conclusions.

Part 1: fuel chemistry approach

This line of research started in May 2005 with the graduation thesis by the author on the effects of (oxygenated) fuel chemistry on (diesel) particle formation and builds further on earlier work initiated some years before (see Chapter 1) at the Department of Mechanical Engineering (Technical University of Eindhoven, Combustion Technology Group). The purpose of the graduation project was to study fuel effects on soot formation, in particular that of so-called oxygenates (i.e. C_xH_yO_z). More specifically, the purpose was to study which fuel properties, other than fuel oxygen mass fraction, could account for observed differences in oxygenate performance with respect to soot reduction.

Based on the encouraging results in the graduation thesis it was decided to continue research on oxygenated fuels as part of a PhD position in the Combustion Technology Group). This research was sparked by the unexpected behavior of one particular oxygenate: cyclohexanone (C₆H₁₀O).

The systematics of this part is as follows. The underlying mechanism(s) via which relevant oxygenate properties exert their influence on soot emissions was investigated in a series of consecutive subprojects conducted either in-house (chapters 1 and 3) or externally (chapters 2, 4 and 5). Each successive chapter aims to answer an open research question of the preceding chapter.

Chapter 1 - Carbon sequestration or promotion of curvature?

Research question

Which of the two, at that time hypothesized, mechanisms explains the effectiveness of cyclohexanone in abating soot emissions at a given fuel oxygen weight percentage (wt-%)?

Mechanism I: carbon sequestration

An extensive literature study presented in this chapter shows that carbon sequestration, i.e. the ability of fuel-bonded oxygen atoms to prevent carbon atoms from participating in the soot formation process, is the most frequently referenced mechanism in literature pertaining to oxygenate performance. Herein, the ideal distribution of oxygen atoms in the fuel is such that each oxygen atom is bonded to two carbon atoms and no carbon atom is attached to more than one oxygen atom. In other words, this mechanism assumes that the functional oxygen group (alcohol, keton, aldehyde, ...) determines the effectiveness of an oxygenate.

Mechanism II: promotion of curvature

The same literature study revealed some evidence of a more exotic mechanism, namely the ability of certain fuels to form curved poly-aromatic hydrocarbons (PAH) (see figures 2(a) vs. 2(b) for an illustration of this mechanism). Soot formation is normally incited via merging of small unsaturated hydrocarbons (acetaldehyde, propargyl...) to the first aromatic rings. These rings then combine into planar (i.e. flat) PAH arrays (figure 2(a)) and stack to form so-called crystallites, which are essentially the building blocks of soot particles. In the event the PAH are curved rather than planar, the vanderwaals forces bonding the arrays together in crystallites become weaker, resulting in a more readily oxidizable soot nanostructure. In this mechanism, phenoxy radicals were found to play a pivotal role in soot formation. Accordingly, it was decided to add an oxygenate to the fuel matrix which best resembled such radicals: cyclohexanone.

Methodology

A large number of cyclic and non-cyclic oxygenated hydrocarbons were tested in several heavy-duty direct-injected (HDDI) engines under various operating conditions.

Results

Cyclohexanone clearly outperformed previous best-in-class oxygenates. This was particularly the case in combination with exhaust gas recirculation (EGR), where the adverse effect of EGR on soot emissions, the so-called Diesel Dilemma, was not observed

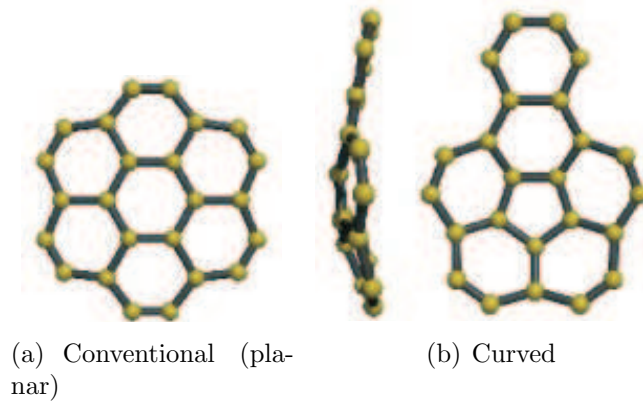


Figure 2: Distinct types of PAH

and near-zero soot and NO_x emissions could be realized. In addition, cyclohexanone had a markedly longer ID.

Discussion & conclusion

Based on the double-bonded oxygen (C=O) bond in cyclohexanone, one would expect from a carbon sequestering point of view that this fuel would yield higher soot emissions than for example other tested oxygenates such as tri-propylene mono methyl ester (TPGME), which has better spaced (C-O-C) oxygen atoms. Accordingly, mechanism I is found not to be in-line with experimental results and is therefore discarded as an explanation for the exceptional performance of cyclohexanone. Although the favorable results for cyclohexanone are in line with mechanism II, it cannot be established at this stage whether or not this mechanism is indeed responsible. Moreover, cyclohexanone had a markedly longer ID, suggesting a more premixed combustion which might also account for its exceptional performance. If this is the case, the strength of cyclohexanone lies not in enhanced oxidation of soot (i.e. via weaker soot nanostructure) but rather in improved suppression of soot formation via better pre-mixing. This observation lead to the formulation of a third, at this stage hypothetical, mechanism.

Mechanism III: longer ignition delay

Cyclohexanone yields lower soot emissions than non-cyclic variants because of its relatively long ID: longer delays allow for more premixing and hence lead to lower soot emissions.

Chapter 2 - Promotion of curvature or longer ignition delay?

Research question

It is clear that the results in chapter 1 are in-line with both mechanism II and III. In order to discard one of the two, an experiment had to be designed from which it becomes clear whether the soot formation is being suppressed or soot is being more efficiently oxidized. In other words, is the observed reduction in soot (with

cyclohexanone) the result of enhanced soot oxidation (due to curvature in PAH) or suppression of soot formation (due to improved premixing)?

Methodology

A second series of experiments with cyclic and non-cyclic oxygenates was conducted, this time in an optically accessible HDDI engine. Soot luminosity and ID in particular were studied. For given operating conditions, the amount of soot luminosity is an indicator for the soot formed.

Results

Cyclohexanone yielded a significantly lower luminosity than its non-cyclic counterparts. In a given engine workpoint, lower luminosity correlates well with the ID, with longer delays resulting in less luminosity.

Discussion & conclusion

The absence of soot luminosity is indicative of better suppression of soot, rather than of enhanced oxidation. Enhanced oxidation would likely have a more or less neutral impact on luminosity, as nearly all formed soot is combusted in the flame anyway, regardless of operating conditions or fuel composition. Accordingly, mechanism II does not appear to agree with the observations and is therefore not considered to be the dominant mechanism at work in the case of cyclohexanone. Mechanism III, conversely, agrees well with the experimental data and is therefore investigated further in chapter 3. It is clear that the ignition delay is an important parameter. In the next chapter, it will be investigated whether or not the importance of ignition delay holds irrespective of oxygenate structure (cyclic, straight-chained...). In other words, is the ignition delay leading with respect to soot regardless of oxygenate structure?

Chapter 3 - Molecular shape or cetane number?

Research question

If the ID is indeed more important for oxygenate performance, the soot emissions should display a correlation with the cetane number (CN). The CN is a well-known measure for fuel reactivity and correlates well with ID. Accordingly, the following research question can be formulated. What is the dominant fuel property with respect to soot emissions: molecular shape (e.g. cyclic for cyclohexanone) or CN?

Methodology

The first series of experiments is reinvestigated, laying more emphasis on the significance of CN with respect to soot emissions.

Results

Irrespective of oxygenate molecular shape, the ability of an oxygenate to abate soot emissions is clearly linked to its respective CN, with lower CN's manifesting in lower

soot emissions.

Discussion & conclusion

The fact that oxygenate molecular shape of functional oxygenate group does not appear to be of primary importance, is another confirmation that mechanisms I and II are not the primary mechanisms at work here. Mechanism III still appears to hold, but from the literature study conducted in this chapter a possible fourth mechanism was identified.

Mechanism IV: Longer flame-lift-off-length

It has been well established above that soot emissions correlate with the CN. Apart from the obvious (positive) effect on premixing (via longer ID), there is some evidence in literature that suggests a lower CN fuel leads to a longer so-called flame lift-off length (FLoL, see figure 1). A longer FLoL, in turn, allows for more air to be entrained upstream of the prevailing diffusion flame and also in the quasi-stationary phase of spray combustion. Consequently, a longer FLoL could translate into a leaner mixture in the spray core and ultimately in lower soot formation rates.

Chapter 4 - Longer ignition delay or flame lift-off length (part A)?

Research question

The relation between CN and ID has been well-established in literature. Accordingly, it is assumed in this chapter that both parameters are coupled. Experimental results in chapter 3 clearly demonstrate a correlation between oxygenate CN and soot emissions. Both Mechanisms III and IV have been linked in literature to the CN, so either of the two could be the dominant mechanism at work. An experiment has been devised to determine which of the two is dominant: ID or FLoL?

Methodology

Such an experiment is not trivial given the fact that, typically, both an ID and FLoL are encountered in compression-ignition engines. After much consideration, it was decided to conduct experiments in an industrial diffusion burner under stationary conditions, in which case the ID is non-existent. Accordingly, ID and FLoL could be effectively decoupled.

Results

Once again, the ability of an oxygenate to abate soot emissions is clearly linked to its respective CN, with lower CN's manifesting in lower soot emissions. This was found to hold irrespective of oxygenate molecular structure.

Discussion & conclusion

Given the fact that the correlation between CN and soot emissions still holds in a stationary burner, it is likely that the ID can not be the primary mechanism at work. Conversely, mechanism IV still holds, although the FLoL was not measured in the experiments. This remaining piece of research is presented in the final chapter of this part. However, when the ID becomes so long that nearly all fuel is premixed prior to auto-ignition, no diffusion flame (figure 1) can settle and the ID effect will begin to outweigh the FLoL effect.

Chapter 5 - Longer ignition delay or flame lift-off length (part B) ?

Research question

It becomes clear from the previous chapters that the FLoL mechanism could be the dominant mechanism at work, at least for conventional DI combustion (i.e. containing a diffusion-controlled combustion phase). The obvious question still remaining is therefore: does the FLoL correlate with the CN and therefore with the soot emissions?

Methodology

In order to measure the FLoL, experiments with cyclohexanone and other oxygenates are conducted in the same optically accessible HDDI engine used in chapter 2.

Results

From the results it becomes clear that, in accordance with literature, lower CN fuels generally yield longer FLoL's and lower soot emissions (in terms of soot luminosity) than higher CN fuels.

Discussion & conclusion

The experimental data presented in this thesis is in-line with the assumption that oxygenate performance with respect to soot is governed by its fuel reactivity (e.g. captured here via the CN). Given the results, the impact of fuel reactivity on the FLoL appears to be the most important underlying mechanism.

Summary

A summary of part I is provided in table 1.

Table 1: Summary of part I: in search of the *dominant* underlying mechanism with respect to soot performance of oxygenates studied in this thesis

<i>Chapter</i>	<i>Mechanism</i>			
	I Sequestration	II Curvature	III ID	IV FLoL
1	discarded ^a	introduced	-	-
2	-	discarded	introduced	-
3	-	-	holds	introduced
4	-	-	partly holds	holds
5	-	-	-	<i>holds</i>

Part 2: combustion concept approach

From the previous part it can be concluded that the fuel-air mixing process in compression-ignition engines can be improved by a modification of the fuel formulation. Alternatively, the mixing can be enhanced by switching to a new combustion concept, in this case premixed charged compression ignition (PCCI). With PCCI, the ID is sufficiently long to outlast the fuel injection process. As a result, the formation of the soot and nitric oxides (NO_x) forming diffusion flame (figure 1) is, in the ideal case completely suppressed. In the previous part, the positive effect of a longer ID has been clearly demonstrated. In this part, the ID will not be prolonged by fuel modification, but rather through a modification of the engine intake management and fueling strategy.

Chapter 6 - Optimization of operating conditions in the early direct injection premixed charge compression ignition regime

In this chapter a particular form of PCCI is discussed, namely so-called Early Direct Injection (EDI) PCCI. In EDI PCCI, an increase in ID is achieved by injecting the fuel into the combustion chamber relatively early in the cycle, typically around two-thirds of the compression stroke. At this time, gas temperatures, elevated by compression, are high enough for fuel to evaporate, but low enough to postpone auto-ignition towards TDC. While EDI PCCI leads to significantly lower soot emissions, two important drawbacks must be addressed. One drawback is auto-ignition before TDC, resulting in poor thermal efficiency and therefore fuel economy. The second

^aalthough not significant for the investigated workpoints and oxygenates at a given fuel oxygen content, enhanced sequestration is the general mechanism at work, with respect to abating soot emissions, in the case more oxygen is introduced to the fuel

drawback is a phenomenon known as wall-wetting. This involves collision of liquid fuel against the combustion chamber walls, leading to high UHC emissions and dilution of engine oil. The dilemma of resolving both issues is of a thermal nature. With respect to wall-wetting, a higher in-cylinder temperature is desirable for obvious reasons. Conversely, prevention of premature auto-ignition, but also reduction of NOx emissions, calls for a cooler in-cylinder temperature.

Research question

The research question in this chapter can be defined as follows. Can the negative impact of an early fuel injection timing on UHC emissions be curbed without negatively impacting (i.e. further advancing) the combustion phasing?

Methodology

A series of engine-based measures are investigated, which are itemized below.

- use of hot EGR
- higher fuel pressure
- higher fuel temperature
- higher intake pressure
- smaller nozzle holes
- narrower nozzle cone angle

Results

From the results it becomes clear that all measures manifest in a decrease in UHC emissions, without, or only marginally, impacting the combustion phasing or fuel economy.

Discussion & conclusion

While the results show that UHC emissions can be lowered significantly, it remains unclear whether or not this is attributable to reduced wall-wetting.

Chapter 7 - Spray impingement in the early direct injection premixed charge compression ignition regime

Research question

As concluded above, from chapter 6 it is not clear whether or not the reduction in UHC emissions is due to reduced wall-wetting^b. This research question is addressed in this chapter.

^bwall-wetting is referred to as spray impingement in this chapter

Methodology

The spray evolution, penetration and evaporation in particular, are modeled in the CFD code STAR CD for relevant cases of the previous chapter. Intermediate results are validated against experimental data.

Results

Combined modeling and earlier experimental results demonstrate that the modeled spray impingement correlates well with measured HC emissions.

Discussion & conclusion

Accordingly, it may be assumed that spray impingement is responsible for the high UHC emissions and that the optimized engine settings are able to mitigate this drawback of EDI PCCI.

Part 3: hardware approach

In Parts 1 and 2, an alternative fuel chemistry and combustion concept were proposed, respectively, to improve the fuel-air mixing process. In the final part of this thesis, a third approach is presented in which the mixing process is improved by modifying the engine hardware.

Chapter 8 - PFAMEN: porous fuel air mixing enhancing nozzle

There are many ways to improve the mixing process when the engineer is allowed to modify the engine hardware. The real challenge, however, is to develop a hardware modification which is effective, but not too intrusive and costly. In this chapter, a modification of the injector nozzle is proposed and investigated with both finite element modeling and experiments in an optically accessible high pressure chamber.

Research question

Can the mixing process be positively impacted by utilizing the porous injector nozzle?

Methodology

Combustion experiments with the conventional and porous nozzle are performed in the Eindhoven High Pressure Cell (EHPC), which can mimic combustion chamber conditions in a controlled environment.

Results

From the acquired high-speed movies it becomes clear that a) the ID for given cell conditions is considerably shorter for the porous nozzle and b) total flame volume is markedly higher (i.e. more air appears to be participating in the combustion process) for the porous nozzle.

Discussion & conclusion

Both results indicate that the mixing process could be improved by the porous design. Ultimately, however, engine experiments (scheduled for early 2010) are necessary to provide more insight into the effect on UHC and soot emissions.

Part I
Fuel Chemistry

Carbon Sequestration or Promotion of Curvature?

This paper reports on a study of a large number of blends of a low-sulfur EN-590 type diesel fuel respectively of a Swedish Class 1 fuel and of a synthetic diesel with different types of oxygenates. Oxygen mass fraction of the blends varied between 0 and 15 %. For comparison, the fuel matrix was extended with non-oxygenated blends including a diesel/water emulsion. Tests were performed on a modern multi-cylinder HD DAF engine equipped with cooled EGR for enabling NO_x-levels between 2.0 and 3.5 g/kWh on EN-590 diesel fuel. Additional tests were done on a Volvo Euro-2 type HD engine with very low PM emission. Finally, for some blends, combustion progress and soot illumination was registered when tested on a single cylinder research engine with optical access. The results confirm the importance of oxygen mass fraction of the fuel blend, but at the same time illustrate the effect of chemical structure : some oxygenates are twice as effective in reducing PM as other well-known oxygenates. In combination with conventional CI combustion with extended ignition delay, such fuel blends will produce extremely low PM levels without the necessity of very high amounts of EGR, suggesting a possible alternative pathway towards clean diesel combustion.

The content of this Chapter has been taken from:

M.D. Boot, P.J.M. Frijters, R.J.H. Klein-Douwel, R.S.G. Baert. Oxygenated Fuel Composition Impact on Heavy-Duty Diesel Engine Emissions. *SAE Paper*, 2007-01-2018, 2007.

Minor edits have been made to streamline the layout of the thesis chapters. The contribution of the author is related to the motivation and selection of the "X"-fuels and relevant operating conditions (with the exception of the ROSI 15 wt-% EGR workpoint), along with the results, discussion and conclusions thereof. The introduction and overall discussion and conclusions were realized in a joint effort. Experiments were carried out in the engine lab of the Eindhoven University of Technology.

1.1 Introduction

Air quality concerns result in increasingly stringent emissions regulations for automotive vehicles. To meet with these regulations, in the next few years, selective catalytic NO_x reduction technology will be introduced on the majority of the heavy-duty trucks. Alternatively, some manufacturers may prefer to implement advanced air management systems allowing for high levels of (cooled) EGR and combine these with high pressure FIE and/or PM catalyst technology [1, 2]. By 2012, the emissions targets for heavy-duty (HD) vehicles will see a further sharp reduction. To cope with this challenge all of the above technology will be needed, maybe even in combination with PCCI-like combustion in part of the engine operating range.

One route towards cleaner heavy-duty emissions that has been receiving less attention is that of changing the fuel composition. Of course, in the near future limited amounts of so-called first generation biofuels (i.e. fatty acid methyl esters) will be blended into regular diesel fuel. But this has been motivated mainly by the expected positive contribution of this measure towards energy diversification and greenhouse gas abatement. In view of the negative impact of the emissions regulation on heavy-duty vehicle investment and running costs, changing fuel composition for achieving better emissions is becoming an increasingly interesting option.

Over the last 15 years, a number of studies have demonstrated that blending oxygenated hydrocarbons (that is molecules containing not only hydrogen and carbon but also oxygen) with diesel can be a very effective route for particulate reduction with heavy-duty engines. A wide variety of such oxygenates have been tested and the results have been described in a large number of publications. Only a few of them will be referred to here. In a large number of these studies, a strong relation was found between the fuel oxygen content and the amount of PM produced [3–7]. Most authors accredit the beneficial impact of fuel oxygen on particulate emissions to enhanced trapping or sequestering of fuel carbon into non-sooting species (e.g. partially oxidized C1-C2 hydrocarbons). In other words, by means of already chemically bonding oxygen to carbon in the fuel, fewer carbon atoms are available to mature into (potential) soot precursors (e.g. ethylene, acetylene, etc.). At a fixed fuel-oxygen level, however, carbon sequestration was often found to be dependent on the type of functional oxygen groups ((e.g. alcohols, ethers, esters, etc.) involved).

Generally speaking, oxygenates containing either a single C-C-O group (e.g. ethanol) or a repetition of C-C-O (e.g. glymes) were amongst the best performing oxygenates with respect to abating PM emissions. There is however as yet no clear understanding on this issue. Delfort et al. [8] for instance found that CN had no effect, and they could confirm the O-effect only within a specific group (or class) of oxygenates with carbonate type oxygenates being most effective in PM reduction. Yeh et al. [9] on the other hand confirmed the importance of oxygenate class, but they found that carbonates and esters were less effective than ethers and alcohols. Also Mueller and Martin observed that an ester (DiButylMaleate or DBM) was much less effective than Tripropylene Glycol Monomethyl Ether or TPGME) when blended with diesel to a similar O-content [10]. In a more recent study it was shown that there would even be a difference in PM forming tendency between 1,4-DBM, 2,3-DBM and 1-butyl-DBM [11].

The majority of the more detailed studies of oxygenated fuel combustion and soot

formation were in optical engines running at relatively low load. In the literature there are some indications that the effectiveness of an oxygenate would also change with engine load [9], but little other information was found on this. In [12] some of the present authors noticed an effect of load, but this effect was small. In view of these observations, the objective of the study presented here was to try and further examine the impact of oxygenate fuel structure respectively engine load on PM reduction, i.e. aiming for future very clean combustion concepts.

1.2 Oxygenate fuel effects on soot production: a literature review

When analyzing the effect of fuel-bound oxygen on soot production, use can be made of the conceptual model for the (quasi-steady, mixing controlled phase of the) conventional compression ignition DI combustion process in heavy-duty diesel engines [13, 14]. According to this model, in the mixing controlled phase, diesel combustion is a 2-stage process. First, newly entered fuel atomizes and the fuel droplets entrain hot ambient gas; after a relatively short distance, the resulting vapor/gas mixture enters a high temperature zone. This stationary zone, which resembles the lift-off region of a quasi-steady turbulent jet, has been described by Dec as a steady rich premixed flame zone (with equivalence ratio between 2 and 4). A mixture of partial combustion products and remaining unburnt fuel leaves this premixed flame zone at relatively high temperatures (1300-1600 K), conditions that are ideal for soot formation. As this mixture moves towards the turbulent diffusion flame region soot nuclei form and particles start growing. In the diffusion flame both soot formation and oxidation takes place (Figure 1.1). Of course, soot oxidation continues when particles leave the diffusion flame region and as these products mix with remaining air (depending on overall air-fuel ratio / temperature level this goes on well into the expansion stroke). According to the above model, adding oxygen to the fuel molecule will affect soot formation through a number of mechanisms:

- In quasi-steady conditions (that is, for relatively long injection durations) turbulent diffusive combustion will be concentrated in the region where fuel and oxygen meet in (on average) stoichiometric proportions. When oxygen is present in the fuel molecules, this region will shift towards the injector tip. For a fixed injection velocity, this will reduce the time available for soot formation in the products of the primary rich reaction zone..
- A change in oxygen mass fraction at the flame lift-off location (FLOL) location will have a considerable effect on soot formation. If it is hypothesized that diesel FLOL (and therefore primary reaction zone location) is the result of local flame spreading rate being balanced by local mixture velocity, then this location could also be influenced by fuel oxygenation. Indeed, if we assume similarity between fuel-bound oxygen and increased ambient gas oxygen concentration, one would expect flame lift-off length at a shorter distance from the injector tip. Nevertheless, because of the fuel-bound oxygen, the effective local fuel/oxygen ratio would not change that much. There is however little experimental data to

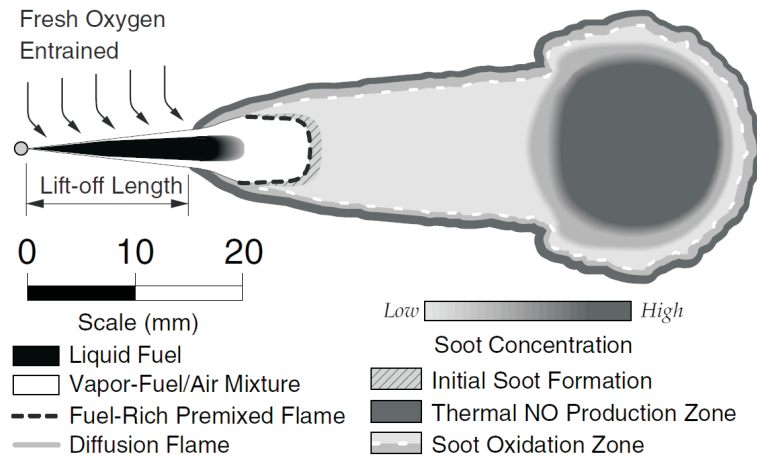


Figure 1.1: Visualization of the conceptual model for diffusion controlled CI diesel combustion (as proposed by Dec [13] and presented by Musculus et al. in [15]).

back this hypothesis. Musculus and Dietz [16] found little effect of fuel quality on FLOL (at typical medium load - 1 MPa imep - conditions). Pickett and Siebers [17] on the other hand noticed a strong fuel effect on FLOL location. Obviously this is still subject of further research.

- A higher heat of vaporization (e.g. with alcohols) will result in lower temperatures throughout the combustion process (in the primary reaction zone and up to the diffusion flame region).
- Also other (physical) fuel properties may influence fuel air-mixing : fuel compressibility, viscosity and density will interact with fuel spray penetration and spreading rate.
- The reduced lower calorific value of oxygenated fuels will have little or no effect on the diffusion flame temperature as it will be balanced by the lower stoichiometric air-fuel ratio [18]. If we assume a constant effective fuel/oxygen ratio in the primary reaction zone, the same argument holds.
- Of course, a lower calorific value will, for a given target torque level and injection pressure, result in a longer injection duration and therefore a combustion process that extends further into the expansion stroke. This will affect NO_x emission, but as a result of the increasing amount of fuel being burnt outside the premixed combustion phase, this could also increase PM production.
- On its own, a lower cetane number (f.i. by adding an additive) will result in less fuel being burnt in the diffusion combustion phase described above; since little or no soot is formed in the prior premixed combustion phase, this will result in lower soot production. Often, the change in cetane number is linked to a fuel composition change, e.g. an increase in aromatics content. Then, the higher soot forming tendency of the aromatics will mask the above effect.

- From experiments with burners and from chemical kinetic principles it is clear that fuels with the same oxygen mass fraction but with different chemical structure will demonstrate differences in soot forming tendency.
- Finally, different fuels are known to produce different soot precursors resulting in soot particles with a different structure. And soot structural differences will affect soot oxidation rate.

Conclusion: the majority of the above mentioned mechanisms are directly related to fuel oxygen mass fraction. Only a few are related to fuel structure. This is of course in line with the observations in the past.

1.3 Multi-cylinder engine experiments

In a previous study [12], results were presented of tests with a large number of blends between EN-590, Swedish Class 1 diesel and a synthetic diesel with different types of oxygenates. The study presented here builds further on these previous tests.

1.3.1 Engine specifications

For the engine tests a turbo-charged and charge-cooled, Euro 3 DAF (PE235C 4V), heavy-duty diesel engine was used (Table 1.1).

Table 1.1: Baseline engine specifications.

Bore/stroke	mm	118/140
No. of cylinders	-	6
CR	-	16 (nom.)
FIE type	-	PLD
Turbo type	-	fixed geometry
Charge cooling type	-	air-to-air
Max. power	kW	235 (2100 rpm)
Max. torque	Nm	1325 Nm (1500 rpm)

This 9.2 liter displacement volume engine has an electronically controlled unit pump type fuel injection system capable of 1400 bar injection pressure. This engine was redesigned for lower engine-out emissions (Euro-4 to Euro-5 like, i.e. 3.5 / 0.02 resp. 2.0 / 0.02 g/kWh NO_x / PM in the European Steady-state - or ESC - emissions test cycle) on regular diesel fuel. For this an external EGR system was implemented as shown in Figure 1.2.

Exhaust gas is recirculated in a long route, starting upstream of the turbocharger turbine and ending upstream of the compressor intake. To avoid compressor fouling, a continuously regenerating (catalytic active) diesel particulate filter (cDPF) is positioned in the EGR circuit just after the EGR control valve. In the EGR circuit the cDPF is followed by an EGR cooler and an EGR flow sensor. The cDPF is positioned shortly after the turbocharger such as to guarantee a temperature level that is sufficiently high for continuous regeneration to occur. For maintaining acceptable air-fuel

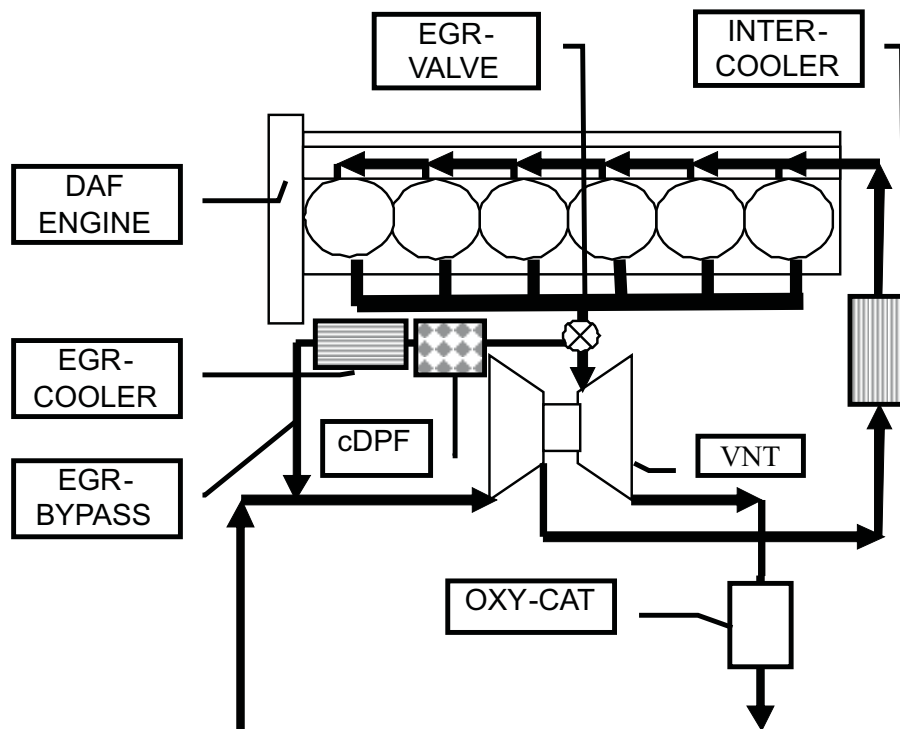


Figure 1.2: Test engine lay-out; details of EGR system and aftertreatment; standard air-to-air charge cooling replaced with air-to-water cooling.

ratio (AFR) levels, even with significant amounts of EGR, the standard fixed geometry turbocharger has been replaced with a variable geometry turbocharger or VGT. Finally, an oxidation catalyst was positioned in the exhaust to reduce the emission of unburnt hydrocarbons, i.e. that of aldehydes originating from oxygenate combustion. This is acceptable as some kind of oxidizing catalyst is expected on future HD engines both without DPF and with cDPF.

On the engine the usual sensors were used to log temperatures and pressures. To determine fuel, intake air and EGR flow rate Micro Motion mass flow meters were used. For measuring gaseous exhaust emissions a Horiba wet UHC and heated dry NO_x analyzer was used and for CO₂, CO and O₂ a Hartmann & Braun dry analyzer was used. The dry measured emissions were corrected to wet measurements. NO_x emissions are also corrected for ambient temperature and humidity. Exhaust smoke level (in Filter Smoke Number or FSN units) was measured using an AVL 415S smoke-meter. In all tests FSN was measured after the oxycat. At this position, particulate matter will consist mainly of carbon matter. It is therefore expected that FSN will correlate well with dry-PM. For determining PM emission, a correlation between PM-emission and FSN was used. This correlation, shown in Figure 1.3 for sulphur-free diesel fuel was found in the past to correlate well with actual dry-PM measurements on other engines.

The engine was equipped with a quartz piezoelectric pressure transducer (AVL GU21C) mounted in the cylinder head (cylinder number 6) to measure cylinder pressure. The fuel injector was equipped with a needle lift sensor. For each operating condition, 10 consecutive cycles of cylinder pressure data were collected at a 0.1 °CA

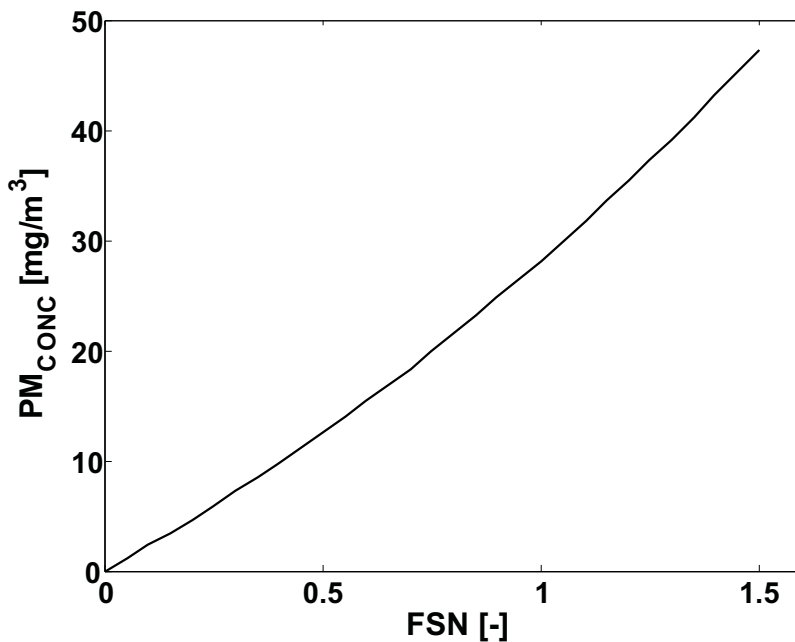


Figure 1.3: Correlation between FSN and dry-PM.

intervals and then averaged. Using a typical first law and perfect gas analysis, apparent rate of heat release (aRoHR) was calculated from an ensemble-averaged cylinder pressure curve which was filtered with a first order, small frame size Savitzky-Golay filter. The part load aRoHR results were filtered for the diffusive combustion part of the signal. For this a low pass filter was used.

1.3.2 Operating conditions

As in [12] measurements were performed at 3 key (speed/load)-combinations : (1340 rpm, 1276 Nm), (1340 rpm, 638 Nm) and (1650 rpm, 463 Nm). The 1340 rpm speed corresponds to the lower speed level considered in the ESC test cycle and 1276 Nm is the maximum load at that speed. In ESC terms the first two operating points are referred to as the A100 and A50 points. The third working point is the so-called ROSI point. In a typical HD truck application this setting gives a vehicle speed of around 85 km/hr. In practice, many HD vehicles will spend a lot of their time at this speed.

With the test engine lay-out described before, for any given torque and speed combination, different operating conditions can be realized through manipulation of VGT-setting and EGR valve position. In this way different combinations of external EGR (EGR_e) and AFR can be imposed. At the same time, changing the start of FIE actuation for fuel delivery (SOD) will give different timings for start of fuel injection (SOI). For each of the engine speed/load combinations realistic values of EGR and SOI were selected to give NO_x emission levels varying between 2 and 3 g/kWh NO_x. At the same time AFR levels were maximized (by closing of the VGT) for minimum PM emission. In practice however it was decided to limit VGT closing (and therefore to limit AFR increase) such as to avoid running with unrealistically negative pressure

drop levels across the engine. Not only would the ensuing increase of internal EGR counteract the effect of AFR increase on PM emissions, but also fuel consumption would suffer and EGR would not be uniquely defined.

Table 1.2: Engine operating conditions.

		ROSI	A100
Imep	Mpa	0.84	1.98
EGR _e	wt-%	15	7
AFR	kg/kg	32	23
Nominal SOD	°CA bTDC	13	9
T _{man}	K	320	320
P _{man}	kPa	147	260
P _{tin}	kPa	178	276
ΔP	kPa	-31	-16
B _{sfc}	g/kWh	213	211
Nox	g/kWh	3	3
FSN	-	1.2	1.11
PM	g/kWh	0.18	0.1
HC	g/kWh	0.21	0.14

Table 1.2 provides an overview of the engine working conditions selected for the results presented here (data are shown for the 3 g/kWh NO_x target and for regular diesel fuel EN590: 2005).

1.3.3 First series of experiments

Fuel matrix

For this study the fuel matrix tested before was extended with three different blends. One was an emulsified water-diesel blend (called PuriNO_xtm); the two other blends were mixtures of regular EN590 diesel fuel with different amounts of rapeseed-methyl ester (RME) and Glycerol Tertiary Butyl Ether (GTBE). The biofuel content in these blends was 5 respectively 20 %.

The positive effect of adding water to diesel (i.e. of the use of PuriNO_x) for diesel engine emissions is well established [19, 20]. The motivation for adding this product to the fuel matrix was the observation that the effect of adding water to the fuel is expected to have mainly physical effects on the soot production process: the added water will act as a diluent and it will lower the fuel concentration in the fuel spray, i.e. it will result in lower temperature levels throughout the reacting mixture (that is within the spray and at the surrounding diffusion flame). Given its relatively high specific heat, this effect will be higher than if the fuel would be diluted with an equivalent amount of extra nitrogen. Although adding water vapor has been mentioned to have also a chemical effect on the soot formation process [15, 21], the diluent effect is generally considered to be far more important. By comparing PuriNO_x with equivalent oxygenated material, some impression of the relative importance of the other soot forming effects (that are more linked to fuel chemistry and therefore fuel structure) should result.

Table 1.3: Principal properties of blend components. Density is at 288 K; boiling point at 0.1013 MPa.

Acronym		TPGME TP	TGM TG	ETOH ET	GTBE GT	RME -	DBM DB
C-H-O	-	C10H22O4	C8H18O4	C2H6O	-	-	C12H20O4
Oxygen	wt-%	32.4	36	34.8	-	11	28.1
CN	-	74.5	> 74.5	8	-	-	<50
LHV (MJ/kg)	MJ/kg	28.1	25.9	27	35.2	36.97	40
ρ	kg/l	0.96	0.986	0.795	0.883	0.88	0.99
Tb	K	515	489	351	-	> 593	554
ν (T)	mm ² /s (K)	2.73 (313)	2.5 (293)	1.08 (313)	-	-	2.78 (313)

GTBE was selected (in combination with RME) as it can be made from glycerine. Glycerine is an important by-product of the esterification process of plant oils (around 10 % of weight of the esters). With the expected strong increase in biodiesel production, turning glycerine into GTBE is considered an interesting additional path for its valorization.

Table 1.4: Some properties of the regular (low sulphur) EN590 diesel fuel, Swedish Class 1 fuel and FT synthetic diesel used in this study.

Acronym		EN590 D	Swedish Class 1 SW1	Syndiesel S
PAH	wt-%	< 11	-	< 0.1
ρ	kg/l	0.8272	0.8177	0.78
CN	-	56.2	54.9	>73
TB,95	K	608	-	-
Sulphur (mg/kg)	mg/kg	35	≤ 10	≤ 0.1
ν (T)	mm ² /s (K)	2.94 (313)	2.0 (313)	3.0 (313)

The properties of the different blend components are shown in Table 1.3. In this Table also some oxygenates are shown that were tested in the previous study. They will be used as a reference for the new test fuels. Table 1.4 gives the composition of the base fuels. Table 1.5 gives a summary of the resulting first set of fuel blends that were tested.

Results

All of the blends were tested in the different operating points listed in Table 1.2. Figure 1.4 shows the PM-NOx trade-off measured for the high load A-100 (7 % EGR) operating point. For comparison, this Figure also shows the trade-offs that were obtained with (a representative selection of) the blends that were tested in [12]. In addition, Figure 1.5 shows the corresponding heat release curves that were measured

Table 1.5: Fuel test matrix; D refers to EN590 diesel fuel, S to synthetic (GTL) diesel fuel.

Acronym	Oxygen wt-%	LHV MJ/kg	CN -
D	0	43.3	56.2
S	0	44	>73
S-TP-9	9.5	39.4	74.8
S-TP-15	15	36.6	74
S-ET-6	6	41	57.9
S-TG-15	15	36.5	>74.8
D-GT1	5.6	-	-
D-GT2	1.3	-	-
PuriNOx	12	-	-

for one specific start of fuel pump delivery (SOD) setting corresponding to a NO_x-level of 3 g/kWh. It is clear from this Figure that needle lift is very repeatable and that needle lift duration is directly related to the volumetric energy density of the fuel. (Note that felling was towards constant torque.) The only exception being the ethanol-syndiesel blend S-ET-6. When running on this fuel a different hydraulic behavior of the fueling system was observed, resulting in a somewhat later start of injection.

For all of the fuels premixed burning at this operating point was almost negligible and the rate of heat release curves show a very similar shape. As a consequence, CN effects will not be visible at this operating point. This is most clear when comparing the syndiesel fuel with the EN590 fuel. Of course, PM emission is reduced when fuel oxygen content increases. Other additional effects (e.g. related to fuel chemistry) are minimal and start demonstrating themselves only at the lowest NO_x-levels (< 2.5 g/kWh). At these low NO_x-levels, also the syndiesel and EN590 curves start diverging.

The PuriNO_x fuel behaves very similar to the 9 wt-% O blends. Because of its water content, with PuriNO_x the residence time of rich reacting mixture in the spray zone decreases as with an oxygenate with a similar amount of oxygen. However, the lower heat of vaporization of the oxygenate should result in higher temperatures and in a thermal acceleration of the (soot related) reaction rates. The results indicate that this effect is more than compensated for by the soot reducing (chemical) impact of the fuel bound oxygen. Also the S-ET-6 blends perform almost similar to the 9 wt-% O blends.

Similar tests were performed at the ROSI operating point. As can be seen from the rate of heat release curves in Figure 6 and 8, premixed combustion is much more important at this low load point. That results in CN-effects starting to play a role.

From these figures it becomes evident that PuriNO_x has a similar ignition delay and RoHR shape as the EN590 fuel. Given their low oxygen content also the D-GT-blends also behave similarly. The syndiesel fuel shows a less prominent premixed combustion peak and so do its blends with TPGME and TGM (who start burning somewhat earlier, in line with their CN). The exception is the blend with ethanol which starts much later (later than would be expected from its CN) and shows a

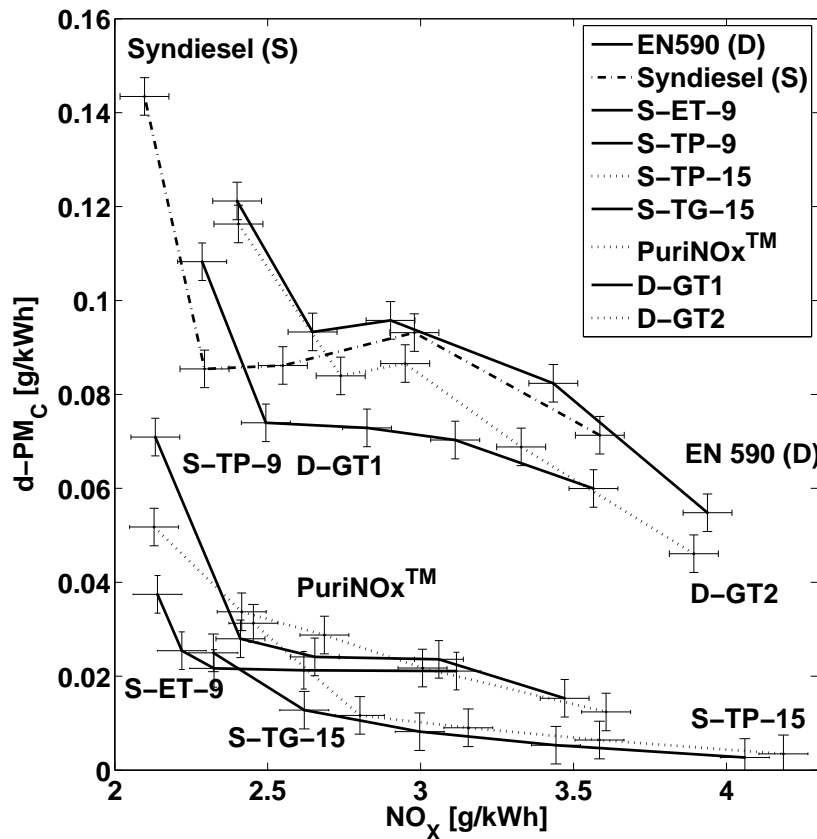


Figure 1.4: PM vs. NO_x, A100, 7% EGR.

strongly differing aRoHR.

How does all of this reflect in the NO_x-PM trade-off? Notwithstanding its short ignition delay (high CN), the syndiesel has a considerably lower soot level than the EN590 fuel. Of course this is linked to its lower aromatics content. At the same time one would expect that the resulting lower soot levels would result in lower radiative heat losses in the hot flame regions and therefore in higher NO_x-levels. This is not confirmed by the measurements.

A possible explanation would be that these fuels show similar in-cylinder soot levels during combustion but faster soot oxidation towards the end of the combustion process.

From Figures 1.4, 1.7 and 1.9 it is clear that the major trend is with oxygen mass fraction. There is however also a clear and strong additional dependency on load and on chemical structure. At high loads, higher temperatures are expected in the soot forming region. This could result in a lower sensitivity to an increase in AFR (because conditions are within the hart of the soot-forming AFR-T region identified in soot modeling studies). Alternatively, at these higher temperatures, soot formation could follow different pathways.

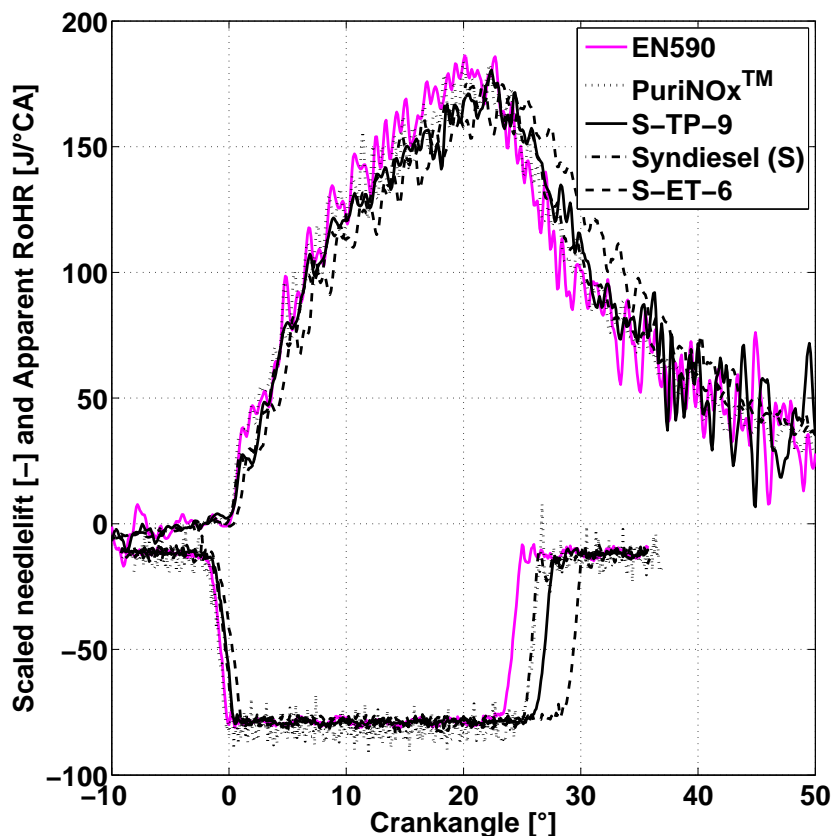


Figure 1.5: aRoHR for 4 blends; A100 point; SOI at - 9 °CA aTDC.

1.3.4 Second series of experiments

Effect of fuel oxygen on the quality of emitted PM

Although information on the quantitative effects of fuel oxygen on PM emissions is abundant, very little is known on the effects of oxygenates on PM quality (i.e. nanostructure). Vander Wal et al. [22, 23] observed the pyrolysis process of a neat oxygenate (e.g. ethanol) utilizing Transmission Electron Microscopy (TEM). They utilized a high temperature (e.g. 1523-1923 K) furnace for the synthesis of soot particles from various fuels (e.g. ethanol, acetylene and benzene). Note that the internal (tube) furnace environment is an inert one. They found the particles generated from ethanol to consist of characteristically curved or fullerene-like PAH segments. Conversely, pyrolysis of benzene and acetylene yielded predominantly planar PAH. They subsequently reported that curvature of layer planes substantially increased the particle oxidative reactivity. From [23] becomes clear that the curved nanostructure, seen for ethanol particles, is preserved regardless of residence time in the furnace. Pyrolysis of benzene and acetylene, conversely, displayed a strong dependency of soot nanostructure on residence time (e.g. at 1923 K), manifesting in a predominantly curved and graphitic nanostructure at short and long residence times respectively [23].

It is interesting to note that TEM experiments conducted by Su et al. [24, 25]

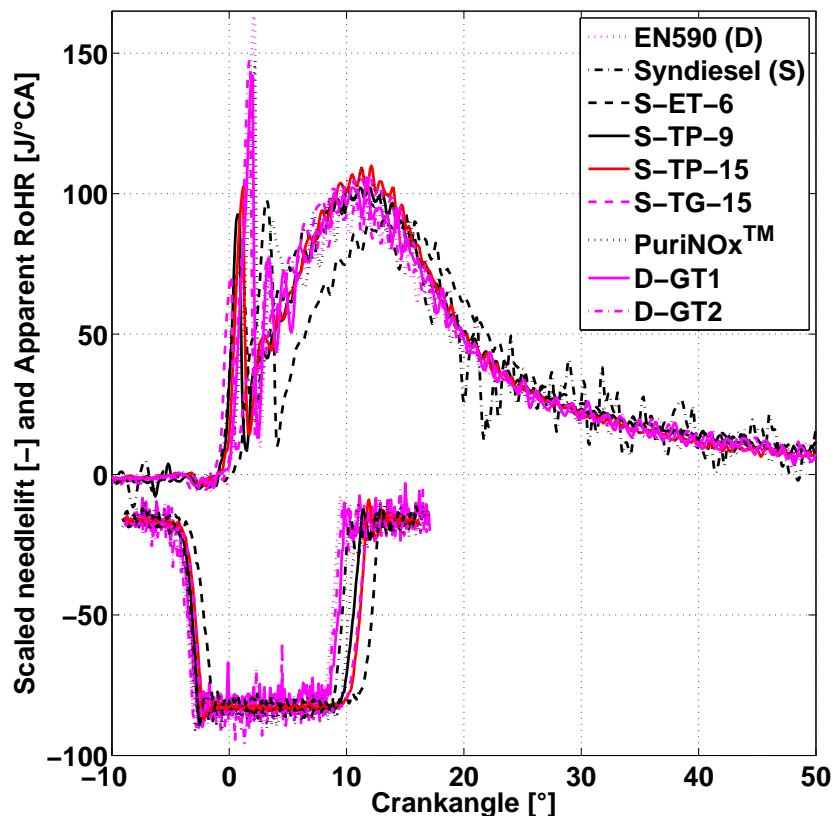


Figure 1.6: aRoHR for ROSI, 15 wt-% EGR.

disclosed a similar curved nanostructure in PM collected from a modern (i.e. Euro-4 diesel engine) operating on non-oxygenated fuel. The higher fuel injection pressures, typically seen for modern engines, are likely to lead to shorter in-spray residence times of soot particles. Shorter residence times, in turn, as concluded in [23], can eventuate in curved PAH segments even for non-oxidized fuels.

All of this suggests that a curved nanostructure can be formed independent of fuel identity provided that the residence time of soot particles at high temperature is relatively low. Curvature, however, appears to favor an oxygenated fuel. It is unclear at this point, however, whether or not a curved nanostructure is unique to ethanol or characteristic for any oxygenated fuel.

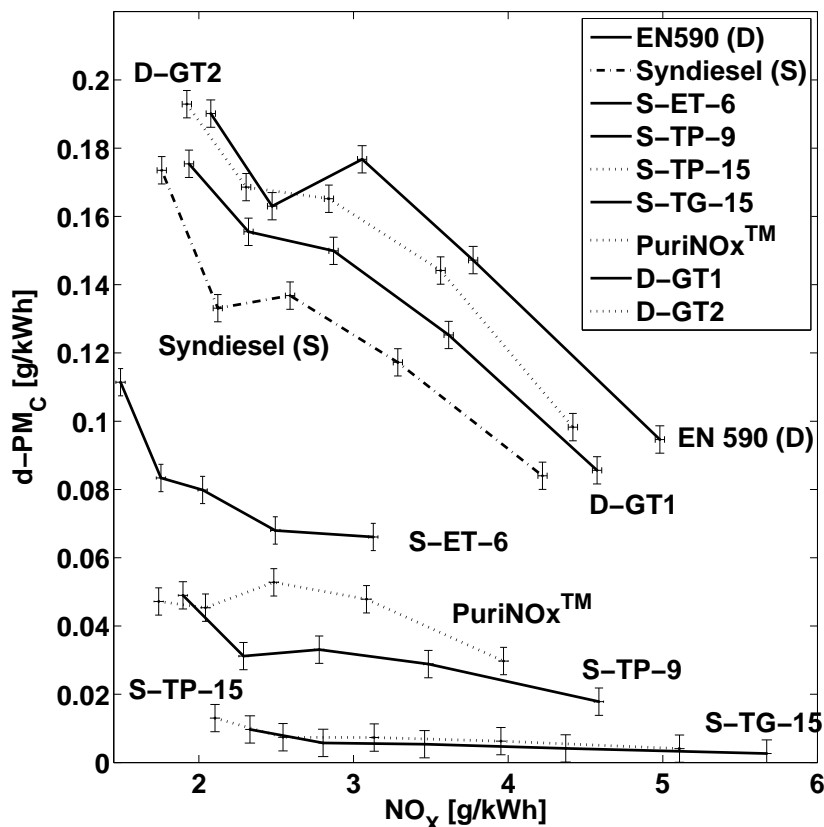


Figure 1.7: PM vs. NO_x; ROSI, 15 wt-% EGR.

Fuel matrix

One important conclusion made by Vander Wal et al. [23] is that a curved nanostructure is inherently less stable than its planar (i.e. graphitic-like) counterpart. Inspired by this conclusion, it was decided to select a number of molecules of which was thought that their pyrolysis products would help boost the degree of curvature in PAH. This would supposedly help to reduce PM emissions, either by the enhanced soot oxidation rate of the curved soot and/or because the curved soot nuclei would be less prone to grow into larger particles (i.e. because of reduced soot formation). A total of four hydrocarbons (X1-X4), amongst which one oxygenate (X1), were selected on the basis of this (hypothesized) ability to promote curvature. X1-X4 all have a similar non-linear molecular structure, varying only in carbon number and/or the presence of a functional oxygen group. The properties of X1-X4 are given in Table 1.6.

Inclusion of an oxygenate was motivated by the question whether or not oxygenate molecular structure could have a significant impact on PM emissions at an equal oxygen level. To this end, two oxygenates (e.g. TPGME and DBM) from the previous measurements [12] were included in the second fuel matrix. They were blended with Swedish Class 1 fuel; blend composition is as in Table 1.5: acronym of main fuel acronym oxygenate oxygen percentage (e.g. SW1-TP-5).

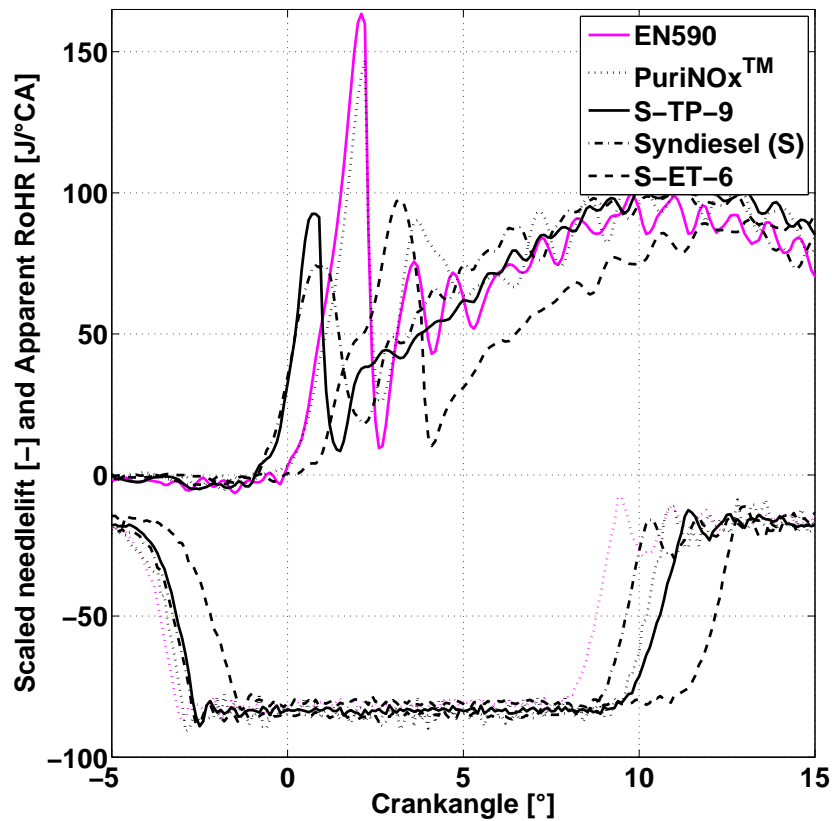


Figure 1.8: Detailed figure of aRoHR for ROSI (reduced amount of fuels from figure 1.6).

Table 1.6: Second test fuel matrix; LHV-data are calculated; kinematic viscosity data for 293.5 K.

	Oxygen wt-%	LHV MJ/kg	T_b K	CN -	ρ kg/	ν mm ² /s
D	0	43.4	450	56	0.83	2.9
X1	16	31.6	430	13-18	0.95	2.3
X2	0	41	350	13-18	0.77	1.3
X3	0	41.3	320	-	0.75	0.6
X4	0	38.3	430	-	0.99	-

Results

Variation of Start of Delivery

Species X1-X4 were blended to the reference diesel fuel EN590 to 30 vol-%. This specific value was selected because it corresponds to 5 wt-% oxygen in X1; this facilitates a comparison of X1 to the 5 wt-% oxygen blends of DBM and TPGME from the first fuel matrix. The lines in Figure 1.10 correspond to a sweep in SOD from -18 to -8 [°CA aTDC] in the ROSI operating point. Engine specifications have been provided

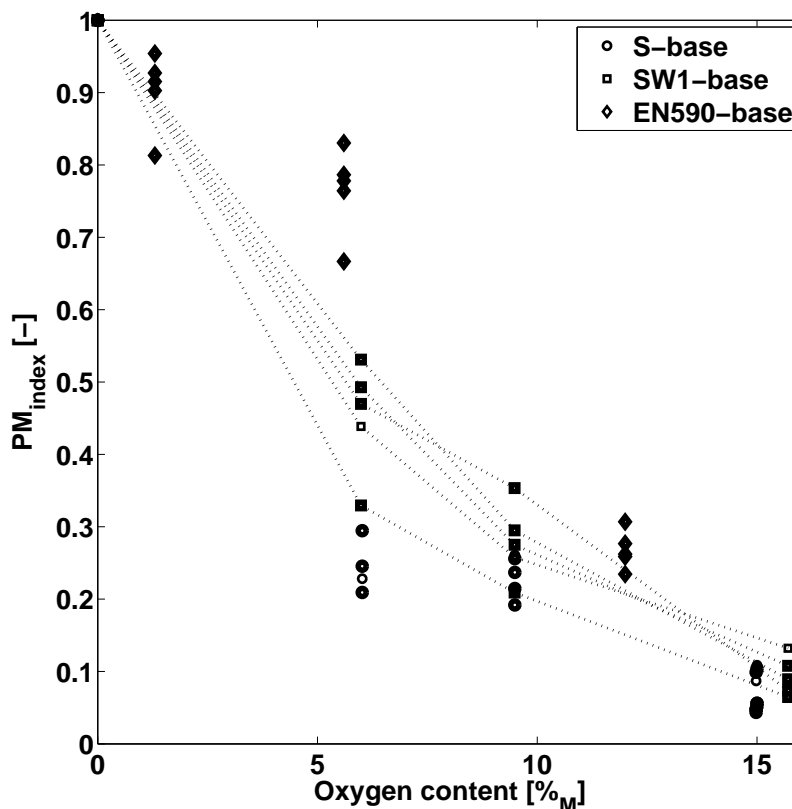


Figure 1.9: Relative PM_C reduction for the 3 different base fuels. For every base fuel all working points are shown, except for the SW1 blends. For the SW1 blends an averaged value is shown for every engine working point.

earlier in this paper (Table 1.2).

It can be observed from Figure 1.10 that the non-oxygenated fuel X2 has a considerable lower PM emission level than the pure diesel (see Figure 1.7). Also the performance of X1 at 5 wt-% fuel oxygen is comparable to that of DBM and TPGME at 9 wt-%. A similar observation was made when comparing a 9 wt-% X1-blend with DBM and TPGME at 15 wt-% (not shown).

On the basis of the data in Figure 1.10, one can conclude that the non-linear molecular structure appears to have a favorable effect on the NO_x/PM trade-off both with (X1) and without (X2 in particular) functional oxygen group. Indeed, the experiments with the X1 blend support the idea that, at a given fuel oxygen content, fuel identity can have an important (additional) beneficial impact on PM emissions. Given the additional apparent benefit of a functional oxygen group (Figure 1.10), subsequent testing was focused on the oxygenated variant X1.

It is evident from Figure 1.10 that, at the applied EGR level (e.g. 15 wt-%), the NO_x is in nearly all cases higher than the aspired EURO V level of 2 [g/kWh] for the investigated range of SOD. Consequently, it was decided to test the various oxygenates at higher EGR levels in order to meet (at least) the Euro V benchmark for NO_x.

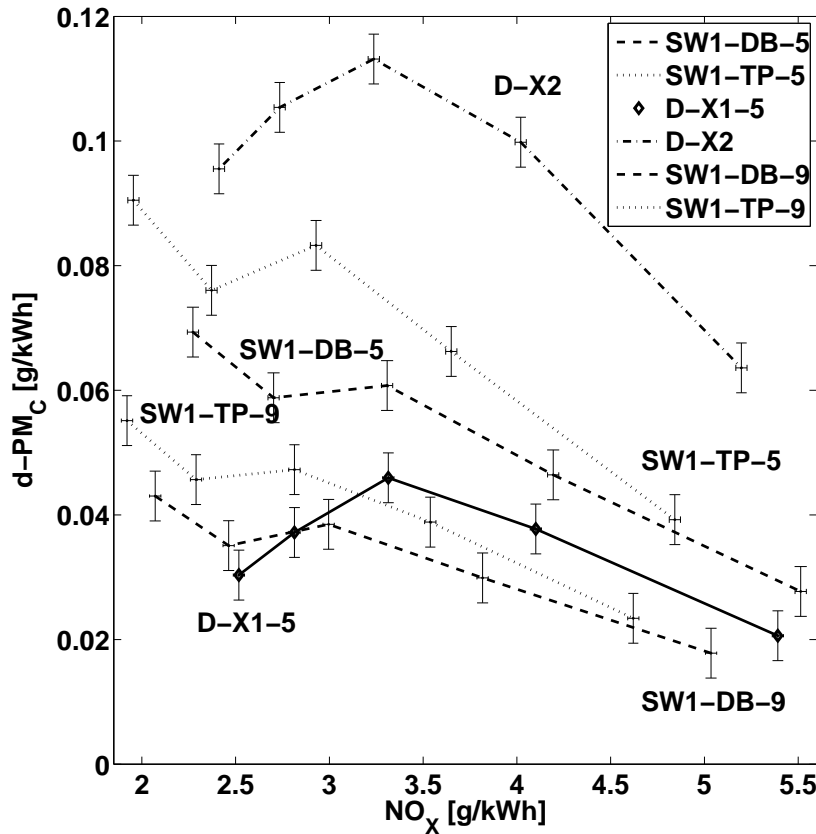


Figure 1.10: $d\text{-PM}_C$ vs NO_x at ROSI 15 wt-% EGR, SOD sweep, for different fuels.

Variation of Applied Exhaust Gas Recirculation Level

An EGR-sweep was performed while fuel SOD was kept constant at -13°CA aTDC; EGR-variation was achieved through EGR valve position modulation at fixed VGT position. Due to the setup of the test rig AFR decreases as EGR increases as shown in Figure 1.11.

As discussed earlier, it is well-known that the impact of the accompanying decrease in in-cylinder oxygen concentration is such that often exponentially rising PM emissions are observed with increasing EGR concentration. This downside of EGR utilization is clearly visible in Figure 1.12, in which the effect of EGR on the NO_x/PM trade-off is plotted for DBM and TPGME at 9 wt-% fuel oxygen, as well as for EN590 and X1 at 5 and 9 wt-% fuel oxygen.

Perhaps the most important conclusion which may be drawn from this Figure is that the data suggest that the effects of fuel identity become more important at lower combustion temperatures (implied by the lower NO_x values). Indeed, the out-performance of X1 compared to DBM and TPGME becomes more pronounced with increasing EGR level, which coincides with lower NO_x values.

It should be noted that the measured rise in specific PM emissions for X1 at 9 wt-% fuel oxygen is attributable solely to increased fuel consumption at the higher

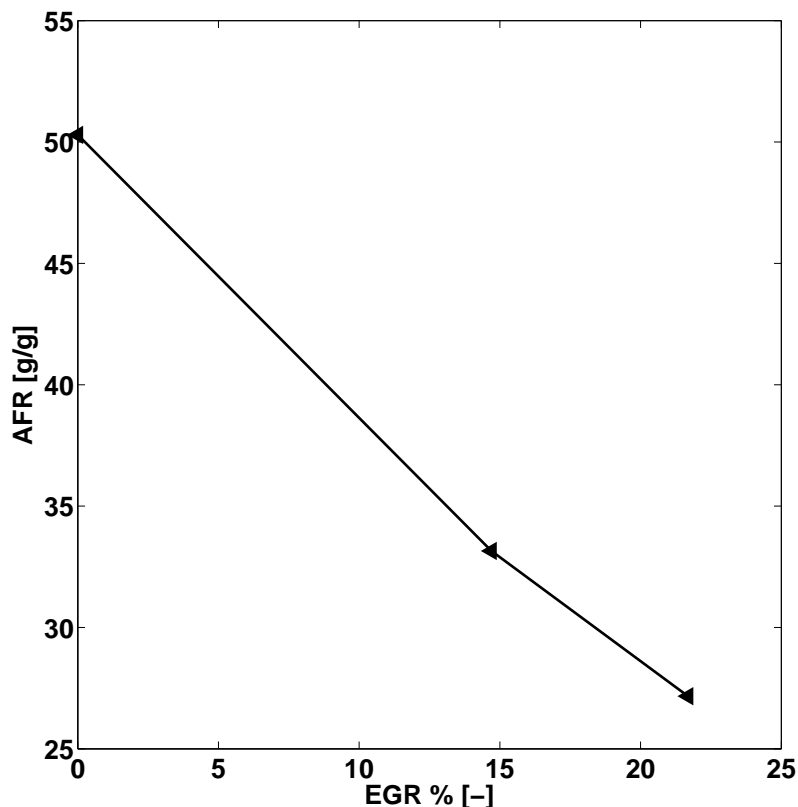


Figure 1.11: AFR vs EGR wt-% for EGR sweep on EN590 base fuel, during ROSI. SOD and VGT position is kept constant, comparable to earlier performed experiments.

EGR concentrations (Figure 1.13). Smoke emissions for this particular blend were actually seen to slightly decrease with increasing EGR percentage.

Apart from a sub-Euro-5 NO_x (Figure 1.12) and a near Euro-4/5 PM level, CO (Figure 1.14) and UHC (Figure 1.15) emissions for the X1 blends are well below the norm, save for the CO level at EGR concentrations in excess of 20 wt-%. It is stressed, however, that all emissions were measured upstream of the incorporated oxidation catalyst.

From this section it may be concluded that clearly factors other than fuel oxygen content alone are responsible for the exceptional performance of X1. In the next section it will be attempted to arrive at a better understanding of the behavior of this oxygenate by closely examining the heat release curves associated with the data pointed used in Figures 1.12-1.15.

As a final remark, it is worth while pointing out that in our experiments no consistent difference between DBM and TPGME blends could be identified, contrary to the findings in [9, 10].

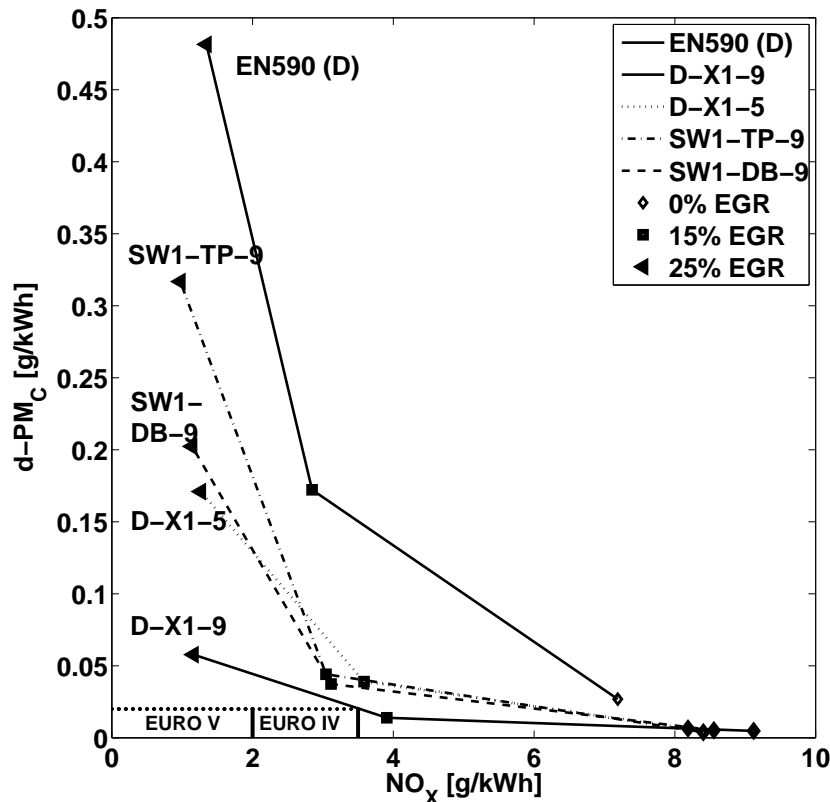


Figure 1.12: d-PM_C vs. NO_x for different blends during EGR sweep, ROSI.

1.3.5 Heat release analysis

In Figure 1.16, the heat-release curves and needle lift profiles are plotted for the reference fuel EN590, and for blends with TPGME, with DBM and with X1 (all at 9 wt-% O) at various EGR levels in the ROSI workpoint. SOD was kept constant at -13 °CA aTDC. It becomes evident from this Figure that fuel X1 manifests in considerably more premixed combustion than both EN590 and TPGME and DBM. Moreover, the contribution of premixed relative to diffusion combustion becomes larger at elevated EGR levels.

All operating conditions remaining equal, the ratio of premixed to diffusion combustion is governed by the incurred ignition delay, which is ultimately primarily a function of fuel reactivity. As stated earlier, the molecules X1-X4 distinguish themselves by their high non-linearity. It is well-known from literature that nonlinear hydrocarbons such as those with either branched or cyclic carbon skeletons are more resistant to auto-ignition than their linear (e.g. n-paraffins) counterparts. One can observe the effects of molecular structure on ignition delay kinetics in Figure . Here, the ignition delay is plotted against the applied EGR level for the reference fuel EN590, DBM/TPGME (at 9 wt-% O) and X1 (at 5 and 9 wt-% O₂) in the ROSI working point. SOD has been held constant at -13 °CA aTDC.

From Figure 1.17 becomes clear that (at a given EGR concentration) the addition

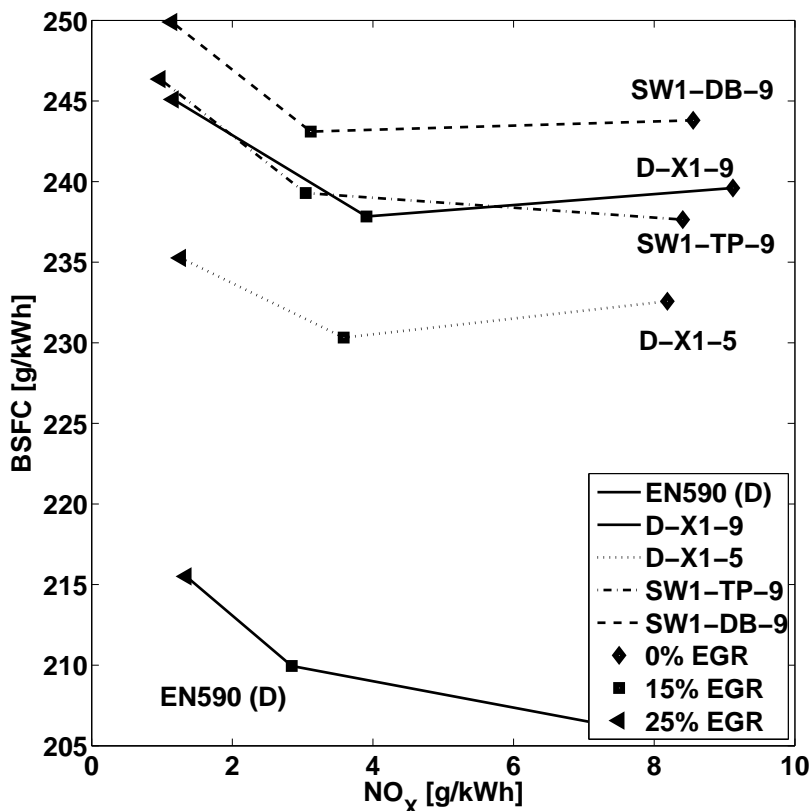


Figure 1.13: BSFC vs NO_x at ROSI, EGR sweep.

of non-linear molecules (e.g. X1 or X2) to EN590 leads to slower auto-ignition chemistry and, that - for all fuels - the lower in-cylinder oxygen concentration intrinsic to EGR decelerates the start of combustion as well.

For a particular fuel, given the intrinsic attenuation of available oxygen, the incurred ignition delay becomes more extended with increasing EGR utilization (see also Figure 1.17 above). For moderate EGR concentrations, the negative effect of oxygen deprivation will outweigh the beneficial impact of increased premixed combustion. Accordingly, PM emissions are typically seen to rise (exponentially) as more EGR is fed to the combustion chamber (see also Figure 18 below). Conversely, at EGR levels in excess of a certain threshold, which is of course dependent on operating conditions, the trend will shift and the positive effect of increasingly more premixed combustion will outweigh the negative effect of decreasing oxygen availability. Under these circumstances PM emissions will decrease with increasing ignition delay. Operating in this regime is better known as high EGR / low temperature combustion.

From Figure 1.18 can be distilled that, at a given EGR ratio, an elongation of the ignition delay, induced by degraded fuel reactivity (e.g. D-X1-9 vs. SW1-TP9), will lead to lower PM emissions. In a sense, the combustion becomes more separated from the injection process. This principle has been the basis for the so-called Modulated Kinetics combustion concept proposed by Kimura et al. [26].

There are, however, several key distinctions between the heat-release curves of

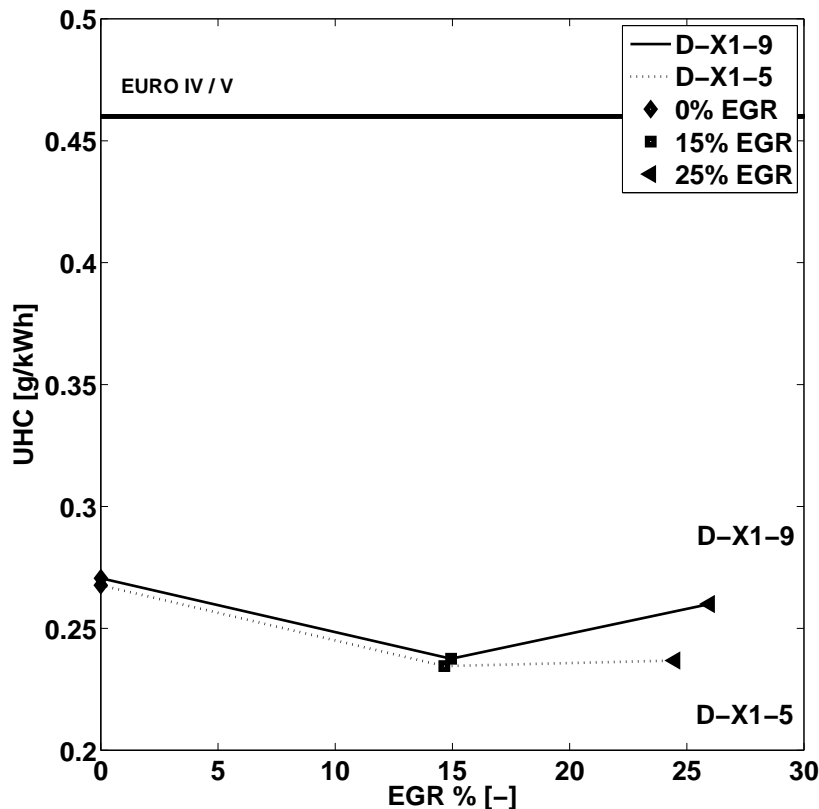


Figure 1.14: UHC vs. EGR wt-%, at ROSI, EGR sweep; fixed SOD.

D-X1-9 and those typically acquired from an engine operating in MK mode.

Consider firstly, the cardinal prerequisite of MK, as defined in [26], namely that there may be no overlap in the injection and combustion events. In the results presented here, in all instances, even at 25 wt-% EGR, there is considerable overlap in the aforementioned events, which is underlined by the emissions of significant concentration of NO_x (Figures 1.10 and 1.12). With true MK, the amount of emitted NO_x would be close to zero, as is also generally the case for any form of premixed charge compression ignition (e.g. PCCI, MK). What is more, the apparent insensitivity of PM emissions to overlap in injection and heat release events, holds the promise to expand the MK range to higher fueling levels (i.e. higher loads).

Secondly, the crank-angle (e.g. 3-7 °CA aTDC at which the heat-release commences for the D-X1-9 blend (Figure 1.16) differs noticeably from the values of 20 °CA aTDC and later which are typically recorded for true MK combustion [26]. An earlier heat-release event will typically lead to both an improved thermal efficiency and lower emissions of UHC and CO in comparison to conventional MK.

One of two conclusions may be drawn from the above comparison of X1 to MK combustion. First of which is that the presence of oxygen in the fuel somehow compensates for the otherwise negative impact of overlap in the injection and combustion events on the PM emissions. Alternatively, another hitherto undisclosed mechanism

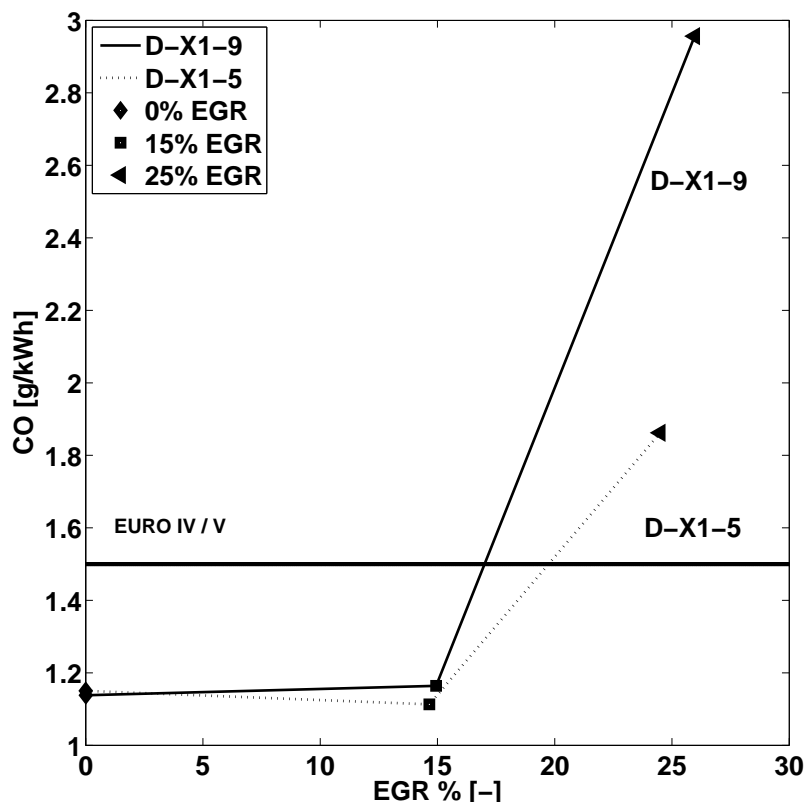


Figure 1.15: CO vs EGR wt-%. At ROSI, EGR sweep, fixed SOD.

is responsible, one possible candidate for which being the premise which motivated the selection of additives X1-X4 in the first place.

Looking solely at the behavior of D-X1-9, one would arrive at the first conclusion. Judging, however, from the similar PM performance of D-X1-5 and SW1-DB-9 (Figure 1.12) - although the former has only half as much on-board oxygen as the latter, and their ignition delay behavior as a function of EGR is comparable (Figure 1.16) - the second conclusion becomes more plausible.

1.3.6 Additional experiments on Volvo test engine

Additional measurements with several of the above mentioned oxygenated fuel blends were performed at TNO Automotive on a VOLVO D7 engine, see Table 1.7 for specifications.

Also this engine was fitted with an oxidation catalyst. Soot was measured using the same AVL415 S smoke meter equipment to calculate a dry PM, but also a mini-dilution tunnel was used for a directly measured dry PM. This Euro-2 engine was running without EGR.

Figures 1.19 and 1.20 show the results. From these figures it can be concluded that for low to medium ESC engine speed D-X1-5 produces more d-PM_M but results in the largest FSN reduction, compared to the other two fuels tested. At the C engine

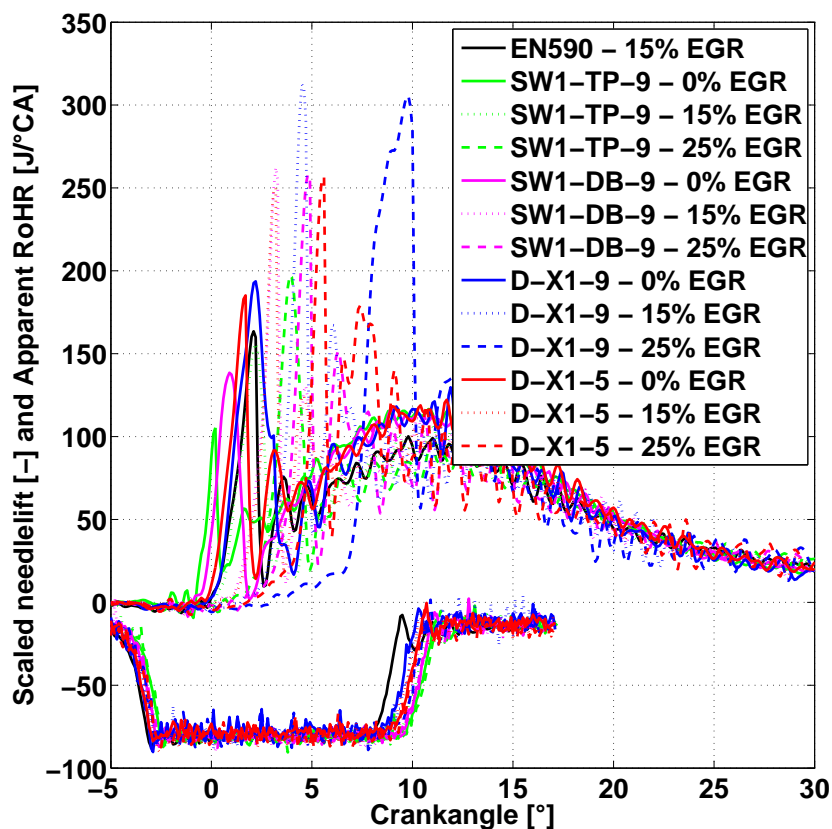


Figure 1.16: aRoHR for 3 EGR levels; ROSI; 4 different blends and EN590 as reference fuel.

Table 1.7: Specifications of the Volvo test engine.

Bore/stroke	mm	105/130
No. of cylinders	-	6
CR	-	18 (nom.)
FIE	-	Line pump
Turbo	-	Fixed geometry
Charge cooling	-	air-to-air
Max. power	kW	191 (2200 rpm)
Max. torque	Nm	1100 (1300 rpm)

speed and low load D-X1-5 is favorable. For the high load case (C-speed) D-X1-5 is also not producing the least amount of soot.

1.4 Optical engine experiments

In order to arrive at a better understanding of the combustion process of blends with X1 in particular, additional tests were done, this time in an optically accessible engine

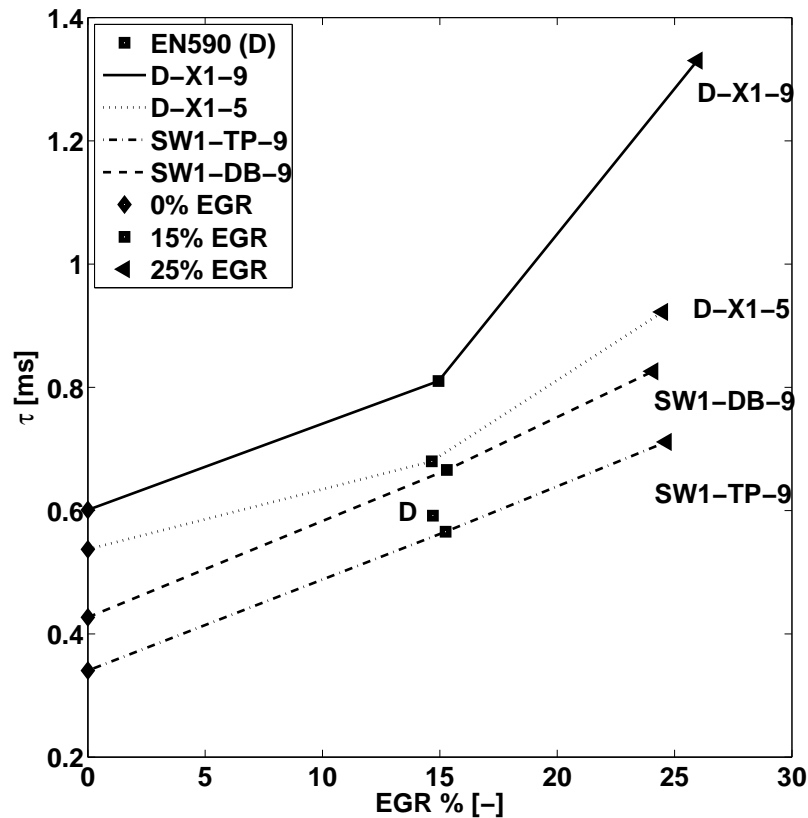


Figure 1.17: Ignition delay τ versus EGR wt-% at ROSI, EGR sweep. One point only for EN590, at 15 wt-% EGR.

at the Radboud University in Nijmegen [27].

1.4.1 Engine specifications

The engine utilized is derived from a 6-cylinder 11.6 liter DAF WS engine (130 mm bore, 146 mm stroke). Several modifications, however, have been made to facilitate optical measurements. Several modifications, however, have been made to facilitate optical measurements.

- Compression ratio was lowered to 15:1 (this was compensated by increasing intake temperature and boost pressure levels)
- One cylinder has been adapted to a Bowditch configuration in order to accommodate optical accessibility through a quartz insert of the flat piston.
- The original line pump has been replaced by common rail system
- Continuous firing was replaced by skip-firing (e.g. 1:30 ratio)

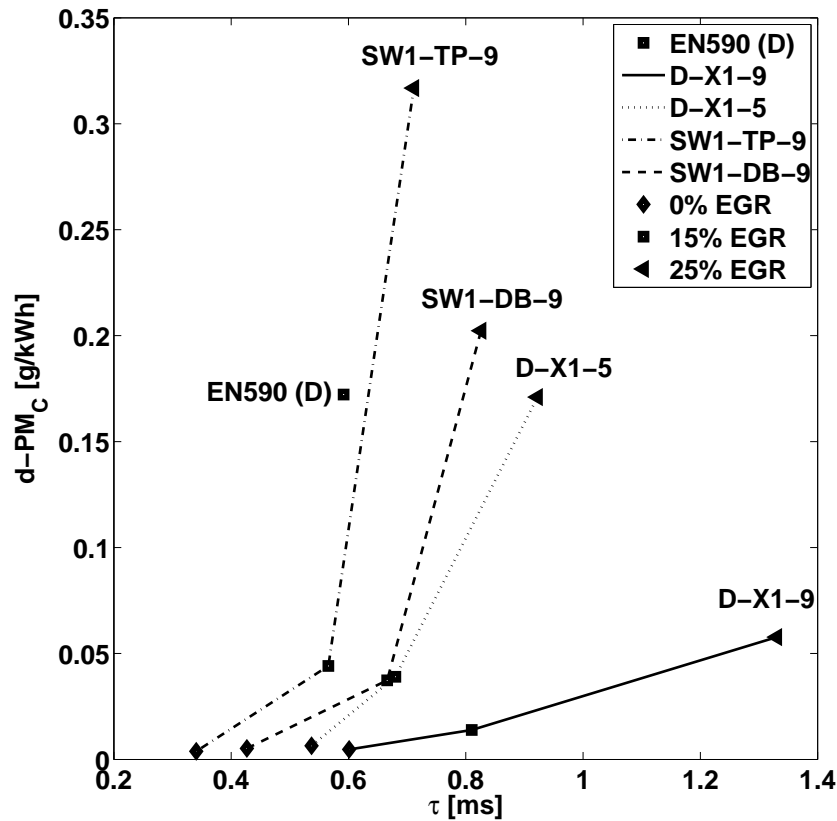


Figure 1.18: $d\text{-PM}_C$ vs. ignition delay at ROSI, EGR sweep.

In-cylinder soot luminosity was recorded with a Phantom V7.1 high-speed camera. Engine operating conditions at which the experiments were conducted are listed in Table 1.8 below.

Table 1.8: Setup of the RUN optical accessible engine.

Speed	rpm	1430
Rail pressure	MPa	120
SoA	$^{\circ}\text{CA aTDC}$	-13
Intake pressure	MPa	0.14
Load (IMEP)	MPa	0.5
Injector diameter	mm	0.128
No. of holes	-	8
Injection pressure	MPa	120

1.4.2 Results

In Figure 1.21 the soot luminosity is shown for the period -2.1 thru 12.9 $^{\circ}\text{CA aTDC}$ at intervals of 3 $^{\circ}\text{CA aTDC}$ for the S-TP-9 (left) and S-X1-9. The luminosity signal

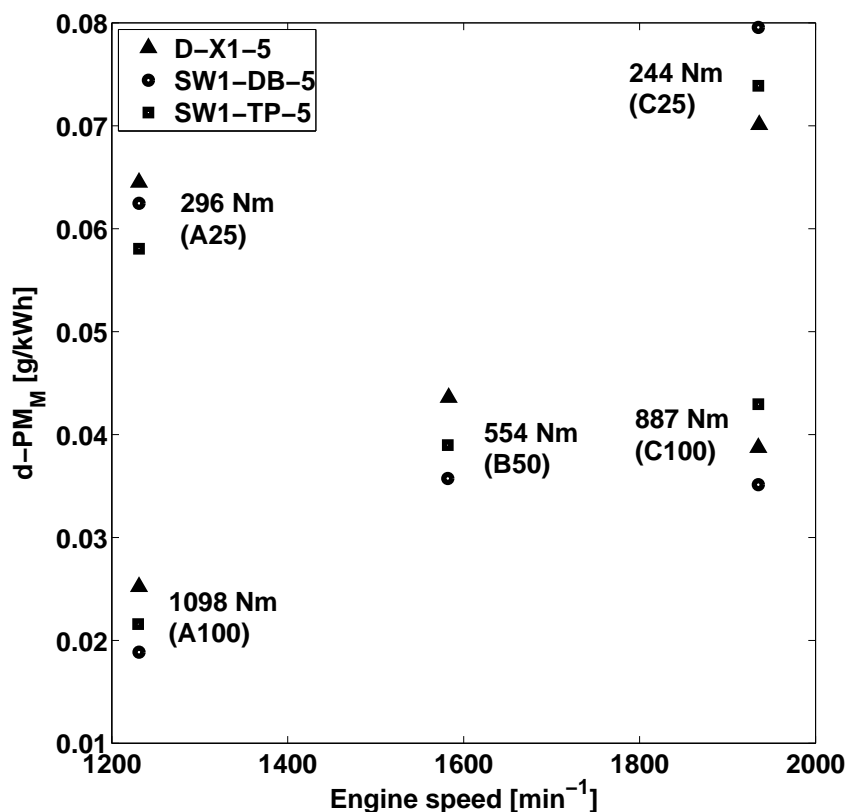


Figure 1.19: d-PM_C vs engine speed for different ESC loads.

passed through a filter that was transparent in the blue-to-green wavelength range only. Note that the recorded images have been inverted. Accordingly, the degree of blackness in Figure 1.21 can be considered as a rough measure for the amount of hot (radiating) soot particles. Of course soot luminosity is also a (strong) function of the temperature of the particles. To correct for this, soot temperature levels could be estimated using the well-known 2-wavelength method. First (rough) estimates of temperature differences in the hottest (stoichiometric) regions for the 2 fuels do not allow (by far) to explain the luminosity difference.

It is also worth mentioning here that when running the optical engine on the S-X1-9 fuel no fouling of the windows occurred. All other fuels demanded for intermittent window cleaning.

If it is assumed that the luminosity is to a large extent an indicator of soot mass, then these data would suggest that the low PM emissions measured in earlier experiments for the various X1 blends (Figure 1.12) would be the result of PM suppression rather improved PM oxidation.

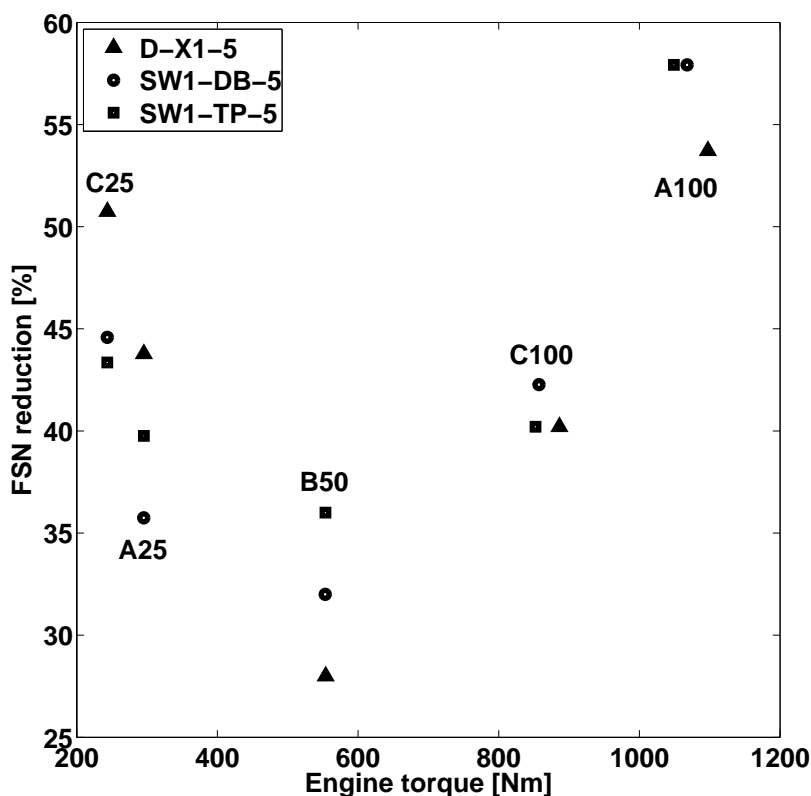


Figure 1.20: FSN reduction (in %, compared to EN590 fuel) vs. engine torque for different ESC points.

1.5 Conclusions

- The results presented in this study confirm earlier findings : oxygen content has a pronounced effect on PM reduction, but chemical structure effects can be almost of the same order.
- The effectiveness of oxygenates in PM reduction changes with engine (speed/load) condition. It is hypothesized that this effect may be linked to the change in (AFR, T)- conditions within the soot formation region that coincides with these (speed/load)- changes. At high loads, conditions may be at the hart of the soot formation region, hence the positive effect of oxygenate addition would be reduced. Alternatively, at these higher T, reactions may follow different paths. This aspect needs further study/analysis.
- As could be expected, the non-linearity of X1- X4 gives rise to, in some cases, a significant increase in ignition delay. Accordingly, addition of these molecules to a reference diesel fuel will manifest in a relatively high premixed burn fraction. It is well-known from literature that for a given gas composition (e.g. EGR level), a longer ignition delay, and therefore more premixed combustion, has a favorable effect on PM emissions. A well-known example of this phenomenon is

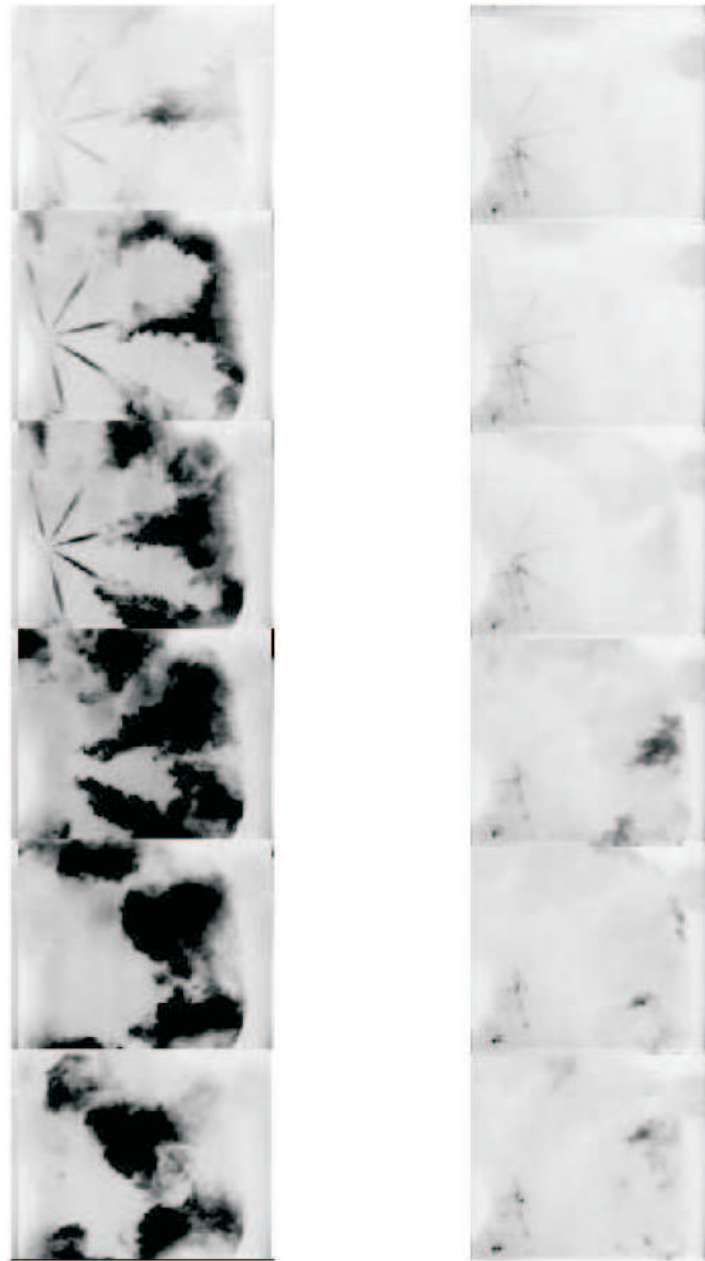


Figure 1.21: Six consecutive frames of a high-speed video recording of soot luminosity of S-TP-9 and SX1-9 blends from -2.1 to 12.9 °CA aTDC.

Nissan MK combustion.

- From the experiments becomes clear, however, that the beneficial impact of a longer ignition delay is not the only PM reduction mechanism at work here. Fuels SW1-DB-9 and D-X1-5, for example, have both comparable auto-ignition behavior and PM emissions, while the latter blend has only half the fuel oxygen content than the former fuel. This distinction underlines the assumption that, although auto-ignition behavior may be important, clearly another, currently undisclosed, mechanism is somehow responsible for the exceptional performance of the X1 blends. With the knowledge at hand, however, it is uncertain whether or not the mechanism in question is somehow linked to curvature in PAH layers.
- Optical in-cylinder measurements have revealed that, compared with S-TP-9, a S-X1-9 blend produces a considerable lower level of soot luminosity throughout the combustion process. If it is assumed that this is the result of a reduced amount of soot, this information would imply that the strength of S-X1-9 would be more in the suppression of PM formation, rather than enhanced PM oxidation. This needs to be confirmed by further ongoing experiments.

Bibliography

- [1] M. Parche. *Is it already time to plan for Euro 6 ?* Proc. EU 5&6 Global Diesel Emissions Strategies Conference. Amsterdam, Netherlands, June, 2006.
- [2] S. Meinrad. *Future Emission Regulations for trucks: Global harmonisation and technology development.* Proc. EU 5&6 Global Diesel Emissions Strategies Conference. Amsterdam, Netherlands, June, 2006.
- [3] N. Miyamoto, H. Ogawa, N.M. Nurun, K. Obata, and T. Arima. Smokeless, low NO_x, high thermal efficiency, and low noise diesel combustion with oxygenated agents as main fuel. *SAE Paper*, 980506, 1998.
- [4] N. Miyamoto, H. Ogawa, T. Arima, and K. Miyakawa. Improvement of diesel combustion and emissions with addition of various oxygenated agents to diesel fuels. *SAE Paper*, 962115, 1996.
- [5] B.E. Hallgren and J.B. Heywood. Effects of oxygenated fuels on DI diesel combustion and emissions. *SAE Paper*, 2001-01-0648, 2001.
- [6] M. Natarajan, E.A. Frame, D.W. Naegeli, T. Asmus, W. Clark, W. Garbak, M.A. González-D, E. Liney, W. Piel, and J.P. Wallace. Oxygenates screening for advanced petroleum-based diesel fuels: Part 1. screening and selection methodology for the oxygenates. *SAE Paper*, 2001-01-3631, 2001.
- [7] González-D M.A., W. Piel, T. Asmus, W. Clark, J. Garbak, E. Liney, M. Natarajan, D.W. Naegeli, D. Yost, E.A. Frame, and J.P. Wallace. Oxygenates screening for advanced petroleum-based diesel fuels: Part 2. the effect of oxygenate blending compounds on exhaust emissions. *SAE Paper*, 2001-01-3632, 2001.

-
- [8] B. Delfort, I. Durand, A. Jaecker-Voirol, T. Lacombe, F. Paille, and X. Montagne. Oxygenated compounds and diesel engine pollutant emissions performances of new generation of products. *SAE Paper*, 2002-01-2852, 2002.
- [9] L.I. Yeh, D.J. Rickeard, J.L.C. Duff, J.R. Bateman, R.H. Schlosberg, and R.G. Caers. Oxygenates: An evaluation of their effects on diesel emissions. *SAE Paper*, 2001-01-2019, 2001.
- [10] C.J. Mueller and G.C. Martin. Effects of oxygenated compounds on combustion and soot evolution in a DI diesel engine: Broadband natural luminosity imaging. *SAE Paper*, 2002-01-1631, 2002.
- [11] B.A. Buchholz, C.J. Mueller, A. Upatnieks, G.C. Martin, W.J. Pitz, and Ch.K. Westbrook. Using carbon-14 isotope tracing to investigate molecular structure effects of the oxygenate dibutyl maleate on soot emissions from a DI diesel engine. *SAE Paper*, 2004-01-1849, 2004.
- [12] P.J.M. Frijters and R.S.G. Baert. Oxygenated fuels for clean heavy-duty diesel engines. *Int.J. Vehicle Design*, 41:242–255, 2006.
- [13] J.E. Dec. A conceptual model of DI diesel combustion based on laser-sheet imaging. *SAE Paper*, 970873, 1997.
- [14] P.F. Flynn, R.P. Durrett, G.L. Hunter, A.O. zur Loye, O.C. Akinyemi, J.E. Dec, and C.K. Westbrook. Diesel combustion: an integrated view combining laser diagnostics, chemical kinetics, and empirical validation. *SAE Paper*, 1999-01-0509, 1999.
- [15] M.P.B. Musculus, J.E. Dec, D. Daly, D. Langer, Ryan Th.W., and A.C. Mathéaus. Effects of waterfuel emulsions on spray and combustion processes in a heavy-duty DI diesel engine. *SAE Paper*, 2002-01-2892, 2002.
- [16] M.P.B. Musculus and J. Dietz. Sand2005-0189: Effects of diesel fuel combustion-modifier additives on in-cylinder soot formation in a heavy-duty DI diesel engine. Technical report, Sandia, 2005.
- [17] L. Pickett and D.L. Siebers. Fuel effects on soot processes on fuel jets at DI diesel conditions. *SAE Paper*, 2003-01-3080, 2003.
- [18] Md.N. Nabi, H. Ogawa, and N. Miyamoto. Nature of fundamental parameters related to engine combustion for a wide range of oxygenated fuels. *SAE Paper*, 2002-02-2835, 2002.
- [19] F. Barnaud, P. Schmelzle, and Ph. Schulz. Aquazole: an original emulsified water-diesel fuel for heavy-duty applications. *SAE Paper*, 2000-01-1861, 2000.
- [20] P.D. Basar, D.A. Duncan, and D.A. Langer. Step forward in diesel engine emissions reduction: system incorporating a novel low emission diesel fuel combined with a diesel oxidation catalyst. *SAE Paper*, 2001-01-2491, 2001.

-
- [21] M.S. Skjøth-Rasmussen, P. Glarborg, M. Østberg, J.T. Johannesssen, H. Livberg, A.D. Jensen, and T.S. Christensen. Formation of polycyclic aromatic hydrocarbons and soot in fuel-rich oxidation of methane in a laminar flow reactor. *Combust. Flame*, 136:91–128, 2004.
- [22] R.L. Vander Wal and A.J. Tomasek. Soot oxidation: Dependence on initial nanostructure. *Combust. Flame*, 134:1–9, 2003.
- [23] R.L. Vander Wal and A.J. Tomasek. Soot nanostructure: Dependence upon synthesis conditions. *Combust. Flame*, 136:129–140, 2004.
- [24] D.S. Su, R.E. Jentoft, and J.O. Muller. Microstructure and oxidation behavior of euro IV diesel engine soot: a comparative study with synthetic model soot substances. *Catalysis Today*, 90:127–132, 2004.
- [25] D.S. Su, R.E. Jentoft, J.O. Muller, D. Rothe, E. Jacob, and R. Schlogl. Fullerene-like soot from euro IV diesel engine: consequences for catalytic automotive pollution control. *Topics in Catalysis*, 30/31:241–245, 2004.
- [26] S. Kimura, O. Aoki, Y. Kitahara, and E. Aiyoshizawa. New combustion concept for ultra clean and high efficiency small DI diesel engines. *SAE Paper*, 1999-01-3681, 1999.
- [27] K. Verbiezen, R.J.H. Klein-Douwel, A.P. van Vliet, A.J. Donkerbroek, W.L. Meerts, N.J. Dam, and J.J. ter Meulen. Attenuation corrections for incylinder NO LIF measurements in a heavy-duty diesel engine. *Appl. Phys. B*, 83:155–166, 2006.

Promotion of Curvature or Longer Ignition Delay?

Cyclic fuels have recently been demonstrated to be very efficient in soot and NO_x abatement, based on exhaust gas analysis [1]. High-speed imaging, chemiluminescence spectroscopy and thermodynamical characterization are applied in order to compare ignition delay and sooting behavior of bio-derived, oxygenated fuels and various reference fuels during combustion. The fuels concerned include the bio-derived fuels Jatropha oil (pure), Jatropha-methylester (JME) and rapeseed-methylester (RME), all containing $\approx 10\%_{mass}$ oxygen, and fossil oxygenated fuels tripropylene-glycolmonomethylether (TPGME) and cyclohexanone, both mixed with synthetic fuel to have similar total oxygen content. Commercial diesel, model fuel IDEA, a synthetic diesel fuel and a blend containing cyclohexane serve as reference fuels. The start of hot combustion is derived from OH and CH* chemiluminescence as observed through a spectrograph. Both species appear at about the same time. Soot incandescence is recorded by high-speed imaging at 0.3° crank angle resolution (200 images/cycle). Ignition delays derived from soot incandescence and chemiluminescence are compared to those determined from the heat release rate. The heat release rate and exhaust NO concentrations are used as indicators of average and peak temperatures during combustion, respectively. The soot incandescence is estimated to scale with T^{13} for our experimental conditions, so that local temperature becomes a decisive factor for the interpretation of natural luminosity images. All data are combined to get a relative measure for each fuel's sooting propensity. Both the fuel molecular structure and its oxygen content are found to be important for soot abatement. The cyclic fuels cyclohexane and especially cyclohexanone are found to produce the least amount of soot during combustion.*

The content of this Chapter has been taken from:

R.J.H. Klein-Douwel, A.J. Donkerbroek, A.P. van Vliet, **M.D. Boot**, L.M.T. Somers, R.S.G. Baert, N.J. Dam, J.J. ter Meulen. Soot and chemiluminescence in diesel combustion of bio-derived, oxygenated and reference fuels. *Proc. Combust. Inst.*, 32:2817 - 2825, 2009.

Minor edits have been made to streamline the layout of the thesis chapters. The contribution of the author is related to the motivation and selection of the test fuels and relevant operating conditions, along with the results, discussion and conclusions thereof. The introduction and overall discussion and conclusions were realized in a joint effort. Experiments were carried out in the engine lab of the Radboud University of Nijmegen.

2.1 Introduction

Air quality concerns result in increasingly stringent emissions regulations for automotive vehicles regarding NO_x and soot. To meet the legislative requirements, several strategies are possible, like aftertreatment, exhaust gas recirculation (EGR) or improved fuel injection techniques for better mixing.

An alternative route receiving less attention is changing the fuel composition. Much work has been done on oxygenated fuels from either biological [2] or fossil feedstock [1, 3–10], and clear differences have been found in sooting characteristics between various oxygenated fuels and between oxygenated and conventional fuels [5–11].

The effect of oxygenated fuels is studied extensively for dibutylmaleate (DBM) and TPGME in Refs. [5, 11], which find that TPGME outperforms DBM. The oxygenate molecular structure is found to have an effect on soot formation, with esters being less effective in soot abatement [3], as opposed to earlier studies (references in [3]). Literature reveals that an elevated oxygen concentration in the particle synthesis zone, for instance via fuel-bound oxygen, alters the particle nanostructure [12] and also that the soot oxidation rate of curved particle nanostructures is about 5 times higher than that of crystalline ones [13].

Effects of fuel structure, composition and oxygen content are reviewed by Tree & Svensson [14], which includes over 25 different oxygenates, but no cyclic ones. In earlier work of our laboratory it was found that a cyclohexanone blend outperforms both DBM and TPGME in terms of soot reduction [1].

One of the main objectives of this research is to determine how the cardinal conclusion from previous work on a full-metal (i.e. non-optical) engine [1], namely that fuel molecular structure (for both oxygenated and non-oxygenated fuels) is pivotal for the net (exhaust) soot production, manifests itself during the combustion in an optical engine. In Ref. [1] more fuels are tested than in this work and also their oxygen content is varied (5 - 10%), but only the engine performance and exhaust emissions are studied there. In the current work, however, optical access provides a direct view at the onset of soot formation, and although the fuel oxygen content is not varied here, significant differences in sooting propensity between the tested fuels are still observed. Temperature effects on soot incandescence are discussed by considering heat release rates and exhaust NO measurements for average and peak temperatures, respectively [15–17].

Chemiluminescence of OH* and CH* has been used as indicator of hot combustion [18–20]. We have used a spectrograph to resolve the spectral difference between chemiluminescence (specific features) and soot incandescence (featureless background). Finally, rather than merely presenting snapshots [11, 18, 21, 22], a statistical analysis of the high-speed data based on multiple consecutive cycles is presented here.

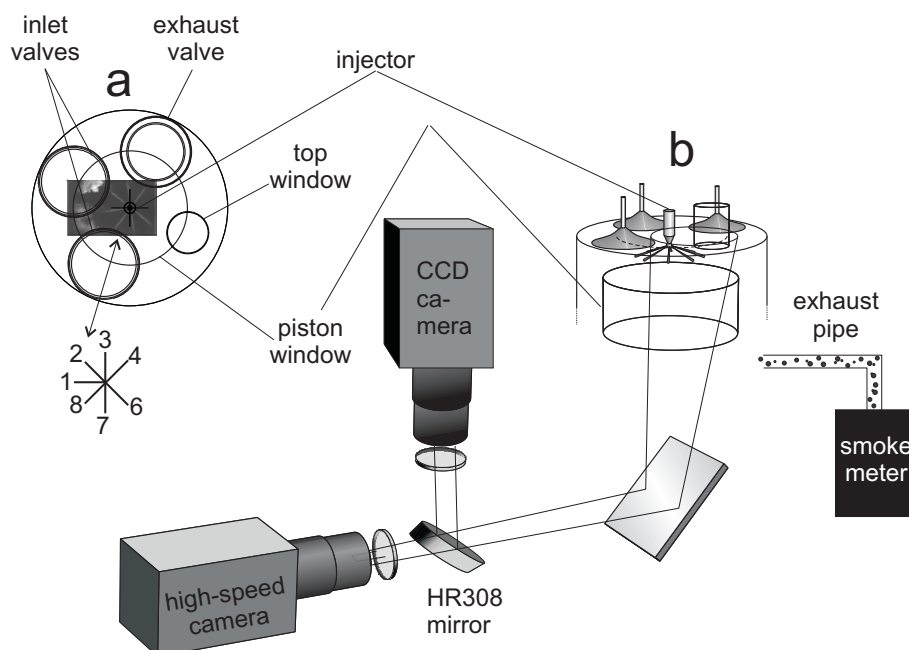
2.2 Experimental setup

2.2.1 Engine

All measurements are performed on a six cylinder, heavy-duty Diesel engine (DAF Trucks). One of the cylinders is modified for optical access through quartz windows at

Table 2.1: Engine parameters.

bore	130	mm
stroke	146	mm
compression ratio	14.9	
swirl ratio	1.8	
piston bowl	flat	
skip firing	1:35	
injection pressure	120	MPa
boost pressure	0.14	MPa (abs)
boost pressure (eff)	0.11	MPa (abs)
EGR	21 or 15	% O ₂
speed	1430	rpm

**Figure 2.1:** Schematic representation of the experimental setup (spectrograph and CCD camera observing side window not shown).

various locations, see Figure 2.1. The engine settings and specifications pertaining to the modified cylinder are given in Table 2.1. The piston window (flat geometry) gives a view of a large part of the combustion chamber. Fuel is injected through a central eight-hole nozzle, driven by a common-rail system. The engine speed is constant to $\pm 2\%$. It is air-aspirated, and swirl is clock-wise in the images presented here. More details can be found in Refs. [23, 24].

The common-rail pressure, needle lift signal and cylinder pressure signals are recorded during injection and averaged over 20 cycles. The delay between injector activation and start of delivery (SoD) of fuel into the cylinder is determined from rail pressure curves, taking injector characteristics into account [25]. An example is given in Figure 2.2. Details of exhaust NO measurements and analysis are given in Refs. [24, 26].

Two inlet air conditions have been employed, one with normal (dry) air, and one

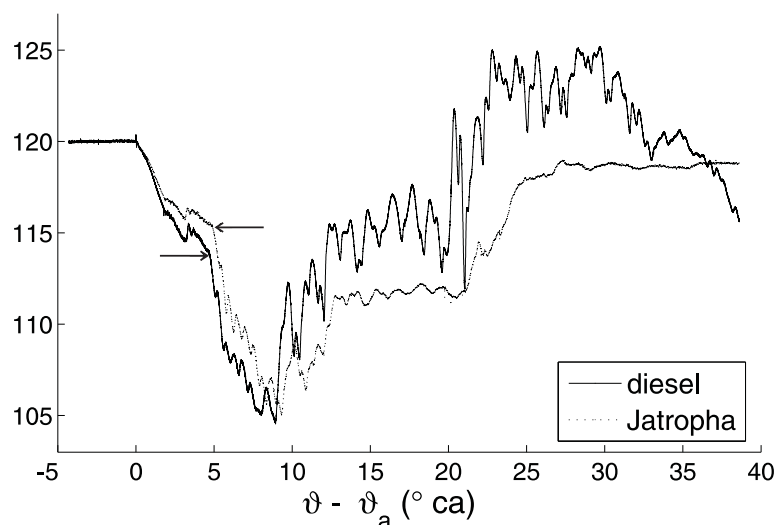


Figure 2.2: Common rail pressure transients during injection of Jatropha oil and regular diesel, corresponding to the measurements presented in Figs. 2.6 and 2.7, respectively. Up to the end of injection, all transients reproduce to within 1% of each other. The Jatropha injections proceed slightly slower and exhibit much smaller pressure oscillations than all other fuels. Note that the horizontal scale is relative to the injector activation timing ϑ_a . Arrows indicate the actual start of fuel delivery. ϑ_{SoD} is given by $\vartheta_a + 3.5 \pm 0.3^\circ$ CA. In recording the transients there is an additional delay of $\approx 1.2^\circ$ CA (diesel) or $\approx 1.4^\circ$ CA (Jatropha oil) due to the time it takes the pressure waves to travel back from the nozzle opening to the pressure sensor. The sharp pressure increase at the end of injection (“water hammer” effect) is visible for diesel at $\vartheta_a + 20.1^\circ$ CA and for Jatropha oil at $\vartheta_a + 21.4^\circ$ CA.

with nitrogen enriched air containing only 15% oxygen, to mimic EGR conditions. The majority of measurements presented here have been obtained with normal 21% oxygen inlet air, and this condition applies unless stated otherwise.

2.2.2 Fuels

The bio-derived fuels used are commercially available rapeseed methylester (RME), pure Jatropha oil (raw vegetable oil) and its methylester JME. Other fuels used are commercial diesel (EN590), synthetic diesel fuel (SD; straight-chain alkanes), oxygenated fuel TPGME mixed with SD, model fuel IDEA (70% n-decane and 30% α -methylnaphthalene, designed to have a heat release rate very similar to that of diesel), cyclohexanone + SD (abbreviated here as CHxnO, both fuels 50% by weight) and cyclohexane + SD (CHxn, both fuels 50% by weight). Elementary data (and their references) about the fuels used in the experiments is given in Table 2.2, from which it is clear that the oxygen content is approximately equal for all oxygen-containing fuels.

The low cetane number cyclohexanone is blended with SD to obtain a cetane number similar to the three bio-derived fuels. Note that cyclohexanone is marked ‘X1’ and cyclohexane is marked ‘X2’ in Chapters 1, 3 and 4. Fuel molecular structures are given as supplementary material (online version): CHxnO and CHxn have a cyclic molecular structure, that of Jatropha oil is branched and for TPGME, JME and RME

Table 2.2: Fuels used. ^ain %_{mass}. ^bin kg/m³. ^ccetane number. ^dlower heating value in MJ/kg. ^eRef. [1]. ^fRef. [27]. ^gcyclohexane + SD. ^hcyclohexanone + SD. ⁱ+SD. ^jRefs. [2, 28, 29]. ^kRefs. [2, 30–32].

	O ^a	ρ^b	CN ^c	Hu ^d
diesel ^e	0	827	56.2	43.2
IDEA ^f	0	817	55	43
SD ^e	0	778.3	>74.8	44
CHxn ^{e,g}	0	774	≈45	42.2
CHxnO ^{e,h}	9	864	≈45	37.5
TPGME ^{e,i}	9.49	818.3	74.8	39.4
Jatropha ^j	≈10	919	46.3±6.2	36
JME ^j	≈10	882	52.3±2.3	36.5
RME ^k	≈10	879	54.5±4.9	37.3

it is linear.

2.2.3 Chemiluminescence

The combustion luminosity is recorded through various windows (Figure 2.1). An intensified CCD camera (Roper Scientific, CCD 512T, 512² pixels, 16 bit dynamic range) coupled to a spectrograph (ARC SpectraPro 500i) equipped with a UV Nikkor f/4.5 105 mm lens is observing through the side window, recording one image per fired cycle. A grating of 600 grooves/mm is used, resulting in a simultaneously observable spectral range of 40 nm. Thus, chemiluminescence of OH* (310 nm) and CH* (430 nm) could not be observed simultaneously; they have been recorded here in separate measurements under nominally identical conditions. The volume observed in the combustion chamber is about 23 mm high and 5 mm wide [24]. Spectra have been recorded with an exposure time of 60 μ s (\sim 0.52 °CA).

2.2.4 High-speed imaging

A digital, non-intensified high-speed camera (Phantom V7.1, 160 kHz maximum frame rate, 12 bit dynamic range) observes the combustion luminosity through the piston window (Figure 2.1). The spectral sensitivity of this camera starts at around 317 nm (supplementary Figure online), and it is used here to record soot incandescence. To avoid overexposure in intensity measurements, an exposure time of 2 μ s (the shortest possible) is used together with a filter combination transmitting roughly between 460 and 640 nm (Schott BG 18 and GG 475). Thus, possible chemiluminescence contributions due to OH* and CH* are explicitly rejected. Combined with the camera quantum efficiency, the system spectral response is flat within \approx 10%. The camera response linearity was checked separately. Detection of the fuel start of delivery (SoD) is enabled by illumination of the spray region in the combustion chamber by a continuous-wave Ar⁺ laser (Spectra Physics; Figure 2.1) and recording elastic scattering with a longer exposure time of 24 μ s. This also allows better localization of the first weak soot incandescence.

The camera is synchronized to the crankshaft of the engine and operated in the

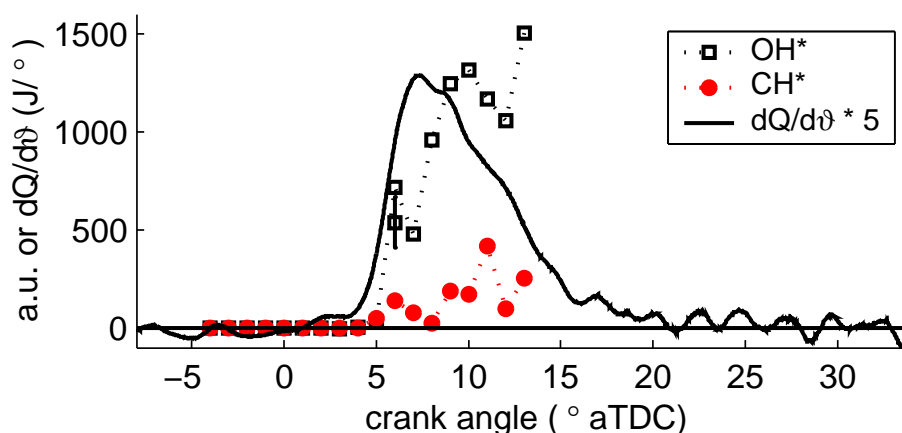


Figure 2.3: $dQ/d\vartheta$ and net OH^* and CH^* chemiluminescence signal for CH_xO combustion (latter two derived from Figure 2.4, in same arbitrary units; $\vartheta_{\text{SoD}} = -4.5^\circ$ aTDC, $\vartheta_{dQ} = 4.4^\circ$ aTDC). Error bar for OH^* indicated.

memory gate mode. Image acquisition is triggered by injector actuation and enabled for 7 ms, after which it is halted until the next injection. Images are recorded every 0.3° CA ($\approx 35 \mu\text{s}$), resulting in ≈ 200 images per injection event. A spatial resolution of typically $275 \mu\text{m}$ per pixel is obtained ($158 \mu\text{m}$ per pixel for the diesel series).

2.3 Data acquisition and analysis

2.3.1 Injection and thermodynamics

Figure 2.3 presents the heat release rate $dQ/d\vartheta$ versus crank angle ϑ for a typical engine run with CH_xO . The crank angle ϑ_{SoD} at which SoD occurs is determined from camera images with an accuracy of 0.3° CA and the delay between injector actuation and ϑ_{SoD} thus determined is $3.5 \pm 0.3^\circ$ CA, irrespective of fuel, which corresponds very well to values obtained from common-rail pressure curves (Figure 2.2). The indicated mean effective pressure of all experiments reported here lies between 450 and 520 kPa; it is approximately constant per fuel for the conditions used here.

The heat release ignition delay τ_{dQ} is determined by fitting a straight line to the region of steepest slope in $dQ/d\vartheta$, which intersects $dQ/d\vartheta = 0$ at ϑ_{dQ} and whence $\tau_{dQ} = \vartheta_{dQ} - \vartheta_{\text{SoD}}$. Since the steep increase in the heat release rate is well defined, this method of determining ϑ_{dQ} is very insensitive to noise.

2.3.2 Chemiluminescence

Chemiluminescence spectra of OH^* and/or CH^* were often found to be contaminated by soot incandescence. Spectra obtained from CH_xO combustion are shown in Figure 2.4, from which it is clear that the thermal soot incandescence background increases while combustion proceeds. While in general OH^* remains visible for a long time, CH^* is often detectable for only a few degrees, before drowning again in the increasing soot signal (depending on fuel sooting propensity). Net average chemiluminescence signals are obtained by background subtraction (2nd degree polynomial fit), followed

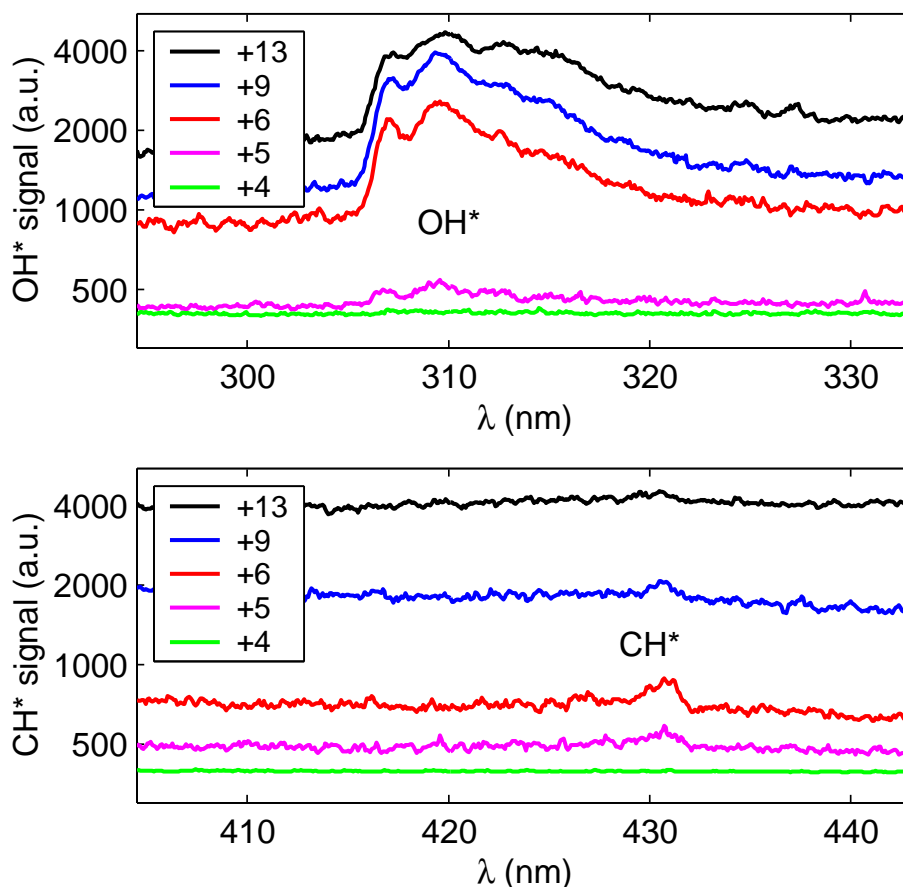


Figure 2.4: Raw dispersion spectra of OH* and CH* from CH_xO combustion (2 separate experiments; selected crank angles indicated [$^{\circ}$ aTDC]), $\vartheta_{SoD} = -4.5^{\circ}$ aTDC. Note the logarithmic ordinate and the increase in background signal level with crank angle (due to soot incandescence).

by integration of the remaining signal. Examples of OH* and CH* evolution are presented in Figure 2.3. Data like this is used to determine the crank angle ϑ_{cl} at which chemiluminescence becomes detectable and to obtain the chemiluminescence ignition delay $\tau_{cl} = \vartheta_{cl} - \vartheta_{SoD}$. The uncertainty is about $\pm 25\%$ in the chemiluminescence intensity and about $\pm 0.5^{\circ}$ in ϑ_{cl} .

2.3.3 Flame structure development

Phase averaged images of 10 consecutive injections (21% O₂) are shown in the left column of Figure 2.5 for diesel, CH_xO, JME and Jatropa oil, the latter three chosen for their very different chemical structure (see above). Corresponding heat release rates $dQ/d\vartheta$ are shown in Figs. 2.6 (oxygenates) and 2.7 (non-oxygenates). We have chosen to compare fuels under conditions of fixed Start of Delivery, $\vartheta_{SoD} = -4.5^{\circ}$ CA, except for CH_xO.

Since the ignition delay τ_{dQ} is much larger for CH_xO than for the other fuels (see below), data with an earlier ϑ_{SoD} are selected for this fuel, such that the fast rise in $dQ/d\vartheta$ occurs at about the same crank angle for all fuels. The images shown in

Figure 2.5 are all taken at 1.2° CA after maximum $dQ/d\vartheta$, since around that time the early soot structure is well developed.

The phase averaged images (Figure 2.5, left column) reveal clear differences in the early soot location for different fuels. This is corroborated by the corresponding standard deviation images (Figure 2.5, right column), which exhibit the same fuel dependence of spatial structure, in addition to showing cycle-to-cycle variability.

Diesel and JME have quite similar behavior, in that (i) the earliest soot is detected between the end of the liquid spray and the cylinder wall, and (ii) the soot vapor region expands both towards the injector and along the cylinder wall. (See supplementary material for more images and movies.) For CH_xNO , very weak soot incandescence is first detected along the full perimeter of the cylinder, and only slightly later a brighter region of soot grows towards the liquid core. Jatropa oil, however, behaves markedly different: soot originates leeward of the liquid spray, but only along its downstream half. Then it slowly grows towards the cylinder wall, eventually covering the whole perimeter of the field of view.

Under (quasi-)steady-state conditions the closest distance of the flame to the injector (flame lift-off length, FLoL) is a measure for the amount of air that has been entrained by the spray before combustion starts. A larger distance could contribute to reduced soot formation because of enhanced air entrainment. Both the OH^* (or CH^*) chemiluminescence and the soot luminosity can be used as a measure for the flame lift-off length. The former is the more direct indicator of the flame location, but measurement of OH^* chemiluminescence was beyond the capabilities of our high-speed camera. Therefore, the location of most upstream soot luminosity, the SLoL, is used here as indicator for air entrainment.

The analysis of the SLoL was not straightforward, due to the occurrence of a background ('haze') the origin of which remains unclear. We have strong reasons to believe that it is not simply related to the combustion luminosity. Its intensity was not proportional to the total luminosity, the haze persisted until late in the stroke (up to at least 70°CA , that is, after combustion has finished), and it was absent in experiments in which the combustion volume was illuminated by the Ar^+ laser. A camera artefact cannot be excluded. Figure 2.8 shows the typical time development of the haze intensity for a position between two sprays close to the injector. The haze initially showed up closely around the soot, spreading within around 3^{circ} (i.e. 10 camera frames) homogeneously over the full image. The asterisk at the start of the plateau in Figure 2.8 has been taken as the haze intensity.

As a first step in the analysis, the image was noise-filtered by a 3×3 neighborhood-sized median filter. Subsequently, the haze was subtracted. Then, to assess the soot lift-off length, the closest distance to the injector was determined where the intensity on a single pixel basis is above a certain threshold value. In this sense, we followed the method described by Higgins and Siebers [20] for (OH^* -based) flame lift-off assessment. The analysis was restricted to a cone around the spray axis, slightly rotated in the swirl-wise direction, as shown in Figure 2.9. The threshold was set to 25% of the maximum haze-corrected pixel value occurring in the cone of analysis. The result for the SLoL of the oxygenates as a function of crank angle is shown in Fig. 2.10. From this Figure it appears that the SLoL converges slowly to a kind of common quasi-steady-state, which, however, is not really reached within the injection duration. The reproducibility of the SLoL-data is good, judging from the rather

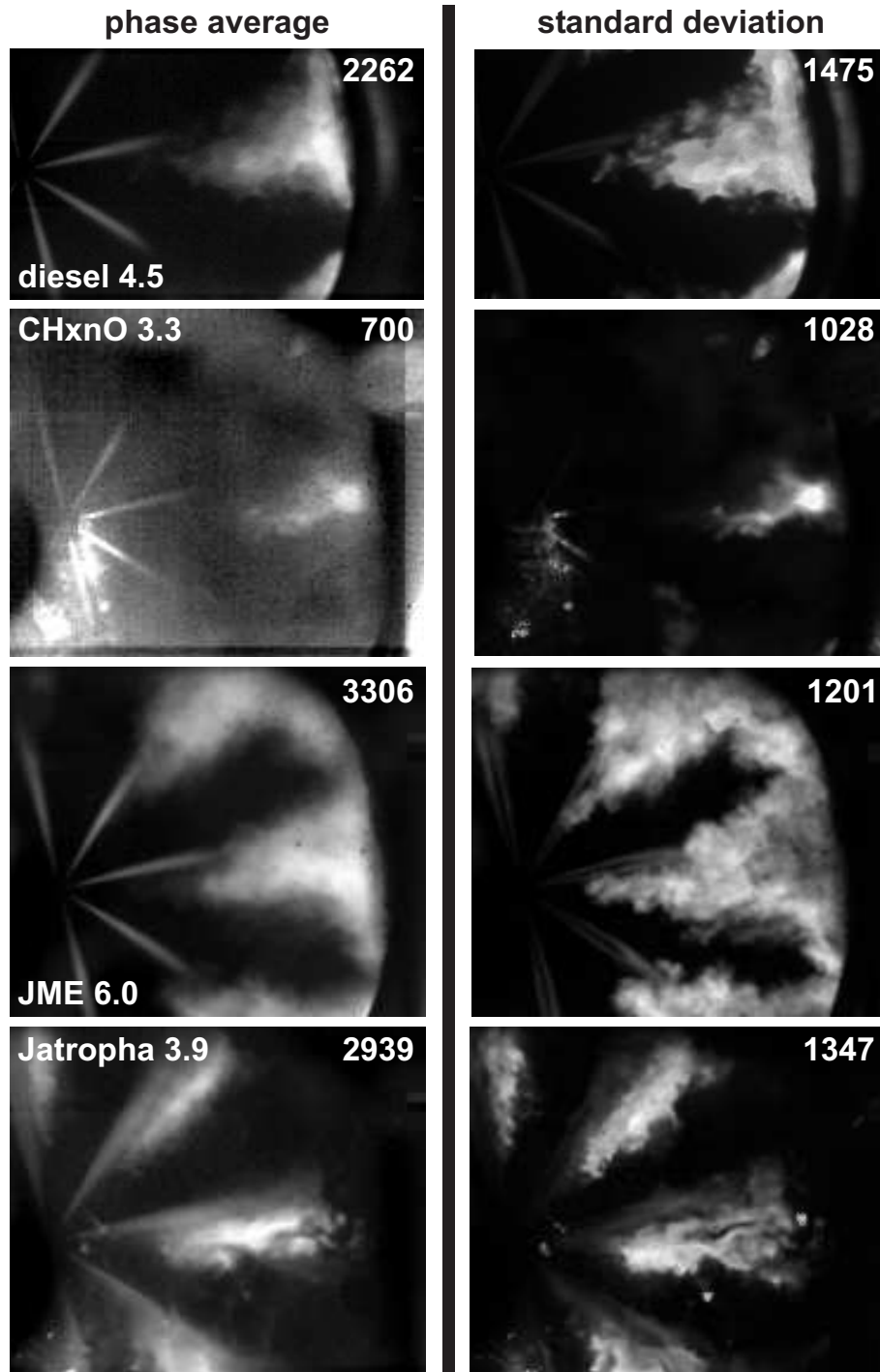


Figure 2.5: Phase average over 10 injections (left column) and corresponding standard deviation (right column) of the spontaneous luminosity of various fuels. The crank angle of each recording [in $^{\circ}$ aTDC] follows the fuel name. $\vartheta_{SoD} = -4.5^{\circ}$ aTDC, except CHxnO for which $\vartheta_{SoD} = -9.5^{\circ}$ aTDC). CHxnO images show residual light scattering below the injector. The dark segment in the lower left corner of some of the images is an artefact of the optical setup. Swirl is clock-wise. Pixel values for white are indicated in the upper right corners (black is minimum).

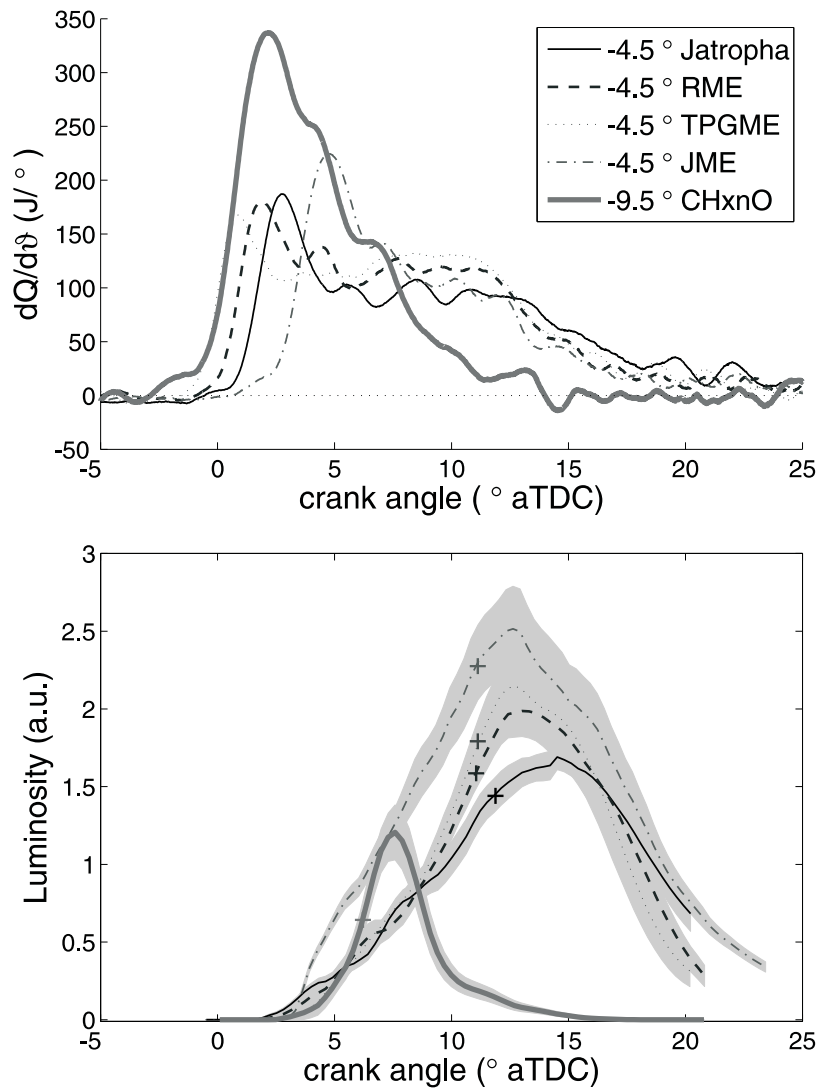


Figure 2.6: Heat release rates and integrated luminosity for oxygenated fuels (ϑ_{SoD} indicated). Shaded grey area represents standard error of phase averages. The crosses indicate the end of injection for each fuel.

narrow ranges of standard deviations. Again, Jatropa behaves markedly different from the other fuels tested. Interestingly, regular diesel fuel has a relatively large SLoL.

Under conditions of reduced oxygen (mimicking EGR) the concept of SLoL loses its meaning, since combustion only starts at the piston bowl wall.

2.3.4 Intensity analysis of luminosity

The total signal in a cone around a single spray, that is considered representative for the others (Figure 2.9) was taken as the measure for soot luminosity. The liquid core was excluded from the analysis, even though the light scattered by it will largely have been due to the natural luminosity. The analysis of the luminosity was not straightforward, due to the occurrence of the background ('haze'), addressed in section

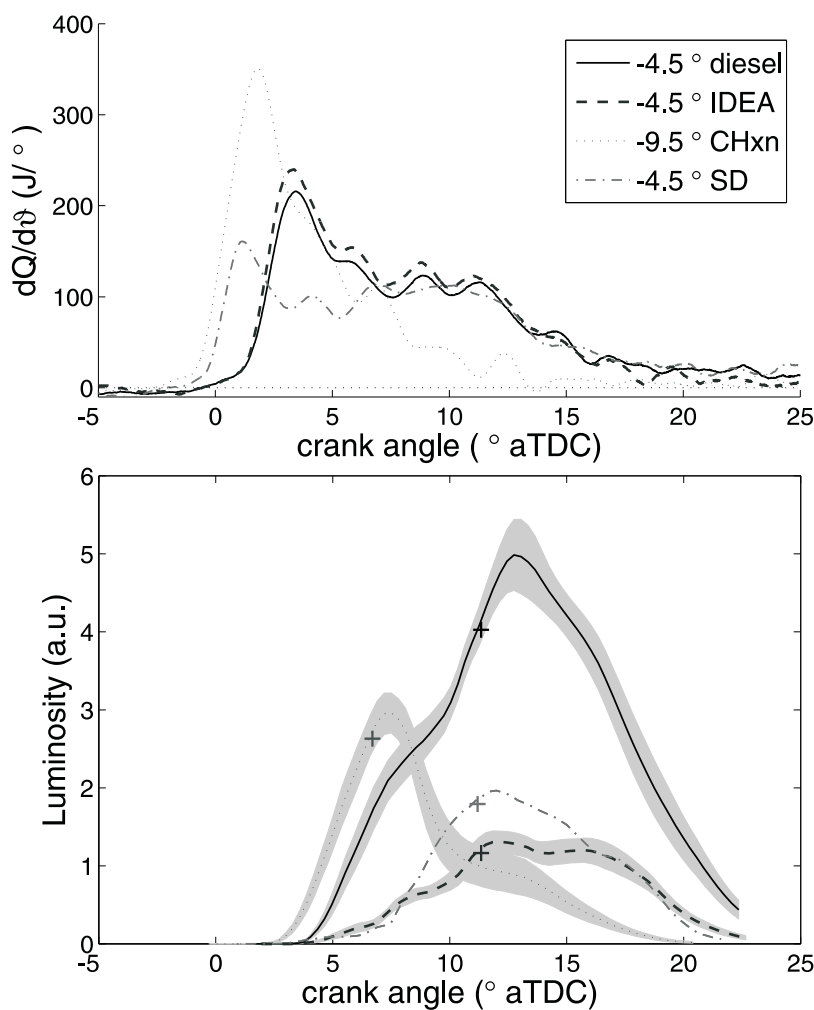


Figure 2.7: Similar to Figure 2.6 (identical ordinates), now for non-oxygen containing fuels. For SMDS, data from only one injection were available.

2.3.3. Only pixels with intensity values at least 15% above the haze were regarded as pixels showing soot luminosity. The total luminosity was determined by integration, after haze subtraction. The resulting values were not critically dependent on the intensity threshold value, because pixels that are just above the threshold do not have a large contribution to the total luminosity anyway. For the pixels that are above the threshold, the average intensity at the luminosity maximum is comparable to the haze intensity.

As a check of our method of haze correction, the luminosity data recorded with $2 \mu s$ and $11 \mu s$ exposure time are compared in Fig. 2.11. The curves are very similar and differ by a simple scaling factor of 5.5, as would be expected from the difference in exposure time. Without haze correction, the curves differ at most by a factor of 1.5.

Figures 2.6, 2.7 and 2.14 present the total soot incandescence intensity, integrated over the field of view (an earlier ϑ_{SoD} is selected for CHxn as well, similarly to CHxnO). The crank angle at which the first soot is detected, ϑ_{soot} , is determined from the high-speed sequences and a soot ignition delay $\tau_{soot} = \vartheta_{soot} - \vartheta_{SoD}$ is calculated.

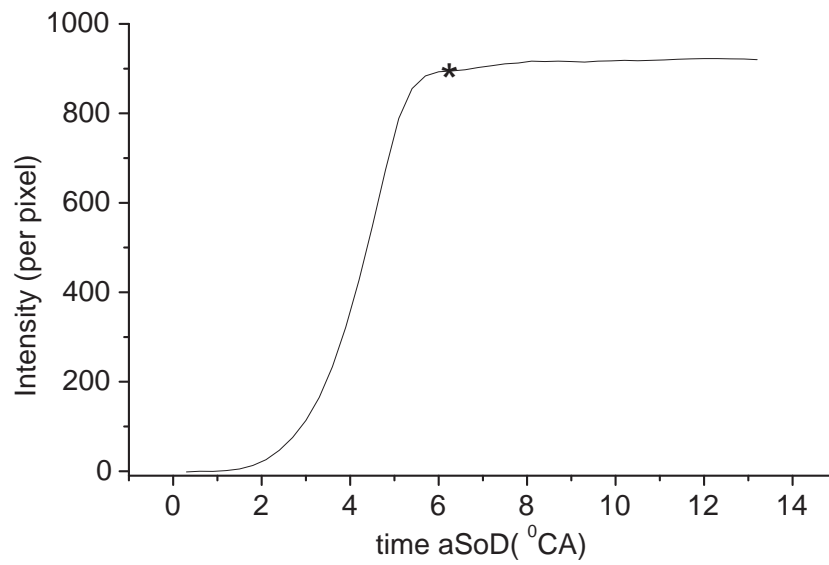


Figure 2.8: Background haze as a function of the frame number after the start of ignition. (See text for details.)



Figure 2.9: Typical CMOS camera snapshot for diesel as a fuel. The wide cone extending till the end of the field of view indicates the area where the luminosity is determined. The spray area contains scattering from liquid fuel, and is excluded from analysis. The '+' indicates the SLoL.

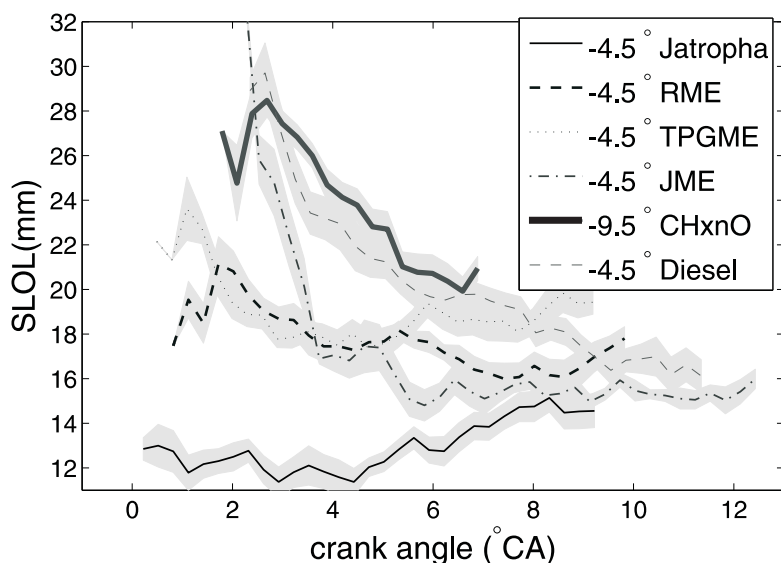


Figure 2.10: Soot lift-off length (SLoL) for the oxygenates and for regular diesel, all under standard operating conditions. The gray bands indicate the standard error calculated over 10 injections.

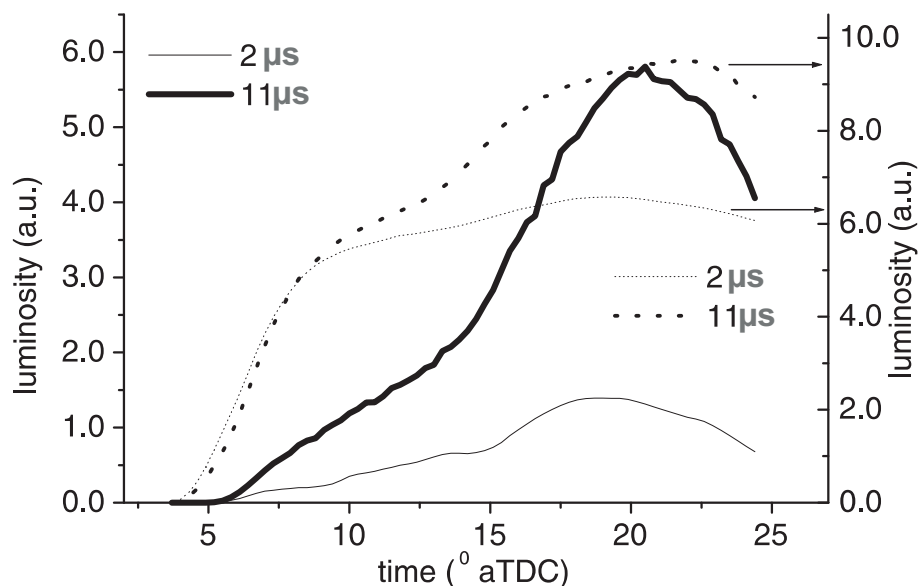


Figure 2.11: Luminosity for n-heptane, both for haze correction (left ordinate) and no haze correction (right ordinate). n-Heptane was injected from 4.5° bTDC to 21.0° aTDC, normal inlet air, for two different camera exposure times. The nominal boost pressure was 0.11 MPa. An average of 9 injections was taken for both exposure times.

Mueller & Martin [11] have provided an excellent discussion of possibilities and pitfalls for evaluation of soot luminosity data. Their approach is followed here as well. The crucial point is that the spectral selectivity of a luminescence detector may give rise to a much steeper temperature dependence than the T^4 -relation that would hold for a black absorber. The spectral emittance of soot is governed by its temperature distribution: a higher T not only results in a higher total amount of radiation ($\propto T^4$), but also may move the emittance maximum closer to the spectral observation window. For the particular case of our detection system's spectral response (section 2.2.4), we conclude that the observed soot incandescence will scale approximately with T^{13} over the range of 1800 – 2700 K (T^{11} was found for the conditions of Ref. [11]). Clearly, the hottest soot will dominate the recorded signal. This hot soot is expected to be present at the rich side of the diffusion flame enveloping the reacting jet [11]. This is observed in Figure 2.5.

For a heavily sooting fuel the soot cloud may be optically thick, causing some incandescence to be obscured by soot particles closer to the detector. This would lead to an underestimation of the total soot incandescence and hence of the amount of soot. The soot volume fraction and particle size distribution, which can in principle be determined by laser-induced incandescence [33, 34], therefore may affect the observed incandescence, but its influence cannot be estimated in the scope of this work.

The degree of attenuation due to window fouling has been assessed globally by comparing luminosity measurements under identical conditions at various points in time during a measurement cycle. For the two cyclic fuels, CH_{xn} and CH_{xn}O, no significant change in recorded luminosity intensity was observed. For the other fuels a gradual decrease in recorded luminosity by typically 10% per series of 10 consecutive injections was found. We have no indications that this depends on whether or not EGR-like conditions are used. The relatively viscous Jatropha oil requires particular care in cleaning between measurement cycles. In the luminosity data shown, the estimated corrections for window fouling are included.

2.4 Discussion

2.4.1 Ignition delays and cetane number

As discussed in the previous section, several measures for the ignition delay can be derived from our data, based on heat release rate, chemiluminescence, or soot incandescence, respectively. Ignition delays τ_{dQ} (heat release), τ_{cl} (chemiluminescence of OH* and/or CH*), and τ_{soot} (soot incandescence) are presented in Figure 2.13a for the same operating points as used for Figs. 2.6 and 2.7. The lower abscissa in Figure 2.13 is labeled by the experiment sequence number; the fuel legend is included in panel (a). For all runs $\vartheta_{SoD} = -4.5$ °CA, except for #3,6 for which it is -9.5 °CA. Ignition delays are approximately independent of ϑ_{SoD} for all fuels (shown here only for CH_{xn}O and CH_{xn}, #1-6), and they only increase for more extreme values of ϑ_{SoD} (data not shown). A general trend of decreasing ignition delay with increasing cetane number is observed, with Jatropha oil and RME being notable exceptions. It must be noted, however, that the cetane number uncertainty for bio-derived fuels is relatively large (Table 2.2), and also that Jatropha oil is preheated (≈ 34 °C) in order to reduce

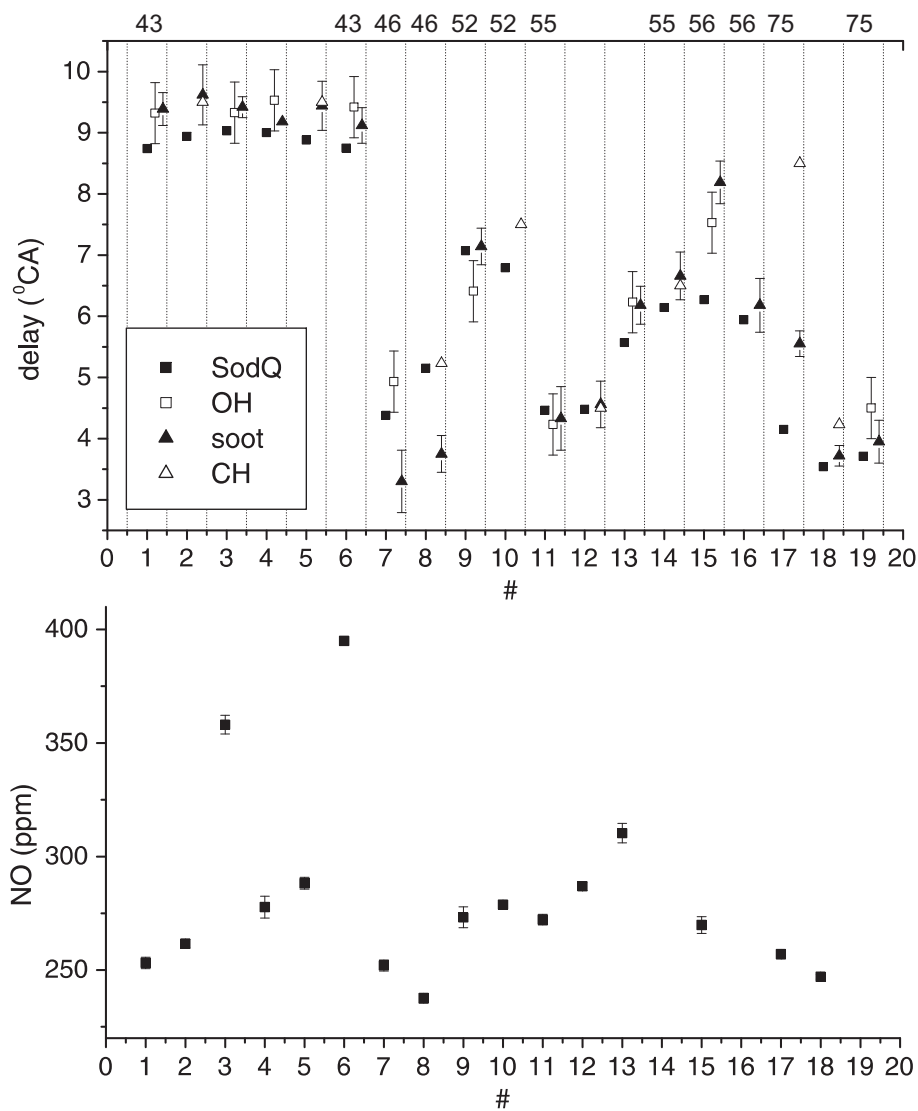


Figure 2.12: (a) Ignition delays τ_{dQ} (constituting an upper limit), τ_{cl} and τ_{soot} (results for OH* and CH* from separate but identical runs given for most fuels) versus cetane number (shown on top axis, uncertainty not indicated; $\vartheta_{SoD} = -4.5^\circ$ aTDC except #3,6, where it is -9.5° aTDC). The different ignition delays are shifted slightly along the abscissa for the sake of clarity. Fuels corresponding to the numbers at the lower abscissa: 1,2,3: CH_xO, 4,5,6: CH_x, 7,8: Jatropha pure, 9,10: JME, 11,12: RME, 13,14: IDEA, 15,16: diesel, 17: SMDS, 18,19: TPGME (b) corresponding NO exhaust concentration

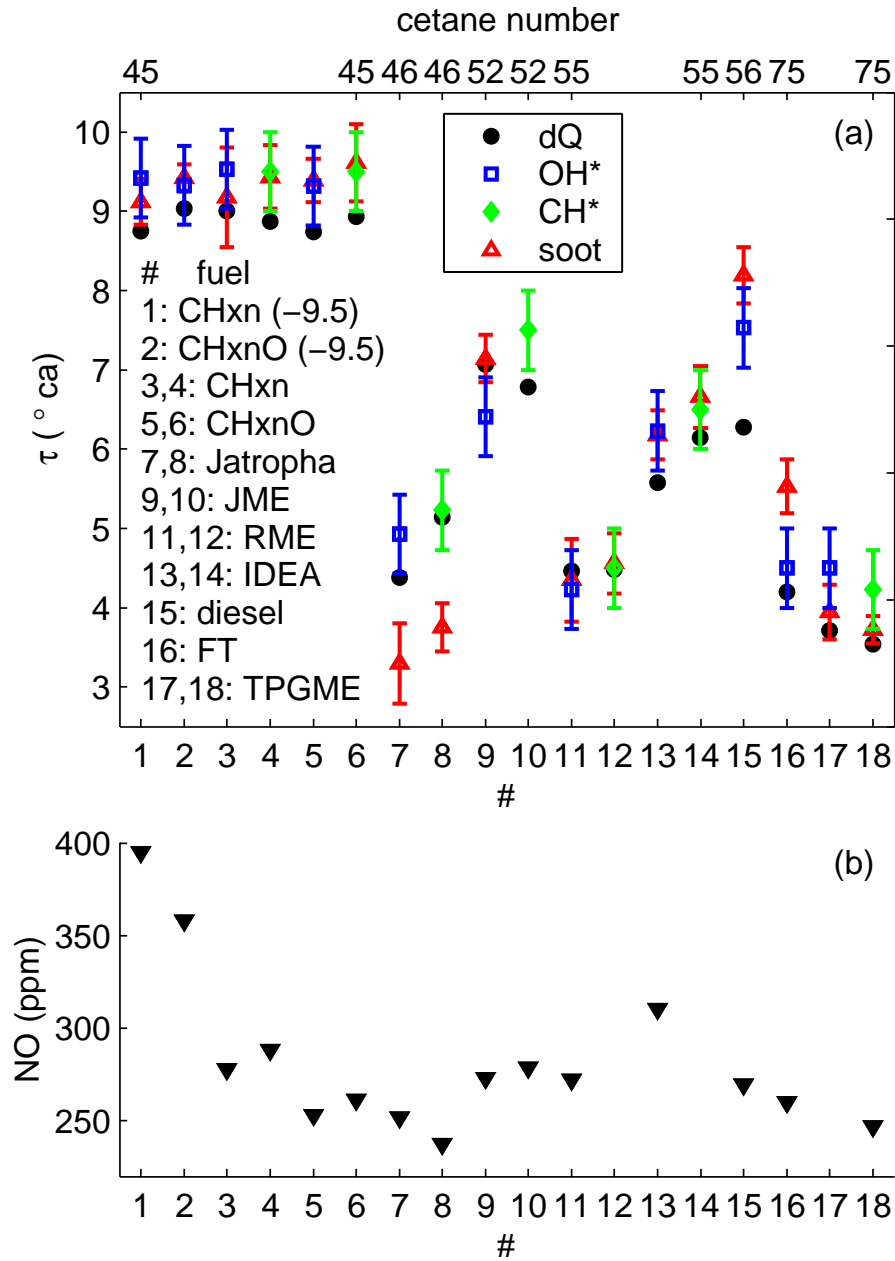


Figure 2.13: (a) Ignition delays τ_{dQ} , τ_{cl} (separately for OH* and CH*, where available) and τ_{soot} versus cetane number (shown on top axis. $\vartheta_{SoD} = -4.5^\circ$ aTDC for all runs (numbered along the lower abscissa) except for #1,2, where it is -9.5° aTDC); (b) corresponding NO concentration in the exhaust gas (uncertainty approximately symbol size).

its high viscosity [35] for pumping purposes. Heating increases its cetane number [36], and may (partly) explain its short ignition delay. Nevertheless, it is not unexpected that some fuels do not follow the general trend of lower ignition delay with higher cetane number, since it is known that the cetane number is not a very good indicator of ignition delay for fuels whose ignition characteristics depend on temperature in a different manner than primary reference fuel blends [37, 38].

For regular diesel (#15) $\tau_{dQ} < \tau_{cl} < \tau_{soot}$. For most other fuels used, these differences are much smaller or insignificant, and it also depends on the fuel in which order

heat release, chemiluminescence and soot incandescence are observed. In general, the differences are not large for a given fuel (typically $< 1^\circ\text{CA}$), and of course it should be kept in mind that τ_{cl} and τ_{soot} relate to single spray only, whereas τ_{dQ} is a global parameter. From the data presented it is clear that τ_{cl} is largely independent of the species detected, so that either OH^* or CH^* can be used as an indicator for the local start of hot combustion. From Figure 2.4 it follows that OH^* yields more signal and less background.

2.4.2 Soot location

With respect to the soot formation, significant differences between fuels can be observed in Figure 2.5. (More examples in the Supplementary material of the original article) Varying ϑ_{SoD} by $\pm 5^\circ\text{CA}$ for each fuel does not yield noticeable differences, nor is the load variation ($\leq 15\%$ from fuel to fuel) expected to contribute significantly. Ignition delay and air entrainment (which are related), however, are expected to correlate with soot incandescence.

CH_xnO has a larger τ_{dQ} (Figure 2.13) and soot is observed at a larger distance from the injector (Figure 2.10) than for the other fuels in Figure 2.5. An interpretation would be that more air entrainment results in a postponed diffusion flame, and consequently a larger SLoL. However, the SLoL may not be the best indicator for the air entrainment during the steady-state diffusion burn, prior to ignition. To exclude the effect of soot inception time, the flame lift-off length (based on OH^*) should be studied as well.

For Jatropha oil, its high viscosity (40 - 54 cP [29, 35], compared to 4.6 - 5.6 cP for its esterified counterpart JME and 3.5 - 5 cP for commercial diesel [29]) results in poor fuel atomization [36]. Combined with its relatively short ignition delay (as discussed above), this may explain why soot is observed much closer to the injector for Jatropha oil than for the other fuels (Figs. 2.5 and 2.10). Note also that the Jatropha SLoL quickly stabilizes relatively close to the injector (at about 14 mm), while for the majority of other fuels the incandescence progresses to the injector during the first few $^\circ\text{CA}$ after its initial appearance. A short ignition delay on its own is not enough for a short SLoL. For instance, the soot incandescence location of TPGME (which has a similar ignition delay as Jatropha oil, Figure 2.13) is much larger than that of Jatropha and even larger than that of JME, which has a larger ignition delay. For reasons not yet fully understood, it is believed that the dissimilarity in viscosity is at least partly responsible for the observed differences in soot location for Jatropha oil.

The large SLoL we find for regular diesel fuel is surprising, judging literature. Pickett and Siebers [39] studied different fuels in a single spray in a high pressure high temperature vessel. They found that soot incandescence stabilizes markedly closer to the injector for diesel than for some oxygenates tested, including TPGME blended with an ignition improver. Ito et al. [40] show comparable results. A possible explanation might be that our fuels contain less oxygen. More speculatively, in the bio-derived fuels the soot reduction due to oxygen may be counterbalanced by the double bonds present, which tend to enhance soot production [14].

2.4.3 Comparison of heat release, temperature and soot incandescence

Standard inlet air (21% O₂)

The general shape of the soot incandescence curves (Figs. 2.6, 2.7 and 2.14) is influenced by the amount of soot and, in a strongly non-linear way, its temperature, as discussed above. An average temperature indication can be derived from the heat release rate, but locally temperatures and hence soot incandescence may deviate appreciably. As a measure for the local peak temperature the exhaust NO concentration has been used, since in diesel combustion most NO is formed through the thermal process [26]. The expected correlation of increasing NO emission with higher flame temperatures has been verified experimentally in divided-chamber [15, 16] and direct injection diesel engines [17]. This relation is assumed to hold qualitatively for the conditions presented here as well.

The results of exhaust NO measurements, using standard inlet air with 21% O₂, are presented in Figure 2.13b. They clearly indicate that, under conditions of constant timing of the steep rise in the heat release rate, both CH_xnO and CH_xn have a much higher NO production than all other fuels tested here. A higher NO production by cyclohexanone and cyclohexane blends was also observed in Ref. [1]. Consequently, the peak temperature is expected to be higher as well during combustion of these two fuels. This is corroborated by the peak heights of the $dQ/d\vartheta$ curves of Figs. 2.6 and 2.7. Since for our experimental conditions the detected incandescence signal is estimated to scale with T^{13} (see above), the soot incandescence in the case of the cyclic fuels is expected to be strongly enhanced due to the relatively high combustion temperature, as compared to the other fuels. Yet, CH_xnO has the lowest of all soot incandescence signals presented here (and for $\vartheta_{SoD} = -4.5^\circ$ aTDC [data not shown] it is even lower), and for CH_xn the incandescence yield is merely comparable to that of the other fuels. Besides that, circumstantial evidence comes from the absence of window fouling during combustion of the cyclic fuels (section 2.3.4). The fast decrease in incandescence in comparison to the other fuels suggests that the soot that is produced, is rapidly oxidized. In conclusion, therefore, these measurements strongly indicate that CH_xnO combustion produces by far the least amount of soot from all fuels discussed here.

It may be argued that, rather than oxygen content or fuel molecular structure, the relatively large ignition delay of CH_xnO may be primarily responsible for its lower soot production, since the large ignition delay leaves more time for mixing and combustion in regions closer to stoichiometric, thus reducing soot formation. However, Boot et al. [1] compared a fuel blend of cyclohexanone with only 5% oxygen to a DBM blend containing 9% oxygen. The ignition delays (τ_{dQ}) of these two mixtures were found to be almost identical, as were their particulate matter (soot) emissions. So in that case the mixing times are equal, yet with much less oxygen incorporated, the cyclohexanone blend reaches the same soot reduction. Thus, although ignition delay may be important in soot abatement, clearly another yet undisclosed mechanism, of physical or chemical nature, is expected to be responsible for the large soot reduction capabilities of cyclohexanone blends.

In the case of TPGME and the biofuels JME, RME and Jatropha oil, the heat

release rates, soot incandescence and NO exhaust concentrations are all rather similar for normal inlet air conditions. JME shows the highest incandescence intensity. Therefore, the esterification of Jatropha seems to give rise to an elevated soot production. Indeed, esters have been reported [3] to be not so effective in soot abatement. Figure 2.10 shows that JME forms soot close to the injector. From the oxygenates, only Jatropha shows a shorter SLoL.

Regular diesel shows the highest peak luminosity (Figure 2.7b), in line with expectation. Even though CHxn has a higher luminosity than SD and IDEA, higher combustion temperatures are expected for CHxn, judging from the rate of heat release (Figure 2.7a) and the NO concentration in the exhaust gas. Thus, while the consideration of temperature makes it hard to conclude how the peak amount of soot of CHxn relates to that of the other fuels, the fast decrease in CHxn luminosity suggests that its low soot emission is due to efficient oxidation of soot, rather than due to a low soot production by itself. In comparison to the other non-oxygenated fuels tested here, this suggests that chemical structure effects alone may already be important for soot abatement.

A comparison of commercial diesel with IDEA, which is designed to have very similar heat release properties, may yield information about the role of polycyclic aromatic hydrocarbons (PAH's) in soot formation. In accordance to regulations, diesel contains a maximum of 11%_{mass} PAH (maximum 35%_{mass} aromatics in total). Of these PAH's, an undisclosed fraction is larger than two rings. IDEA, however, contains 30%_{mass} of 2-ring PAH's by design. Although $dQ/d\vartheta$ of IDEA is only marginally higher than that of diesel (Figure 2.7a), its exhaust NO concentration is significantly higher (Figure 2.13b), indicating that peak temperatures may be higher in IDEA combustion. Yet, the IDEA soot incandescence signal is much lower than that obtained with regular diesel fuel, which indicates that IDEA combustion forms less soot during combustion. From this it may be argued that larger PAH's are much more important for soot formation than 2-ring PAH's, even if the latter's density is higher (as in IDEA).

Oxygen-depleted inlet air (15% O₂)

Under EGR conditions, the low sooting tendency of CHxnO is even more distinct, as depicted in Figure 2.14b. The data presented there have been recorded with a 24 μ s exposure time. A longer exposure time was used because the quality of some images recorded with the previously used 2 μ s exposure time was poor, especially for CHxnO as a fuel. Besides, for the oxygenates at EGR conditions, the light levels are generally lower than for the normal inlet air condition. Yet, for TPGME, RME, and CHxn the luminosity is slightly underestimated, as in some images a small number of pixels was overexposed. Again, a higher combustion temperature is expected for CHxnO, judging from its rate of heat release and the exhaust-gas NO_x concentration (20 ppm rather than around 10 ppm for other fuels). Note, however, that EGR increases the ignition delay even more, so that when the soot incandescence shows up for CHxnO, the fuel injection is already over and spray conditions do not hold anymore. Therefore, it cannot be concluded directly from the higher temperature of combustion that the soot temperature is higher for CHxnO as well. Still, because the incandescence of CHxnO is that much lower in comparison to the other fuels, our measurements suggest that CHxnO increasingly suppresses soot formation with

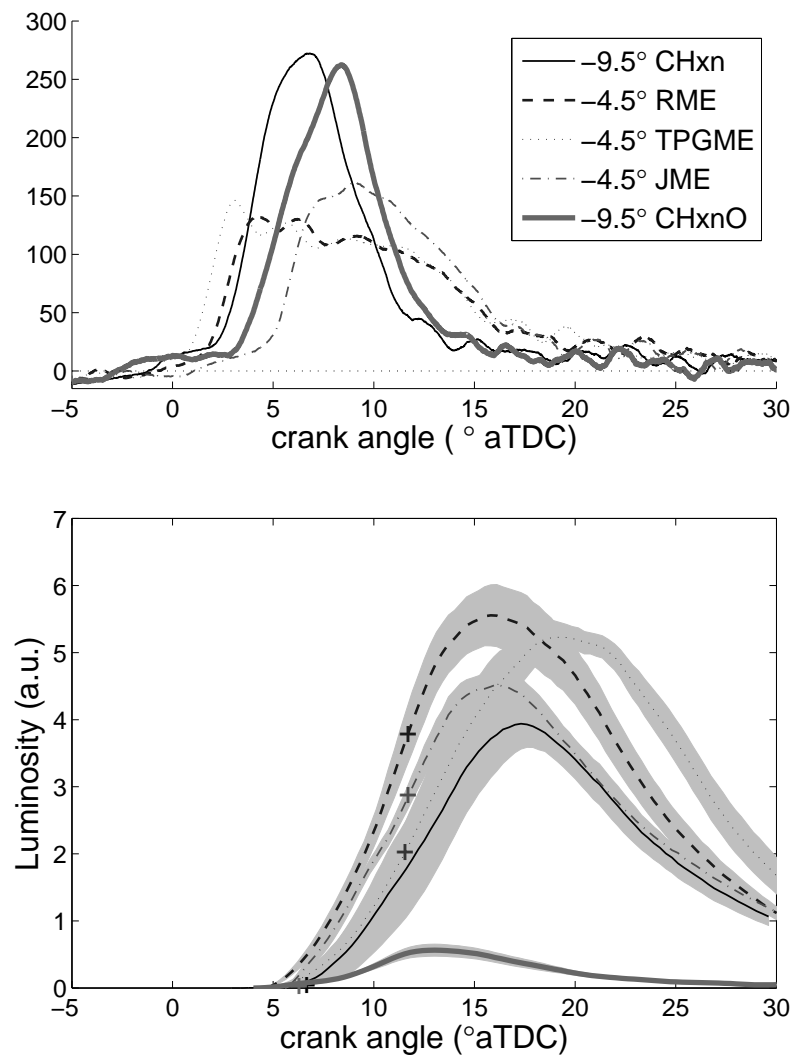


Figure 2.14: Heat release rates and soot incandescence for oxygenated fuels and CHxn at EGR conditions. (ϑ_{SoD} indicated). Shaded grey area represents standard error of phase averaging, '+' indicates the end of injection of the respective fuel.

decreasing oxygen concentration, in line with the exhaust gas measurements reported by Boot et al. [1].

At the 15% oxygen condition, it is hard to draw conclusions on CHxn in comparison to the other fuels, mainly due to the fact that the luminosity only shows up after the injection is already over. Again, the temperature effect on the luminosity is expected to be appreciable, but its evaluation is complicated for CHxn, as the injection is already over when its luminosity is around the maximum.

JME shows a slightly lower incandescence than RME. This might be attributed to the higher ignition delay of JME and the reader is advised against ascribing the lower incandescence to molecular structure effects on soot formation.

2.5 Conclusions

The sooting and chemiluminescence behavior of bio-derived, oxygenated and various reference fuels is studied in an optically accessible heavy-duty diesel engine by high-speed imaging, chemiluminescence spectroscopy and thermodynamical characterization techniques, applying standard inlet air (containing 21% O₂). The sooting behavior has also been studied under EGR-like conditions (15% O₂ in the inlet air). Ignition delays have been determined on the basis of first appearance of OH* chemiluminescence, CH* chemiluminescence, soot incandescence, and the heat release rate. Soot incandescence images are recorded every 0.3° CA. Since the incandescence intensity is estimated to scale with a large power of the temperature (T^{13} for our experimental conditions) we have used measured exhaust NO concentrations as indicator of peak combustion temperatures.

Jatropha oil combustion behaves markedly different from the other fuels, in that soot forms leeward of the liquid spray, whereas for most other fuels soot is first observed further downstream near the spray tips. From the combined luminosity and NO data it may be concluded that the cyclic additives cyclohexane and especially cyclohexanone are more efficient in soot abatement than the other fuels tested. For cyclohexanone, this behavior is even more pronounced under EGR-like conditions. These two cyclic fuels are also more efficient in reducing soot emissions than esterified fuels like JME and RME, in line with literature ([3] and references therein). On the basis of our results, we attribute the low smoke emissions measured in Ref. [1] under EGR conditions to reduced soot formation during combustion, rather than to improved burnout of soot formed in the initial diffusion flame.

Comparison of the results for IDEA and diesel indicates that 2-ring PAH's are less important for the fuel sooting propensity than larger PAH's. Under normal inlet air conditions, combustion of esterified Jatropha (JME) produces more soot than combustion of Jatropha oil itself.

Bibliography

- [1] M.D. Boot, P.J.M. Frijters, R.J.H. Klein-Douwel, and R.S.G. Baert. Oxygenated fuel composition impact on heavy-duty diesel engine emissions. *SAE Paper*, 2007-01-2018, 2007.
- [2] E.L.M. Rabé. Jatropha oil in compression ignition engines. Technical report, Eindhoven University of Technology, 2006. Graduation thesis.
- [3] C.K. Westbrook, W.J. Pitz, and H.J. Curran. Chemical kinetic modeling study of the effects of oxygenated hydrocarbons on soot emissions from diesel engines. *J. Phys. Chem. A*, 110:6912 – 6922, 2006.
- [4] P.J.M. Frijters and R.S.G. Baert. Oxygenated fuels for clean heavy-duty diesel engines. *Int. J. of Vehicle Design*, 41:242 – 255, 2006.
- [5] C.J. Mueller, W.J. Pitz, L.M. Pickett, G.C. Martin, D.L. Siebers, and C.K. Westbrook. Effects of oxygenates on soot processes in di diesel engines: Experiments and numerical simulations. *SAE Paper*, 2003-01-1791, 2003.

-
- [6] N. Miyamoto, H. Ogawa, N.M. Nurun, K. Obata, and T. Arima. Smokeless, low nox, high thermal efficiency, and low noise diesel combustion with oxygenated agents as main fuel. *SAE Paper*, 980506, 1998.
- [7] N. Miyamoto, H. Ogawa, T. Arima, and K. Miyakawa. Improvement of diesel combustion and emissions with addition of various oxygenated agents to diesel fuels. *SAE Paper*, 962115, 1996.
- [8] B.E. Hallgren and J.B. Heywood. Effects of oxygenated fuels on di diesel combustion and emissions. *SAE Paper*, 2001-01-0648, 2001.
- [9] M. Natarajan, E.A. Frame, D.W. Naegeli, T. Asmus, W. Clark, W. Garbak, M.A. González-D, E. Liney, W. Piel, and J.P. Wallace. Oxygenates screening for advanced petroleum-based diesel fuels: Part 1. screening and selection methodology for the oxygenates. *SAE Paper*, 2001-01-3631, 2001.
- [10] M.A. González-D, W. Piel, T. Asmus, W. Clark, J. Garbak, E. Liney, M. Natarajan, D.W. Naegeli, D. Yost, E.A. Frame, and J.P. Wallace. Oxygenates screening for advanced petroleum-based diesel fuels: Part 2. the effect of oxygenate blending compounds on exhaust emissions. *SAE Paper*, 2001-01-3632, 2001.
- [11] C.J. Mueller and G.C. Martin. Effects of oxygenated compounds on combustion and soot evolution in a di diesel engine: Broadband natural luminosity imaging. *SAE Paper*, 2002-01-1631, 2002.
- [12] R.L. Vander Wal and A.J. Tomasek. Soot nanostructure: dependence upon synthesis conditions. *Combust. Flame*, 136:129 – 140, 2004.
- [13] R.L. Vander Wal and A.J. Tomasek. Soot oxidation: dependence upon initial nanostructure. *Combust. Flame*, 134:1 – 9, 2003.
- [14] D.R. Tree and K.I. Svensson. Soot processes in compression ignition engines. *Progr. Energy Combust. Sci.*, 33:272 – 309, 2007.
- [15] S.L. Plee, T. Ahmad, J.P. Myers, and G.M. Faeth. Diesel NOx emissions - a simple correlation technique for intake air effects. *Proc. Combust. Inst.*, 19:1495 – 1502, 1982.
- [16] K.J. Wu and R.C. Peterson. Effects of flame temperature and burning rate on nitric oxide emission from a divided-chamber diesel engine. *Proc. Combust. Inst.*, 21:1149 – 1157, 1986.
- [17] T. Ahmad and S.L. Plee. Application of flame temperature correlations to emissions from a direct-injection diesel engine. *SAE Paper*, 831734, 1983.
- [18] J.E. Dec and C. Espey. Chemiluminescence imaging of autoignition in a DI diesel engine. *SAE Paper*, 982685, 1998.
- [19] J.E. Dec and P.L. Kelly-Zion. The effects of injection timing and diluent addition on late-combustion soot burnout in a DI diesel engine based on simultaneous 2-d imaging of OH and soot. *SAE Paper*, 2000-01-0238, 2000.

- [20] B. Higgins and D. Siebers. Measurement of the flame lift-off location on DI diesel sprays using OH chemiluminescence. *SAE Paper*, 2001-01-0918, 2001.
- [21] C.F. Edwards, D.L. Siebers, and D.H. Hoskin. A study of the autoignition process of a diesel spray via high speed visualization. *SAE Paper*, 920108, 1992.
- [22] C. Espey and J.E. Dec. Diesel engine combustion studies in a newly designed optical-access engine using high-speed visualization and 2-d laser imaging. *SAE Paper*, 930971, 1993.
- [23] K. Verbiezen, R.J.H. Klein-Douwel, A.P. van Vliet, A.J. Donkerbroek, W.L. Meerts, N.J. Dam, and J.J. Ter Meulen. Quantitative laser-induced fluorescence measurements of nitric oxide in a heavy-duty Diesel engine. *Proc. Combust. Inst.*, 31:765 – 773, 2007.
- [24] K. Verbiezen. *Quantitative NO measurements in a Diesel engine*. PhD thesis, Radboud University Nijmegen, 2007. URL http://webdoc.uhn.ru.nl/mono/v/verbiezen_k/quannomei.pdf.
- [25] X.L.J. Seykens, L.M.T. Somers, and R.S.G. Baert. Detailed modeling of common rail fuel injection process. *Mecca, J. of Middle European Construction and Design of Cars*, III:30 – 40, 2005.
- [26] K. Verbiezen, A.J. Donkerbroek, R.J.H. Klein-Douwel, A.P. van Vliet, P.J.M. Frijters, X.L.J. Seykens, R.S.G. Baert, W.L. Meerts, N.J. Dam, and J.J. Ter Meulen. Diesel combustion: In-cylinder NO concentrations in relation to injection timing. *Combust. Flame*, 151:333 – 346, 2007.
- [27] J.T. Farrell, N.P. Cernansky, F.L. Dryer, D.G. Friend, C.A. Hergart, C.K. Law, R. McDavid, C.J. Mueller, and H. Pitsch. Development of an experimental database and kinetic models for surrogate diesel fuels. *SAE Paper*, 2007-01-0201, 2007.
- [28] A.S. Ramadhas, S. Jayaraj, and C. Muraleedharan. Use of vegetable oils as I.C. engine fuels - a review. *Renewable Energy*, 29:727 – 742, 2004.
- [29] W.M.J. Achten, L. Verchot, Y.J. Franken, E. Mathijs, V.P. Singh, R. Aerts, and B. Muys. Jatropha bio-diesel production and use. *Biomass & Bioenergy*, :1064 – 1084, 2008.
- [30] A. Tsolakis and A. Megaritis. Exhaust gas assisted reforming of rapeseed methyl ester for reduced exhaust emissions of CI engines. *Biomass & Bioenergy*, 27:493 – 505, 2004.
- [31] A. Tsolakis, A. Megaritis, and D. Yap. Application of exhaust gas fuel reforming in diesel and homogeneous charge compression ignition (HCCI) engines fuelled with biofuels. *Energy*, (in press):, 2007. doi: 10.1016/j.energy.2007.09.011.

-
- [32] J.H. Van Gerpen. Cetane number testing of biodiesel. In J.S. Cundiff, E.E. Gavett, C. Hansen, C. Peterson, M.A. Sanderson, H. Shapouri, and D.L. Vandyne, editors, *Proceedings, Third Liquid Fuel Conference: Liquid Fuel and Industrial Products from Renewable Resources*, pages 197 – 206, St. Joseph, MI (USA), 1996. American Society of Agricultural Engineers. paper 22-15.
- [33] C. Schulz, B. Kock, M. Hofmann, H. Michelsen, S. Will, B. Bougie, R. Suntz, and G. Smallwood. Laser-induced incandescence: Recent trends and current questions. *Appl. Phys. B*, 83:333 – 354, 2006.
- [34] B. Bougie, L.C. Ganippa, A.P. van Vliet, W.L. Meerts, N.J. Dam, and J.J. Ter Meulen. Soot particulate size characterization in a heavy-duty diesel engine for different engine loads by laser-induced incandescence. *Proc. Combust. Inst.*, 31:685 – 691, 2007.
- [35] D. Agarwal and A.K. Agarwal. Performance and emissions characteristics of jatropha oil (preheated and blends) in a direct injection compression ignition engine. *Appl. Thermal Engineering*, 27:2314 – 2323, 2007.
- [36] O.M.I. Nwafor. Emission characteristics of diesel engine running on vegetable oil with elevated fuel inlet temperature. *Biomass & Bioenergy*, 27:507 – 511, 2004.
- [37] D.L. Siebers. Ignition delay characteristics of alternative diesel fuels: implications on cetane number. *SAE Paper*, 852102, 1985.
- [38] R.E. Canaan, J.E. Dec, R.M. Green, and D.T. Daly. The influence of fuel volatility on the liquid-phase fuel penetration in a heavy-duty DI diesel engine. *SAE Paper*, 980510, 1998.
- [39] L.M. Pickett and D.L. Siebers. Fuel effects on soot processes of fuel jets at DI diesel conditions. *SAE Paper*, 2003-01-3080, 2003.
- [40] T. Ito, T. Kitamura, M. Ueda, T. Matsumoto, J. Senda, and H. Fujimoto. Effects of flame lift-off and flame temperature on soot formation in oxygenated fuel sprays. *SAE Paper*, 2003-01-0073, 2003.

Molecular Shape or Cetane Number?

Combustion behavior of various oxygenated fuels has been studied in a DAF heavy-duty (HD) direct-injection (DI) diesel engine. From these fuels, it is well-known that they lead to lower particle (PM) emissions; however, for a given fuel oxygen mass fraction, there are significant differences in PM reduction. Although this can be traced back to the specific molecular structure of the oxygenate in question, no consensus can be found in the literature as to the explanation hereof. In this study, the sooting tendency (smoke number) of three oxygenates [viz. tri propylene glycol methyl ether (TP), dibutyl maleate (DB), and cyclohexanone (X1)] was compared to that of commercial diesel fuel (EN590, D). The results suggest that the cetane number (CN) (i.e. fuel reactivity) may play an important role. More specifically, the low reactive oxygenate X1, with its cyclic carbon chain, was found to perform exceptionally well compared to the more reactive linear and branched oxygenates DB and TP, respectively. Cyclic oxygenates are abundant in nature. Cellulose, the most common organic compound on earth, is the best-known example. Although it is not trivial, liquid cyclic oxygenates can be made from lignocellulosic biomass. Particularly, the production of C6 oxygenates (e.g. guaiacol, cyclohexanone, phenol, etc.), which can be derived from lignin, is the subject of current investigation. Fuels produced from such biomass (e.g. plant waste or the nonedible part of plants) are referred to as second-generation biofuels and are expected to play a pivotal role in the near future.

The content of this Chapter has been taken from:

M.D. Boot, P.J.M. Frijters, C.C.M. Luijten, L.M.T. Somers, R.S.G. Baert, A.J. Donkerbroek, R.J.H. Klein-Douwel, N.J. Dam. Cyclic oxygenates: A new class of second generation biofuels for Diesel engines?. *Energy and Fuels*, 23(4): 1808-1817, 2009.

Minor edits have been made to streamline the layout of the thesis chapters. The contribution of the author is related to the motivation and selection of the "X"-fuels and relevant operating conditions, along with the results, discussion and conclusions thereof. The contribution also includes the literature review. The introduction and overall discussion and conclusions were realized in a joint effort. Experiments were carried out in the engine lab of the Eindhoven University of Technology.

3.1 Introduction

For the heavy-duty (HD) diesel industry, it is very difficult to keep up fuel economy while still complying with legislated soot (PM) and nitric oxide (NO_x) targets. Measures needed to meet future (EPA 10 or EURO 6) emission legislation call for combined measures, such as after treatment (particle filters, de-NO_x catalysts, etc.) and/or exhaust gas recirculation (EGR). Both measures, however, increase pumping losses and therefore lead to lower engine efficiency.

Also, a non-optimal (e.g. retarded) combustion phasing will most likely be needed, which, although favorable to reduce engine-out NO_x emissions, lowers the thermodynamic efficiency of the engine even further. On the long term (beyond 2015), this methodology will be unfavorable because the industry will face stringent CO₂ legislation as well.

Alternative pathways are still using conventional CI engines but using an oxygenated fuel or even choosing more revolutionary approaches, such as premixed charge compression ignition (PCCI), at modest engine loads. This study will focus on oxygenated fuels used in a conventional HD diesel engine, more specifically, on the impact of oxygenate cetane number (CN) (i.e. reactivity) on the PM performance.

It is the aim of the authors to provide the reader with an overview of the literature that deals with the impact of (oxygenated) fuel reactivity (CN) on the soot formation process. In addition, the authors will present their own work dedicated specifically to this topic.

The dependency of soot formation on CN is important because legislators worldwide are pressing for a minimum CN (i.e. ~ 50) for biofuels. Although first-generation biofuels (vegetable oils or their esterified counterparts) are generally in compliance with such legislation, second-generation biofuels, produced from lignocellulosic feedstock will most likely fall short of the minimum CN.

The reason why this will be the case becomes clear when one considers the molecular structure of the feedstock. First-generation biofeedstock typically comprises monomers of long-chained molecules, which intrinsically have relatively high CN (i.e. > 50). Conversely, molecules that constitute the second-generation biofeedstock are inherently polymers of a cyclic nature.

As will be demonstrated later in the paper, these polymers are built up exclusively from C4-6 cyclic oxygenates, which are linked together via C-O-C bonds. When the polymer is broken up and treated catalytically, cyclic C4-6 oxygenates can be produced, which typically have a very low reactivity (CN $\sim 5-20$). In this study, one such oxygenate, cyclohexanone (X1; CN $\sim 10-15$), will be compared to conventional (i.e., noncyclic, fossil-based oxygenates) in a 9.2 L DAF HD DI diesel engine under various operation conditions. Particularly, the effect of a low CN on smoke opacity and NO_x emissions is of interest. Note that in Chapter 2 the cyclohexanone blend with synthetic diesel is denoted by 'CH_xnO' Chapter 2.

3.2 Impact of fuel reactivity on sooting tendency: a literature review

There is no consensus in the reviewed literature surrounding the influence of fuel CN on soot emissions. Two trends can be distinguished in the literature: (1) a higher CN leads to less soot [1–4] and (2) a higher CN leads to more soot [5–8]. To comprehend why two distinct trends are measured, one must discern how the variation in CN was achieved in the experiments. Three main approaches have been identified: (1) variation of aromatic content [1–5], (2) use of CN boosters [6, 7, 9, 10], and (3) comparison of fuels with equal aromaticity but with a different CN [8, 11, 12].

3.2.1 Aromatics

Karonis et al. [1] measured the emitted PM mass from 68 diesel fuels in a single-cylinder diesel engine. The CN range in question was 42–58. The CN correlated well with the aromatic content, with the CN rising as the total aromatic fraction of the fuel decreased. A near linear decrease of PM mass with increasing CN (i.e., decreasing aromatic content) was reported.

Zannis and Hountalas [2] used a single-cylinder Lister LV1 experimental DI diesel engine to compare the smoke opacity of three diesel fuels with a spread in CN from 60 to 64. The variation in CN was attributed to the difference in aromatic content. Smoke opacity was seen to decrease with increasing CN.

Wu et al. [3] added synthetic diesel fuel to commercial diesel fuel at fractions ranging from 0 to 100 vol-%. As more purely paraffinic, high CN synthetic fuel was introduced, the aromatic content of the blend decreased, resulting in the gradual rising of the CN from 52 to 75. Smoke opacity, measured from a HD turbo-charged DI diesel engine, decreased with increasing CN (i.e., increasing fraction of synthetic fuel).

Bielaczyc et al. [4] tested four specially prepared diesel fuels with varying CN (range of 45–63) in a 2.0 L DI turbo-charged common rail diesel engine. The variation in CN is ascribed to the aromatic content. A general trend observed was that the emitted particle mass decreased with increasing CN.

Most authors recognize the conflicting effects that aromatics have on the soot formation process. On the one hand, aromatics are known soot precursors. Moreover, because the formation of the first aromatic ring is generally considered to be the rate-determining step in the formation process, aromatics already present in the fuel have a significant impact on the sooting tendency.

On the other hand, because aromatics are intrinsically relatively inert, the CN of a fuel will decrease with increasing aromatic content. Consequently, longer ignition delays can be expected, and the non-sooting premixed burning period becomes more dominant. Ultimately, however, the former mechanism outweighs the latter, and higher soot emissions are generally observed as the degree of aromaticity is increased.

A notable exception to the trend discussed above can be expected when a high aromaticity coincides with a very low CN. Kalghatgi et al. [5] demonstrated that a DI diesel engine fueled with gasoline (CN \sim 10) can run virtually soot-free in a wide range of operating conditions. The low soot emissions were ascribed to a nearly fully premixed combustion, which was the result of the long incurred ignition delays. It should be noted that low soot was achieved only when the incurred ignition

delay was sufficiently long to completely separate the injection and heat-release event. Accordingly, a form of fuel-induced PCCI is realized.

3.2.2 CN Boosters

Lü et al. [9] studied the effect of a CN booster on the sooting tendency (i.e. smoke opacity) of fuels tested in a high-speed DI diesel engine. In all cases, an increased CN booster concentration led to an increase in smoke opacity.

Ladommatos et al. [6] investigated the effect of fuel CN improver on diesel pollutant emissions on a single-cylinder ASTM co-operative research engine with IDI. The CN booster was added in various concentrations to a base fuel, resulting in a CN spread from 40 to 62. Increased smoke opacity was observed as more CN booster was added.

In another study by Lü et al. [7], the effect of the CN improver on the heat-release rate and emissions was investigated on a high-speed DI diesel engine. The CN booster was added to an ethanol-diesel blend at various concentrations. Measured smoke opacity increased as more CN booster was added to the oxygenated blend.

Schultz et al. [10] studied the influence of the CN booster concentration (isopropyl-nitrate) on a one-cylinder engine dedicated for CN testing. CN in this study ranged from 50 to 64, and the measured particle mass increased as more CN improver was added.

In all reviewed literature, the use of a CN booster had a negative impact on soot emission, regardless of the engine type, operating conditions, or base fuel specifications. Most authors attribute this result to a reduction in non-sooting premixed burn duration as a result of shorter ignition delays.

3.2.3 Equal aromaticity but different CN

Apart from varying the aromatic fraction or introducing a CN booster, one can compare the soot performance of fuels with equal aromatic content but with a different CN. For a given class of saturated hydrocarbons (e.g. n-, iso-, and cyclo-paraffins), CN mainly depends upon the carbon number or molecular weight, with heavier molecules having consistently higher CN.

When saturated classes at a given carbon number are compared, the fuel that is the most compact will generally have the lowest CN. Accordingly, the CN will decrease in the order n- f iso- f cyclo-paraffin. For example, the CN of a given straight hydrocarbon (n-hexane) can be reduced from 42-45 to 23-34 by introducing branching (3-methyl-pentane) and further down to 13-18 by cyclization (cyclohexane).

Alternatively, one can increase the CN of hexane to 52-56 or 64-65 by elongating the chain with one (n-heptane) or two (n-octane) carbon atoms, respectively. In all cases, the molecules are not considered soot precursors, but the variation in CN will have a significant effect on the yielded soot emissions.

Svensson et al. [11] investigated the impact of hydrocarbon molecular structure on soot production (via line-of-sight extinction) of a reacting fuel spray in a constant volume combustion vessel. A comparison between n-heptane and n-undecane was made, with the former and latter species having a CN of 53-56 and 79-83, respectively.

A higher soot concentration was observed for n-undecane, which was credited to a shorter ignition delay and less dominant non-sooting premixed burn period.

n-Heptane was subsequently compared to toluene, an aromatic molecule with a significantly lower CN of approximately 5-10. Toluene yielded a significantly higher soot concentration, which was attributed to the fact that toluene, being an aromatic, can be considered a soot precursor. The authors conclude with the remark that, depending upon how a change in CN is realized, it can have either a positive or negative impact on soot concentration.

In an earlier study [12], the low CN hydrocarbon cyclohexane (CN \sim 10) was blended to commercial diesel fuel (CN \sim 55) and subjected to a series of engine experiments in a DAF HD DI diesel engine. The authors reported a significant reduction in smoke opacity compared to the neat base fuel. In related work by Klein-Douwel et al. [8], cyclohexane was blended to a high CN (\sim 75) synthetic diesel fuel. The soot luminosity resulting from combustion of the blend (CN \sim 45) in a DAF HD DI diesel engine was compared to that of neat synthetic fuel. A clear decrease in soot luminosity was observed as a result of cyclohexane addition.

Further insight into the influence of fuel CN on soot formation is provided by Pickett et al. [13]. In their experiments, the soot formation process was observed in an optically accessible constant volume combustion chamber via laser extinction and planar laser-induced incandescence. By studying a quasi-steady fuel jet, the aforementioned beneficial impact of a long ignition delay is no longer of significance. Nevertheless, a correlation between the fuel CN and sooting tendency was still found. In general, lower CN fuels produced less soot. The authors attributed this trend to the apparent relation between fuel reactivity (i.e. CN) and flame-lift-off-length (FLOL). According to the authors, a longer FLOL will yield a more favorable equivalence ratio in the soot synthesis zone, which lies downstream of the FLOL. Lower CN fuels yield longer FLOL, which in turn manifested in less soot being produced.

3.2.4 Overview

Aromatics generally lead to a lower CN and increased soot emissions. In other words, when the CN of fuel is increased by removing soot precursors, this will have a beneficial impact on soot. Nevertheless, it should be noted that, when a high aromaticity coincides with a very low CN, the resulting prolonged ignition delays are likely to lead to low soot emissions. This appears only to be the case when the fuel injection process and heat-release event are completely separated, effectively creating a form of PCCI combustion [5].

In the reviewed literature, CN boosters lead to a higher CN and increased soot emissions. Most authors attribute this trend to a smaller fraction of fuel that is consumed in the non-sooting premixed burn period.

A comparison of fuels with an equal aromaticity but with a different CN will typically show a trend wherein the higher CN fuels lead to higher soot emissions. It is believed that this trend can be credited to a smaller fraction of fuel, which is consumed in the non-sooting premixed burn period.

A correlation appears to exist between fuel reactivity (i.e. CN) and FLOL. In general, the lower the CN, the longer the FLOL, the more favorable the equivalence ratio in the particle synthesis zone, and ultimately, the lower the soot production. Although

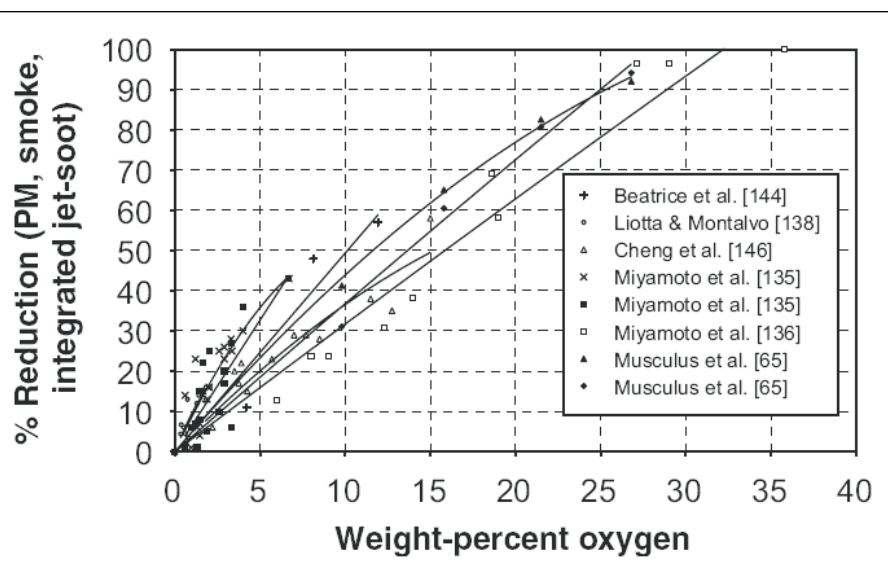


Figure 3.1: Soot reduction versus fuel oxygen: a literature review. NB references in the legend correspond to those used in the original publication [14].

this relation seems intuitively correct, it should be noted that more research in this particular area is still needed to further substantiate the aforementioned correlation.

3.3 Impact of fuel oxygen on sooting tendency: a literature review

Over the past 15 years, a large number of studies have demonstrated that blending oxygenated hydrocarbons with diesel can be a very effective route for PM reduction. A wide variety of such oxygenates have been tested, and the results have been described in a large number of publications. Only a few of them will be referred to here.

3.3.1 Fuel oxygen concentration

In the majority of these, a strong relation was found between fuel oxygen content and the amount of PM produced [8, 12, 14–25].

Tree and Svensson [14] for example collected data on this dependency for 21 oxygenates from a large number of independent studies (Figure 3.1). Soot-free combustion is typically observed, regardless of oxygenate structure, when the fuel oxygen concentration is between 30 and 40 wt-%. From this data, it can be concluded however that, a general trend notwithstanding, fuel oxygen content alone cannot account for the observed reduction in PM.

It is clear from this figure that, for a given fuel oxygen mass fraction, there are indeed significant differences in PM reduction. Although this can be traced back to the specific molecular structure of the oxygenates in question, no consensus can be found in the literature as to the explanation hereof. There is some indication,

however, that oxygenate effectiveness is linked to the distribution of oxygen atoms in the oxygenated molecules.

3.3.2 Oxygenate effectiveness

The beneficial impact of fuel oxygen on particulate emissions is often credited to enhanced trapping or sequestering of fuel carbon into non-sooting species (e.g. partially oxidized C1-C2 hydrocarbons). In other words, by means of already chemically bonding oxygen to carbon in the fuel, fewer carbon atoms are available to mature into (potential) soot precursors (e.g. ethylene, acetylene). At a fixed fuel-oxygen level, however, carbon sequestration was often found to depend heavily upon the type of functional oxygen group(s) (e.g. alcohols, ethers, and esters) involved.

In many studies, oxygenates in which each oxygen atom is connected to two carbon atoms tend to yield the lowest soot emissions [15–20]. One can imagine that, in alternative distributions, an oxygen atom may trap only one (C=O) or one-half (O-C-O) of a carbon atom instead of up to two (C-O-C) carbon atoms in the preferred embodiment.

Oxygenate classes that are in accordance with the optimal sequestering configuration are ethers. Many authors who investigated the impact of oxygenate molecular structure on sooting tendency report that ethers are the most effective. Herein, tripropylene glycol methyl ether (TP) and glycol ethers (also known as glymes) are named as being particularly effective at reducing soot emissions [15–20].

Conversely, there are studies that show classes other than (glycol) ethers (i.e., classes with lower expected sequestering efficiencies) to be the most effective [8, 12, 21, 22].

Stoner and Litzinger [21] for example reported that, in an optically accessible DI diesel engine, in-cylinder soot concentrations (measured via laser light extinction) were lower for maleates (i.e., esters; O-C=O) than was the case for glycol ethers.

An earlier in-house study [12] conclude that, in a DAF HD DI diesel engine, regardless of engine operating conditions, a cyclic ketone (cyclohexanone; C=O) leads to lower smoke opacities than both glymes and ethers even though the fuel oxygen concentration was kept constant.

In a related study by Klein-Douwel et al. [8], cyclohexanone was blended to a synthetic diesel fuel. The soot luminosity resulting from combustion of the blend in a DAF HD DI diesel engine was compared to that of an ether (TP) blend with the same synthetic fuel. The authors report significantly lower soot luminosity for the cyclohexanone blend, a constant fuel oxygen content notwithstanding.

Ren et al. [22] studied the combustion and emissions of a DI diesel engine fueled with various diesel-oxygenate blends. Low CN oxygenates (for example, ethanol) performed better with respect to smoke opacity than high CN fuels (for example, diglyme).

3.3.3 Combination of fuel oxygen and EGR

Although soot emissions attenuate strongly with the introduction of fuel oxygen, NO_x emissions are typically left little affected by the use of oxygenates. An exception to this observation can be found when the range of CN of investigated oxygenated blends

is relatively large [8, 12]. It has been proposed by many authors to combine the use of oxygenates with EGR [12, 18, 23, 24, 26]. Accordingly, soot and NO_x can be addressed simultaneously. The negative effect of lower flame temperature (via EGR) on soot oxidation is (partially) countered by the enhanced suppression of particle formation (via fuel oxygen).

Murayama et al. [23] studied the combined use of EGR and oxygenated fuel (dimethyl carbonate) on smoke opacity in a low-emission DI diesel engine. The authors conclude that the expected sharp rise of smoke opacity, typically observed when using EGR to reduce NO_x, can be partially countered by the simultaneous use of fuel oxygen.

Song et al. [24] examined the effect of oxygenated fuel (e.g., glycol ethers) on the combustion and emissions in a light-duty turbocharged DI diesel engine. At low load, the combination of high levels of EGR and fuel oxygen leads to a concurrent decline in both particle mass and nitric oxide emissions. The authors attributed these findings to suppression of soot precursors and a reduction of the flame temperature, respectively.

In a similar study performed by Bertoli et al. [26], the influence of fuel oxygenation and EGR on engine-out emissions was investigated on a single-cylinder DI diesel engine. Pertaining to the combined use of EGR and oxygenation, a simultaneous reduction of particle mass and nitric oxides is reported. In addition, the authors conclude that fuel composition becomes less important at high EGR levels (30 wt-%) and is negligible at 45 wt-%.

The favorable impact of the combination of EGR and oxygenates on emissions has also been observed by Miyamoto et al. [18]. In the used single-cylinder DI diesel engine, the smoke increase because of EGR is significantly suppressed by the presence of fuel oxygen.

Boot et al. [12] examined the influence of oxygenated fuel and the use of EGR on the sooting tendency of the combustion process on a HD DI diesel engine. The authors reported that the adverse smoke-NO_x tradeoff typically observed when implementing an EGR circuit is improved when oxygenates are blended to commercial diesel fuel.

3.3.4 Overview

In general, soot emissions tend to drop more or less linearly with the amount of oxygen present in the fuel. Near zero-soot operation is found in several studies when the fuel oxygen is in excess of 30-40 wt-%.

In all reviewed literature, differences in soot performance are observed between various oxygenates with a constant fuel oxygen content.

Many authors believe the soot performance of an oxygenate at a given fuel oxygen content is affected by the (qualitatively estimated) carbon sequestering efficiency [15–20]. In general, oxygenates in which the individual oxygen atoms are connected to two carbon atoms [e.g., (glycol) ethers], the optimal configuration with respect to sequestering potential, tend to yield the lowest soot emissions.

In general, the negative impact of EGR on soot emissions can be at least partially countered by the simultaneous use of oxygenated fuels.

No clear correlation between oxygenate CN and soot emissions could be found in the reviewed literature. A general observation that can be made when studying the

seemingly conflicting literature, a few exceptions notwithstanding, is that, when the spread in CN is relatively low, the oxygenate with the better (expected) sequestering efficiency [e.g., (glycol) ethers] will produce the least soot. Alternatively, when the range of investigated CN is wider, soot emissions tend to decrease with a decreasing CN. This positive correlation between low CN and soot is likely linked to a higher premixed burnt fraction and/or a longer FLOL (see the Overview of the previous section).

As discussed earlier, results of Pickett et al. [13] suggest that, for given operating conditions, the FLOL is a function of mainly the CN. Conversely, the oxygen content of the fuel does not appear to be of importance in this respect. For a given FLOL, however, the presence of fuel oxygen will naturally lower the equivalence ratio in the flame, effectively shifting it into a more favorable region in the well-known temperature (T)-equivalence ratio (ϕ) map. Considering the fact that oxygenates, such as glymes, which have a considerably higher CN than diesel fuel, can still lead to significantly lower soot emissions, it is plausible that the presence of fuel oxygen outweighs the negative effect of a lower degree of mixing, because of both the (expected) shorter FLOL and shorter ignition delay. According to this theorem, low CN oxygenates should therefore hold an advantage over their high CN counterparts via enhanced mixing as a result of both the extended ignition delay and longer FLOL. The main objective of this and ongoing work is to test this hypothesis.

3.4 Experimental setup and test procedure

For the engine tests, a modified Euro-3 DAF PE235C HD DI diesel engine was used. Specifications of the engine and a schematic representation of the engine can be found in Table 3.1 and Figure 3.2, respectively.

Table 3.1: Test engine specifications.

Bore / Stroke	mm	118 / 140
No. of Cylinders	-	6
CR	-	16
FIE	-	PLD (Pump Line Nozzle)
Turbocharger	-	Yes, VNT
Charge Cooling	-	Air-to-water
EGR	-	Yes, with cDPF
Max. Power	kW	235 (2100 RPM)
Max. Torque	Nm	1325 Nm (1500 RPM)
Oxidation Catalyst	-	Yes
Emission Norm	-	Euro 3

This 9.2 L engine has an electronically controlled unit pump- type fuel injection system, capable of delivering over 1400 bar injection pressure. This engine was redesigned for lower engine- out emissions (Euro-4) on regular diesel fuel. To this end, an external EGR system was implemented (Figure 3.2). In the EGR circuit, a catalytic diesel particulate filter (cDPF) was mounted.

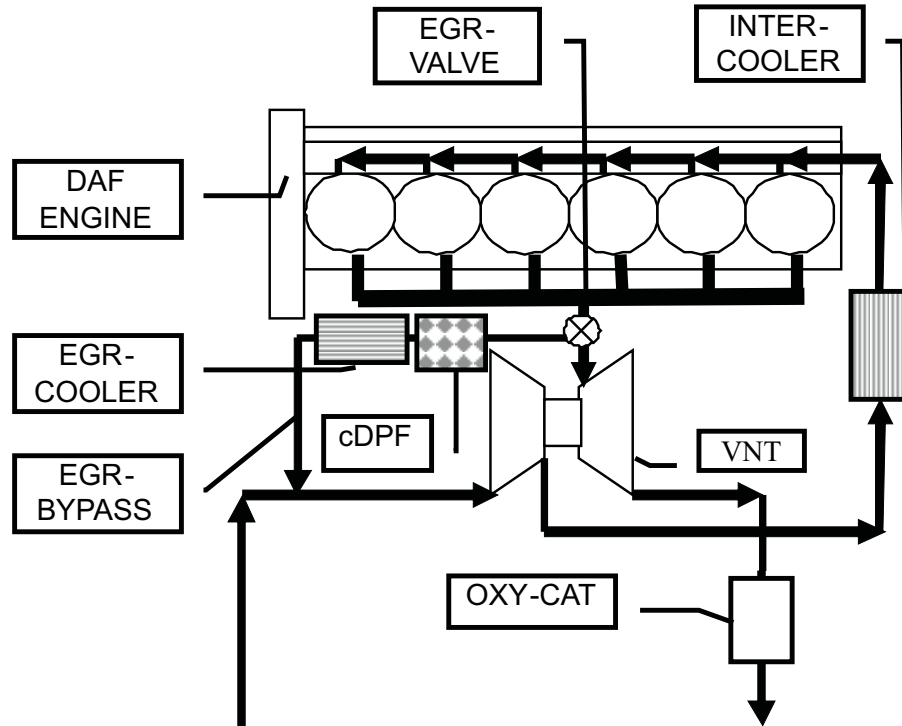


Figure 3.2: Test engine lay-out; details of EGR system and aftertreatment; standard air-to-air charge cooling replaced with air-to-water cooling (see Chapter 1).

Downstream, in the exhaust circuit, a diesel oxidation catalyst (DOC) was installed to be able to measure dry PM (i.e., smoke opacity) emissions. To optimize (within limits) the air-to-fuel ratio (AFR) for a given amount of EGR or NO_x level, the fixed geometry turbocharger was replaced by a variable nozzle turbine (VNT) turbocharger. Note that standard air-to-air charge air cooling (CAC) has been replaced with air-to-water cooling.

Engine torque and speed were kept constant when switching between fuels, mimicking the drivers desire for constant vehicle performance independent of fuel quality. In addition, the standard fuel injection equipment (FIE) was not modified. Taking into account that the FIE of the test engine was cam-driven and the relatively low heating values and fuel densities of various test blends, this implied longer injection durations for some fuels. This was particularly the case for the low boiling ethanol blends. The formation of vapor bubbles in the FIE lead to elongated injection durations to maintain the desired engine torque/speed.

Moreover, the VNT/EGR-valve position was not altered when switching fuels. Naturally, this will have some effect on the engine gas exchange process (i.e., AFR and EGR) and combustion phasing. This, in turn, will affect the corresponding NO_x emissions [12, 25]. In this work, however, the authors aim to establish emission trends rather than to compare exact values. The aforementioned effect of gas exchange on NO_x is therefore not considered an issue in this study.

A description of the used emission measurement equipment and other relevant data acquisition is provided elsewhere [12, 25].

3.5 Fuel matrix

A total of 15 blends have been prepared between various base fuels and neat oxygenates, with fuel oxygen levels ranging from 5 to 15 wt-% [12, 25]. In Table 3.2 below, the acronyms and CN of the tested base fuels, neat oxygenates, and blends can be found. A blend acronym has the following format: base fuel-oxygenate fuel-fuel oxygen wt-% (e.g. D-ET-15).

Table 3.2: Base fuel properties.

Base fuel	Acronym	CN	Aromatics
		-	wt-%
Swedish Class 1	SW1	53	5-10
EN590	D	56	20-25
Synthetic diesel	S	75	0

From earlier experimental results [12, 25], it has been concluded that tri-propylene glycol methyl ether (TP) and dibutyl maleate (DB) were among the best performing oxygenates. These oxygenates, blended with SW1 to a fuel oxygen content of 9 wt-%, have been compared to a third oxygenate, cyclohexanone (X1). X1 is a member of a hitherto scarcely discussed class, viz., cyclic oxygenates. These results have been discussed earlier as well [12].

X1 has been blended with D, which has a CN and density comparable to those of SW1. CN for all blends other than the X1 blends has been determined by Shell Global Solutions. The CN for the X1 blend has been determined by applying Kays mixing rule (i.e. a linear dependence on mole fractions) [27].

Contrary to TP and DB, X1 is a cyclic rather than branched (TP) or linear (DB) molecule. It is well-known that such a cyclic character results in a relatively poor reactivity (low CN), as can be seen in Table 3.3. It is believed that, by investigating so wide a range in CN, more insight can be obtained with respect to the effect of fuel reactivity on the smoke opacity performance of oxygenated fuels.

Table 3.3: Neat Oxygenate Properties.

Oxygenate	Acronym	CN	Density	T _b	Oxygen	LHV
		-	kg/m ³	K	wt-%	MJ/kg
Ethanol	ET	8	0.82	351	38.8	27.7
Cyclohexanone	X1	10	0.95	428	16.3	33.6
Dibutyl maleate	DB	28	0.99	554	26	28.23
Ethanol with CN booster	ET+	55	0.82	351	34.8	27.7
Tri-propylene glycol methyl ether	TP	65	0.96	515	31	32.5
Triglyme	TG	120	0.99	489	26	26.2

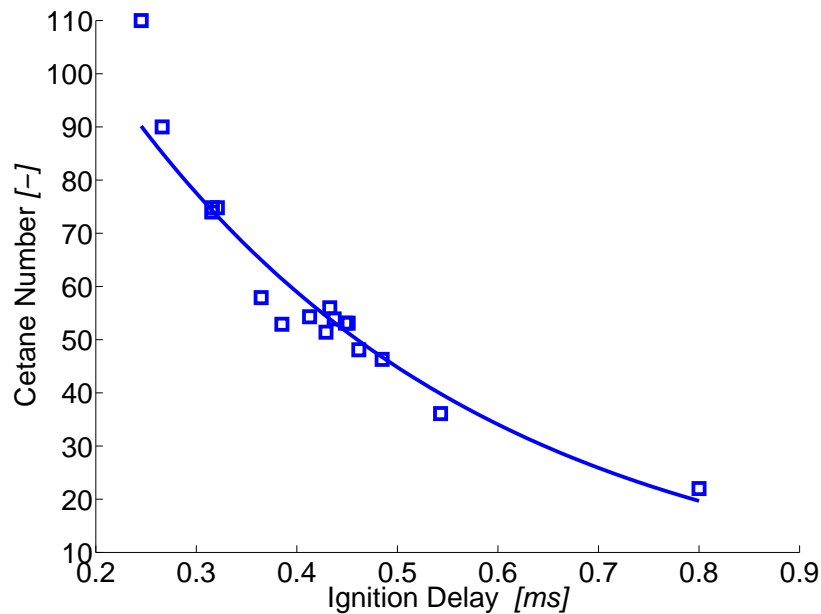


Figure 3.3: CN versus ignition delay for a wide range of oxygenates blended to various fuel oxygen contents (e.g., 5-15 wt-%) with various base fuels.

3.6 Results

Experimental results discussed in this study have been measured in the so-called ROSI [25] work point (i.e. 1650 rpm at 463 Nm). For this particular engine, this is a representative engine operating point for typical use during highway cruising. For all experiments, the start of injector actuation (SoA) has been fixed at -13°CA aTDC. The default EGR level was set at 15 wt-%. Unless mentioned otherwise, the data presented in this section was measured in the ROSI work point at the aforementioned EGR and SoA settings.

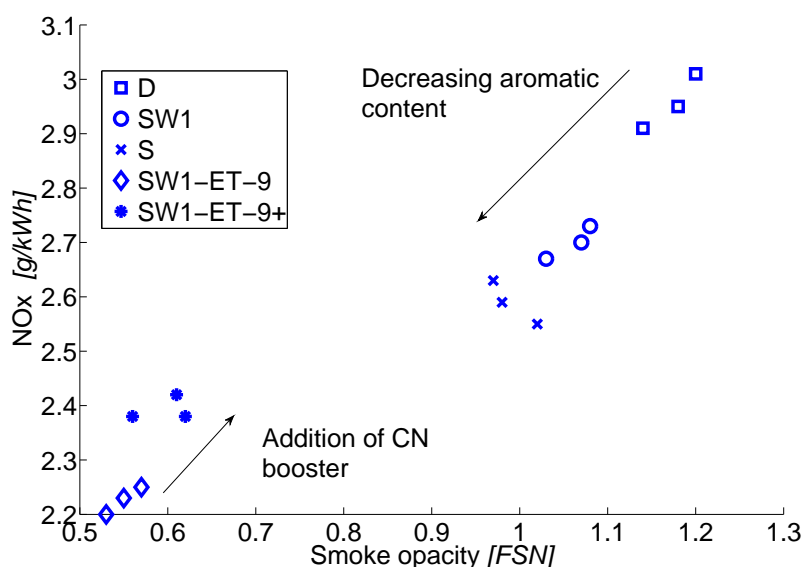
3.6.1 Impact of fuel CN on ignition delay

As discussed earlier, fuel reactivity will have an impact on the premixed burn period. In Figure 3.3, the measured ignition delays (via heat-release analysis) are plotted against their respective CN for all fuels listed in Table 3.4 in the ROSI work point. The ignition delay is defined as the difference in crank angles or time between the points of 50% injector needle lift (opening) and start of heat release (computed from the measured in-cylinder pressure) at a threshold of $30 \text{ J}/^{\circ}\text{CA}$.

It can be seen that a clear correlation exists between ignition delay and CN regardless of fuel oxygen content and/or base fuel characteristics. Ignition delays become rapidly shorter as the CN of fuel in question rises. Accordingly, fuels with a low and high CN will lead to a large and small non-sooting premixed burn fraction, respectively.

Table 3.4: Oxygenated blend properties.

Blend	CN	Blend	CN
SW1-ET+-6	51	SW1-ET-9	36
SW1-DB-6	48	S-TG-9	90
SW1-TP-6	53	S-TP-9	75
S-ET+-6	58	D-X1-9	22
D-X1-5	33	S-TG-15	110
SW1-ET+-9	53	S-TP-15	74
SW1-TP-9	54	SW1-TP-15	54
SW1-DB-9	46		

**Figure 3.4:** NO_x versus smoke opacity for the three base fuels and the 9 wt-% O ethanol blend (with and without a CN improver).

3.6.2 Impact of aromatic content and CN boosters on NO_x/smoke tradeoff.

As discussed in the literature review, a boost in CN can have either a positive or negative impact on particle emissions (e.g., smoke opacity) depending upon how it is realized. Plotted in Figure 3.4 below are the smoke and NO_x emissions for the three base fuels produced in the ROSI work point. It can be seen that a reduction in the aromatic content of the base fuel from 20-25 wt-% (D) to 5-10 wt-% (SW1) and finally to 0 (S) has a positive impact on smoke opacity. In this case, the reduction in smoke opacity coincides with an increase in CN.

An additional decrease in smoke can be achieved by blending an oxygenate (e.g. ET) to SW1. Conversely, when a CN improver is added to the oxygenated blend, the smoke opacity appears to be negatively affected. Both trends are in accordance with

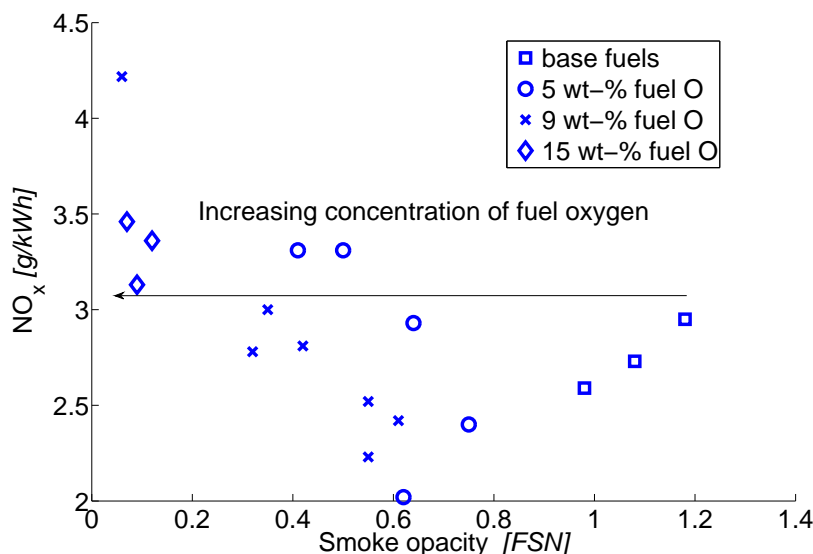


Figure 3.5: NO_x versus smoke opacity for all oxygenated blends (at various fuel O wt-%) and base fuels.

the reviewed literature discussed earlier.

3.6.3 Impact of fuel oxygen on NO_x/Smoke tradeoff.

In comparison to the base fuel, the NO_x/smoke opacity tradeoff improved significantly when increasing the fuel oxygen content. In Figure 3.5, this is best observed when considering a constant (e.g. ~ 3 g/kWh) NO_x value. The significant reduction of smoke opacity with increasing fuel oxygen content is in line with the reviewed literature discussed earlier.

3.6.4 Impact of blend CN on NO_x/Smoke tradeoff.

To isolate the effect of CN on smoke and NO_x, only oxygenated blends containing 9 wt-% fuel oxygen were considered in the following analysis.

In Figure 3.6 and 3.7, it can be seen that, for a given base fuel, there is some indication that smoke opacity and NO_x emissions tend to increase and decrease, respectively, with increasing CN. This appears to be the case for the X1, DB, TP, and triglyme (TG) blends. Such trends can be expected when considering the impact of CN on the ignition delay or premixed burn fraction discussed earlier.

Exceptions to the trend were the ethanol blends. During engine testing, some vapor bubble formation in the FIE was observed when running on the ethanol (ET) blends. As a result, the injection duration was typically somewhat longer, retarding the combustion process and ultimately leading to lower than expected NO_x (Figure 3.7) and higher than expected smoke opacity (Figure 3.6).

A more distinct trend is obtained, however, when plotting the NO_x emissions against the smoke opacity (Figure 8). Here, a clear tradeoff can be observed regardless of the base fuel used and blend CN. The lowest smoke values are obtained for the

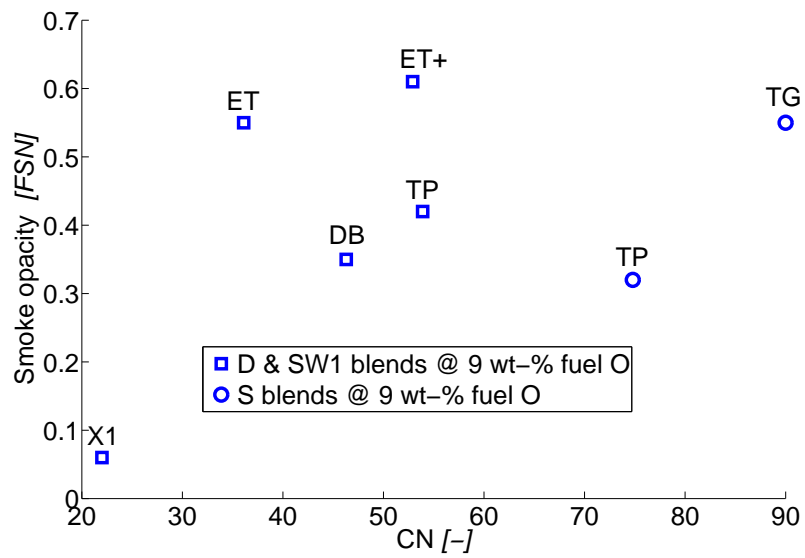


Figure 3.6: Smoke opacity versus CN for all 9 wt-% fuel oxygen blends.

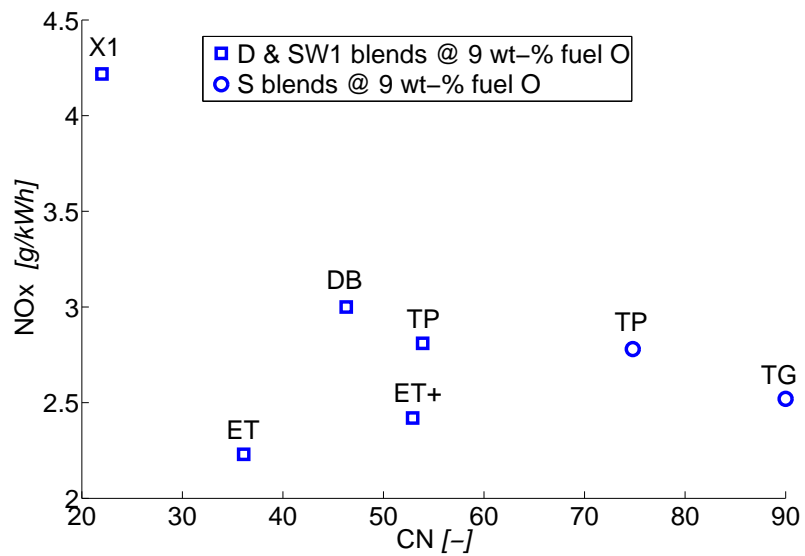


Figure 3.7: NOx versus CN for all 9 wt-% fuel oxygen blends.

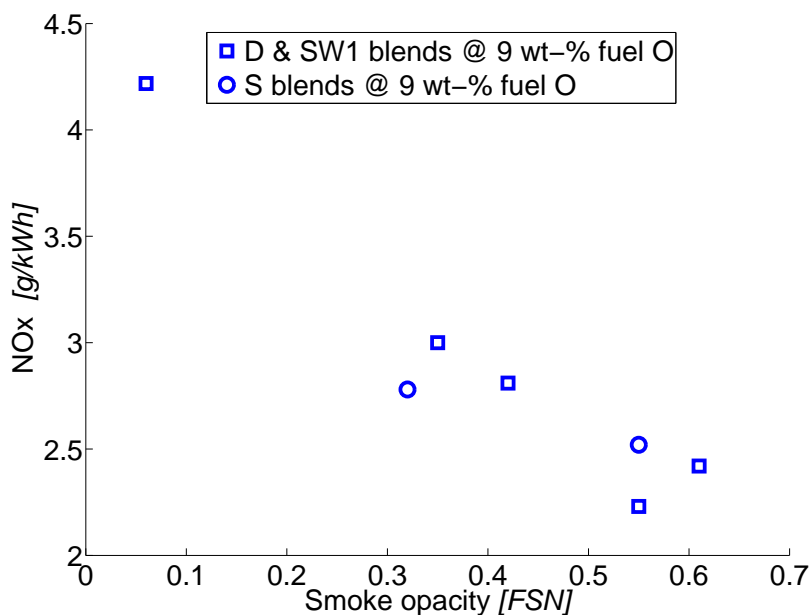


Figure 3.8: NO_x versus smoke for all 9 wt-% fuel oxygen oxygenated blends.

fuels that yield the highest NO_x emissions in accordance with the well-known diesel dilemma.

3.6.5 Influence of EGR on NO_x/Smoke tradeoff.

As can be observed from Figure 9, at a given fuel oxygen level, low smoke opacity can be obtained at the expense of NO_x emissions. To mitigate the adverse effect on NO_x, the EGR level was increased in steps of 2.5 wt-% from 15 to 22.5 wt-%. In this section, only the best performing oxygenated blends, with respect to smoke opacity, are considered. It should be noted that, even with the higher EGR ratios, the engine-out unburnt hydrocarbon and carbon monoxide emissions were within euro IV/V limits [12].

As could be expected, a significant reduction in NO_x can be realized by boosting the EGR fraction. Unfortunately, for the TP and DB blends, this coincides with the typical sharp rise in smoke opacity. Conversely, the X1 blend appears to be left largely unaffected by the otherwise adverse effect of EGR on smoke.

In Figure 10, smoke opacity and NO_x emissions are plotted against increasing ignition delay (e.g., because of EGR). From left to right, the three data points per fuel correspond to the respective emission values at 0, 15, and 25 wt-% EGR. From this figure, it becomes clear that, while all blends display a similar reaction to EGR with respect to NO_x, the negative impact of EGR on smoke seen for TP and DB is not observed for the X1 blend.

When switching between fuels, the injection duration was varied such that engine torque and speed were maintained at the ROSI work point. From the reference EGR level of 15 wt-%, the EGR level was gradually increased up to approximately 25 wt-%. For all fuels considered, the impact of increased EGR is clear, i.e., higher fuel

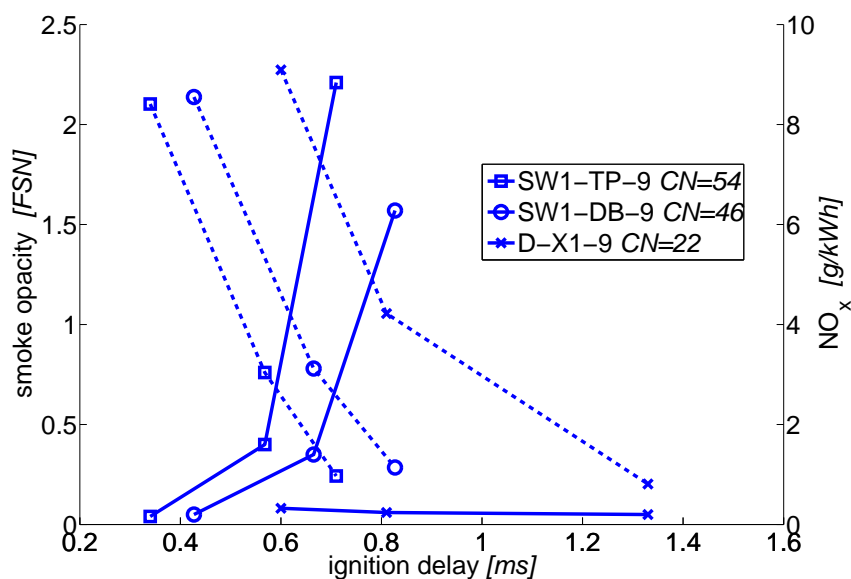


Figure 3.9: NO_x versus smoke opacity at various levels of EGR.

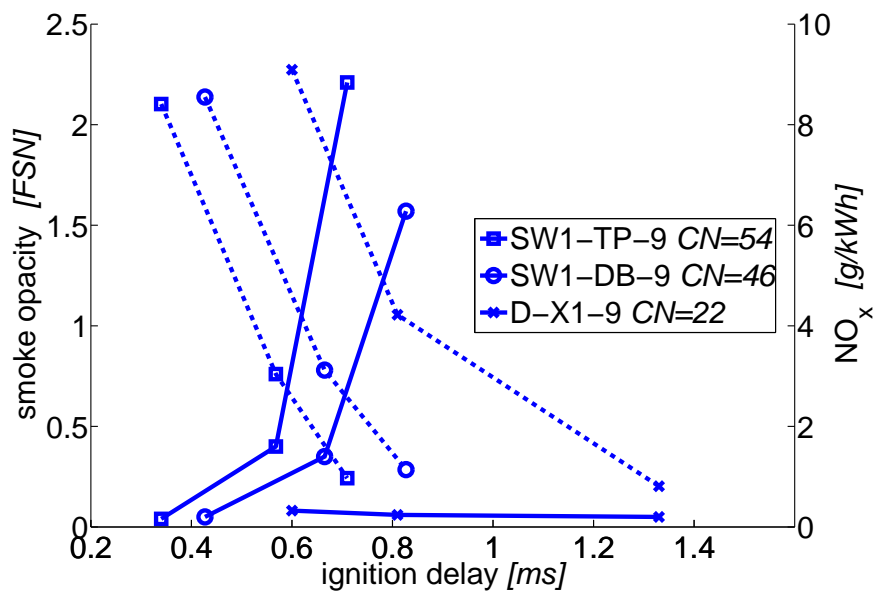


Figure 3.10: Smoke opacity (solid line) and NO_x (dashed line) versus increasing ignition delay (e.g. because of EGR).

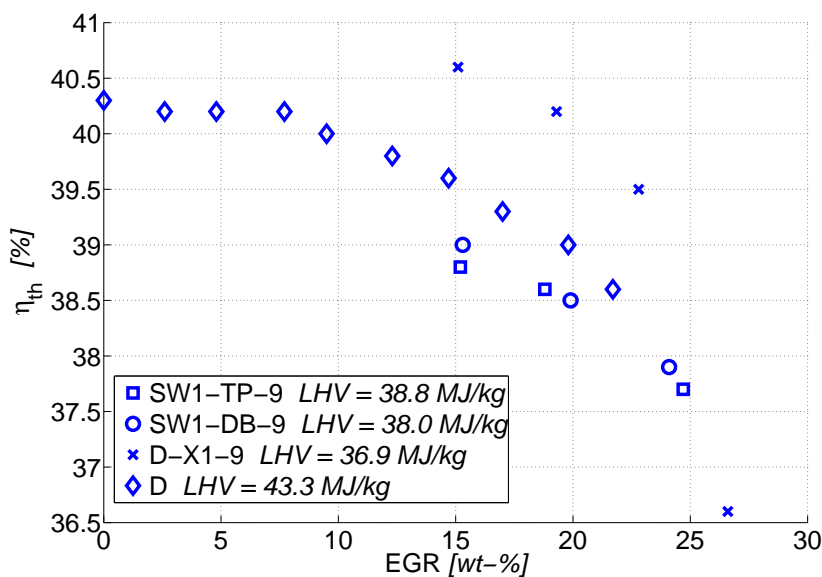


Figure 3.11: Thermal efficiency versus EGR.

consumption and lower thermal efficiency (Figure 3.11). This effect is well-known and is generally attributed to the associated retarded combustion phasing and increased pumping losses.

As could be expected, the presence of 9 wt-% fuel oxygen negatively impacts fuel consumption (i.e. approximately by 10-%). All three oxygenates show comparable behavior here. When expressed in energy consumption, however, all fuels including the non-oxygenated base fuel yield similar results (Figure 3.11). In fact, the distinctions are too small, considering the uncertainty of the LHV in particular, to draw any further conclusions. It is evident from these results that the breaking of the NO_x-PM curve does not come at the expense of thermal efficiency (when compared to the base fuel).

It may be concluded that, as expected, the application of EGR has a positive and negative effect on the NO_x and smoke opacity, respectively. This effect is exacerbated by the fact that the AFR drops as more EGR is fed into the cylinders. The presence of fuel oxygen appears to improve this tradeoff irrespective of the oxygenate concentration or molecular structure. Considerable differences, however, are observed between the various oxygenates, with X1 performing considerably better than TP and DB. These distinctions appear to be masked at low EGR/high NO_x values and are amplified at high EGR/low NO_x levels (Figure 4.3). These conclusions have been drawn earlier by Boot et al. [12] and will be readdressed in the discussion below. It should be noted that an opposite trend was reported by Bertoli et al. [26], who concluded that fuel composition becomes less important with respect to soot at high EGR levels (30 wt-%) and is negligible at 45 wt-%.

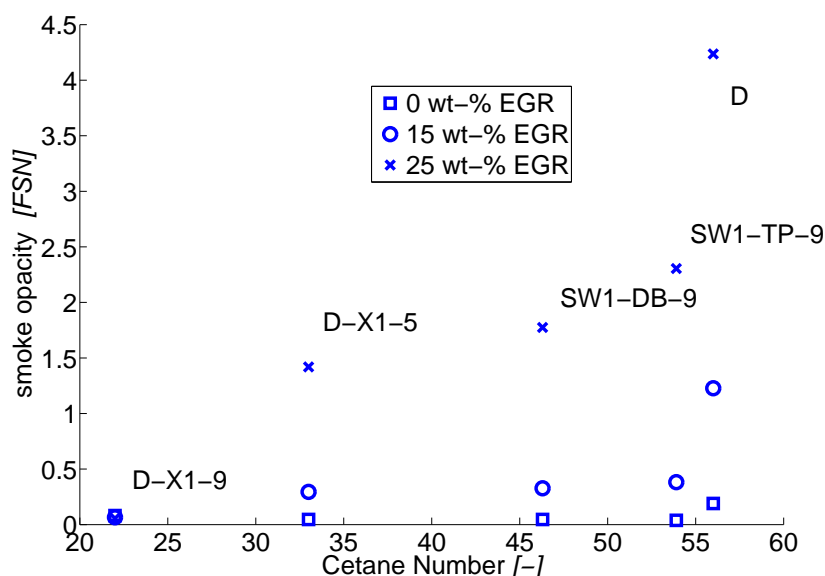


Figure 3.12: Smoke opacity versus CN plotted for various 9 wt-% fuel oxygen blends at three different EGR levels.

3.7 Discussion

3.7.1 Effect of CN

As stated earlier, the main research goal of this study was to investigate the impact of fuel reactivity, expressed here as the CN on smoke opacity. In this section, smoke opacity will be taken as an indication of emitted PM mass. From Figure 3.12, it may be deduced that fuel identity is essentially masked at low EGR levels. In this case, NO_x emissions are relatively high (Figure 4.3) and most PM formed is likely to be readily oxidized in the diffusion flame and post-flame gases. Conversely, at high EGR, NO_x emissions are low, suggesting low flame temperatures and poorer PM oxidation. Here, more influence of the PM formation tendency of the fuel can be expected. This expectation is supported by the data in Figure 3.12, where it can be seen that smoke opacity becomes increasingly sensitive to fuel identity as more EGR is applied.

When investigating the difference in PM performance, one observes that PM emissions correlate quite well with the CN of the fuels. Indeed, PM emissions, at a given EGR level, are seen to decrease in the order SW1-TP-9, SW1-DB-9, and D-X1-9, the CN of which being 54, 46, and 22 respectively. It is striking that the difference in PM performance between the various oxygenates (e.g., at 25 wt-% EGR) is nearly 2 orders of magnitude (Figure 3.12). To emphasize this distinction, the data for X1 at a lower fuel oxygen wt-% (e.g. 5) is plotted in Figure 3.12 as well. It can be observed that, the greater than 40 difference in fuel oxygen wt-% notwithstanding, the DB-9 and X1-5 blends share a similar PM performance. These results suggest that not only fuel oxygen content but also oxygenate reactivity or CN play a significant role in the PM lifecycle, especially at high EGR levels. For the oxygenated blends at 25 wt-% EGR, smoke opacity increases more or less proportionately with the CN. A possible

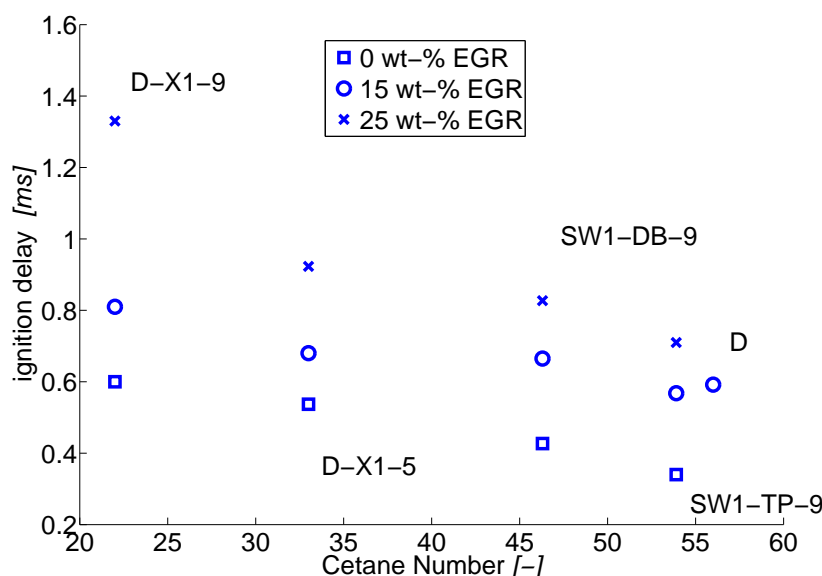


Figure 3.13: Ignition delay versus CN plotted for various 9 wt-% fuel oxygen blends at three different EGR levels.

explanation for this strong dependency upon CN will be discussed below.

A consequence of using EGR and/or lower CN fuel is that the resulting ignition delay (i.e., time between the start of injection and start of combustion) becomes more extended (Figure 3.13).

As a rule, longer ignition delays translate into more premixing of fuel and air prior to auto-ignition. It is generally accepted that most fuel that is injected prior to auto-ignition (i.e., during the ignition delay) will not participate in the PM formation process. By studying Figures 3.12 and 3.13 together, it can be concluded that longer ignition delays indeed coincide with lower smoke opacity. When EGR is applied, with respect to PM emissions, the positive effect of more premixing is generally offset by the negative effect of lower flame temperatures. Accordingly, as can be seen in Figure 3.12, an increase in EGR results in a sharp increase in smoke opacity.

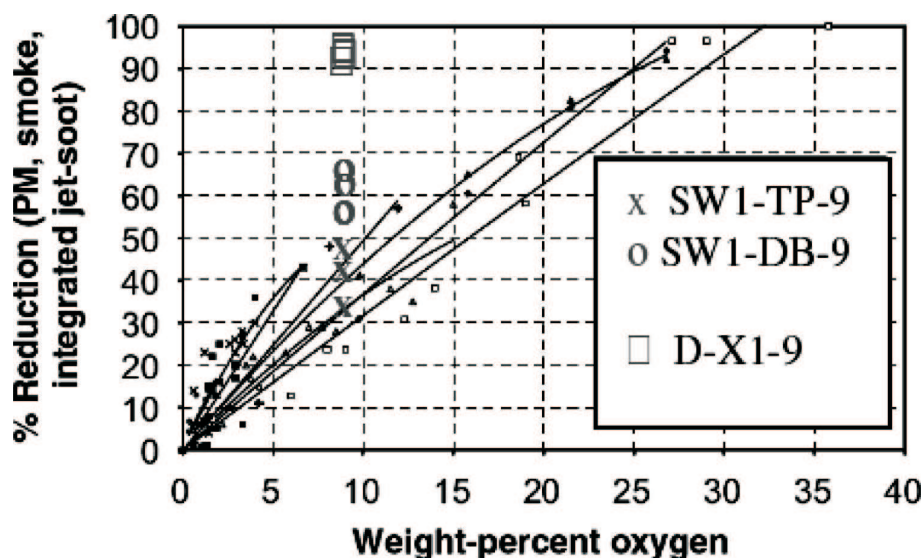
It should be noted that, the longer ignition delays notwithstanding, there still exists considerable overlap between the fuel injection and combustion event. The data in Table 5 show that the start of combustion (SoC) occurs (e.g., for 15 wt-% EGR) well before the end of fuel delivery (EOD). From Figure 4.3, it can be concluded that at this EGR level the breaking of the NO_x/PM tradeoff is already well-established for the X1 blend. Conversely, for premixed combustion concepts, such as homogeneous charge compression ignition (HCCI), Nissans modulated kinetics (MK), and Volkswagens combined combustion system (CCS), the aforementioned events are as a rule separated.

NB while the start of injector actuation (SoA) has been fixed at -13 °CA) aTDC for all experiments, the actual start of delivery (SOD) is nearly 10 later because of delaying effects in the pump-line-nozzle (PLD) fuel injection system.

Alternatively, as discussed earlier, there is some indication in the literature that lower CN fuels lead to longer flame-lift-off-lengths. Longer FLOL's in turn allow for

Table 3.5: Injection and ignition events.

Blend	SOD		EOD		SOC	
	°CA aTDC		°CA aTDC		°CA aTDC	
D	-4		8.8		0.7	
D-X1-9	-3		9.7		5.2	
SW1-DB-9	-3		10.5		1.9	
SW1-TP-9	-3		10.4		1.4	

**Figure 3.14:** Reduction versus fuel oxygen wt-%, collected from numerous experiments reported in the literature [14] and compared to the results of the present study.

more air to be entrained into the fuel jet prior to combustion. Accordingly, a more favorable (i.e. lower) equivalence ratio can be expected in the particle synthesis zone downstream of the FLOL [13], ultimately creating a less conducive environment for soot production.

To put these results in a broader perspective, relevant data from Figure 4.3 has been superimposed (Figure 4.1) onto the literature overview presented in Figure 3.1. An explanation for the omission of cyclic oxygenates and low CN oxygenates in general from fuel matrices in other studies may lie in the dogma that a high CN is beneficial for PM emissions. Although true for conventional fossil fuels, where increased CN is achieved by virtue of the removal of notorious soot precursors (i.e. (poly) aromatics), the presented data clearly suggests otherwise for oxygenated fuels. Moreover, such a pronounced influence of CN as presented in Figures 3.12 and 3.13 is visible only for high EGR/low NO_x levels.

In light of the good results obtained with the X1 blend, the use of cyclic oxygenates in combustion processes has been secured by the Eindhoven University of Technology in three patents. The subject of the current investigation is to develop a commercially viable production route for C₆ cyclic oxygenates, such as X1, from a biological feedstock. A preliminary study is presented in the following section.

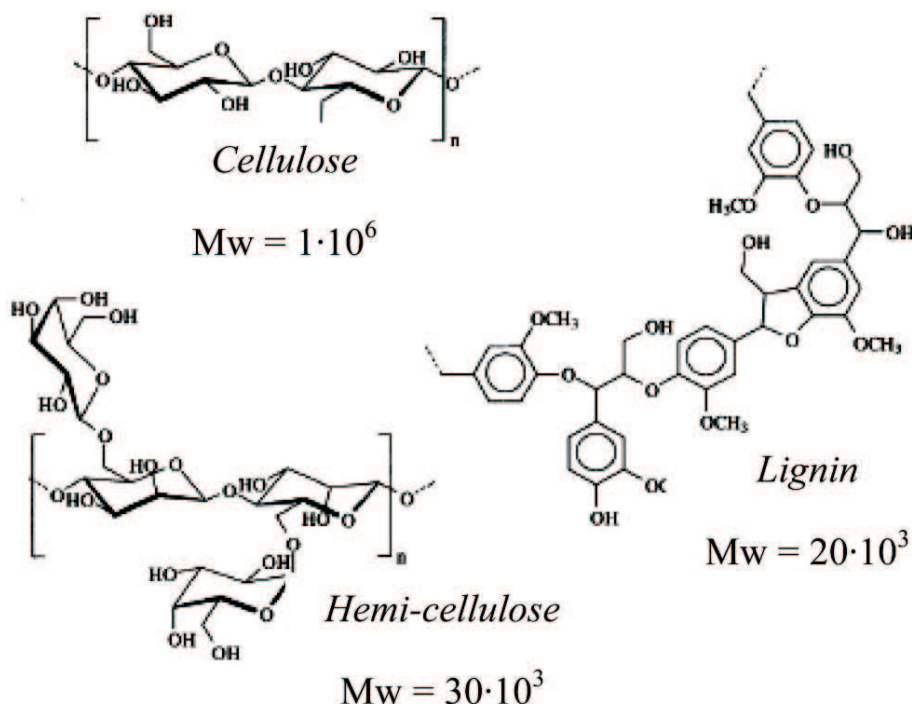


Figure 3.15: Cyclic oxygenated structures of the various lignocellulosic molecules. Molecular weight (MW) in g/mol [28].

3.7.2 Production routes for cyclic oxygenates

Cyclic paraffins are the most abundant (30-60 wt-%) chemical compounds in crude oil [29]. Rings with 6 carbon atoms (e.g. cyclohexane) are the most dominant species by far. Partial oxidation of cyclohexane to X1 is quite straightforward, which might explain why cyclohexanone (X1) could be purchased at less than a fourth of the price of TP and DB. What is more, distillates such as diesel, jet fuel, and heating oil, contain at least about 20 vol-%, generally from about 20 to about 40 vol-%, of six-membered cyclic paraffins. In other words, an economically viable feedstock for X1 is available at any neighborhood gas station. Even on-site and/or on-board refining is within the realm of possibilities.

Even more ambitious is the production of cyclic oxygenates (e.g., X1) from a biological feedstock, more specifically, from lignocellulosic biomass (also known as plant waste/residue). Principal components of such biomass include cellulose (35-50%), hemicellulose (25-30%), and lignin (15-30%) [28], as can be seen in Figure 3.15, all of which are five- and six-membered cyclic oxygenates. Unfortunately, these compounds are large polymers with molecular weights 2-4 orders of magnitude higher than conventional fuels [28]. The production of liquid cyclic oxygenates from such heavy molecules is not straightforward.

Meier and Berns [30] discuss the isolation of phenol from the phenol-like lignin molecules and report conversion rates of 12.8%. Jianliang et al. [31], in turn, studied the conversion of phenol (C₆H₆O) to cyclohexanone (X1) and reported conversion rates in excess of 80%.

Hewgill and Legge [32] have isolated the model component for lignin, guaiacol

(C₆H₄(OH)(OCH₃)), with an efficiency of 88%. Cyclohexanol (C₆H₁₂O) can be subsequently produced via direct hydrogenation.

It deserves attention that all species discussed above are C₆ cyclic oxygenates (like X1) and soluble (to a certain extent) in commercial diesel fuel. The CN of these C₆ molecules is in the range of 5-20 and is expected to have a similar smoke opacity performance as X1.

The design of a commercially viable production process of these species is a current subject of investigation. In the meantime, the above species will be purchased in neat form and tested in a HD DI diesel engine by some of the authors in the near future.

3.8 Conclusions

When the extraordinary sooting behavior of the cyclic oxygenate cyclohexanone (X1) was first observed, many fuel properties were considered as potentially responsible. Foremost herein were the fuel reactivity, oxygen content, and functional oxygen groups (e.g. so-called carbon sequestering efficiency).

The main objective of this work was to examine earlier data more closely in an attempt to ascertain which of the above parameters is the most important. From the Discussion, it follows that the impact of fuel reactivity (CN) on soot, via its derivatives flame-lift-off-length (FLOL) and ignition delay, appears to outweigh that of carbon sequestering efficiency and, in some cases, even that of the amount of oxygen present in the fuel. The results suggest that the importance of CN grows as higher levels of EGR are applied.

With respect to the breaking of the NO_x/PM curve, the authors have demonstrated that for the D-X1-9 blend this occurs at EGR levels as low as 15 wt-%. At such low EGR, there exist still considerable overlap between fuel injection and heat release. For combustion concepts geared toward creating a homogeneous mixture (e.g. HCCI, MK, and CCS), breaking of the NO_x/PM curve has indeed also been observed. Such combustion concepts, however, are characterized by the absence of the aforementioned overlap.

There are process routes known from the literature to produce X1 and similar C₆ cyclic oxygenates from lignocellulosic material. An investigation of a viable production route is the subject of current investigation. When produced from such feedstock, X1 or similar C₆ cyclic oxygenates will qualify as second-generation biofuels.

Bibliography

- [1] D. Karonis, E. Lois, S. Stournas, and F. Zannikos. Correlations of exhaust emissions from a diesel engine with diesel fuel properties. *Energy Fuels*, 12:230–238, 1998.
- [2] T. Zannis and D. Hountalas. DI diesel engine performance and emissions from the oxygen enrichment of fuels with various aromatic content. *Energy Fuels*, 18: 659–666, 2004.
- [3] T. Wu, Z. Huang, W.G. Zhang, J.H. Fang, and Q. Yin. Physical and chemical properties of GTL-diesel fuel blends and their effects on performance and

- emissions of a multicylinder DI compression ignition engine. *Energy Fuels*, 21:1908–1914, 2007.
- [4] P. Bielaczyc, M. Kozak, and J. Merkisz. Effects of fuel properties on exhaust emissions from the latest light duty DI diesel engine. *SAE Paper*, 2003-01-1882, 2003.
- [5] G. Kalghatgi, P. Risberg, and H-E. Ångström. Advantages of fuels with high resistance to autoignition in late-injection, low-temperature, compression ignition combustion. *SAE Paper*, 2006-01-3385, 2006.
- [6] N. Ladommatos, M. Parsi, and A. Knowles. The effect of fuel cetane improver on diesel pollutant emissions. *Fuel*, 75:8–14, 1996.
- [7] X. Lü, J. Yang, W. Zhang, and Z. Huang. Effect of cetane number improver on heat release rate and emissions of high speed diesel engine fueled with ethanol-diesel blend fuel. *Fuel*, 83:2013–2020, 2004.
- [8] R.J.H. Klein-Douwel, A.J. Donkerbroek, A.P. van Vliet, M.D. Boot, L.M.T. Somers, R.S.G. Baert, N.J. Dam, and J.J. ter Meulen. Soot and chemiluminescence in diesel combustion of bio-derived, oxygenated and reference fuels. *Proc. Combust. Inst.*, 32:2817–2825, 2009.
- [9] X.C. Lü, J.G.. Yang, W.G. Zhang, and H. Zhen. Improving the combustion and emissions of direct injection compression ignition engines using oxygenated fuel additives combined with a cetane number improver. *Energy Fuels*, 19:1879–1888, 2005.
- [10] H. Schulz, G. Bandeira De Melo, and F. Ousmanov. Volatile organic compounds and particulates as components of diesel engine exhaust gas. *Combust. Flame*, 118:179–190, 1999.
- [11] K.I. Svensson, M.J. Richards, A.J. Mackrory, and D.R. Tree. Fuel composition and molecular structure effects on soot formation in direct-injection flames under diesel engine conditions. *SAE Paper*, 2005-01-0381, 2005.
- [12] M.D. Boot, P.J.M. Frijters, R.J.H. Klein-Douwel, and R.S.G. Baert. Oxygenated fuel composition impact on heavy-duty diesel engine emissions. *SAE Paper*, 2007-01-2018, 2007.
- [13] L.M. Pickett and D.L. Siebers. Fuel effects on soot processes of fuel jets at DI diesel conditions. *SAE Paper*, 2003-01-3080, 2003.
- [14] K.I. Tree, D.R.; Svensson. Soot processes in compression ignition engines. *Prog. Energy Combust. Sci.*, 33:272–309, 2007.
- [15] J. Song, V. Zello, A.L. Boehman, and F.J. Waller. Comparison of the impact of intake oxygen enrichment and fuel oxygenation on diesel combustion and emissions. *Energy Fuels*, 18:1282–1290, 2004.
- [16] F.J. Liotta and D.M. Montalvo. The effect of oxygenated fuels on emission from a modern heavy-duty diesel engine. *SAE Paper*, 932734, 1993.

- [17] C. Beatrice, C. Bertoli, and N.D. Del Giacomo. New findings on combustion behavior of oxygenated synthetic diesel fuels. *Combust. Sci. Technol.*, 137:31–50, 1998.
- [18] N. Miyamoto, H. Ogawa, N.Md. Nurun, K. Obata, and T. Arima. Smokeless, low NO_x, high thermal efficiency, and low noise diesel combustion with oxygenated agents as main fuel. *SAE Paper*, 980506, 1998.
- [19] C.J. Mueller and G.C. Martin. Effects of oxygenated compounds on combustion and soot evolution in a DI diesel engine: Broadband natural luminosity imaging. *SAE Paper*, 2002-01-1631, 2002.
- [20] M. Gonzalez, W. Piel, T. Asmus, W. Clark, J. Garbak, E. Liney, M. Natarajan, D.W. Naegeli, D. Yost, E.A. Frame, and J.P. Wallace. Oxygenates screening for advanced petroleum-based diesel fuels: Part 2. the effect of oxygenate blending compounds on exhaust emissions. *SAE Paper*, 2001-01-3632, 2001.
- [21] M. Stoner and T. Litzinger. Effects of structure and boiling point of oxygenated blending compounds in reducing diesel emissions. *SAE Paper*, 1999-01-1475, 1999.
- [22] Y. Ren, Z. Huang, H. Miao, Y. Di, D. Jiang, K. Zeng, B. Liu, and X. Wang. Combustion and emissions of a DI diesel engine fuelled with diesel-oxygenate blends. *Fuel*, 87:2691–2697, 2008.
- [23] M. Tadashi, M. Zheng, T. Chikahisa, Y.T. Oh, Y. Fujiwara, S. Tosaka, M. Yamashita, and H. Yoshitake. Simultaneous reductions of smoke and nox from a di diesel engine with egr and dimethyl carbonate. *SAE Paper*, 952518, 1995.
- [24] J. Song, K. Cheenkachorn, J. Wang, J. Perez, and A.L. Boehman. Effect of oxygenated fuel on combustion and emissions in a light-duty turbo diesel engine. *Energy Fuels*, 16:294–301, 2002.
- [25] P.J.M. Frijters and R.S.G. Baert. Oxygenated fuels for clean heavy-duty diesel engines. *Int. J. Vehicle Des.*, 41:242–255, 2006.
- [26] C. Bertoli, C. Beatrice, M.Na. Migliaccio, and N. Del Giacomo. Evaluation of combustion behavior and pollutants emission of advanced fuel formulations by single cylinder engine experiments. *SAE Paper*, 982492, 1998.
- [27] W.B. Kay. Density of hydrocarbon gases and vapors. *Ind. Eng. Chem.*, 28: 1014–1019, 1936.
- [28] R. Santen and G. Centi. *Catalysis for Renewables*. Wiley-VCH: Weinheim, Germany, 2007.
- [29] G. Kvesitadze, G. Khatishvili, T. Sadunishvili, and J. Ramsden. *Biochemical Mechanisms of Detoxification in Higher Plants*. Springer: Heidelberg, Germany, 2006.
- [30] D. Meier, A. Oasmaa, and G.V.C. Peacocke. Properties of fast pyrolysis liquids: status of test methods. *Biomass Bioenergy*, 7:99–105, 1994.

-
- [31] L. Jianliang, L. Hui, and L. Hexing. Liquid-phase selective hydrogenation of phenol to cyclohexanone over pd-ce-b/hydrotalcite catalyst. *Chin. J. Catal.*, 28: 312–316, 2007.
- [32] F.R. Hewgill and F. Legge. On the antioxidant activity of phenols obtained by hydrogenation of eucalyptus diversicolor wood. *Wood Sci. Technol.*, 10:125–129, 1976.

Longer Ignition Delay or Flame Lift-Off Length (Part A) ?

Different strategies are being investigated towards reducing engine-out emission levels of soot and NO_x of modern Diesel engines. A fuel-based strategy currently under investigation, entails the use of low cetane number (CN; i.e. low reactive) oxygenates. Previous research has shown that low CN oxygenates (e.g. cyclohexanone, X1), compared to their higher CN counterparts, perform exceptionally well with respect to abating soot emissions. An accepted mechanism, which could account for the observed reduction, is associated with the ignition delay (ID). As the ID effect does not apply to burners, experiments with various oxygenated blends over a wide range of CNs in a yellow (diffusion) flame burner have been conducted to establish whether or not this is the only mechanism responsible for the measured soot reduction. From the experiments can be observed that emitted soot mass is closely correlated to CN in burners as well. Accordingly, the results suggest that another mechanism is, at least partially, responsible for the observed reduction in emitted soot mass.

The content of this Chapter has been taken from:

M.D. Boot, C.C.M. Luijten, R.S.G. Baert, R. Edenhofer, H. Dirks, K. Lucka and H. Khne. Sooting behavior of oxygenated fuels in a diffusion burner. *In Proc. of the 4th European Combustion Meeting*, Vienna, Austria, 2009.

Minor edits have been made to streamline the layout of the thesis chapters. The contribution of the author is related to the motivation and selection of the "X"-fuels and relevant operating conditions, along with the results, discussion and conclusions thereof. The contribution also includes the Background section. The introduction and overall discussion and conclusions were realized in a joint effort. Experiments were carried out in the burner lab of the Oel-Waerme-Institut GmbH in Herzogenrath, Germany.

4.1 Introduction

The drive for increasingly lower regulated emissions (CO, UHC, NO_x and soot) will result in the implementation of powerful catalytic aftertreatment technology on next generation Diesel engines. At the same time reducing engine-out emission levels is still a major development effort as this will relax the requirements on the aftertreatment system and at the same time could result in a larger overall cost-of-ownership (in particular fuel and eventual additive consumption).

Of the different paths towards reducing engine-out emission levels, fuel-based strategies are among the promising. For more than hundred years, engines have been optimized to cope with the available fossil-based fuels. When looking at fuel-based strategies, the engine is taken as a given, and fuels are designed which have optimal properties for the prevailing combustion process. An important enabler for such tailored fuels in the future will be the development of synthetic fuels (XTL = anything to liquid). Basically, XTL entails the gasification of an arbitrary, preferably renewable, source of hydrocarbons to a desired liquid fuel via specialized catalytic routes. This opens the possibility to produce a dedicated fuel, tailored specifically for the conventional combustion engines.

In this paper a brief recapitulation of previous work on such a tailored fuel is given. From this summary it will become clear that some questions still remain open. The burner setup which is used to shed some light on these questions will be presented and a discussion on experimental results and final conclusions will follow.

4.2 Background

Previous work [1–4] by some of the authors has demonstrated that it is possible to achieve near-zero soot and NO_x emissions in modern diesel engines with cyclic oxygenated fuels (e.g. cyclohexanone, X1). Several questions, however, have remained unanswered thus far. A brief overview is presented below.

A first study on X1 was published in [1]. This paper reports on the combustion properties of a large number of blends of different types of oxygenates with a low-sulfur EN-590 type diesel fuel, a Swedish Class 1 fuel and a synthetic diesel, respectively. Oxygen mass fraction of the blends varied between 0 and 15 wt-%. Tests were performed on a modern multi-cylinder heavy-duty DAF engine equipped with cooled exhaust gas recirculation (EGR) for enabling NO_x-levels between 2.0 and 3.5 g/kWh on EN-590 diesel fuel.

The results (Figure 4.1) confirmed the importance of oxygen weight fraction in the fuel blend, but at the same time illustrate the effect of chemical structure. At an equal oxygen content, some oxygenates (X1) are twice as effective in reducing soot as other well-known oxygenates (dibutyl maleate (DB) and tri-propylene glycol mono-methyl ether (TP)).

It became clear that X1 had excellent combustion properties. The mechanism responsible for the observed soot reduction, however, was not yet understood. High-speed imaging, spectroscopy and thermodynamical characterization were therefore applied to an optically accessible, heavy-duty diesel engine in order to compare sooting and chemiluminescence behavior of various oxygenated fuels [2].

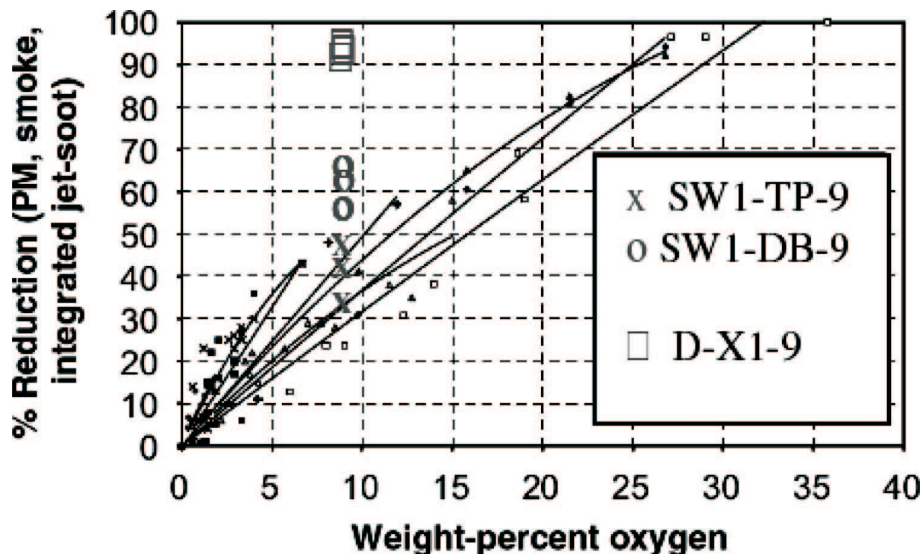


Figure 4.1: Reduction versus fuel oxygen wt-%, collected from numerous experiments reported in the literature and compared to the results of the present study (see chapter 3).

The start of hot combustion was derived from OH^* and CH^* chemiluminescence, as observed through a spectrograph that was used to separate the molecular signals from thermal soot radiation. Both species occur at about the same time, CH^* signal being weaker. Soot incandescence was observed two-dimensionally at 0.3°CA resolution (200 images/cycle). Ignition delays, derived from soot incandescence and chemiluminescence, were compared to those determined from heat release. In line with earlier work [1] large differences in sooting behavior were observed between oxygenated fuels at an equal fuel oxygen content [2], see figure 1.21.

The heat release rate and exhaust NO concentrations were used as indicators of average and peak temperatures, respectively. Both the fuel molecular structure and its oxygen content were reported to be important for soot abatement, a low reactive cyclic structure having the most significant effect.

Another conclusion drawn from the optical experiments was that the cyclic molecule X1 had a considerably longer ignition delay (ID), related to its relatively low cetane number (CN, measure for reactivity) of ~ 10 . It is well known from literature that longer IDs tend to have a favorable effect on soot emissions. Accordingly, it was decided to re-examine data from [1] to establish whether or not a correlation could be found between the soot emissions and ID.

The results, reported in [3] indicate that the low CN (via ID) may indeed play an important role with respect to soot suppression. More specifically, the low reactive oxygenate X1, with its cyclic carbon chain, was found to perform exceptionally well compared to the more reactive linear and branched oxygenates DB and TP (Figure 4.3).

To verify whether or not ignition delay is the dominant factor in the above par soot reduction potential of low CN X1 blends, it was decided to perform a series of experiments on stationary burners with various fuels, having a wide range in CN. Contrary to the situation in engines, fuels burnt in stationary burners do not incur an ID. Accordingly, the presence of a correlation between CN and soot would suggest

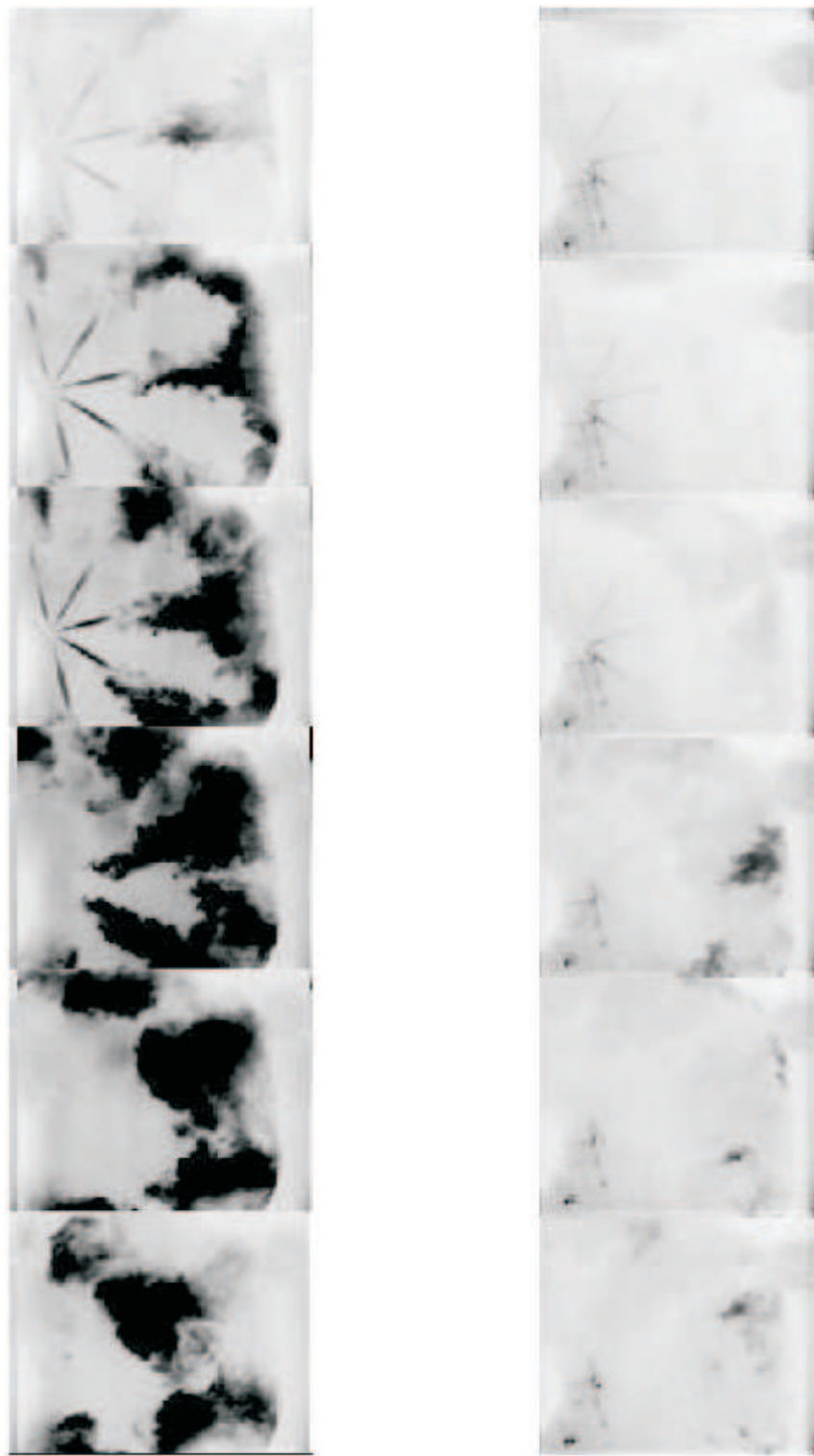


Figure 4.2: Six consecutive frames of a high-speed video recording of soot luminosity of S-TP-9 and SX1-9 blends from -2.1 to 12.9 °CA aTDC.

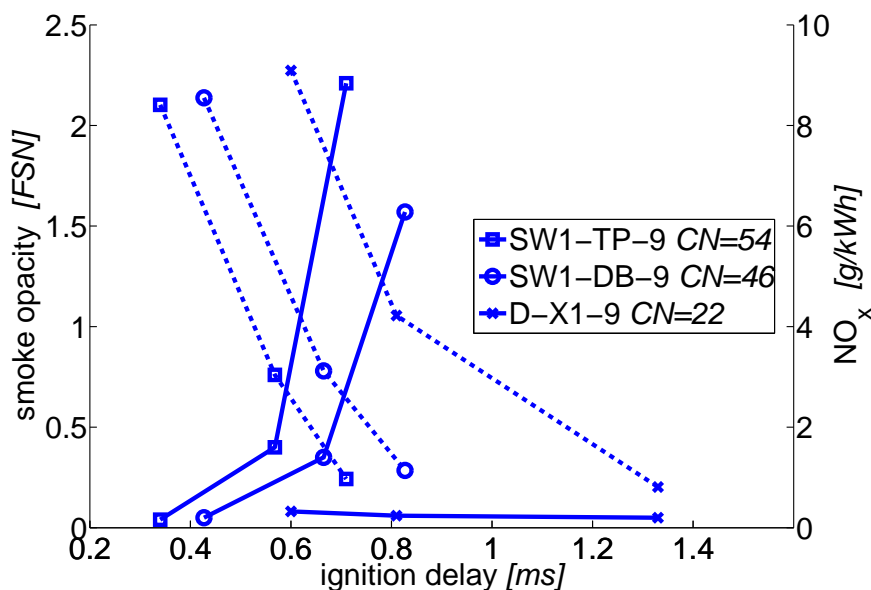


Figure 4.3: Smoke opacity (solid lines: FSN, measure for soot) and NO_x (dashed lines) versus ID for 9 wt-% fuel oxygen blends of X1, DB and TP at three different EGR levels (i.e. from left to right: 0, 15 and 25 wt-%).

a different, hitherto unknown, mechanism is at work.

4.3 Fuel matrix

The base fuel (D) used for the blends is a commercially available low sulphur fuel oil with a sulphur content of 9 ppm. This base fuel oil is blended with oxygenates up to an oxygen concentration of 9 wt-% in the blend. As oxygenates different types of compounds are used: an alcohol (hexanol (HX)), a cyclic ketone (X1) and an ether (Tri Propylene Glycol Methyl Ether (TP)), see Table 4.1. As a result a matrix with a range of functional oxygen groups and CN is formed (Table 4.2).

Table 4.1: Properties of neat compounds.

Property	Unit	X1	HX	TP	D
Density	kg/m ³	0.95	0.81	0.97	0.84
Molar mass	g/mol	98	102	206	-
CN	-	10	23	65	50
Oxygen	wt-%	16	16	31	-
Functional oxygen group		ketone	alcohol	ether	-

Knowing the properties of the pure species, it is assumed that the blend CN (Table 4.2) can be roughly estimated using the Kay mixing rule [3, 5]:

Table 4.2: Properties of tested blends. Note the fractions refer to the oxygenate content in the blend.

Blend property	D-X1-9	D-HX-9	D-TP-9
Vol. fraction	0.52	0.58	0.24
Mass fraction	0.55	0.57	0.27
Molar fraction	0.7	0.71	0.25
CN	21	31	54

4.4 Experimental setup

The combustion of the oxygenated blend fuels is accomplished in a yellow flame burner in stationary mode at its nominal heat input of 18 kW, mounted on a low temperature boiler providing an exhaust gas temperature of 130 °C. In their standard configuration with an equivalence ratio of about $f = 0.83$ the soot number measured in accordance with the German standard DIN 51402, part 1, reaches values between 0 and 1 (on a scale from 0 to 10). In order to see an effect as large as possible comparing the soot emissions of standard and oxygenated fuels, the equivalence ratio of the burner is adjusted to $f = 0.96$, which rises the soot number of the exhaust gas to values between 3 and 4.

Previous to each test run the burner and the boiler are checked for soot deposits and cleaned if necessary. After each test with one of the oxygenated fuels a run with pure fuel oil is done to check and, if necessary, adjust the settings of the yellow flame burner. The determination of the total suspended particles (TSP) is executed by differential weighing of filter membranes before and after exposure to the soot-loaded exhaust gas, following the European standard EN 13284-1 (April 2002). Figure 4.4 shows a schematic drawing of the test rig.

The combustion air enters the burner through a fine filter with a filtration efficiency of (Di-Octyl Phthalate) DOP 0.3 at μm greater than 99.998 %, in order to avoid contamination by external particles. The pressure loss due to the filter is compensated by an additional fan placed between the filter and the burner. Due to the compression heat of the fan the intake air is heated up to about 30 °C.

In the chimney there are sensors for pressure and temperature of the exhaust gas as well as a sampling point feeding the gas analysis system. A partial flow of the exhaust gas is extracted iso-kinetically by the probe head and lead through the measurement filter. The filter housing is heated to the temperature of the exhaust gas in order to avoid condensation of vapor components on the filter. The design of the probe head and the filter housing is according to the requirements of the VDI (Verein Deutscher Ingenieure) directive 2066, part 7.

Because the rotary vane pump and the gas meter are not resistant to corrosion due to humidity and aggressive gas components, the exhaust gas is cooled, scrubbed and dried downstream of the filter. The adjustment of the partial gas flow in order to ensure iso-kinetic extraction is done by a choke valve just before the pump. The determination of the exhaust gas flow rate at the probe head is done by calculating the flow rate from the heat input and the equivalence ratio. The fuel-related data necessary for this calculation, such as the specific exhaust gas flow etc., are determined by an elementary analysis of the fuel. For the present setup this method has proven

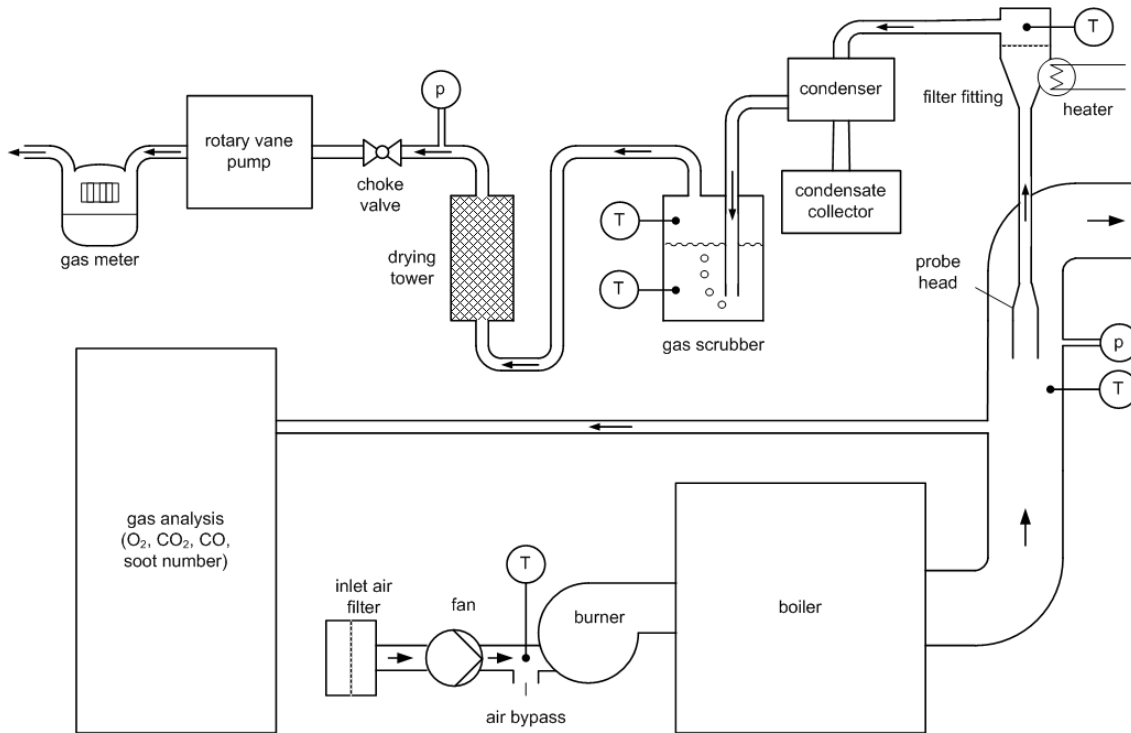


Figure 4.4: Schematic drawing of the test setup.

more accurate than direct measurement of the exhaust gas flow rate (due to the high turbulence of the gas flow which complicates measurement using a Prandtl-probe).

complicates measurement using a Prandtl-probe). Filtration of the particles from the partial gas flow takes place by a Teflon-coated borosilicate fibre membrane with a filtration efficiency of DOP $0.3 \mu\text{m} = 96.4 \%$ according to ASTM D 2986-95A and a temperature resistance up to $315 \text{ }^\circ\text{C}$. According to the requirements of EN 13284-1 (April 2002) the filter membranes are dried at a temperature of $180 \text{ }^\circ\text{C}$ for 1 hour and equilibrated several hours in an exsiccator before the initial weighing. In the time between the initial weighing and the application in the filter housing the membranes are stored in the exsiccator (i.e. dryer).

Directly after removal from their housing, the loaded filters are dried for 1 h at a temperature of $160 \text{ }^\circ\text{C}$ and subsequently equilibrated inside the exsiccator. Each weighing of the loaded membranes is executed at least twice with an additional drying cycle between the weighings. This procedure is repeated until two subsequent weighings give identical results in order to ensure a complete evaporation of volatile components and a good repeatability of the measurement.

It should be noted that atmospheric conditions are considered here, rather than the typical high pressure environment that prevails in the combustion chamber of an engine. It is assumed, however, that pressure has only a modest effect on the diffusion flame.

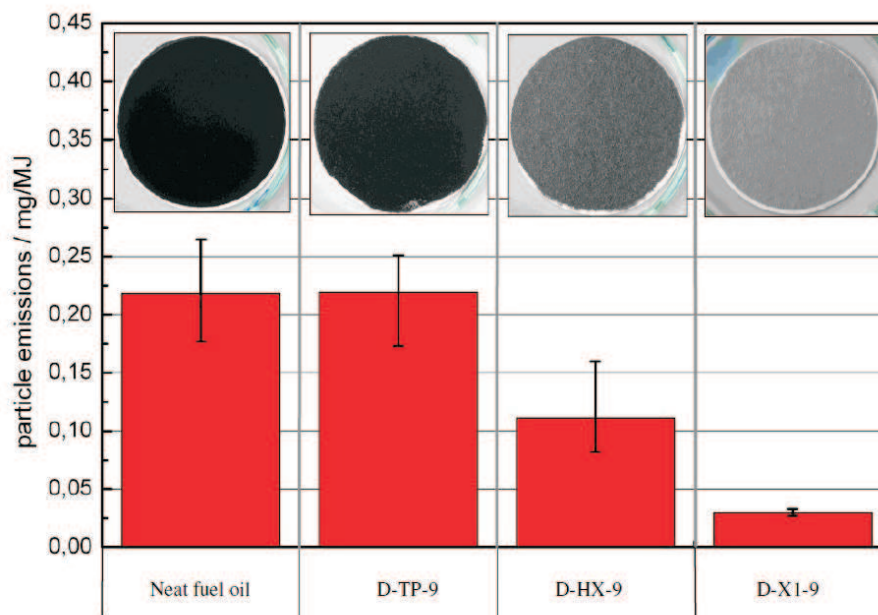


Figure 4.5: Averaged test results with the oxygenated fuels compared to pure fuel oil. Test duration is half an hour, equivalence ratio $\phi = 0.96$. The error bars display the total range of the individual measurements. Featured above each fuel is a photograph of the collected filter sample.

4.5 Experimental results

In Figure 4.5, the results of the measurements with the oxygenated fuels related to the tests with the pure fuel oil are shown. For comparison of the results the particle mass on the filters is related to the heat input of the fuel and given in mg/MJ. Each of the tests is conducted with a duration of half an hour, the test settings are mentioned in the previous section. In order to get at least a minimum of statistics and estimate the repeatability of the results, each test is carried out between two and five times.

The tests with D-TP-9 show nearly identical results to D without improvement of particulate matter emissions. The filters are as black as with pure fuel oil. The weighing confirms the optical impression. In contrast to the test with D-TP-9 there is an improvement using D-HX-9. The particle emissions decrease obviously, the filters are colored dark grey. The mean of the three tests is 0.10 mg/MJ.

In the last test with this blend two problems occurred: the sealing of the filter holder broke and the oil nozzle changed its behavior. The damages on the oil nozzle could not be identified by inspection using a microscope, but the emissions with pure fuel increased severely and the burner could no longer be adjusted to the previous settings. The damaged components were replaced with new ones and the burner settings adjusted to the standard (see previous section).

The best results concerning the particle emissions are achieved with D-X1-9, the value is 0.03 mg/MJ and the filters are light grey. But with this fuel similar problems occurred as with D-HX-9, i.e. the oil nozzle broke and a leakage at the sealing of the oil pump occurred.

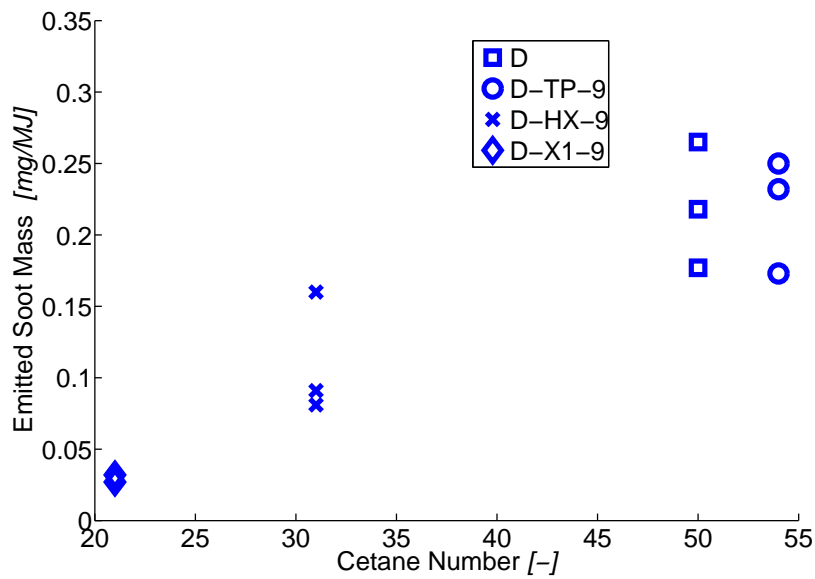


Figure 4.6: Measured soot mass versus blend CN.

4.6 Discussion

As stipulated earlier, the specific objective of this work is to verify whether the ID is the dominant factor with respect to the above par soot reduction potential of the low CN X1 blends reported in earlier work [1–3]. According to this theory, oxygenates with a different CN but equal oxygen wt-% should yield similar soot emissions. Soot, after all, is largely a function of the incurred ignition delay, which is not applicable for stationary diffusion burners for long periods (e.g. 30 minutes).

Another striking observation is the more or less equal performance of the D-TP-9 blend and the diesel base fuel (D). Although both have a similar CN, one would expect the presence of 9 wt-% fuel oxygen in the former blend would have a positive effect on soot, as is the case in most engine experiments cited in literature (Figure 4.1). Apparently, at least in a stationary burner, the CN is of more significance with respect to soot than the available fuel oxygen. Bearing in mind the insignificance of the ID effect, the mechanism of the soot reduction observed in Figure 4.6 is not straightforward.

Some insight into the influence of fuel CN on soot formation in diffusion flames is provided by Pickett and Siebers [6]. In their experiments, the soot formation process was observed in an optically accessible constant volume combustion chamber via laser extinction and planar laser-induced incandescence. By studying a quasi-steady fuel jet, as is the case in the diffusion burner, the beneficial impact of a long ID is no longer relevant. Nevertheless, a correlation between the fuel CN and sooting tendency was found. In general, in line with the data in Figure 4.6, lower CN fuels produced less soot. The authors attributed this trend to the apparent relation between fuel reactivity (e.g. CN) and flame-lift-off-length (FLOL). According to the authors, a longer FLOL will yield a more favorable equivalence ratio in the soot synthesis zone, which lies downstream of the FLOL. Lower CN fuels yield longer FLOL, which in

turn manifests itself in less soot being produced. An investigation into the relation between CN and FLOL in engines is currently subject of research by some of the authors.

4.7 Conclusions

Based on the experimental data the following conclusions are drawn:

- The Cetane Number (CN) of oxygenated blends plays an important role in the emitted soot mass in stationary diffusion burners.
- Given an equal CN, the presence of fuel oxygen does not appear to have the same positive effect on soot as is commonly experienced in engines.
- A clear correlation between soot and blend CN is observed, regardless of the presence of different functional oxygen groups (e.g. ether, ketone and alcohol).
- There are indications from literature that low CN may have a beneficial impact on soot in diffusion flames, via an elongation of the flame lift-off length (FLOL). Accordingly, more air is entrained upstream of the soot synthesis zone.
- This, together with the observations reported in the present work, would explain the results of earlier engine experiments [1–3] where, for the same ignition delay (ID), low CN oxygenated fuels showed lower soot levels than oxygenates with similar oxygen mass fraction but higher CN.

Bibliography

- [1] M.D. Boot, P.J.M. Frijters, R.J.H. Klein-Douwel, and R.S.G. Baert. Oxygenated fuel composition impact on heavy-duty diesel engine emissions. *SAE Paper*, 2007-01-2018, 2007.
- [2] R.J.H. Klein-Douwel, A.J. Donkerbroek, A.P. van Vliet, M.D. Boot, L.M.T. Somers, R.S.G. Baert, N.J. Dam, and J.J. ter Meulen. Soot and chemiluminescence in diesel combustion of bio-derived, oxygenated and reference fuels. *Proc. Combust. Inst.*, 32:2817–2825, 2009.
- [3] M.D. Boot, P.J.M. Frijters, C.C.M. Luijten, L.M.T. Somers, R.S.G. Baert, A.J. Donkerbroek, R.J.H. Klein-Douwel, and N.J. Dam. Cyclic oxygenates: A new class of second-generation biofuels for diesel engines? *Energy Fuels*, 23:18081817, 2009.
- [4] P.J.M. Frijters and R.S.G. Baert. Oxygenated fuels for clean heavy-duty diesel engines. *Int. J. Vehicle Design*, 41:242–255, 2006.
- [5] W.B. Kay. Density of hydrocarbon gases and vapors. *Ind. Eng. Chem.*, 28:1014–1019, 1936.
- [6] L.M. Pickett and D.L. Siebers. Fuel effects on soot processes of fuel jets at diesel conditions. *SAE Paper*, 2003-01-3080, 2003.

Longer Ignition Delay or Flame Lift-Off Length (Part B) ?

The relation between ignition delay and flame lift-off length (based on OH^ chemiluminescence) has been studied in an optically accessible heavy-duty diesel engine. Soot production has been studied as well, using both exhaust soot data and high-speed imaging of the in-cylinder natural luminosity. Since the luminosity is estimated to scale with T^{13} for our experimental conditions, the local temperature becomes a decisive factor in the interpretation of natural luminosity images. The fuels used include regular diesel and blends of various oxygenates (cyclohexanone, anisole, and dibutyl maleate) with synthetic diesel, to cover a wide range of cetane numbers and oxygen content. Based on a literature review, we hypothesize that the flame speed only determines an upper limit for the flame lift-off length (rather than its exact position). Under conditions that promote auto-ignition, the lift-off length may be shorter, and is likely governed by ignition chemistry. For the oxygenated fuels, the flame lift-off length is found to increase with ignition delay. An inverse correlation is found between the soot luminosity and the oxygen ratio at the lift-off length. The anisole-blend does not produce measurable amounts of exhaust soot as long as the injection duration is shorter than the ignition delay. Under cooled EGR-like conditions, the ignition delay is so large that anisole is considered a candidate fuel for soot-free operation of heavy-duty diesel engines up to medium load.*

The content of this Chapter has been taken from:

A.J. Donkerbroek, **M.D. Boot**, C.C.M. Luijten, N.J. Dam, J.J. ter Meulen. Flame lift-off length and soot production of oxygenated fuels in relation with ignition delay in a DI heavy-duty diesel engine. *Submitted to Combust. Flame*, October 2009.

Minor edits have been made to streamline the layout of the thesis chapters. The contribution of the author is related to the motivation and selection of the "X"-fuels and relevant operating conditions, along with the results, discussion and conclusions thereof. The contribution also includes the literature reviews. The introduction and overall discussion and conclusions were realized in a joint effort. Experiments were carried out in the engine lab of the Radboud University of Nijmegen.

5.1 Introduction

For more than a hundred years, engines have been optimized for the available fossil-based fuels. Meeting future emission legislation, however, should be reached in a two-way synergetic approach. In addition to adapting the engine hardware to the existing fuel, a fuel could be tailored to the engine. An important enabler for such tailored fuels in the future is the development of synthetic fuels (XTL = ‘anything to liquid’). Basically, XTL entails the gasification of an arbitrary, preferably renewable, source of hydrocarbons into a desired liquid fuel via specialized catalytic routes. This opens the possibility to produce a dedicated fuel, on a large scale, tailored specifically for use in either conventional combustion engines or in modern concepts such as premixed charge compression ignition (PCCI).

This is not to say that fossil-based fuels have not improved over the years. For example, large investments have been made to cut the aromatic content of diesel fuel. Besides lower soot emissions, a result of the reduction in aromatic content is a higher Cetane Number (CN). In conventional diesel fuels, a higher CN typically results in smoother running of the (diesel) engine and lower soot emissions. It is stressed here that this reduction in soot is caused by the lower aromatic content. The fact that fewer aromatics (which are key soot precursors) in the fuel leads to a higher CN is a by-product. An increase in CN can either have a positive or negative effect on net soot production, depending on how it is realized. This dependency is discussed at length in [1].

The dogma, however, of ever increasing requirements for the cetane number (CN) has come under pressure in light of amounting interest in premixed charge compression ignition (PCCI) combustion in diesel engines [2–4]. In PCCI mode, the combustion and injection processes do not overlap, thereby avoiding the formation of the (jet) diffusion flame responsible for soot and NO_x in the fuel rich core and near-stoichiometric periphery, respectively. Instead, a more or less premixed mixture is created, which burns volumetrically, thereby largely avoiding fuel rich zones and hot pockets. Unfortunately, PCCI, which requires long ignition delays, is extremely difficult to achieve in a controlled way with the available high CN diesel fuels, especially at higher loads. Extreme measures (e.g. reduced compression ratio, or large amounts of exhaust gas recirculation) need to be employed in order to counteract the high reactivity of the fuel [2–5].

Alternatively, PCCI-like combustion can be achieved with more or less stock engine hardware when running on low CN fuels [1]. A lot of research has been performed by the authors on low CN fuels, particularly oxygenated (i.e. fuel-bonded oxygen) variants. This work, performed both on engines and burners, has recently been summarized in [6]. The results demonstrate that near-zero soot and NO_x emissions can be achieved with low CN diesel-oxygenate blends. More importantly, both in the burner and engine experiments, a clear correlation was found between blend CN and soot, with the latter decreasing sharply with reduced CN. With respect to the engine experiments, the low soot production is believed to be linked to an increasing premixed burn fraction for lower CN blends, which exhibit longer ignition delays [1–4, 6–8].

The ignition delay mechanism, however, does not explain the occurrence of the same CN-soot trend in (co-flow diffusion) burner experiments [6]. In the utilized burners, combustion is continuous, with experiments lasting an average of over 30

minutes. Any effects of ignition delay are therefore irrelevant as the flame is ignited by an external agent such as a match or a lighter. A potential mechanism might involve the Flame Lift-off Length (FLoL, i.e. the location downstream of the injector where the reaction zone stabilizes after auto-ignition), which indicates to a large extent how much air is entrained upstream of the diffusion flame [6]. A longer FLoL means more air entrainment. Consequently, a lower equivalence ratio is established in the jet core, ultimately leading to the formation of less soot [9, 10].

5.1.1 Impact of ignition behavior on flame lift-off length

For more than 50 years the widely accepted flame propagation model, first suggested by Vanquickenborne and Van Tiggelen [11], assumes that at the position of the FLoL the turbulent flame propagation velocity is exactly equal and opposite to the downstream convective flow velocity. In other words, at given operating conditions, the FLoL is governed by flame propagation. This model is based on experiments using gaseous fuels on a turbulent jet diffusion burner. Later, Kalghatgi [12] validated this model for various gaseous fuels over a wide range of jet diameters and flow velocities. It is noteworthy that both studies were conducted under atmospheric conditions. A literature review of related research can be found in [13].

Although the propagation model was found to hold for various gaseous fuels under atmospheric conditions, recent studies [9, 14–19] suggest that, at least for lifted turbulent diffusion flames with both gaseous and liquid fuels under high temperature and/or pressure, auto-ignition behavior contributes to a large extent to the position of the FLoL.

Spray combustion in constant volume vessels

Pickett and Siebers [9] studied the impact of CN, amongst other fuel and spray properties, on FLoL in an optically accessible constant-volume vessel at typical DI diesel conditions using OH chemiluminescence imaging. They conclude that in general fuels with shorter ignition delays tend to have shorter lift-off lengths.

In related work [14], Pickett et al. add that the premixed flame speed of large hydrocarbon fuels is known not to change significantly with varying CN. Accordingly, differences in FLoL appear not only attributable to flame propagation. Further evidence that corroborates the importance of auto-ignition behavior is presented as well. The authors studied the timescale for jet mixing from the injector tip to the FLoL for a range of temperatures. They conclude that this timescale collapses to an Arrhenius-like expression over a wide range of conditions, akin to that which describes the ignition delay as a function of the reactants temperature. Since for larger hydrocarbons, the flame speed is not likely to significantly depend on molecular structure and the number of carbon atoms [20, 21], the correlation between FLoL and ignition delay does not stem from a correlation between FLoL and flame speed.

Pauls et al. [15] investigated the relation between auto-ignition behavior and FLoL in a heated high-pressure vessel using OH chemiluminescence. In agreement with the work of Pickett et al. [9, 14], the authors report that the experiments suggest that the FLoL is determined by auto-ignition, but argue that flame propagation remains important to stabilize the flame front.

Pertaining to the mechanism connecting auto-ignition and FLoL, both Pickett et al. [14] and Pauls et al. [15] detected the presence of local auto-ignition events, involving small pockets of premixed fuel and air, upstream of the FLoL, which subsequently propagate downstream towards the flame front. Once merged with the flame front, a reduction in the FLoL was observed. Moreover, Pickett et al. [14] report the presence of formaldehyde (CH_2O), a known precursor for first-stage ignition chemistry, upstream of these local ignition kernels.

More recently, Pickett et al. [19] studied this ignition-island mechanism by pulsed laser-igniting a diesel fuel jet upstream of the natural FLoL position. Via this approach, ignition spots could be artificially created. The formation of such islands resulted in an upstream movement of the FLoL. Only after a significant amount of time, far longer than dictated by the convective downstream velocity, did the FLoL move back to its original position.

Research conducted on co-flow burners

Research on FLoL is not limited to automotive-related studies. Gordon et al. [16] studied auto-ignition processes involving hydrogen in a (hot) co-flow turbulent diffusion burner. The authors conclude that ignition behavior has a strong influence on FLoL. The same conclusion was found in a related study, now using methane, performed by Gordon et al. [17]. In both studies ignition precursors (hydroperoxyl radicals (HO_2) [16] and CH_2O [17]) were detected upstream of the FLoL. Moreover in [17], ignition kernels (identified by OH) were measured upstream of the FLoL.

Oldenhof et al. [18] reported similar ignition kernels upstream of the FLoL in a co-flow diffusion burner fueled with natural gas, under atmospheric pressure with a heated co-flow (max. temperature of roughly 1500 K). A model, which can predict both the random process of kernel formation and growth, was found to be in good agreement with the measurements. The authors conclude that the mechanism determining the average FLoL is not upstream propagation of the flame front, but the apparently random process of auto-ignition and subsequent growth and downstream transport of ignition kernels. With a probability model, the observed shortening of the FLoL with increasing ambient gas temperature (also seen in the aforementioned constant-volume vessel experiments) can be explained by an enlarged probability of auto-ignition.

Summary of literature study

Table 5.1 provides a summary of the reviewed literature. In all but the last study the authors conclude that the FLoL is governed largely by ignition processes rather than by flame propagation. This conclusion appears to hold for a wide range of liquid and gaseous fuels irrespective of operating pressure, but is not in agreement with the widely accepted flame propagation model [11, 12]. Why this is the case requires further investigation, but the applied air/co-flow temperature might be of significance. While in [11, 12] the air was at room temperature, the air/co-flow temperature in [9, 14–19] was elevated to 750–1500 K. At the former conditions, auto-ignition processes are not supported and hence it is improbable that auto-ignition behavior will influence the FLoL. In all likelihood, the FLoL will then be governed by flame propagation. At the

Table 5.1: Summation of FLoL literature review. 1T_g refers to gas temperature in vessel, 2T_g refers to co-flow temperature, CN = Cetane Number, CVV = Constant Volume Vessel, CFB = Co-Flow (turbulent diffusion) Burner, G = gas, L = liquid

Ref.	Setup	Fuel properties		Conditions			Observation	Conclusion
		Phase	CN	T_g (K)	p_g (bar)	ρ_g (kg/m ³)	Ignition precursors upstream of FLoL	Does FLoL correlate with ignition delay?
[9]	CVV ¹	L	42-80	800-1300	-	7.3-30	-	Yes, but no one-to-one correlation
[14]	CVV ¹	L	43-80	800-1300	-	7.3-30	CH ₂ O and kernels of OH	Yes, but no one-to-one correlation
[15]	CVV ¹	L	41-56	800	50	-	Kernels of OH	Yes
[16]	CFB ²	G	-	1045	1	-	HO ₂	Yes
[17]	CFB ²	G	< 0	1355-1475	1	-	CH ₂ O and kernels of OH	Yes
[18]	CFB ²	G	< 0	1600	1	-	Kernels of OH	Yes
[19]	CVV ¹	L	46	750-900	-	14.8	Kernels of OH	Yes
[22]	Engine	L	53					Not with chemical ID

latter conditions, however, temperatures are high enough to facilitate auto-ignition chemistry and indeed it appears from [9, 14–19] that this chemistry influences the FLoL. In the last study listed in Table 5.1 [22], it is concluded that the ignition delay and the lift-off length are not correlated. Differences in the FLoL are most likely the result of differences in the amount of mixing needed with hot combustion products containing air, for ignition of the fuel.

A hypothesis based on the literature review is that the prevailing oxidizer temperature determines whether or not auto-ignition behavior upstream of the FLoL is important with respect to the location of FLoL. Herein, a combination of effects is imaginable, with upstream auto-ignition events driving the ‘nominal’ FLoL, as determined by flame propagation, closer to the injector. In other words, the balance between flame speed and injection velocity determines an upper limit for the FLoL. In the event of upstream ignition events, however, the FLoL will be ‘pulled’ closer to the injector orifice and ignition chemistry will, along with flame propagation, determine the location of the FLoL.

An analogy can be drawn to knock in spark-ignition engines. The normal mode of combustion in spark-ignition engines is flame propagation. In some cases, however, the unburnt mixture, downstream of the moving flame front, can heat up (due to compression via expansion of the burnt products) to such an extent that undesired auto-ignition (or knock) occurs. In the event of knock, the propagating flame front will be strongly influenced by this auto-ignition process.

5.1.2 Objective

Although a lot of data on the relationship between FLoL and ignition behavior can be found in literature, the associated experiments have been conducted either on burners or in high-pressure vessels. We are aware of only two related engine-based studies, which, however, do not explicitly investigate this relationship. Musculus et al. [23] presented results which suggest a weak correlation between ignition delay and FLoL. The study of Cheng et al. [24] also suggests such a correlation for primary reference fuel blends, but only early in the stroke. Later in the stroke, the FLoL decreases and becomes virtually identical for the blends.

The objective and added value of our present paper is to investigate specifically the effects of auto-ignition (represented here by the CN and prevailing ignition delay) on both FLoL and soot production in an optically accessible direct-injected (DI) heavy-duty diesel engine. Both parameters are measured simultaneously for various oxygenated fuels, with equal fuel oxygen content, but with widely varying auto-ignition behavior. The results of this study are subsequently compared to those reported in the constant volume vessel and burner literature as indicated above [9, 11–19].

5.1.3 Fuel selection

The fuels investigated in this study are regular diesel and the oxygenated fuels dibutyl maleate (DBM, $C_{12}H_{20}O_4$), cyclohexanone ($CH_{10}O$, $C_6H_{10}O$) and anisole ($C_6H_5OCH_3$). In a previous work [1], $CH_{10}O$, DBM and other oxygenates were investigated in a DAF heavy-duty direct-injection diesel engine. From oxygenated fuels, it is well-known that they lead to lower soot emissions; however, for a given fuel oxygen mass fraction, there are significant differences in soot reduction. The results suggest that the CN may play an important role. More specifically, the low CN oxygenate $CH_{10}O$, with its cyclic carbon chain, was found to perform exceptionally well in terms of soot reduction, compared to the more reactive linear oxygenate DBM.

In Ref. [1], it was proposed to produce $CH_{10}O$ from lignin. Lignin is a polymer of phenolic-like molecules, which share the hexagonal carbon skeleton, albeit in aromatic rather than aliphatic bonds, of $CH_{10}O$. Consequently, to produce $CH_{10}O$ from lignin, the phenolic-like molecules need to be hydrogenated, a catalytic process which requires hydrogen. Anisole, an aromatic oxygenate, has been included in this study in order to ascertain the impact of aromaticity on combustion behavior. In the event anisole exhibits a similar or superior combustion behavior to $CH_{10}O$, it might prove to be a more viable alternative to produce from lignin than $CH_{10}O$, since the production cost increasing hydrogenation step can be skipped. DBM has been included in the matrix so as to expand the investigated range in CN. DBM and anisole have been blended with synthetic diesel (SD) to a fuel oxygen content of 9% by weight. The same holds for $CH_{10}O$ ($CH_{10}O(9\%)$), but a second blend ratio (i.e. 5% fuel oxygen by weight) is also investigated for $CH_{10}O$ ($CH_{10}O(5\%)$) as it was found to have similar ignition behavior as the aforementioned DBM blend in previous work [1, 5, 8]. Elementary data and some references about the fuels and blends of two fuels used in the experiments are given in Table 5.2.

Table 5.2: Fuels used. ^ain %_{mass}. ^bin kg/l. ^cCetane Number. ^dlower heating value in MJ/kg. ^eRef. [5]. ^fRef. [25]. ^gRef. [26]. ^hestimation.

	[O] ^a	% SD by volume	ρ^b	CN ^c	CN of pure fuel
diesel ^e	0	0	0.83	56.2	56.2
SD ^e	0	100	0.778	75	75
DBM	9	73	0.84	62	30 ^f
CH _x nO(5%) ^e	5	74	0.82	58	10 ^h
CH _x nO(9%) ^e	9	50	0.87	43	10 ^h
Anisole	9	45	0.90	21	-24 ^g

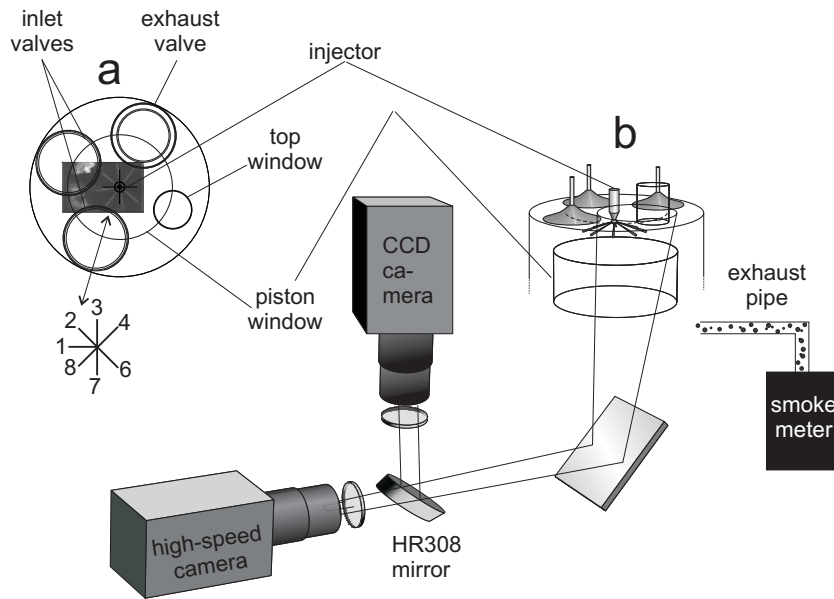


Figure 5.1: Schematic representation of the setup. (a) top view, indicating the field of view of the high-speed camera, along with a schematic view of the (numbered) sprays. Spray 5 was blocked. (b) View of the measurement cylinder and the high-speed and CCD camera.

5.2 Experiment

5.2.1 Engine

In Table 7.1, the specifications of the optical six-cylinder heavy-duty diesel engine are listed, and Fig. 5.1 shows the layout of the optical setup. The engine is designed for laser diagnostic measurements. For that reason, some modifications are present that are not required for the measurements presented here. One of these modifications are two slots (12 mm high and 9.5 mm wide, 180° separation) machined in the piston crown allowing observation and laser access through both side windows even at top dead center (TDC). Fuel injection into the measurement cylinder is achieved by a home-built common-rail (CR) system, providing the possibility to start and end the fuel injection at will. Because of previous experiments not addressed here [27], one of the eight injector holes (annotated as spray 5) was blocked, as indicated in Fig. 5.1. All results presented in this paper pertain to spray 1. To avoid overheating, the non-lubricated measurement cylinder is skip-fired with a ratio of 1:35 (1:10 when exhaust-

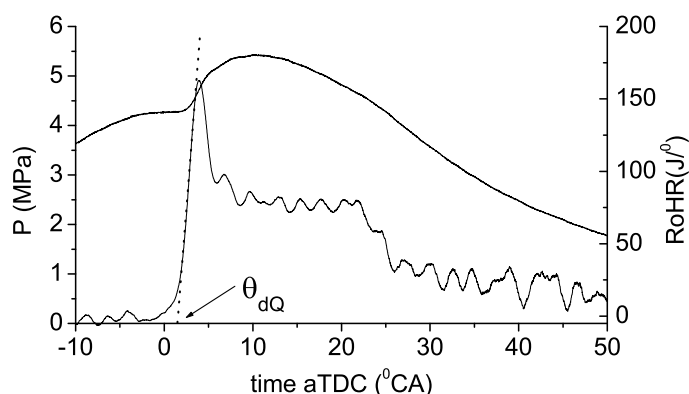


Figure 5.2: Typical pressure curve for diesel (left ordinate), normal inlet air, injection between -4.5° and 21° aTDC. Indicated mean effective pressure (IMEP): 727.4 kPa. For the RoHR curve derived from the pressure curve (right ordinate), the steepest ascent fit to determine ϑ_{dQ} is depicted as a dotted line.

gas measurements were performed). The engine speed is set at 1430 revolutions per minute and separate measurements reveal that it is constant to $\pm 2\%$. With respect to temperature, steady-state conditions are mimicked by (pre-)heating the cooling water to operational temperatures of around 65°C . Unless stated otherwise, the inlet-air temperature was pre-heated to 40°C and the effective boost pressure was 1.1 bar.

Two different inlet air compositions have been employed, one containing 21% O_2 (normal air) and one serving as synthetic cooled EGR, containing N_2 -enriched air with only 15.3% O_2 . The 15.3% O_2 dry air was provided by a pack of 16 gas bottles, 200 bar, 50 liter each (Messer).

5.2.2 Thermodynamics

For diesel, the start of fuel delivery (SoD), i.e. the *effective* start of injection was determined from high-speed imaging (see Fig. S1 in [8] for a more elaborate description). For the other fuels, no high-speed images were available. The SoD was retrieved from the rail-pressure trace and the needle-lift. In all cases the SoD occurs about 3.5° after triggering the injection system.

The start of combustion was retrieved from the rate of heat release (RoHR) [28], derived from the in-cylinder pressure trace. A straight line was fit to the region of the steepest ascent during the rapid rise of the RoHR. The timing of the start of the RoHR (ϑ_{dQ}) was then determined as that time where this straight line intersects the time-axis as shown in Fig. 5.2. This method is very insensitive to noise and yields an upper limit of ϑ_{dQ} . The ignition delay (via the heat release) is then determined as the difference between ϑ_{dQ} and the start of fuel delivery (SoD). An example of typical pressure traces for diesel, along with the rate of heat release, is depicted in Fig. 5.2. All the fuels were injected at 120 MPa.

The pressure in the common rail as a function of time is depicted in Fig. 5.3. The pressure fluctuates between 1075 and 1200 bar (i.e. the injection speed varies over 6%), and therefore the injection rate is not exactly a top-hat profile [29], like

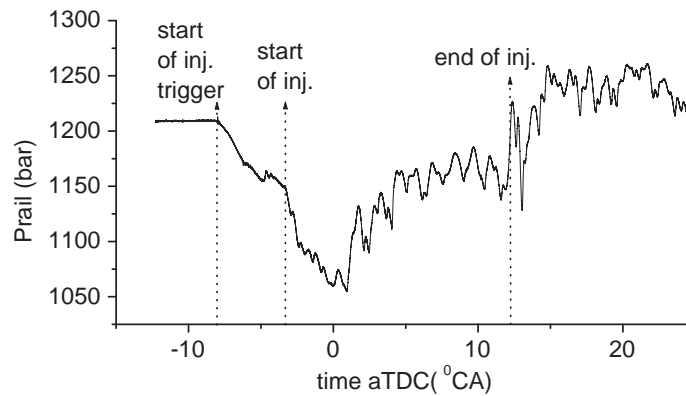


Figure 5.3: (a) Common rail pressure for diesel for an effective injection between -4.5° and 11.0° aTDC. The fuel injection system was triggered between -8.0° and 4.0° aTDC.

employed in many of the lift-off measurements in a single spray by the Sandia group [14, 30]. However, the pressure, and along with it the fuel injection speed, was shown to reproduce very well from fuel to fuel (Ref. [8], supplementary material). Therefore a comparison of the FLoL between different fuels is not complicated by different injection pressures over the course of the injection. For the results presented here, all the oxygen-containing blends were injected from 4.5° bTDC to 13° aTDC, while diesel was injected from 4.5° bTDC to 21° aTDC.

Temperatures and pressures have been derived from in-cylinder pressure measurements. The temperature of the in-cylinder air entrained by the spray has been assessed both before the start of combustion and during the combustion.

5.2.3 OH chemiluminescence measurements

It has been shown by Tacke et al. [31] that in a lifted, turbulent diffusion flame, near stoichiometric combustion occurs at the lift-off length. The high temperatures at this condition give rise to a high concentration of OH, which is partly electronically excited (indicated as OH^{*}). Because of its abundance and short lifetime, OH^{*} can conveniently be used as a marker of the high temperature reactions in which it is formed, and as such, of the lift-off length.

Two dimensional line-of-sight chemiluminescence measurements of OH were performed using an intensified CCD camera (16 bit dynamic range, Princeton Instruments), equipped with a UV Nikkor f/4.5 lens. This camera can only record 1 image per engine cycle. OH emits strongly around 310 nm [32]. To isolate light around this wavelength, a WG305 filter, along with a custom filter set (312 nm bandpass and 358 nm short-wave pass, CVI) was used, as advised by Dec and Coy [33]. The 312 nm bandpass filter transmits between 305 and 321 nm (FWHM) with a maximum transmission of 78 %. Although the 358 nm short-wave pass filter blocks the visible and infrared soot luminosity very effectively, the light transmitted in the wavelength range selected does have a contribution from soot, as shown in earlier experiments [8]. The typical gatewidth of 100 μ s averaged out some degree of turbulence and spray dynamics. The spatial resolution was typically 0.24 mm/pixel, differing slightly from

fuel to fuel.

5.2.4 High-speed imaging

The combustion process was recorded through the piston window by a high-speed camera (Phantom V7.1, 160 kHz maximum frame rate, 12 bit dynamic range), as indicated in Fig. 5.1. Separate tests, using a spectrograph and an oxyacetylene flame ($O_2 + C_2H_2$) as a bright OH^* chemiluminescence source, revealed that the spectral sensitivity of this camera starts at around 317 nm, so OH^* signal cannot be detected at high speed.

Unless stated otherwise, an exposure time of 3 μs has been used. Without spectral filtering, the camera would then still be overexposed due to the bright soot incandescence. Therefore a filter combination (BG 18 and GG 475 Schott filters, just as in the measurements presented in [8]) was used, transmitting roughly between 460 and 640 nm. This avoided overexposure under all circumstances.

The camera was synchronized to the crankshaft of the engine and operated in the memory gate mode: image acquisition was triggered by injector activation and enabled for around 8 ms, after which it was halted until the next injection, in order to rapidly record multiple injections and use camera memory more efficiently. Images were recorded every 0.3° crank angle (CA) ($\approx 35 \mu s$), resulting in around 230 images per injection event. A spatial resolution of 0.19 mm per pixel has been obtained. In order to determine the reproducibility of the results, at least 10 injections were performed for each experimental setting (fuel, engine operating condition).

5.2.5 Soot exhaust measurements

The filter smoke number (FSN) of the measurement cylinder has been determined in the exhaust, using an AVL 415S smoke meter. The correlation between the FSN and soot (mg/m^3), as given in the manual, has been used together with the indicated mean effective pressure (IMEP) to calculate the amount of soot per kWh. The skip-fired operation of the engine necessitated a conversion to a continuous operation mode. The conversion scales the skip-fired mode result by the skip-fire ratio and an additional factor accounting for the fact that the sampling occurs non-isokinetically (see Sec. 5.6). For normal inlet air, the measured FSN was below the sensitivity limit. Therefore, only results for EGR conditions are reported.

5.3 Analysis of the lift-off length

A typical OH chemiluminescence image in case of DBM as a fuel is shown in Fig. 5.4a. As a first step in the analysis, the CCD camera image was noise filtered by a 3×3 neighborhood median filter. All pixel values were corrected first for the background intensity mainly due to scattering from the cylinder head. This scatter was relatively homogeneous, and therefore the intensity close to the injector in between the liquid sprays, where no combustion occurs, was taken as representative of this background intensity. The liquid core of the spray, as indicated in Fig. 5.4a, was excluded from the analysis. In principle, the FLoL, being defined as the closest position to the injector where significant OH chemiluminescence is observed, could be overestimated

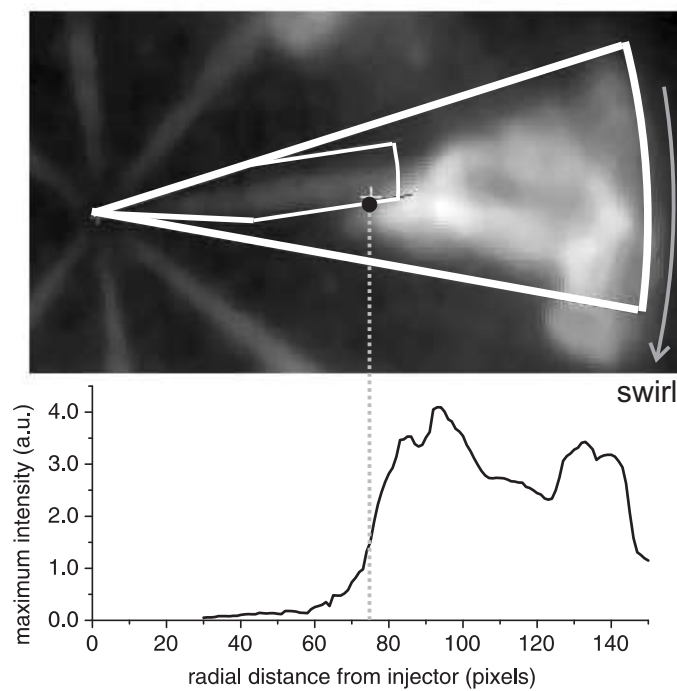


Figure 5.4: (a) Typical OH chemiluminescence image for DBM as a fuel. The intensity is linear in the square root of the pixel value, to enhance contrast at low intensity, i.e. for the liquid spray. The area spanned by the wide cone is the area of analysis. The narrow cone around the liquid spray indicates the area excluded from the analysis. (b). Maximum intensity vs. radial distance from the injector. The FLoL is indicated by the gray dotted line and the black dot.

when chemiluminescence occurs in this excluded area. However, generally the chemiluminescence closest to the injector is at the swirlwise side of the liquid core. The grayscale in the image is linearly proportional to the square root of the pixel values, to enhance contrast in low intensity areas. Then, to assess the flame lift-off length, the closest distance to the injector was determined where the intensity on a single pixel basis is above a certain threshold value. In this sense, the method described by Higgins and Siebers [34] is followed here. The analysis was restricted to a cone around the spray axis, slightly rotated in swirlwise direction, as shown in Fig. 5.4a. The threshold was set to a certain percentage of the maximum pixel value occurring in the cone of analysis. In Fig. 5.4b, the maximum pixel value vs. the radial distance from the injector for the image in Fig. 5.4a is depicted. Clearly at a certain distance, the intensity rises steeply. This makes the FLoL relatively insensitive to the precise value of the threshold. This dependence over a reasonable range of variations of the threshold (between 10 and 35% of the maximum intensity) was generally weaker than the variations in FLoL between single injection events. In the present paper, the threshold is set at 25% of the maximum. The data points depicted for the FLoL in the remainder of this paper represent an average over typically five injections.

Analogous to the OH-chemiluminescence based FLoL, the soot lift-off length (SLoL) will be defined here as the position closest to the injector where significant soot luminosity is observed. In Fig. 5.5 a typical image measured by the high-speed camera is shown. The liquid core (pencil-like shape) was excluded from the analysis,

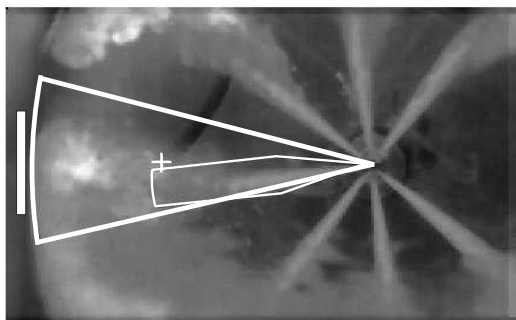


Figure 5.5: Typical high-speed camera snapshot for DBM as a fuel. The big cone, ranging from the injector to the edge indicates the area of analysis, the pencil-like cone the area excluded from the analysis, to avoid taking into account scattering from liquid fuel. The center of the '+' indicates the soot lift-off location.

The high-speed images were further treated like those of the ICCD camera (OH*).

5.3.1 Temperature and density scaling law of FLoL

Since our aim is to compare FLoL data for different fuels, the measurements must be converted to a common set of reference conditions for the in-cylinder air (density and temperature). In an isolated spray (using a diesel fuel), the effect of temperature and density was found by Siebers and Higgins [35] to be given by

$$FLoL = FLoL' \cdot \left(\frac{\rho}{\rho'}\right)^{-0.85} \cdot \left(\frac{T}{T'}\right)^{-3.74} \quad (5.1)$$

where T refers to the temperature and ρ to the density. Primed and unprimed quantities refer to reference and actual conditions, respectively. The dependence on temperature is clearly much larger than the effect of density. The dependence of FLoL on temperature and density depends slightly on the specific fuel [9], but the exact relation is unknown and Eq. 5.1 will be used here.

In an engine, the dependence of the FLoL on temperature and density is expected to be weaker than in a combustion vessel (Eq. 5.1) [36]. Therefore, the result of applying Eq. 5.1 to correct for different in-cylinder conditions from fuel to fuel, constitutes an upper limit for the correction.

5.4 Luminosity

5.4.1 Analysis of intensity

The total signal in the cone around a single spray (Fig. 5.5) was taken as the measure for soot luminosity. Like with the analysis of the SLoL, the liquid core (pencil-like shape) was excluded from the analysis, even though the light scattered by it will largely have been due to the natural luminosity.

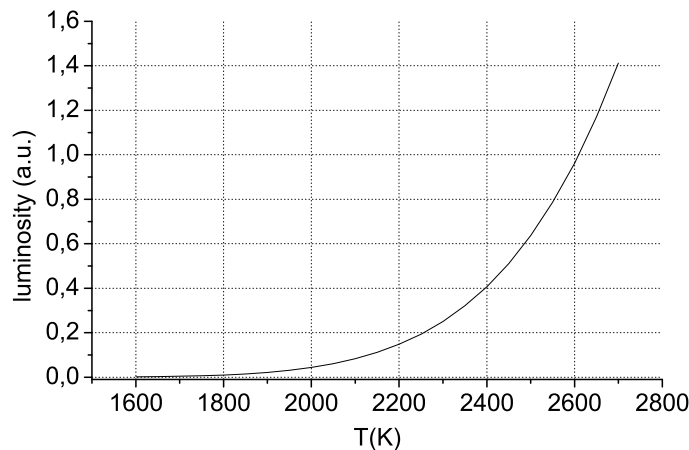


Figure 5.6: Calculated luminosity vs. temperature, for a constant amount of soot.

5.4.2 Factors affecting the luminosity

Mueller and Martin [25] excellently discuss the factors that have to be taken into account when extracting the relative amount of soot from the natural luminosity. We here cover only the factors that are specific to our case, and different from their situation.

Temperature

The temperature of the radiating soot is of paramount importance in the analysis, since it heavily impacts the luminosity, as will be discussed now. The luminosity detected as a function of temperature depends on the blackbody spectral emissive power, the soot particle spectral emittance (Rayleigh regime), the spectral transmittance of the optical filters and the spectral sensitivity of the camera (see Ref. [25] for more details). Combining all these factors, the dependence of the total luminosity S on temperature T (see Fig. 5.6) in our setup is approximated by $S \simeq T^{13}$ for the range between 1800 and 2700 K (T^{11} was found in Ref. [25]). Thus, only the hottest soot is observed, which is expected to be present at the rich side of the diffusion flame enveloping the reacting spray. This soot is expected to have a temperature of around 2350 K [25], based on the adiabatic flame temperature lowered by 300 K as estimated by Mueller and Martin [25]. For the EGR-like condition with inlet air containing only 15.3% O_2 , it is expected to be around 1950 K.

Under otherwise similar conditions, there might be differences in the adiabatic flame temperature between the various fuels, affecting the luminosity of the radiating soot. Nabi et al. [37] suggest, however, that these differences will be small, as the lower heat content of oxygenates is basically balanced by the lower stoichiometric air-fuel ratio. Also Mueller and Martin [25] show by simulation that for their three fuels tested (two oxygenates and one non-oxygenate), the adiabatic flame temperature for all fuels is virtually the same, over a wide range of equivalence ratio's.

Although hardly dependent on the specific type of fuel, the adiabatic flame temperature does depend on the in-cylinder air temperature. At a fixed crank angle,

the in-cylinder air temperature is influenced by the intake air temperature and the accumulated amount of heat released. The method to calculate the in-cylinder air temperature has been described in section 5.2.1. The accumulated RoHR did not vary a lot over the fuels and therefore, the in-cylinder air temperature was virtually the same for all the fuels during the combustion, except from CH_xnO(9%). For this fuel, the intake air temperature was (inadvertently) 20 K higher than for all the other fuels. This results in an in-cylinder averaged temperature at TDC of 883 K rather than 840 K.

Differences in the in-cylinder air temperature influence the adiabatic flame temperature and therefore the temperature of the glowing soot. In order to extract a better measure for the amount of soot formed from the ‘raw’ luminosity data, differences in temperature of the soot have been taken into account in graphs of the integrated luminosity as a function of time (using the T^{13} scaling law). From now on, the term ‘luminosity’ is actually used for the total luminosity corrected for the temperature effect.

Optical thickness

Soot opacity may result in trapping of part of the luminosity. Musculus et al. [23] have shown that for surrogate diesel, the line of sight integrated optical density, perpendicular to the spray axis, can be 1.6, corresponding to a transmission of only 20%. They used a HeNe laser (632.8 nm) as a radiation source. Thus, the recorded luminosities should be interpreted as lower limits for the actually emitted luminosity. Luminosity trapping is not expected to affect the SLoL-determination (given a reasonable amount of symmetry around the spray axis), but it needs to be kept in mind if fuels are compared among each other on luminescence properties. Although Mueller et al. [38] show that in their optical engine, the luminosity scales with the jet integrated amount of soot, this relation does not necessarily hold in general. Since the recorded luminosity depends very strongly on emitter temperature, there is no obvious general relation between spray opacity and recorded luminosity.

Piston window fouling

For all the fuels, loss in signal was apparent over the full engine run (typically 10 operating conditions of 10 to 20 injections each), even though for diesel this effect was more significant than for the other fuels. Therefore, only luminosity data from the first two operating conditions (only the first for diesel) are presented for comparison between different fuels. The decrease in luminosity is attributed mainly to piston window fouling and for only a small part to oil deposits on the engine outcoupling mirror. Only the piston window fouling is covered here. At normal inlet air conditions, the luminosity of diesel has been averaged over only the first 5 injection events since the measurements clearly suffered from piston window fouling. This was derived from the fact that the luminosity dropped by roughly 35% over the 20 injection events recorded for the operating condition applied as first. For the other fuels, no significant loss in signal was observed over the course of one operating condition (of around 20 injection events) and all the injection events were used. For the normal inlet air condition, the injection duration of the oxygenates was shorter than for diesel. Thus, the significant

piston window fouling for diesel during one operating condition does not suggest that the oxygenates form less soot than diesel and/or have a better oxidation, as a longer injection duration causes higher soot emissions.

5.5 Results and Discussion

The Results and Discussion section is divided into two main parts, according to the inlet-air conditions. First, the normal inlet air conditions will be addressed, then the EGR-like conditions. We choose to compare different fuels at identical moments after their respective start of combustion (time after start of RoHR, or ‘time aSodQ (°CA)’), since this time indicates the period elapsed after the burning spray started to develop. For all fuels, and both for EGR (Fig. 5.14a) and normal inlet air (Fig. 5.7a), the FLoL decreases with advancing combustion, as has been observed in other studies [24, 39, 40].

This decrease over time can be explained by the rising in-cylinder air temperature and density due to combustion. Especially a rise in temperature is known to significantly decrease the FLoL in an isolated spray in a combustion vessel, as reported by Siebers and Higgins [35] (Eq. 5.1). A steady-state lift-off length is not readily established, similar to the result shown by Idicheria and Pickett [40] for the 21% O₂ condition. Another contribution to the decrease in FLoL over the injection event might be an increase of the vapor phase spray angle. Such a behavior has been observed for spray development in a constant-volume high-pressure high-temperature environment [41], and is associated with enhanced air entrainment [29].

5.5.1 Normal inlet air

Flame lift-off length and ignition delay

Because of the moving piston, the in-cylinder air conditions change with ignition delay. When investigating the relation between fuel-specific ignition delay and fuel-specific FLoL, both the ignition delay and the FLoL should be scaled to a common set of reference in-cylinder air conditions. Figure 5.7a presents the flame lift-off length (derived from OH*) for normal inlet air, as a function of ϑ_{aQ} . The result of scaling, using Eq. 5.1, is shown in Fig. 5.7b. As reference condition, the in-cylinder air temperature and density for diesel fuel at 3.6° aSodQ have been taken (indicated by the arrow in Fig. 5.7a). The RoHR for the fuels concerned is shown in Fig. 5.7c. The combustion timing of diesel is virtually the same as for CH_xnO(5%) and DBM, although the RoHR is somewhat higher, due to its larger energy content. CH_xnO(9%) ignites slightly later and its RoHR is smaller than for the other fuels. Anisole has a much larger ignition delay than all the other fuels and ignites when the in-cylinder air temperature and density decrease significantly due to the downward piston motion. The lower in-cylinder air temperature and density during the combustion are the reasons for the big effect of scaling on the FLoL of anisole. The scaling constitutes an upper limit, however (see Sec. 5.3.1), and the FLoL of anisole is likely to be larger than the FLoL of diesel and CH_xnO(9%). Also the ignition delay is affected by the density and temperature of the in-cylinder air. Only anisole ignites at considerably lower density

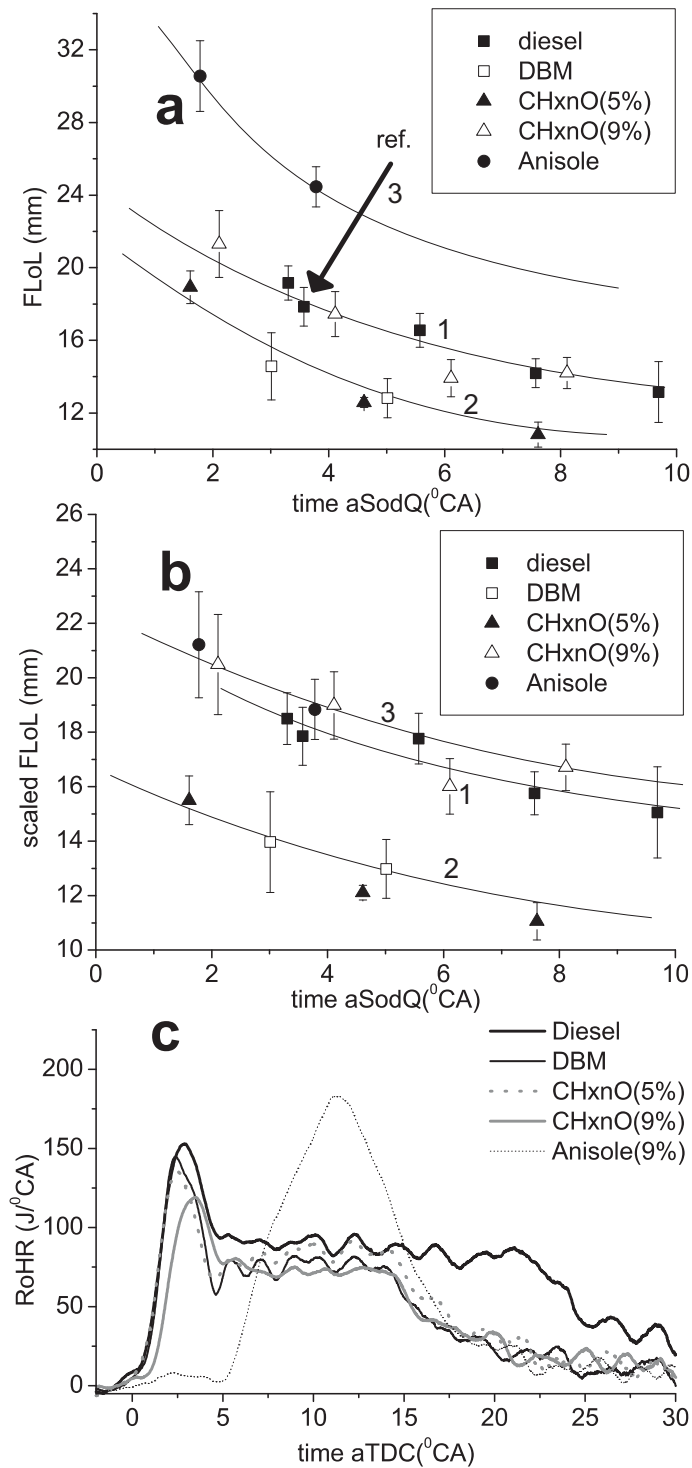


Figure 5.7: (a) FLoL for normal inlet air vs. time aSodQ(°CA). The trend lines for the different fuels are annotated with the numbers indicated in the legend. For anisole, a trend line shaped as generally observed is assumed. (b) FLoL from a) corrected for differences in in-cylinder air conditions. The conditions applying to the data point for diesel, indicated by the arrow in a), have been taken as reference conditions. (c) Corresponding RoHR for the fuels. Note the different horizontal scales.

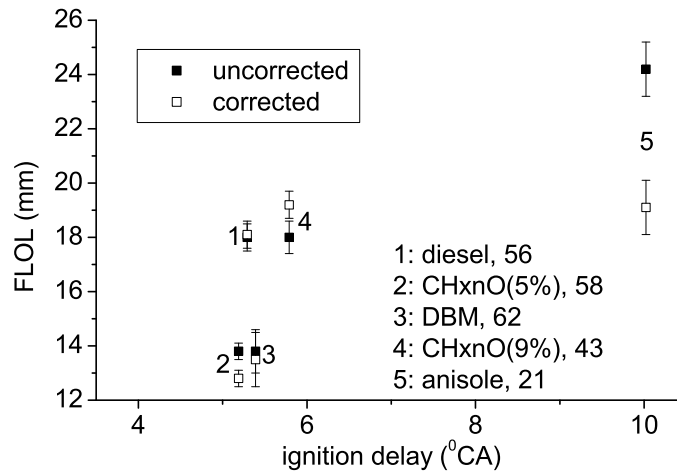


Figure 5.8: FLoL (closed) and scaled (open) FLoL vs. ignition delay for normal inlet air conditions. The fuel associated with each set of two data points is indicated, together with its cetane number.

and temperature than the other fuels^a, because of its large ignition delay. Therefore, for a common set of in-cylinder air conditions, the difference between the ignition delay for anisole and the other fuels would be slightly smaller. The scaled and unscaled FLoL are depicted in Fig. 5.8 vs. the ignition delay^b. Only for anisole the scaled and unscaled FLoL differ considerably. The FLoL at similar conditions as the diesel reference point (i.e. applying a scaling pertaining to our engine rather than to a single spray in a combustion vessel) would be somewhere in between the scaled and unscaled FLoL. The FLoL for DBM and CH_xnO(5%) overlap within experimental accuracy.

Thus, it may be concluded from Fig. 5.8 that the flame lift-off length increases with ignition delay for the oxygenates, even though there is no one-to-one relation. For diesel the FLoL is relatively high. The results presented here are in line with the work of Pickett et al. on a single spray [9, 14], who show that fuels with a shorter ignition delay do generally exhibit shorter lift-off lengths, with some exceptions. Also the engine measurements of Musculus et al. [23] suggest a weak correlation between the FLoL and the ignition delay for the oxygenates they tested, as mentioned already in the introduction.

Note that the higher cetane number fuels diesel, DBM and CH_xnO(5%) have a comparable ignition delay (Fig. 5.8), in correspondence with their cetane numbers. The lowest CN fuels exhibit the largest ignition delay.

Luminosity

Figure 5.9 shows an example of the typical development of the soot luminosity as recorded by the high-speed camera within one injection event, using DBM as a fuel.

^aDifferences in in-cylinder air flow are not considered here.

^bDifferences in density between fuels give rise to different injection velocities (Bernoulli's equation) and proportional differences in the FLoL [35]. The differences in density are small, however (see Tab. 5.2), and the effect on injection velocity is not corrected for.

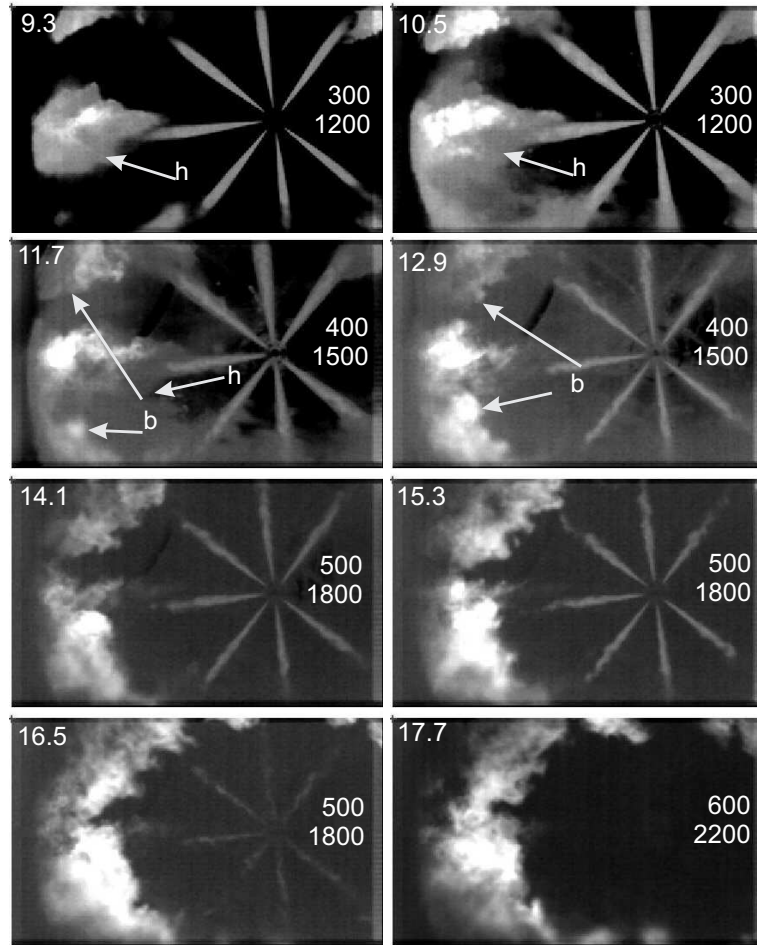


Figure 5.9: Typical sequence of snapshots taken by the high-speed camera within one injection event, for DBM, normal inlet air conditions. See text for details.

High-speed movies can be found in the supplementary material provided at the website given in section 5.6. The numbers at the upper left indicate the time ($^{\circ}\text{CA}$) elapsed after SoD. The numbers at the middle right denote the grayscale lower (black) and upper (white) limit. At first, soot appears mainly at the downswirl side of the spray. Then the luminosity increases in intensity and progresses upstream. A few $^{\circ}\text{CA}$ after the appearance of the first soot, large clouds of soot that have been bounced back from the piston bowl show up, labeled ‘b’. These clouds of soot (and other recirculating combustion gases) progress upstream, obscuring the ‘bowl’ soot.

Figure 5.10 shows typical soot luminosity images for the various fuels at around 8.2° aSodQ. At that time, the early soot structure is well developed. For all fuels, some soot is visible in the recirculation zone, just as in Fig. 5.9. The diesel soot plume starts relatively close to the injector, as will also be shown below by the SLoL analysis. For anisole, the dwell between SodQ and the first soot is longer than for the other fuels and the soot forms only far downstream (labeled ‘s’ at spray 1) and is quickly blurred by the bounced soot cloud.

Figure 5.11 shows the luminosity as a function of time. The gray bands around the curves represent the standard error, derived from the different injection events. Only for the $\text{CH}_x\text{O}(9\%)$ blend, the in-cylinder air temperature differs significantly

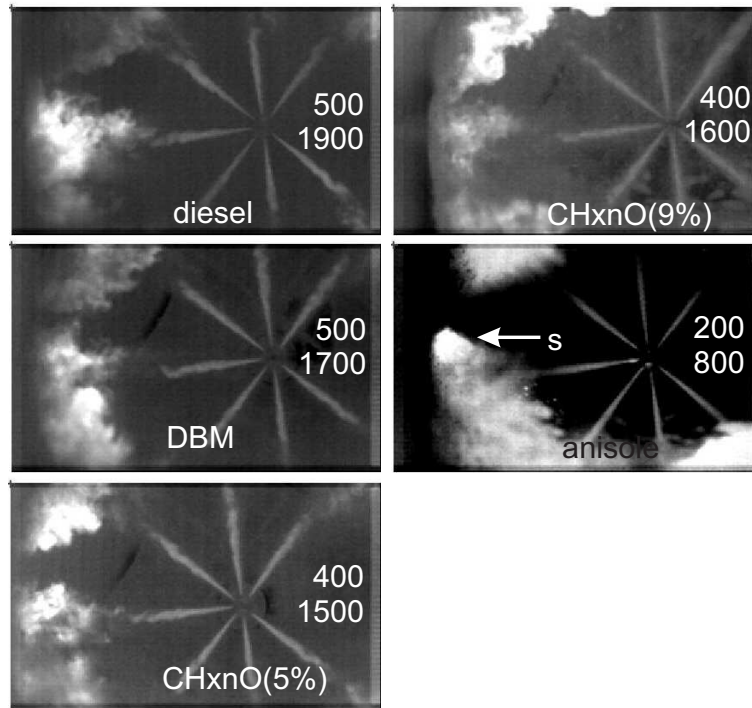


Figure 5.10: Typical snapshots for all fuels tested at 8.2° aSodQ. Minimum (black) and maximum (white) values of the grayscale are indicated.

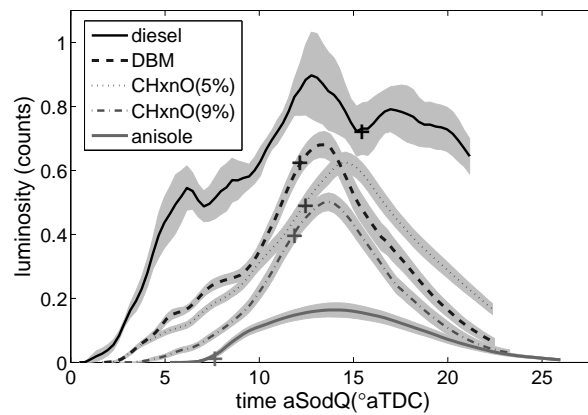


Figure 5.11: Luminosity vs. time for different fuels, normal inlet air conditions. The '+' signs superimposed on the curves mark the end of injection of the respective fuel

from the other fuels; it was calculated to be 43 K higher due to the increased inlet air temperature. The effect of this increased temperature on the adiabatic flame temperature was estimated using a homogeneous reactor simulation (extensive LLNL PRF mechanism [42]) with an equivalence ratio of one, as described in [27]. The adiabatic flame temperature was calculated to be 22 K higher for CHxnO(9%) compared to the other fuels, giving rise to 13% more luminosity. This effect has been corrected for. Moreover, the curves have been scaled by the indicated mean effective pressure (IMEP), since eventually the amount of soot per kWh is of importance. For diesel, which had a longer injection duration, the measured IMEP for an injection duration

equally long as the other fuels was taken. The assumption throughout the article is that the initial part of combustion does not change with injection duration, since the skip-firing prevents the engine from heating up considerably due to combustion.

The curves for DBM and CH_xnO(5%) virtually overlap, at least until the end of the injection. For CH_xnO(9%) it clearly takes longer for soot to appear. Around the end of injection, the luminosity increases in time but is still well below the luminosity of DBM and CH_xnO(5%). Diesel shows the highest luminosity. The interpretation of these observations will be discussed next.

Relation between oxygen ratio at the FLoL and luminosity

The production of soot is possibly affected by a lot of factors, such as the ignition delay, the chemical composition of the fuel, the fuel oxygen content, the in-cylinder air temperature and density, and the FLoL. Therefore, when studying the effect of one of these parameters on the soot production, also the effect of changes in the other parameters needs to be considered.

The FLoL is an interesting quantity to investigate in relation to soot formation, since it is closely related to the amount of air entrained upstream of the closest location of combustion to the injector. As a matter of fact, the oxygen ratio Ω (as introduced by Mueller et al. [38]) at the FLoL, $\Omega(FLoL)$, will be related to the luminosity, rather than the FLoL itself. The oxygen ratio basically describes the total amount of oxygen available in the fuel-air mixture, divided by the amount of oxygen required for stoichiometric combustion. It accounts for both the fuel-bound oxygen and the oxygen in the entrained air. The oxygen ratio is related to the fuel equivalence ratio ϕ by [38]

$$\Omega = \Omega_f + \frac{1 - \Omega_f}{\phi} \quad (5.2)$$

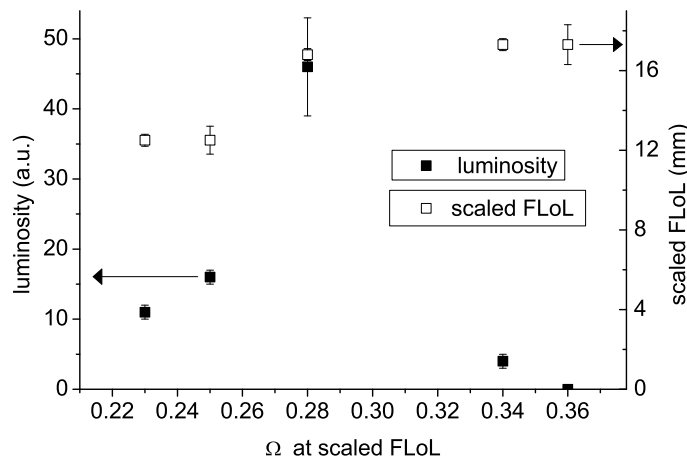
where Ω_f is the oxygen ratio of the fuel, i.e. the amount of oxygen in the fuel relative to the amount of oxygen needed for stoichiometric combustion. Thus, for fuels with no fuel-bound oxygen, the oxygen ratio is the inverse of the equivalence ratio. Using the correlation reported by Naber and Siebers [29], the air (and thus oxygen) entrainment for the fuels at the flame lift-off location can be estimated. The spray angle, required as an input to the penetration correlation, was determined by Schlieren measurements in the Eindhoven high-pressure high-temperature cell [41], for diesel as a fuel and in-cylinder air conditions (temperature 840 K, density 17.4 kg/m³) typical for our engine.

When examining the relation between the soot production and Ω at the fuel-specific FLoL, again both parameters should be scaled to a common set of reference conditions. For the soot production (i.e. the T^{13} -corrected luminosity), this scaling comprises two effects. First, with a change in in-cylinder air temperature and density related to the scaling, the soot formation chemistry is influenced. Second, the change in FLoL (and $\Omega(FLoL)$ accordingly) related to the scaling gives rise to a change in air entrainment at the lift-off location. Even though it is hard to tell to what extent both factors affect the soot production, the direction of the change can be predicted. For CH_xnO(9%), for instance, the higher in-cylinder air temperature increases soot formation^c, more than the lower density is expected to reduce the formation of soot

^cIt also enhances soot oxidation.

Table 5.3: FLoL, scaled FLoL, luminosity at 6° aSodQ, ignition delay (ID), and the oxygen ratio Ω , for normal inlet air. See text for details.

Fuel	FLoL (mm)	scaled FLoL (mm)	Luminosity (a.u.)	ID (°CA)	Ω_f	Ω at scaled FLoL
CH _x nO(5%)	13.4 ± 0.3	12.5 ± 0.3	11 ± 1	5.2	0.0146	0.23 ± 0.01
DBM	13.4 ± 0.7	12.5 ± 0.7	16 ± 1	5.4	0.0289	0.25 ± 0.02
Diesel	16.0 ± 0.2	16.8 ± 0.3	46 ± 7	5.3	0	0.28 ± 0.01
CH _x nO(9%)	16.0 ± 0.3	17.3 ± 0.3	4 ± 1	5.7	0.0285	0.34 ± 0.01
Anisole	20.8 ± 1	17.3 ± 1	0	10.0	0.0307	0.36 ± 0.02

**Figure 5.12:** Luminosity and scaled FLoL vs. Ω at the scaled FLoL, normal inlet air conditions. Lines to guide the eye are indicated.

[10]. A larger FLoL relative to the unscaled FLoL increases the amount of air entrained by the spray before combustion starts at the lift-off location, thereby reducing the soot formation [35]. Thus, both the change in in-cylinder air temperature and change in FLoL at the scaled condition give rise to a lower estimated soot formation for CH_xnO(9%) at the reference condition. This way of reasoning will be used below for the other fuels as well.

In Table 5.3 the FLoL, scaled FLoL, the oxygen ratio, and luminosity at 6° aSodQ (around 2° after the start of the diffusion burn) are given. The FLoL has been extracted from the trend lines drawn in Fig. 5.7a. Error estimates are included in the table. The uncertainties for anisole and DBM at 6° aSodQ are relatively large, since the trend lines at this point in time are based on an extrapolation of only two data points. Fig. 5.12 shows the luminosity and the scaled FLoL vs. Ω at the scaled FLoL. For the oxygenates, there is an inverse correlation between Ω at the scaled FLoL and the luminosity. This correlation is even clearer when the soot production is scaled to the common set of reference conditions.

To put the connection between lift-off length and oxygen entrainment into perspective, differences in the amount of oxygen entrained by the various fuels at the

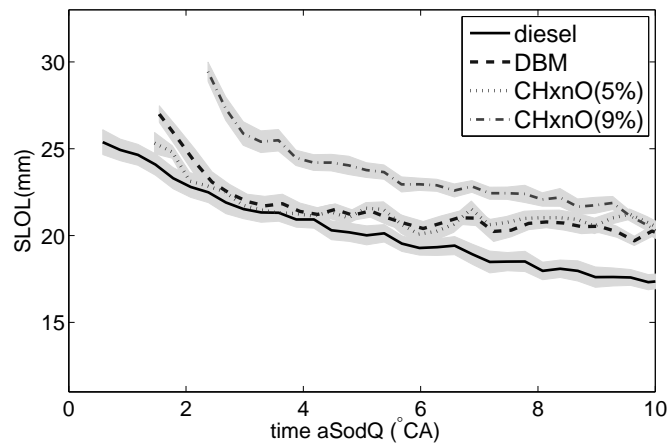


Figure 5.13: SLoL for normal air. The gray bands indicate the standard error from the different injection events.

scaled lift-off length are compared to differences in the fuel-bound oxygen content. As can be seen by comparing Ω and Ω_f in Table 5.3, only a small part of the oxygen content in the fuel air mixture at the lift-off location is fuel-bound oxygen whereas the majority originates from entrained air. Fig. 5.12 shows that for the oxygenates, the largest values of Ω occur at the largest values of the scaled FLoL, suggesting that the FLoL is of importance for the amount of oxygen present at the scaled lift-off length. The importance of the FLoL can be illustrated by comparing for example DBM and CHxnO(9%). Both blends need comparable amounts of oxygen for combustion and are assumed to have similar physical spray characteristics, so differences in Ω at the FLoL are mainly caused by differences in the FLoL itself. The difference is 0.09, around a factor of three more than Ω_f . Therefore, the variation in oxygen entrainment at the lift-off location between the individual fuels is expected to significantly contribute to variations in the soot formation, even though fuel bound oxygen is probably more effective for soot abatement than entrained oxygen [9, 23, 43].

SLoL

Figure 5.13 shows the SLoL for the tested fuels. The data for anisole are not included, since for that fuel soot is present mainly after the end of injection, when the SLoL concept loses its meaning. The reproducibility of the SLoL-data is good, judging from the narrow ranges of standard deviations. For all the fuels, the SLoL decreases over the course of the injection, just as the FLoL does.

Comparing Figs. 5.11 and 5.13, the SLoL and the peak luminosity appear to inversely correlate, as was also observed by Pickett and Siebers [9]. It can be argued that a longer SLoL implies a lower overall soot production. Net soot destruction is believed to start at a fixed oxygen carbon ratio (oxygen both from air and fuel), independent of the specific kind of fuel [9]. Therefore, the more downstream the soot is formed, the less time it has to accumulate and grow before net oxidation sets in. Hence, all other factors being equal, a larger SLoL would imply a smaller soot production, in agreement with the observed inverse correlation between the luminosity and SLoL.

CH_xnO(9%) clearly has the largest SLoL, in line with its FLoL. The SLoL data for CH_xnO(5%) virtually overlap those of DBM, as do those of luminosity and FLoL. Diesel exhibits the smallest SLoL, in contrast to its FLoL, indicating that it has the shortest soot inception time, possibly due to a combination of its zero oxygen content and non-zero aromatic content. The soot inception time indicates the time it takes for soot to form after reactions have begun. According to Dec's conceptual model [44], the position of the first reactions where soot precursors are formed, is close to the FLoL, inside the diffusion flame core. ^d Thus, a reasonable measure for the position of the first reactions is the FLoL [9]. The soot inception time is taken here, like in Ref. [9], as the time it takes for a package of fuel to cover the distance from the FLoL to the SLoL. Accordingly, the fuel velocity unlikely to be dependent on fuel, the distance between the SLoL and the FLoL is proportional to the soot inception time. The soot inception time is used here as an indicator of the effect of the chemical composition of the fuel on soot formation. Thus, for diesel fuel, having a small soot inception time, the soot-enhancing effect of the chemical composition (aromatics) outweighs the soot-reducing effect of the relatively large FLoL.

CH_xnO(9%) has a lower luminosity than DBM. The soot inception time is roughly equal for both fuels, considering the difference between the SLoL and FLoL (Fig. 5.7a and 5.13). The difference in ignition delay of only 0.3° is not expected to make a significant contribution to the difference in luminosity either, since it is a short period relative to the diffusion combustion phase of around 10°. Thus, the fuel-bound oxygen content being equal, the difference in sooting propensity between both fuels may be related to the difference in the FLoL.

DBM and CH_xnO(5%) exhibit the same FLoL and SLoL and also comparable luminosity. Thus, the 5% oxygen of CH_xnO(5%) seems equally efficient in reducing soot formation as the 9% oxygen of DBM.

Anisole combustion results in the lowest luminosity. In fact, (hot) soot only shows up around the end of injection. Since anisole contains aromatics, it is quite surprising that the soot does not show up already closely after the start of combustion and just downstream of the FLoL, just like with diesel. A reason might be that the in-cylinder air temperature and density during combustion are lower than for diesel, because of the retarded combustion, slowing down the process of soot formation.

5.5.2 Effects of EGR

Flame lift-off length and ignition delay

Figure 5.14 shows data analogous to those in Fig. 5.7, but for simulated (cooled) EGR conditions. These data show more scatter and are less easily interpreted. The FLoL of diesel, only recorded early in the combustion stroke, is smaller than that of CH_xnO(9%) but clearly larger than that of DBM, as can be seen in Fig. 5.14a. Unfortunately, the single data point for CH_xnO(5%) does not permit comparison with other fuels. Figure 5.14b shows the lift-off length, corrected for density and temperature effects, using the same reference condition as for Fig. 5.7b. Trend lines are indicated. In Fig. 5.14c, the RoHR for the different fuels is depicted. The values

^dThe exact position depends slightly on operating condition citeSAE2006-01-3434 and possibly also on fuel.

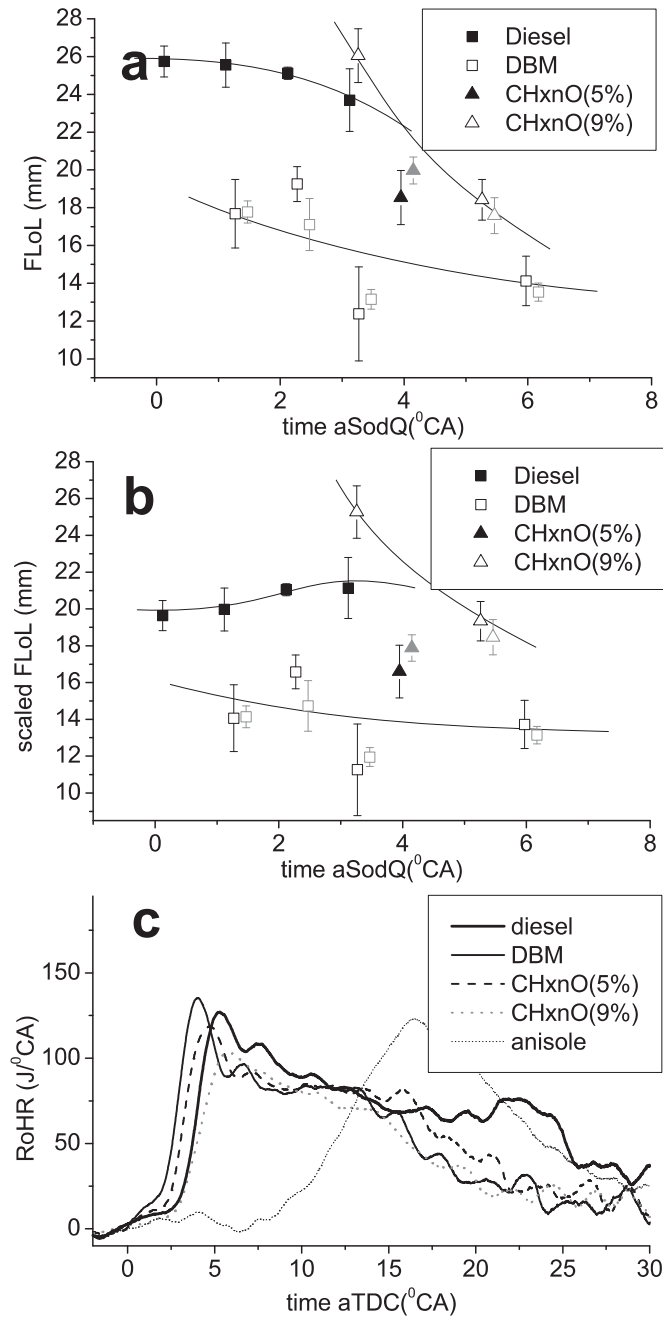


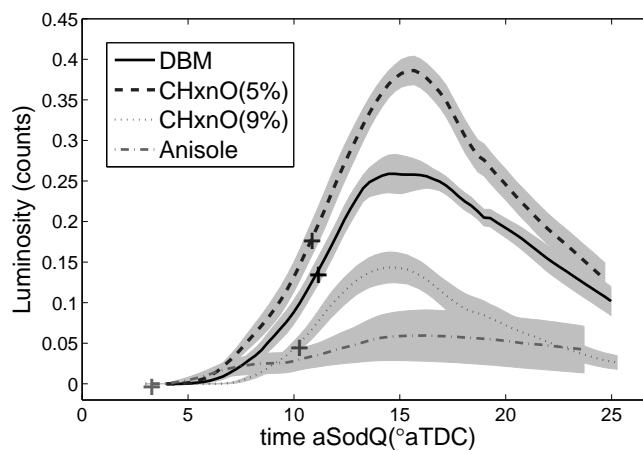
Figure 5.14: (a) FLoL for EGR. For CHxnO(9%), a trend line shaped as generally observed is assumed (b) FLoL from a) corrected for differences in in-cylinder air conditions. (c) Corresponding RoHR for the fuels, on a different horizontal scale.

for the ignition delay and representative (scaled) FLoL, extracted from Fig. 5.14b are listed in Table 5.4. DBM has both the smallest ignition delay and lift-off length. The ignition delays of diesel and CHxnO(9%) are comparable, while the lift-off length of CHxnO(9%) is larger.

Note that for diesel and CHxnO(9%), the FLoL at EGR conditions is larger than with normal inlet air, as expected from studies of Siebers et al. [30] and Ito et al. [45]. For DBM however, the FLoL at EGR conditions is comparable to that at normal inlet air conditions, within the measurement uncertainty.

Table 5.4: Ignition delay ID, the FLoL, and scaled FLoL Ω at 3.2° aSodQ, the luminosity (addressed in section 5.5.2) at the end of injection, EGR conditions.

Fuel	FLoL	Scaled FLoL (mm)	Luminosity (a.u.) at end of injection	ID (°CA)
DBM	15.7 ± 1	14.1 ± 1	0.13 ± 0.02	6.5
Diesel	23.7 ± 0.5	21.2 ± 0.5	-	7.7
CHxnO(9%)	26.0 ± 1	25.2 ± 1	0.042 ± 0.008	7.5
CHxnO(5%)	-	-	0.165 ± 0.02	6.8

**Figure 5.15:** Luminosity, scaled by the IMEP of the respective fuels, vs. time for EGR inlet air conditions. CHxnO(9%) has been corrected for its higher soot temperature. The ‘+’ signs superimposed on the curves mark the end of injection of the respective fuel.

The difference in FLoL between diesel and DBM is larger relative to the 21% O₂ inlet air condition. The explanation might lie in the fact that the incorporated oxygen becomes increasingly important at EGR conditions. No indications have been found in literature, however, that the FLoL of oxygenates decreases relative to the FLoL of non-oxygenates at EGR conditions.

Luminosity and exhaust soot

The luminosity of the oxygenates at EGR conditions as a function of time and scaled by the IMEP of the respective fuels, is depicted in Fig. 5.15. Again, the effect of the higher inlet air temperature on the luminosity has been taken into account for CHxnO(9%). Anisole is hard to compare with the other fuels, since the temperature of the soot is hard to estimate as the soot only shows up when the spray has already ceased to exist. The reason for the large standard deviation for anisole is probably the large ignition delay, which reduces the coupling between injection and combustion. Diesel was not included since we did not have information on the degree of window fouling. As can be seen in Table 5.4, CHxnO(9%) has a longer FLoL but a lower luminosity than DBM. Thus, also at EGR conditions, the soot reducing capability of

Table 5.5: Soot in the exhaust at EGR conditions for two injection durations ΔInj

Fuel	soot(mg)/kWh,	
	$\Delta Inj = 17.5^\circ$	$\Delta Inj = 25.5^\circ$
Diesel	-	250.1 ± 25
DBM	18 ± 2	102 ± 10
CHxnO(5%)	25 ± 3	123 ± 12
CHxnO(9%)	6 ± 1	79 ± 8
anisole	0	59 ± 6

CHxnO(9%) may be related to the long FLoL.

The low luminosity of CHxnO(9%) relative to DBM and CHxnO(5%) is more pronounced in the EGR case (Fig. 5.15) than for the normal inlet air case. This corresponds to the fact that CHxnO(9%) performs increasingly well in reducing the exhaust-gas soot concentration with rising EGR levels, as reported by Boot et al. [5]. Exhaust gas measurements have also been performed with a longer injection duration (i.e. 25.5° CA); these results are given in Table 5.5. With longer injections, the relative importance of the premixed combustion phase is reduced. Again, CHxnO(9%) shows a lower exhaust soot concentration than DBM and CHxnO(5%), indicating that it is not the larger ignition delay that is mainly responsible for the low soot production. At an inlet air temperature of 40°C for CHxnO(9%), the amount of soot in the exhaust would likely be even smaller. This was concluded from separate measurements applying a 5° earlier injection timing, where the experiment with 40°C inlet air temperature produced around two times less soot than the experiment ran at 60°C . Thus, the low soot concentration of CHxnO(9%) in the exhaust is at least partly linked to the long FLoL. The SLoL data cannot be used in the EGR case to infer the soot inception time and derive from it some information on the influence of the chemical composition. The reason is that the soot observed has all been formed close to the piston bowl. This indicates that the soot is formed further downstream than at normal inlet air conditions, in line with expectation [30].

In Fig. 5.16, the luminosity at the end of injection (from Fig. 5.15) is plotted vs. the PM in the exhaust. As indicated by the trend line, the exhaust soot rises with luminosity, suggesting that for the fuels tested here, the luminosity is a good measure for the net amount of soot produced and that the oxidation is not drastically different. Even though some other studies also suggest a correlation between luminosity and exhaust soot [25], there is no *a priori* reason for such a correlation. In fact, Lapuerta et al. [46] mention in their review article on the emissions of biodiesels that soot from biodiesels is probably more easily oxidized than soot formed by the combustion of regular diesel.

The exhaust gas measurements for the low-CN fuel anisole show that, as long as the injection duration is shorter than the ignition delay, this aromatic-containing fuel does not produce any soot. Since at EGR conditions the ignition delay is exceptionally long (1.7 ms), anisole might be used even at medium load operation to make diesel engines run virtually soot free. Stournas et al. [26] have also shown that addition of aromatics that increase the ignition delay can result in lower soot emissions. For the longer injection duration, anisole produces almost an equal amount of soot in the

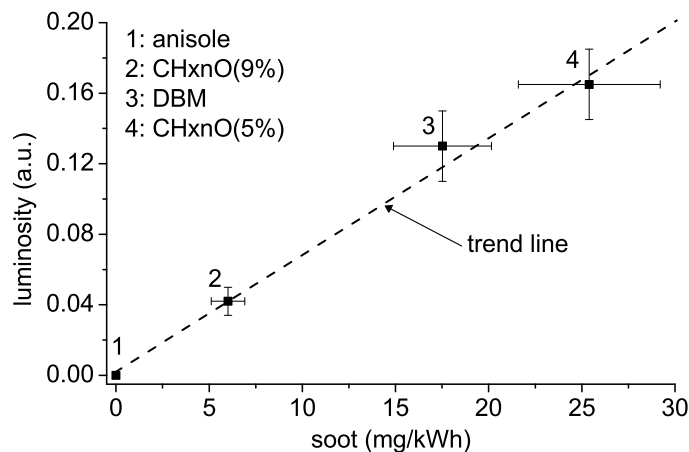


Figure 5.16: Luminosity at the end of injection vs. the amount of soot in the exhaust.

exhaust as CH_xnO(9%), while the soot-promoting diffusion phase is much shorter than that of CH_xnO(9%). This clearly indicates the stimulating effect of aromatics on soot formation, once the formation process has started. More research is needed on the combustion behavior of anisole. The performance with respect to NO_x emissions should be studied, for example, since the large ignition delay likely boosts NO_x emissions. Also the combustion stability and hydrocarbon emissions, amongst others, need to be investigated for anisole.

5.6 Conclusions

The effect of ignition delay on the flame lift-off length and soot production has been tested in an optically-accessible heavy-duty DI diesel engine. The fuels tested include diesel and blends of oxygenated fuels with a wide range of cetane numbers. Both normal inlet air conditions and simulated cooled EGR (15% O₂) were applied. The in-cylinder soot production was measured with a high-speed camera and for the EGR condition, the exhaust-gas soot was measured by a smoke meter. The OH*-based flame lift-off length was measured by an intensified CCD camera.

From a literature study of lift-off measurements in different environments and at different conditions, the hypothesis here is that flame speed determines merely an upper limit for the FLoL. When the oxidizer temperature and in-cylinder air density are high enough to promote auto-ignition before the fuel reaches the lift-off location, the FLoL is likely governed by ignition chemistry. To our knowledge, this is the first paper to explicitly investigate the relation between ignition delay and flame lift-off length in a diesel engine. Indeed, the ignition chemistry seems to play an important role in establishing the FLoL, since the flame lift-off length increases with ignition delay for the oxygenated fuels, at both inlet air conditions. It is suggested that the ignition quality of a fuel impacts the soot formation via the FLoL, since for the oxygenates, the (total) oxygen ratio at the (scaled) flame lift-off length inversely correlates with luminosity at the normal inlet air condition. At either inlet air condition, the lower

luminosity (and exhaust soot at the EGR-like inlet air condition) of CH_xnO(9%) compared to the DBM blend with the same oxygen content may be related to the large FLoL of CH_xnO(9%), rather than to the fuel's chemical predisposition to form soot.

Despite its relatively large lift-off length, diesel exhibits the shortest SLoL and produces the highest amount of soot. This illustrates the well known importance of the chemical composition, in this case the soot enhancing effect of the aromatics contained in diesel.

At EGR conditions, the luminosity seems a good predictor of the amount of exhaust soot. Even though the low-CN fuel anisole contains aromatics, it suppresses soot formation due to its exceptionally large premixed combustion phase. Besides, the low exhaust soot may be linked to the large FLoL. At EGR-like conditions, the ignition delay is so large that anisole might be a good candidate as a low sooting fuel, even at relatively high loads. Further research is needed however, addressing amongst others engine performance, NO_x and unburned hydrocarbons in the exhaust.

Supplementary material

Supplementary material associated with this article, presenting common-rail pressure transients, fuel molecular structures, camera UV sensitivity and high-speed image sequences and movies, can be found in the online version.

Acknowledgments

The authors would like to acknowledge Arjan van Vliet and Peter Claus for their technical assistance. Robert Klein-Douwel is acknowledged for his help with the analysis software and Bart Somers for his help with the adiabatic flame temperature calculations. The research is financially supported by Technology Foundation STW.

Appendix: Exhaust soot in skip-fired operation

To do reliable soot exhaust measurements, the AVL smoke meter needs to integrate over at least a few seconds. Thus, the soot concentration in a single cycle cannot be resolved. The hot combustion gases have another speed, pressure, and density than the exhaust of a motored cycle. This affects the sampled volume and therefore, one cannot simply multiply the amount of soot for the skip-fired mode by the skip-fire ratio. The same approach is followed as the approach for the NO exhaust measurements by Verbiezen et al. [47]. The exhaust gas of the fired cycles proved to be sampled more effectively and the measured soot concentration is given by

$$[soot]_{meas}(n_m) = \frac{\zeta[soot]_{actual}}{n_m + \zeta} \quad (5.3)$$

with $[soot]_{meas}(n_m)$ the measured soot concentration, $[soot]_{actual}(n_m)$ the concentration that would have been obtained applying no skip-firing, n_m the number of motored cycles in between every single fired cycle and ζ the bias factor towards a fired cycle. To obtain ζ for our experiment, the number of motored cycles was varied for diesel,

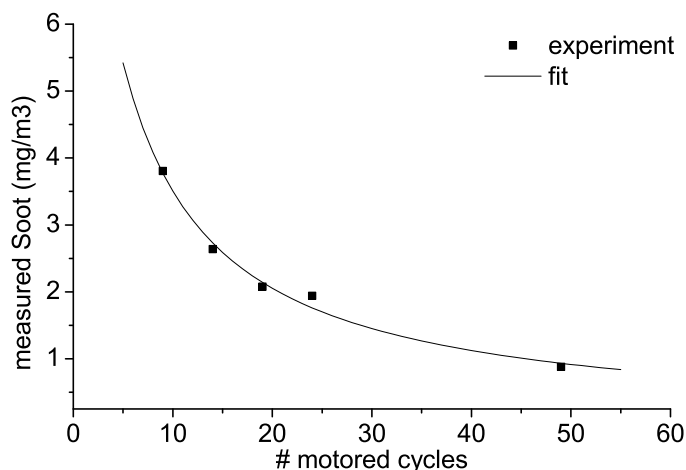


Figure 5.17: The measured and fitted amount of soot in the exhaust as a function of the number of motored cycles in between a fired cycle.

injected from -9.5° until 16° aTDC applying normal inlet air. The experimental result and a fit, using Eq. 5.3 with ζ and $[soot]_{actual}$ as fit parameters, is given in Fig. 5.17. A bias factor (ζ) of 4.14 was obtained and we have used this value for all fuels tested here. The bias factor is probably smaller for conditions where less energy per injection event is released, i.e. for the shorter injection duration, since then the exhaust gas conditions differ less from these of a motored cycle. The bias factor is not expected to vary significantly over the different oxygenated fuels of which soot exhaust measurements have been included, since variations in the heat released between these fuels are small. Therefore, even though the absolute soot exhaust value is probably overestimated for the 17.5° injection duration measurements, a comparison of soot exhaust measurements between different fuels is allowed.

Bibliography

- [1] M. D. Boot, P. J. M. Frijters, C. C. M. Luijten, L. M. T. Somers, R. S. G. Baert, A. J. Donkerbroek, R. J. H. Klein-Douwel, and N. J. Dam. Cyclic oxygenates: A new class of second-generation biofuels for diesel engines? *Energy and Fuels*, 23:1808 – 1817, 2009.
- [2] G. T. Kalghatgi, P. Risberg, and H. E. Ångström. Advantages of fuels with high resistance to auto-ignition in late-injection, low-temperature, compression ignition combustion. *SAE Paper 2006-01-3385*, 2006.
- [3] R. Hanson, D. Reitz, and S. Splitter. Operating a heavy-duty direct-injection compression-ignition engine with gasoline for low emissions. *SAE Paper 2009-01-1442*, 2009.
- [4] V. Manente, P. Tunestal, and B. Johansson. Partially premixed combustion

- at high load using gasoline and ethanol, a comparison with diesel. *SAE Paper 2009-01-0944*, 2009.
- [5] M. D. Boot, P. J. M. Frijters, R. J. H. Klein-Douwel, and R. S. G. Baert. Oxygenated fuel composition impact on heavy-duty diesel engine emissions. *SAE Paper 2007-01-2018*, 2007.
- [6] M. D. Boot, C. C. M. Luijten, R. S. G. Baert, R. Edenhofer, H. Dirks, K. Lucka, and H. Köhne. Sooting behavior of oxygenates fuels in a diffusion burner. In *Proc. of the 4th European Combustion Meeting*, Austria, Vienna, April 2009. ECM 2009.
- [7] M. D. Boot, C. C. M. Luijten, L. M. T. Somers, U. Eguz, D. D. T. M. van Erp, B. A. Albrecht, and R. S. G. Baert. Uncooled EGR as a means of limiting wall-wetting under early direct injection conditions. *SAE Paper 2009-01-0665*.
- [8] R. J. H. Klein-Douwel, A. J. Donkerbroek, A. P. van Vliet, M. D. Boot, L. M. T. Somers, R. S. G. Baert, N. J. Dam, and J. J. ter Meulen. Soot and chemiluminescence in diesel combustion of bio-derived, oxygenated and reference fuels. *Proc. Combust. Inst.*, 32:2817–2825, 2009.
- [9] L. M. Pickett and D. L. Siebers. Fuel effects on soot processes of fuel jets at DI diesel conditions. *SAE Paper 2003-01-3080*, 2003.
- [10] L. M. Pickett and D. L. Siebers. Soot in diesel fuel jets: effects of ambient temperature, ambient density, and injection pressure. *Combust. Flame*, 138:114–135, 2004.
- [11] L. Vanquickenborne and A. van Tiggelen. Stabilisation mechanism of lifted diffusion flames. *Combust. Flame*, 10:59 – 69, 1966.
- [12] G. T. Kalghatgi. Lift-off heights and visible lengths of vertical turbulent jet diffusion flames in still air. *Combust. Sci. Tech.*, 41:17 – 29, 1984.
- [13] S. Kumar, P. J. Paul, and H. S. Mukunda. Prediction of flame lift-off height of diffusion/partially premixed jet flames and modeling of mild combustion burners. *Combust. Sci. Tech.*, 179:2219 – 2253, 2007.
- [14] L. M. Pickett, D. L. Siebers, and C. A. Idicheria. Relationship between ignition processes and the lift-off length of diesel fuel jets. *SAE Paper 2005-01-3843*, 2005.
- [15] C. Pauls, G. Grünefeld, S. Vogels, and N. Peters. Combined simulations and OH-chemiluminescence measurements of the combustion process using different fuels under diesel-engine like conditions. *SAE Paper 2007-01-0020*.
- [16] R. L. Gordon, A. R. Masri, S. B. Pope, and G. M. Goldin. A numerical study of auto-ignition in turbulent lifted flames issuing into a vitiated co-flow. *Combust. Theory Modeling*, 11:351 – 376, 2007.

- [17] R. L. Gordon, A. R. Masri, and E. Mastorakos. Simultaneous Rayleigh temperature, OH- and CH₂O-LIF imaging of methane jets in a vitiated coflow. *Combust. Flame*, 155:181 – 195, 2008.
- [18] E. Oldenhof, M. J. Tummers, E. H. van Veen, and D. J. E. M. Roekaerts. Temperature and velocity measurements in the delft jet-in-hot-coflow burner. In *Proc. of the 4th European Combustion Meeting*, Austria, Vienna, April 2009. ECM 2009. paper 810-176.
- [19] L. M. Pickett, S. Kook, H. Persson, and Ö. Andersson. Diesel fuel jet lift-off stabilisation in the presence of laser-induced plasma ignition. *Proc. Combust. Inst.*, 32:2793 – 2800, 2009.
- [20] M. Metghalchi and J. C. Keck. Burning velocities of mixtures of air with methanol, isooctane, and indolene at high pressure high temperature. *Combust. Flame*, 48:191 – 210, 1982.
- [21] G. J. Gibbs and H. F. Calcote. Effect of molecular structure on burning velocity. *J. Chem. Eng. Data*, 4:226 – 237, 1959.
- [22] Öivind Andersson. Air entrainment and flame lift-off under diesel conditions, personal communication, 2009.
- [23] M. P. Musculus, J. E. Dec, and D. R. Tree. Effects of fuel parameters and diffusion flame on lift-off soot formation in a heavy-duty DI diesel engine. *SAE Paper 2002-01-0889*, 2002.
- [24] A. S. Cheng, A. Upatnieks, and C. J. Mueller. Investigation of the impact of biodiesel fuelling on NO_x emissions using an optical direct injection diesel engine. *Int. J. Eng. Res.*, 7:297–318, 2006.
- [25] C. J. Mueller and G. C. Martin. Effect of oxygenated compounds on combustion and soot evolution in a DI diesel engine: broadband natural luminosity imaging. *SAE Paper 2002-01-1631*, 2002.
- [26] S. Stournas, E. Lois, F. Zannikos, and D. Karonis. Differentiation of road diesel and heating gasoil by changes in fuel properties and addition of oxygenated components. *Energy and Fuels*, 8:1263–1267, 1994.
- [27] A. J. Donkerbroek, A. P. van Vliet, L. M. T. Somers, N. J. Dam, P. J.M. Frijters, R. J. H. Klein-Douwel, W. L. Meerts, and J. J. ter Meulen. Time- and space-resolved quantitative LIF measurements of formaldehyde in a heavy-duty diesel engine. *Combust. Flame*, 157:155 – 166, 2010.
- [28] J. B. Heywood. *Internal Combustion Engine Fundamentals*. McGrawHill, Singapore, 1988.
- [29] J. D. Naber and D. L. Siebers. Effects of gas density and vaporization on penetration and dispersion of diesel sprays. *SAE Paper 960034*.
- [30] D. Siebers, B. Higgins, and L. Pickett. Flame lift-off in direct-injection diesel fuel jets: oxygen concentration effect. *SAE Paper 2002-01-0890*, 2002.

-
- [31] M. M. Tacke, D. Geyer, E. P. Hassel, and J. Janicka. A detailed investigation of the stabilization point of lifted turbulent diffusion flames. *Proc. Combust. Inst.*, 27:1157–1165, 1998.
- [32] A. G. Gaydon. *The spectroscopy of flames*. Chapman and Hall Ltd., London, 1974.
- [33] J. E. Dec and E. B. Coy. OH radical imaging in a DI diesel engine and the structure of the early diffusion flame. *SAE Paper 960831*, 1996.
- [34] B. Higgins and D. Siebers. Measurement of the flame lift-off location on DI diesel sprays using OH chemiluminescence. *SAE Paper 2001-01-0918*, 2001.
- [35] D. L. Siebers and B. S. Higgins. Flame lift-off on direct-injection diesel sprays under quiescent conditions. *SAE Paper 2001-01-0530*, 2001.
- [36] M. P. B. Musculus. Effects of the in-cylinder environment on diffusion flame lift-off in a DI diesel engine. *SAE Paper 2003-01-0074*, 2003.
- [37] Md. N. Nabi, H. Ogawi, and N. Niyamoto. Nature of fundamental parameters related to engine combustion for a wide range of oxygenated fuels. *SAE Paper 2002-02-2835*, 2002.
- [38] C. J. Mueller, W. J. Pitz, L. M. Pickett, G. C. Martin, D. L. Siebers, and C. K. Westbrook. Effects of oxygenates on soot processes in DI diesel engines: experiments and numerical simulations. *SAE Paper 2003-01-1791*, 2003.
- [39] A. Upatnieks and C. J. Mueller. Investigation of the relationship between DI diesel combustion processes and engine-out soot using an oxygenated fuel. *SAE Paper 2004-01-1400*, 2004.
- [40] C. A. Idicheria and L. M. Pickett. Effect of EGR on diesel premixed-burn equivalence ratio. *Proc. Combust. Inst.*, 31:2931–2938, 2007.
- [41] R. S. G. Baert, P. J. M. Frijters, L. M. T. Somers, C. C. M. Luijten, and W. de Boer. Design and operation of a high pressure, high temperature cell for HD diesel spray diagnostics: guidelines and results. *SAE Paper 2009-01-0649*, 2009.
- [42] H. J. Curran, P. Gaffuri, W. J. Pitz, and C. K. Westbrook. A comprehensive modelling study of iso-octane oxidation. *Combust. Flame*, 129:253–280, 2002.
- [43] K. Schmidt and J. H. van Gerpen. The effect of biodiesel fuel composition on diesel combustion and emissions. *SAE Paper 961086*, 1996.
- [44] J. E. Dec. A conceptual model of DI diesel combustion based on laser-sheet imaging. *SAE Paper 970873*, 1997.
- [45] T. Ito, T. Kitamura, M. Ueda, T. Matsumoto, J. Senda, and H. Fujimoto. Effects of flame lift-off and flame temperature on soot formation in oxygenated fuel sprays. *SAE Paper 2003-01-0073*, 2003.

- [46] M. Lapuerta, O. Armas, and J. Rodríguez Fernández. Effect of biodiesel fuels on diesel engine emissions. *Prog. Energy and Combust. Sci.*, 34:198–223, 2008.
- [47] K. Verbiezen, A. J. Donkerbroek, R. J. H. Klein-Douwel, A. P. van Vliet, P. J. M. Frijters, X. L. J. Seijkens, R. S. G Baert, W. L. Meerts, N. J. Dam, and J. J. ter Meulen. Diesel combustion: in-cylinder NO concentrations in relation to injection timing. *Combust. Flame*, 151:333–346, 2007.

Part II
Combustion Concept

Optimization of Operating Conditions in the Early Direct Injection Premixed Charge Compression Ignition Regime

Early Direct Injection Premixed Charge Compression Ignition (EDI PCCI) is a widely researched combustion concept, which promises soot and CO₂ emission levels of a spark-ignition (SI) and compression-ignition (CI) engine, respectively. Application of this concept to a conventional CI engine using a conventional CI fuel faces a number of challenges. First, EDI has the intrinsic risk of wall-wetting, i.e. collision of fuel against the combustion chamber periphery. Second, engine operation in the EDI regime is difficult to control as auto-ignition timing is largely decoupled from fuel injection timing. In dual-mode PCCI engines (i.e. conventional DI at high loads) wall-wetting should be prevented by selecting appropriate (most favorable) operating conditions (EGR level, intake temperature, injection timing-strategy etc.) rather than by redesign of the engine (combustion chamber shape, injector replacement etc.). This paper presents the effects of EGR concentration, intake temperature, intake pressure, injection timing, injection pressure and fuel temperature on engine performance and emission behavior in EDI PCCI mode. In addition, several minor adjustments to the conventional injector nozzle are investigated. Wall-wetting and engine performance are characterized by the measured emissions (smoke and unburned hydrocarbons) and in-cylinder pressure (CA₅₀ and IMEP). The main contribution of this paper is to investigate the cumulative effects on engine performance and emissions, unburnt hydrocarbons (UHC) in particular, of various known measures designed to address wall-wetting. All experiments have been performed at low load (~ 3-4 bar IMEP) and at an engine speed of 1200 RPM, using a modified 6-cylinder 12.6 liter heavy-duty DI DAF XE 355 C engine. Experiments are conducted in one dedicated cylinder, which is equipped with a stand-alone fuel injection system, EGR circuit and air compressor, fueled with commercial diesel fuel (EN590).

The content of this Chapter has been taken from:

M.D. Boot, C.C.M. Luijten, E.P. Rijk, B.A. Albrecht and R.S.G. Baert. Optimization of operating conditions in the early direct injection premixed charge compression ignition regime. *SAE Paper*, 2009-24-0048, 2009.

Minor edits have been made to streamline the layout of the thesis chapters. Experiments were carried out in the engine lab of the Eindhoven University of Technology.

6.1 Introduction

A lot of research effort is being invested to develop new combustion concepts which capture the advantageous efficiency of the CI and low emissions of the SI engine [1–9]. A shared fundamental characteristic of many of these concepts is that a more or less premixed fuel/air charge is brought to auto-ignition. As a result, both fuel and (flame) temperature are well dispersed in the combustion chamber, ideally resulting in near-zero levels of both soot and NO_x respectively. Collectively, such concepts are referred to as Premixed Charge Compression Ignition. In order to achieve the desired degree of premixing, it is necessary to separate (in time) the injection and combustion event, at least to a large extent. In other words, the ignition delay should be longer than the injection duration. In literature, various methods are proposed to stretch the ignition delay.

6.1.1 Early direct injection PCCI

Early direct injection (EDI) PCCI involves a relatively early injection timing, typically when the piston has reached roughly two-thirds of its upward movement in the compression stroke. The prevailing temperature and pressure is at that time too low to initiate auto-ignition chemistry, but, at least to a certain extent, high enough to facilitate the evaporation process. Accordingly, time is created for mixing prior to auto-ignition in order to achieve PCCI combustion. When utilizing stock HDDI hardware, it is difficult to achieve EDI PCCI, whilst maintaining low soot and unburned hydrocarbon (UHC) emissions. This can largely be attributed to wall-wetting. Apart from poor emissions, there is also the tendency of the relatively reactive diesel fuel to prematurely (i.e. well before TDC) auto-ignite, resulting in poor thermal efficiency and the risk of knock. Lastly, the absence of a clear dependence of the combustion timing on injection timing makes controlling EDI PCCI particularly challenging.

EDI PCCI will most likely be used initially in dual-mode engines [1], i.e. in combination with conventional DI combustion at high load. Dual-mode operation will entail running the engine under EDI conditions at low loads. For cold start and higher loads (upper one-third to one-half of the operating range) conventional DI combustion takes over. Meeting legislated targets for soot and NO_x is becoming increasingly reliant on sophisticated aftertreatment. Because these aftertreatment systems are most often catalytic in nature, they become ineffective when - at low engine loads or during cold start - exhaust temperatures remain below the catalyst light-off temperature. Conversely, at high load there is ample thermal energy to facilitate catalytic conversion of harmful emissions. EDI PCCI promises to be a viable short term solution for meeting legislated NO_x and soot targets in the low engine load regime. A more extensive overview on the drawbacks of EDI, along with various approaches to (partially) overcome these, is presented in [1].

6.1.2 Late direct injection PCCI

Late direct injection (LDI) involves a relatively late injection, typically from around 10 crank angles before TDC (or later). This late timing is combined with high EGR rates (> 25 wt-%) to prolong the ignition delay. Compared to EDI PCCI, the ignition

delay is now markedly shorter, but sufficiently long (i.e. longer than the injection duration) to avoid fuel-rich areas where soot is formed [3]. Meanwhile, NO_x is kept low by means of heavy EGR and the aforementioned premixing. Drawbacks of this concept concern the high injection pressure required to keep injection durations short [3], necessary modifications to the combustion chamber, high UHC emissions and limited operating range [3, 5, 9]. When injection is lasting into the expansion stroke, such combustion has been referred to as Modulated Kinetics (MK). Especially with MK an additional drawback is the need to accelerate mixing times (e.g. through modification of valve/piston geometry [5] and/or high swirl [9]).

6.1.3 Fuel induced PCCI

The above mentioned strategies necessary to achieve PCCI result in large part from the low volatility and high CN of present commercial diesel fuel. It is known from literature that a form of PCCI can be realized in unmodified HDDI diesel engines under more or less conventional operating conditions, when a less reactive fuel is used. Earlier work [6, 7] showed near-zero soot and NO_x emissions from a HDDI diesel engine, in an operating point corresponding to highway cruising, using moderate EGR (< 25 wt-%) and conventional fuel injection equipment. The fuel was a blend of commercial diesel and a low reactive cyclic oxygenate (i.e. cyclohexanone). The favorable results were attributed to the long ignition delays incurred and resulting higher degree of premixing. Kalghatgi [8] performed an extensive study on fuel requirements for PCCI engines and reported that, for injection timings that went up towards TDC, volatile, low reactive fuels such as gasoline are more appropriate for this combustion concept than diesel fuel.

This paper initially focuses on individual measures for minimizing wall-wetting and optimizing IMEP in EDI PCCI mode at low load (~ 4 bar IMEP), performed with a conventional HDDI diesel fuel injection nozzle. Subsequently, these measures will be utilized simultaneously to ascertain the cumulative potential. In a third step, the additional benefits of smaller nozzle holes and a narrower cone angle are investigated. For all nozzles and with all measures utilized, the injection timing is optimized.

6.2 Experimental apparatus

A dedicated engine test rig, referred to as CYCLOPS, has been designed and built at the TU/e. The engine is a 6-cylinder 12.6 liter DI DAF XE 355 C heavy-duty Diesel engine. However, several modifications have been made to allow for investigation of PCCI combustion.

6.2.1 Concept

Essentially, the flywheel side of the DAF engine, comprising cylinders 1 thru 3, has been left in its original state. Operating under the stock DAF engine control unit (ECU), this flank is merely exploited as a means to control the crankshaft rotational speed of the test cylinder (cylinder 6) under both firing and motored operation (Figure 6.1 and Table 6.1). Engine speed and torque are controlled by a water-cooled, eddy-current Schenck W450 dynamometer.

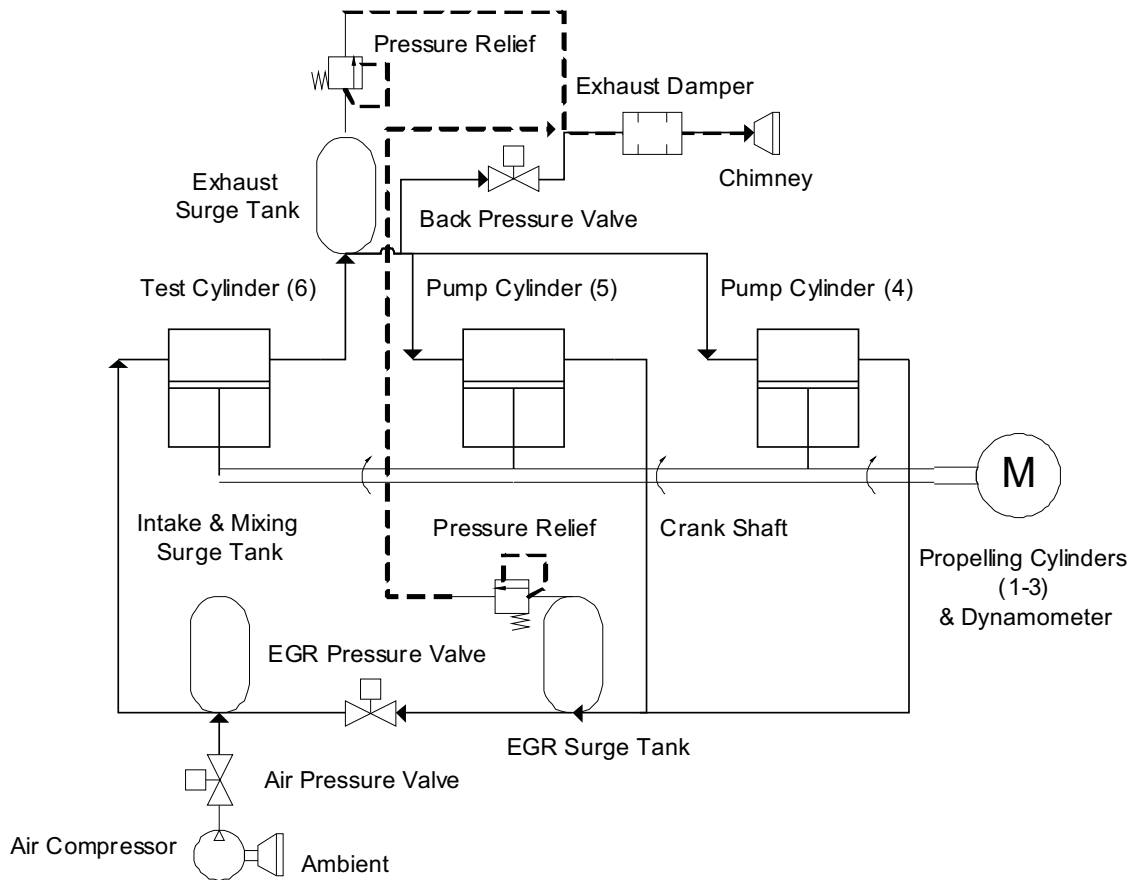


Figure 6.1: Test section of the CYCLOPS engine).

Throughout engine start, warm-up, and whenever the data-acquisition is idle, the CYCLOPS runs solely on the three propelling cylinders. Once warmed up and operating at the desired engine speed, combustion phenomena and emission formation are studied in the test cylinder 6. The test cylinder has been designed to operate independently from the propulsion cylinders with respect to all operating conditions except engine speed. To this end, dedicated air, EGR and fuel delivery circuits have been installed as will be explained below. Note that the compression ratio has been lowered from the stock value of 16 to 11.88 by means of a 3.4 mm thicker head gasket. At the stock value for the compression ratio, the auto-ignition process occurs prematurely, far ahead of TDC, resulting in poor thermal efficiency [1]. Lowering the compression ratio by means of a thicker gasket will alter the chamber characteristics, e.g. spray interaction with bowl and squish flow. These effects, though not investigated, are not believed to significantly influence the qualitative response of the engine to changing operating conditions.

6.2.2 Air

Fed by an Atlas Copco air compressor, the intake air pressure can be boosted to pressures up to 7 bar. For this application, however, the limit is set at 5 bar to pre-

vent the end-of-compression pressure of the test cylinder from reaching the maximum allowable in-cylinder pressure. A surge tank has been mounted downstream of the compressor to muffle any pressure oscillations originating from the compressor. The intake pressure is regulated by a PMA KS 40-1 pressure controller, which receives its input signal from a pressure sensor mounted in the intake manifold of the test cylinder. The set point can be programmed from the engine control room.

6.2.3 EGR

Cylinders 4 thru 6 constitute the considerably more complex, non-stock section of the engine (Figure 6.1). Combustion phenomena and emission formation will be studied exclusively in the test cylinder. Non-firing cylinders 4 and 5 function as EGR pumps, the purpose of this intricate system is to decouple EGR production from test cylinder back pressure and to dampen pressure fluctuations originating from the test cylinder.

Table 6.1: Engine specifications.

Geometric engine data	
Base engine	6 cylinder HDDI diesel
Cylinders	1 isolated for combustion
Bore [mm]	130
Stroke [mm]	158
Compression ratio [-]	11.88 (lowered from 16)
Valve data	
Intake valve open	16 °CA bTDC
Intake valve close	27 °CA aBDC
Exhaust valve open	52 °CA bBDC
Exhaust valve close	14 °CA aTDC
Fuel injection system	
Type	Common rail
No. of holes	8, equally spaced
Nom. hole diameter [mm]	0.19
Cone angle degrees [°]	154

Apart from the mutual cam- and crankshaft, the left engine bank operates autonomously from the right flank. The stand-alone air intake, EGR circuit, and fuel injection equipment have been optimized for maximum flexibility as will be discussed in detail in paragraphs to come. Note that several surge tanks and pressure relief valves have been included in the design, to dampen pressure oscillations and to guard for excessive pressure in the EGR circuit, respectively. Note that the catalytic particle filter (cDPF) in Figure 6.1 has been removed from the setup in order to supply untreated EGR gas into the test cylinder for the experiments presented in this work.

6.2.4 Fuel injection system

The selected double-acting air-driven Resato HPU200-625-2 fuel pump can deliver a fuel pressure up to 4000 bar. Fuel pressure, herein, is regulated by adjusting the air pressure with a Resato R03- 04C high precision pressure regulator. To dampen the pressure fluctuations originating from the pump, a Resato HPA-1 accumulator is mounted downstream of the pump. Corresponding values for the accumulator internal volume and maximum allowable pressure are 1 dm³ and 4000 bar, respectively.

Additionally, a second temperature-controlled (up to 250 °C) buffer is placed near (~0.2 m) the fuel injector to neutralize any pressure waves present in the relatively long (~2 m) fuel line connecting the pump with the injector and to heat up the fuel to the desired temperature. Manufactured in-house, this accumulator can sustain similar pressures as the HPA-1. The internal volume of approximately 0.114 dm³ is significantly smaller to mimic the volume of a typical common rail. Properties of the utilized commercial diesel fuel are listed in Table 6.2.

Table 6.2: Fuel specifications.

Parameter	ASTM Test Method	Value
Density [kg/l] @15 °C	D 4052	0.827
Cetane Index [-]	D 4737	56.2
Viscosity [mm/s] @ 40 °C	D 445	2.69
<i>Distillation</i>		
Recovered @ 250 °C [%v/v]	D 86	30
Recovered @ 350 °C [%v/v]	D 86	98
95 % Recovered [°C]	D 86	335
Sulphur [mg/kg]	D 2622	35
Flash point [°C]	D 93	75.5
Poly-aromatics [%m/m]	391 (IP Test)	< 11
Lower heating value [MJ/kg]	-	43.3

6.2.5 Emission equipment

To determine fuel, intake air and EGR flow rates, Micro Motion mass flow meters were used. For measuring gaseous exhaust emissions a Horiba MEXA 7100 wet UHC and heated dry NOx analyzer were used. Exhaust smoke level (in Filter Smoke Number or FSN units) was measured using an AVL 415S smoke-meter. Note that all experiments presented in this paper were conducted without any form of aftertreatment. The accuracy of this equipment is discussed in reference [6].

6.2.6 Crank angle resolved data acquisition

In-cylinder pressure was measured at 0.1 °CA intervals with an AVL GU21C uncooled pressure transducer. Along with crank angle, pressure data was recorded and processed by a SMETEC Combi data-acquisition system. Important parameters such

as the CA50 and IMEP were calculated online by the SMETEC software and logged for 50 consecutive cycles per operating point in order to establish the standard deviation. Crank angle data in this paper are in degrees crank angle after TDC ($^{\circ}\text{CA aTDC}$). Along with in-cylinder pressure, the pressure in the intake manifold, fuel pressure/temperature (in fuel line approximately 50 mm from injector) and injector actuation current were logged at 0.1 $^{\circ}\text{CA}$ intervals with the SMETEC system. The accuracy of this equipment is discussed in reference [1].

6.2.7 Time resolved data acquisition

Quasi-steady engine data (i.e. in a given work point), such as air/EGR/fuel flows, intake/exhaust pressures/temperatures and emissions were recorded at 20 Hz for a period of 40 s via an in-house data-acquisition system (TUE DACS). The accuracy of this equipment is discussed in reference [1].

6.3 Experimental procedure

6.3.1 Measures under investigation

In literature [1, 2] various measures are described to minimize wall-wetting and optimize IMEP in EDI PCCI mode at low load (~ 4 bar IMEP), most of which will be investigated here. In this work, a division will be made into software-based strategies, involving tuning of engine operating conditions:

- optimizing injection timing;
- raising intake pressure;
- raising fuel injection pressure;
- raising intake temperature (via hot EGR [1]);
- raising fuel temperature;

and hardware-based strategies, involving modifications of the engine hardware:

- decreasing nozzle hole diameter;
- decreasing nozzle hole cone angle.

6.3.2 Engine operating conditions

All measures presented above will be studied by means of parameter sweeps at 1200 RPM and at a load/IMEP of approximately 4 bar. The measuring plan consists of three main parts. In each part, fueling is set such that IMEP is 4 bar at a SoA of $-15^{\circ}\text{CA aTDC}$ and zero EGR. Fueling is subsequently kept constant throughout the performed sweeps. In the fourth part, Siebers engineering correlation for liquid core penetration [10, 11] is used to estimate the degree of wall-wetting in the various cases.

Table 6.3: Operating conditions for Part 1: Investigation of software measures (individual). The applied range or values used in the various parameter sweeps are indicated in **Bold**.

	SoA °CA aTDC	T _{in} K	P _{in} bar (abs.)	P _{fuel} bar (abs.)	T _{fuel} °C	EGR wt-%
SoA sweep [1]	-5:5:-60	303	1.25	750	30	0, 40
T _{in}	-50	303:5:353	1.25	750	30	~ 65
P _{in}	-50	303	00:25.2	750	30	~ 60
P _{fuel}	-50	303	1.5	750, 1100, 1500	30	0
T _{fuel}	-50:5:- 65	303	1.5	1100	30, 100	0

Table 6.4: Operating conditions for Part 2: Investigation of software measures (cumulative). The applied range or values used in the various parameter sweeps are indicated in **Bold**.

	SoA °CA aTDC	T _{in} K	P _{in} bar (abs.)	P _{fuel} bar (abs.)	T _{fuel} °C	EGR wt-%
N1 $\varnothing=190$ $\theta=154^\circ$	-50,-30,-15	353(max)	1.25	750	100(max)	70

- Part 1: Individual assessment of software-strategies (see Table 3)
- Part 2: Cumulative assessment of software-strategies (see Table 4)
- Part 3: Part 2 repeated for two modified nozzles (see Table 5)
- Part 4: Spray modeling to estimate effects of above measures on wall-wetting

Table 6.5: Operating conditions for Part 3: Investigation of hardware measures. The applied range or values used in the various parameter sweeps are indicated in **Bold**.

	SoA °CA aTDC	T _{in} K	P _{in} bar (abs.)	P _{fuel} bar (abs.)	T _{fuel} °C	EGR wt-%
N2 $\varnothing=161$ $\theta=150^\circ$	-50,-30,-15	353(max)	1.25	1600(max)	100(max)	70
N3 $\varnothing=161$ $\theta=100^\circ$	-50,-30,-15	353(max)	1.25	1600(max)	100(max)	75

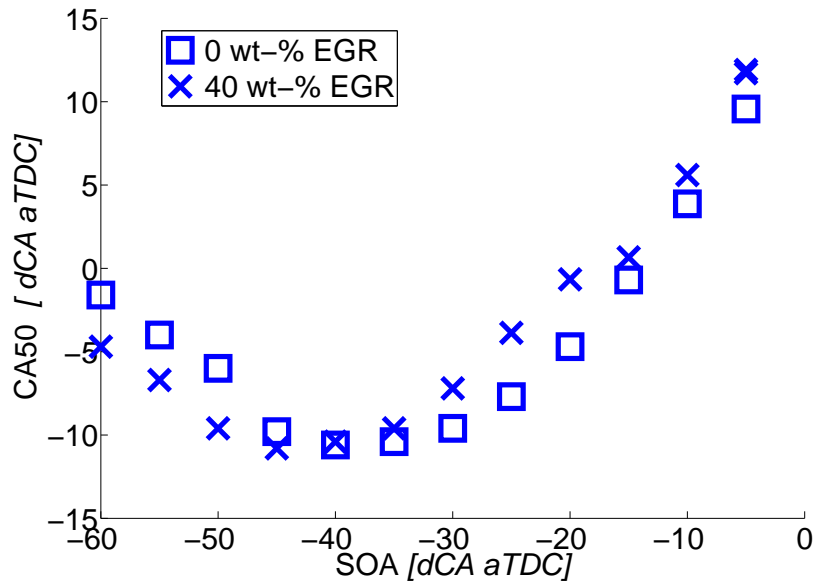


Figure 6.2: Baseline injection timing sweep: CA50).

6.4 Results & discussion: part 1 of 4

6.4.1 Baseline injection timing sweep

As indicated in Table 6.3, the timing of injector actuation is advanced from -5:5:-60 °CA aTDC at two levels of EGR. It should be noted that, at a given engine speed, analysis of logged injector current and injection pressure data shows a constant 3 °CA lag between the SoA and SOI. Plotted in Figure 6.2 thru Figure 6.7, is the response of combustion phasing, engine performance and emissions. Note that the baseline experiments were carried out with nozzle 2 (Table 6.5) instead of nozzle 1 (Table 6.4), because the latter nozzle was not available yet. Note that in this study all parameters related to engine power (i.e. ISFC, NO_x and UHC) are indicated values and not brake-specific.

Combustion phasing

As could be expected, CA50 is initially seen to advance with SoA up to approximately 30 °CA aTDC, from which point a further advancement of SoA has a neutral effect on CA50. The change in slope around 30 °CA aTDC marks the border between conventional DI diesel and EDI PCCI combustion. A further advancement of SoA, deeper into the EDI PCCI regime, appears to lead to a retardation of CA50. The effect of EGR on CA50 is advancing in the EDI PCCI regime compared to the (expected) retarding effect in the conventional DI combustion mode. The intake temperature for the 40 % EGR case was slightly higher at 40-45 °C. These results suggest that the advancing effect of a higher intake temperature is dominant over the retarding effect of a lower oxygen concentration when operating in EDI PCCI mode. The opposite appears to be the case for conventional DI combustion. This behavior correlates well with the observations made in an earlier work [1].

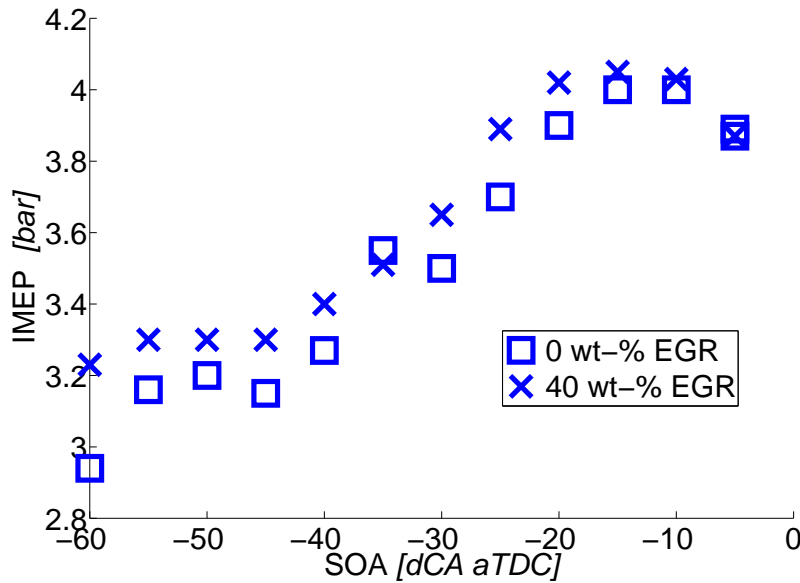


Figure 6.3: Baseline injection timing sweep: IMEP).

Performance

At a given fueling level, engine performance is characterized by IMEP (Figure 6.3) and ISFC (Figure 6.4). Both parameters are coupled and show similar trends with advancing SoA. Both peak around -15°CA , indicating an optimum performance, corresponding to a CA50 around TDC. Later or earlier combustion phasing has a negative effect on thermal efficiency. A slight stabilization, however, is visible when entering the EDI PCCI regime. Here fuel consumption and engine power initially remain unaffected by an advancing SoA. At earlier timings still, both eventually start to deteriorate again.

Emissions

It is clear that the impact of injection timing and EGR on emission behavior is more complex. Starting with NO_x (Figure 6.5), the characteristic rise within the conventional DI regime is clearly visible.

As could be expected, the lower flame temperatures intrinsic to the utilization of EGR, lead to markedly lower NO_x, especially at conventional timings.

Both UHC (Figure 6.6) and smoke (Figure 6.7) reach minimum values around the same SoA where peak values are registered for NO_x. Another trend of interest is the flattening out and even reversal for the zero EGR case of smoke emissions at very early timings, which has been observed elsewhere [12] as well. Decrease of soot forming with increase of EGR is explained in [12] by the reduced combustion temperature of the rich mixture formed on the fuel wall-film.

Baseline

Based on the results of the baseline experiments, two workpoints (Table 6.6) are selected to serve as benchmarks for conventional HDDI diesel and EDI PCCI combus-

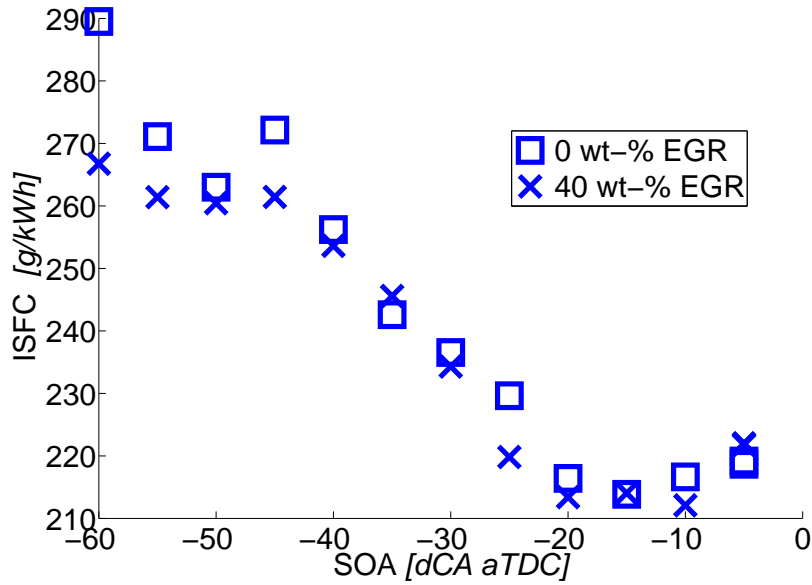


Figure 6.4: Baseline injection timing sweep: ISFC).

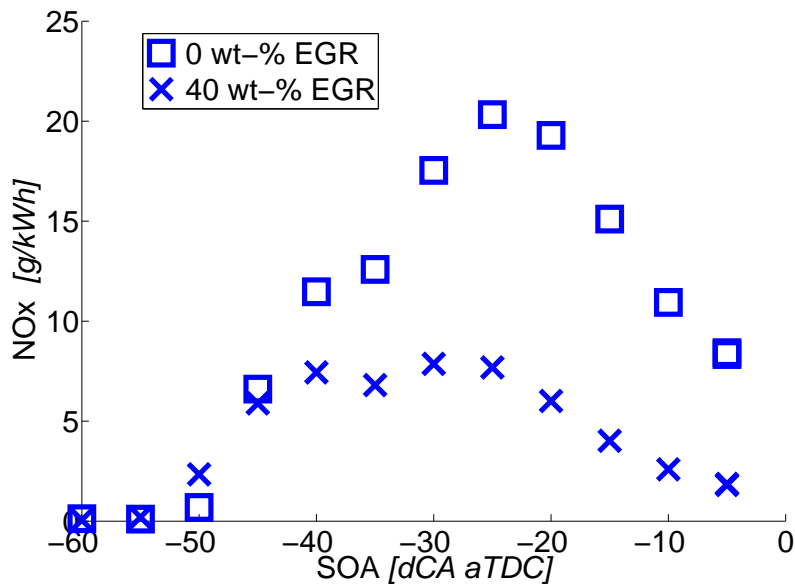


Figure 6.5: Baseline injection timing sweep: NOx).

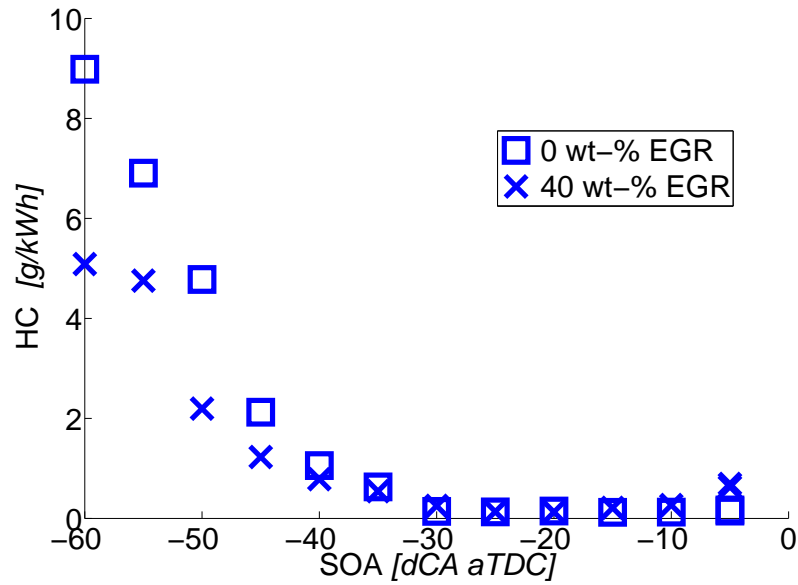


Figure 6.6: Baseline injection timing sweep: UHC).

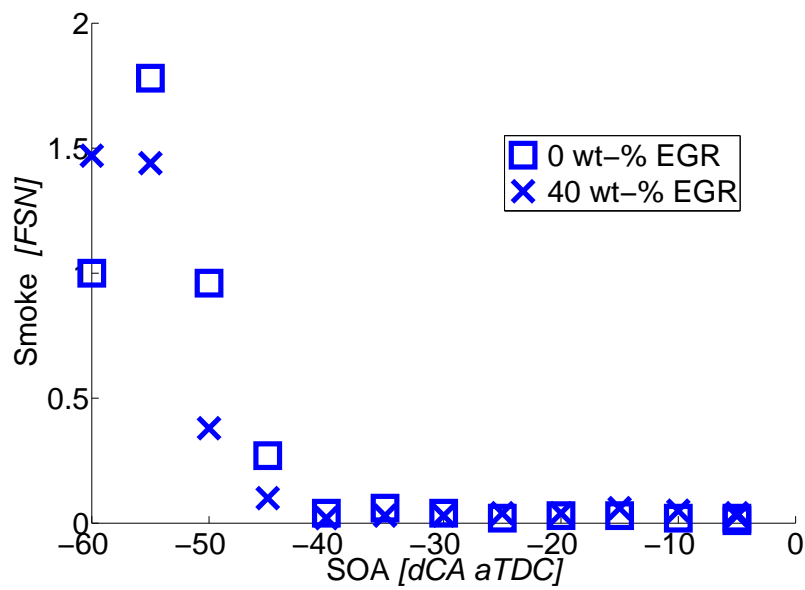


Figure 6.7: Baseline injection timing sweep: Smoke number).

Table 6.6: Normal DI and EDI PCCI baseline conditions (using nozzle 2), performance and emissions. Values in brackets are relative to the normal baseline case.

Parameter	Unit	Normal DI	EDI PCCI
SoA	°CA aTDC	-15	-55
EGR	wt-%	0	40
Pfuel	bar	750	750
λ	-	4.2	3.1
CA50	°CA aTDC	-0.7	-6.7 (-6)
IMEP	bar	4	3.3 (- 18 %)
ISFC	g/kWh	214	260 (+ 21 %)
NOx	g/kWh	15.1	0.20 (- 99 %)
UHC	g/kWh	0.12	4.76 (+ 3867 %)
Smoke	FSN	0.03	1.44 (+ 4700 %)

tion. The motivation for the selected conventional and EDI PCCI workpoints is based on minimal fuel consumption and acceptable NOx (i.e. \sim EPA 2010 (0.27 g/kWh) and $<$ EURO VI (0.4 g/kWh)), respectively.

It is clear that the transition from conventional DI to EDI PCCI comes paired with substantial reduction in NOx, but also leads to an unacceptable increase in soot/UHC emissions and fuel consumption. The latter increases are likely due to wall-wetting and premature auto-ignition, respectively. The goal of the measures presented in the following subsections is to improve smoke/UHC emissions and fuel economy, whilst maintaining low NOx.

Intake temperature

Intake temperature (T_{in}), as measured in the intake manifold, was gradually increased by adding more uncooled EGR to the intake. Due to the intricate system of surge tanks (Figure 6.1), it is quite time consuming to realize an increase in T_{in} from 300 to 350 K. The EGR ratio was initially set to approximately 60-65 wt-% and subsequently raised further to 65-70 wt-% in order to reach the desired maximum T_{in} of 340-350 K. Measurements were performed per 5 K T_{in} increase. It should be noted that, contrary to the baseline measurements, these experiments were carried out with nozzle 1 (see footnote Table 6.3). Listed in (Table 6.7) are the results related to combustion phasing, performance and emissions at the minimum and maximum values for T_{in} . A complete overview of all data points is presented in Appendix A. Values in brackets are relative to the Low T_{in} case to single out the influence of the measure under investigation.

The impact on combustion phasing is quite clear. Even though the increase in EGR leads to a lower oxygen concentration [1], the corresponding increase in T_{in} leads to advancement in CA50. The dominance of temperature over oxygen concentration on the CA50 in the EDI PCCI regime has been observed in earlier work [1] as well. This effect is believed to be even more noticeable as $\lambda \rightarrow 1$. As discussed earlier, the principal motivation for elevating T_{in} is to reduce wall-wetting. From Table 6.7 becomes clear that a hotter T_{in} leads to improved IMEP and ISFC, a less favorable

Table 6.7: Impact of Tin on performance and emissions in the EDI PCCI regime (see Appendix A).

Parameter	Unit	Low Tin	High Tin
EGR	wt-%	60	70
Tin	K	300	350
λ	-	2.6	1.9
CA50	°CA aTDC	-1	-7.6 (-6.6 °CA)
IMEP	bar	3.06	3.14 (+ 3 %)
ISFC	g/kWh	296	284 (- 4 %)
NOx	g/kWh	0.04	0.27 (+ 575 %)
UHC	g/kWh	7.5	5.2 (- 31 %)
Smoke	FSN	1.32	0.32 (- 71 %)

CA50 notwithstanding. UHC and smoke emissions are improved as well. These trends, which are in agreement with earlier work [1], support the assumption that a higher Tin leads to less wall-wetting. NOx increases rapidly with an elevation in intake temperature, even though this increase is realized by an increase in EGR. Like CA50, NOx appears to be more sensitive to temperature than the prevailing oxygen concentration. It should be noted that although the NOx is substantially higher for the high Tin case, the value is still very low (i.e. \sim EPA 2010 (0.27 g/kWh) and $<$ EURO VI (0.4 g/kWh)).

Intake pressure

Intake pressure (Pin) was incrementally increased via the external Atlas Copco compressor (Figure 6.1) from 1 to 2 bar (absolute). In accordance with Table 3, Tin and the EGR ratio were kept constant at 300 K and 60 wt-% respectively. Listed in Table 6.8 are the results related to combustion phasing, performance and emissions at the minimum and maximum values for Pin. A complete overview of all data points is presented in Appendix B. Values in brackets are relative to the Low Pin case to single out the influence of the measure under investigation.

It is evident that an increase in Pin leads to a noticeable advancement of the CA50. Moreover, all performance indicators and emissions have a clear benefit from the leaner mixture, except for NOx. These results are likely attributable to reduced wall-wetting (due to the higher gas density) and improved combustion efficiency (due to the leaner mixture). NOx emissions are higher, but still considered extremely low. It should be noted that exhaust back pressure was kept constant at near-atmospheric pressure regardless of the utilized boost pressure. In reality, the IMEP and ISFC will worsen somewhat as a consequence of the resulting higher back pressure when supplying the higher Pin via a turbocharger.

Fuel injection pressure

(Pfuel) was incrementally increased via the external Resato air-driven fuel pump (Figure 6.1) from 750 to 1500 bar (absolute). In accordance with Table 6.3, Pin, Tin and

Table 6.8: Impact of Pin on performance and emissions in the EDI PCCI regime (see Appendix B).

Parameter	Unit	Low Pin	High Pin
EGR	wt-%	62	55
Pin	bar	1	2
λ	-	2	3.8
CA50	CA aTDC	3.2	-4.8 (-9.8 °CA)
IMEP	bar	2.76	3.72 (+ 35 %)
ISFC	g/kWh	342	248 (- 27 %)
NOx	g/kWh	0.03	0.07 (+ 133 %)
UHC	g/kWh	9.1	6.5 (- 29 %)
Smoke	FSN	1.6	0.52 (- 68 %)

Table 6.9: Impact of Pfuel on performance and emissions in the EDI PCCI regime (see Appendix C).

Parameter	Unit	Low Pfuel	High Pfuel
Pfuel	bar	750	1500
CA50	°CA aTDC	-5.1	-5.5 (- 0.4 °CA)
IMEP	bar	3	3.23 (+ 8 %)
ISFC	g/kWh	280	240 (- 17 %)
NOx	g/kWh	< 0.01	< 0.01
UHC	g/kWh	9.1	7.3 (- 20 %)
Smoke	FSN	1.17	0.9 (- 23 %)

the EGR ratio were kept constant at 1.5 bar, 300 K and 0 wt-% respectively. Listed in Table 6.9 are the results related to combustion phasing, performance and emissions at the minimum and maximum values for Pfuel. Values in brackets are relative to the Low Pfuel case to single out the influence of the measure under investigation. A complete overview of all data points is presented in Appendix C. An increase in Pfuel from 750 to 1500 bar results in a slight advancement of the CA50. This effect on CA50 in EDI PCCI mode, likely attributable to improved mixing, is also found in literature [2]. It is clear that IMEP and ISFC benefit from the higher fuel pressure, although this is not straightforward when considering the advanced CA50. It is assumed here that the higher pressure, and expected improved mixing, leads to less wall-wetting, and therefore improved combustion efficiency. This is supported by the fact that both smoke and UHC emissions show a large improvement at the higher fuel pressure. Reduced smoke emissions in the EDI PCCI regime as a result of higher Pfuel have been reported by others as well [2].

Table 6.10: Impact of T_{fuel} on performance and emissions in the EDI PCCI regime (see Appendix D).

Parameter	Unit	Low T_{fuel}	High T_{fuel}
T_{fuel}	K	303	373
IMEP	bar	3	3.00 (-)
CA50	$^{\circ}\text{CA aTDC}$	-5.2	-5.7 (- 0.5 $^{\circ}\text{CA}$)
ISFC	g/kWh	265	251 (- 5 %)
NOx	g/kWh	0	0.00 (-)
UHC	g/kWh	9.4	7.5 (- 20 %)

Fuel temperature

Fuel injection temperature (T_{fuel}), measured at ~ 50 mm from the injector, was incrementally increased via a heated common rail located at approximately 200 mm from the injector. The relevance of T_{fuel} on the actual fuel temperature at the nozzle was checked in open-air experiments and both were found to correlate quite well. Fueling levels were set such that the IMEP was 3 bar for both fuel temperatures at a SoA of $-50^{\circ}\text{CA aTDC}$. In accordance with Table 6.3, a SoA sweep is subsequently performed from -50 to $-65^{\circ}\text{CA aTDC}$ at two fuel temperatures: 303 and 373 K. All remaining engine operating conditions were kept constant. Listed in Table 10 are the results of the increase in T_{fuel} concerning performance and emissions at a constant SoA of $-50^{\circ}\text{CA aTDC}$. Values in brackets are relative to the Low T_{fuel} case to single out the influence of the measure under investigation. A complete overview of all data points is presented in Appendix D.

The results indicate that both fuel economy and emissions improve when the fuel temperature is raised in the EDI PCCI regime. The advanced CA50, improved ISFC and considerably lower UHC and smoke emissions support the hypothesis that a higher fuel temperature can reduce wall-wetting. This is particularly evident at very early timings for the SoA (Appendix D).

Summary

In this Section, the impact of injection timing, intake temperature, intake pressure, fuel pressure and fuel temperature on engine performance and emission formation has been investigated for EDI PCCI operating conditions. In Table 6.11, a ranking is presented of these software measures with respect to engine performance and emissions. Note that this ranking is purely indicative as some boundary conditions were different for the various measures. It is interesting to note that all measures, while having a neutral to positive effect on performance, smoke and UHC emissions, have a neutral to negative effect on NOx. This is in line with the well-known Diesel Dilemma, which typically holds for conventional HDDI diesel combustion. It is likely that this dilemma holds for EDI PCCI combustion as well when wall-wetting occurs. A penalty in NOx in the EDI PCCI regime, however, is acceptable as the values are typically far below legislated targets.

Another general observation is that all measures lead to an advancement of the

Table 6.11: Summary: Ranking of "software measures".

	CA50	IMEP	ISFC	NO _x	UHC	Smoke
T _{in} ↑	←	0	0	- - -	+++	+++
P _{in} ↑	←	+++	+++	- - -	+++	+++
P _{fuel} ↑	←	+	++	0	++	++
T _{fuel} ↑	←	0	+	0	++	+++

← = advancement || → = retardation
 ± 0-5 % = 0 || ± 5-10 % = + || ± 10-25 % = ++ || > 25 % = +++
 NB a + symbol corresponds to an improvement

CA50. This could be expected given the fact that the measures under investigation are aimed at improving the mixing process. Of all measures, boosting the intake pressure appears to yield the best results, although these will likely worsen somewhat when boosting is achieved via an engine-driven compressor or turbocharger, instead of via an external compressor (Figure 6.1). A similar argument holds for increasing the injection pressure. Moreover, both measures involve improving already complex and expensive technologies. Conversely, increasing the intake temperature (via uncooled EGR) and/or fuel temperature (although less effective in the applied range) can be regarded as more or less cost-neutral and low-tech solutions.

6.5 Results & discussion: part 2 of 4

In this Section, the cumulative impact of the measures discussed in the previous Section is examined (Table 6.4). Maximum values for the intake temperature (353 K) and fuel temperature (373 K) are selected. Unfortunately, a higher injection pressure than 750 bar was not possible due to a malfunctioning at higher pressures in the fuel injector. This was repaired for the later experiments. In addition, although higher pressures appear favorable, the intake pressure was set to 1.25 bar (absolute), as it is assumed that higher boost pressure can not be achieved using conventional engine hardware. At the maximum values for T_{in} and T_{fuel}, a wide SoA timing sweep is performed (Table 6.12) to determine the optimal injection timing. The detailed results are presented in Appendix E.

From Table 6.12 becomes clear that the combination of a high T_{in} and high T_{fuel} leads to a considerable reduction in UHC emissions and smoke. This reduction, however, comes at a price. IMEP and ISFC both worsen, likely due to the further advancement of CA50. NO_x emissions suffer as well, which may be attributed to a large extent to the increase in T_{in}.

Because the operating conditions have changed significantly by introducing heavy uncooled EGR and hot fuel into the combustion chamber, it is interesting to perform a SoA timing optimization. As indicated in Table 12, the SoA is retarded from -50, to -30 and ultimately to -15 °CA aTDC. The effect on engine performance is clear. IMEP and ISFC approach their respective conventional HDDI baseline values for the best SoA timing of -15 °CA aTDC. NO_x emissions are over 95 % lower. UHC and smoke emissions, though still significantly higher than the conventional HDDI values,

Table 6.12: Cumulative (cum.) software measures optimization with a conventional nozzle. Values in brackets are relative to the normal DI baseline case (see Appendix E).

Parameter	Unit	Normal DI baseline	EDI PCCI baseline	SoA 1 cum.	SoA 2 cum.	SoA 3 cum.
nozzle	-	2	2	1	1	1
SoA	°CA aTDC	-15	-55	-50	-30	-15
EGR	wt-%	0	40	70	70	70
T _{in}	K	303	303	353	353	353
T _{fuel}	K	303	303	373	373	373
P _{in}	bar	1.25	1.25	1.25	1.25	1.25
P _{fuel}	bar	750	750	750	750	750
l	-	4.2	3.1	2	1.9	1.9
CA50	°CA aTDC	-0.7	-6.7	-10	-8.9	+0.8 (+1.5)
IMEP	bar	4	3.3	3	3.4	3.9 (- %)
ISFC	g/kWh	214	260	270	233	214 (-)
NO _x	g/kWh	15.1	0.2	1.3	1.6	0.65 (-96%)
UHC	g/kWh	0.12	4.76	3.35	1.42	0.64 (+433%)
Smoke	FSN	0.03	1.44	0.15	0.11	0.09 (+200%)

are but a fraction of the values measured in the EDI PCCI baseline work point.

It is striking that an equal SoA and IMEP/ISFC notwithstanding, the emission behavior is completely different. The emission characteristics in the -15 °CA aTDC EDI PCCI work point are more reminiscent of LDI PCCI behavior. It is known from literature [4, 5], that EDI PCCI is typically realized at a SoA of -10 °CA aTDC or even later and requires high injection pressures and modifications to the combustion chamber geometry (e.g. piston bowl, high swirl) in order to realize near-zero soot emissions and low NO_x. In the experiments presented here, the combustion chamber geometry has not been modified and a relatively low injection pressure was used. The combination of a lower compression ratio of 12 and heavy EGR apparently retard the onset of combustion such that LDI PCCI is achieved at a relatively early SoA.

From Table 6.12 becomes clear that at these operation conditions, given the smooth evolution of engine performance and emissions when retarding the SoA (Appendix E), no clear distinction between the EDI and LDI PCCI regimes can be made. From a control perspective, it is interesting to note that CA50 can be shifted via the SoA in the investigated SoA range.

Table 6.13: Cumulative software measures optimization with smaller nozzle holes (nozzle 2). Values in brackets are relative to the normal DI baseline case (see Appendix F1 and F2).

Parameter	Unit	Pfuel Sweep			SoA Sweep	
		850 bar	1200 bar	1600 bar @ -50	1600 bar @ -30	1600 bar @ -15
nozzle	-	2	2	2	2	2
SoA	°CA aTDC	-50	-50	-50	-30	-15
EGR	wt-%	70	70	70	70	70
T _{in}	K	353	353	353	353	353
T _{fuel}	K	360	360	360	360	360
P _{in}	bar	1.25	1.25	1.25	1.25	1.25
λ	-	1.7	1.7	1.7	1.7	1.7
CA50	°CA aTDC	-10.8	-11.2	-10.2	-8.7	-1 (-0.3)
IMEP	bar	3.6	3.5	3.6	3.81	4.1 (+3%)
ISFC	g/kWh	252	254	255	246	217 (+1%)
NOx	g/kWh	1.4	1.8	1	0.96	0.65 (-96%)
UHC	g/kWh	1.5	1.3	1.1	0.42	0.66 (+450%)
Smoke	FSN	0.15	0.07	0.04	0.03	0.03 (-)

6.6 Results & discussion: part 3 of 4

In this Section, the effect of the cumulative software measures in combination with two hardware measures will be discussed. As described in Table 6.5, experiments with a second nozzle with smaller nozzle holes and a third nozzle with both smaller nozzle holes and a narrower cone angle are performed.

6.6.1 Smaller nozzle holes

First, the combination of a higher P_{fuel} with a high T_{fuel} and T_{in} is studied (Table 6.13, Appendix F) at a constant EDI PCCI SoA timing of - 50 °CA aTDC. From Table 6.13 becomes clear that while IMEP and CA50 remain more or less unaffected by an increase in P_{fuel}, UHC emissions and in particular smoke are noticeably decreased. Likely, this is attributable to a reduction in wall-wetting as a result of improved mixing.

Next, at the highest value for P_{fuel}, the SoA is retarded from -50 to -30 and ultimately to -15 °CA aTDC. As was the case for the previous (conventional) nozzle (Table 6.12), ISFC and IMEP approach their normal DI baseline values, while NOx is reduced by over 95 %. Smoke and UHC emissions, while both significantly higher than the conventional baseline values, are substantially lower than what was the case

in the EDI PCCI baseline work point (column 4, Table 6.12).

The influence of smaller nozzle holes can be studied when comparing the 5th column in Table 6.12 with the 3rd column in Table 6.13, as in both cases the P_{fuel} is around 800 bar. In agreement with literature [10], there is a clear improvement in IMEP and ISFC, but the largest effect ($> 50\%$ decrease) is measured for UHC emissions. It is assumed that the smaller nozzle holes improve the vaporization process and accordingly lead to a reduction in wall-wetting. Smoke and NO_x are more or less unaffected by the change of the nozzle. Once again, from a control perspective, it is interesting to note that CA50 can be shifted via the SoA in the investigated SoA range.

6.6.2 Narrower cone angle

It is known from literature [2] that a narrower cone angle can reduce the occurrence of wall-wetting, because the spray is directed downwards rather than sideways, as is typically the case for conventional diesel nozzles. Details on the utilized nozzles can be found in Table 6.5. The impact of the cone angle can be studied by comparing the 5th column in Table 6.13 with the 5th column in Table 6.14. While the CA50 remains constant, IMEP and ISFC both improve. It is assumed that this is the result of a reduction in wall-wetting. This assumption is supported by the reduction in UHC emissions of over 30 %.

NO_x is little affected by the narrower cone angle, but smoke emissions show a sharp increase in excess of 300 %. A phenomenon known as pool-fire, which is a diffusion-like combustion on the piston surface, might be responsible for this. Described in [2], pool-fire can occur when a narrow cone angle is used under EDI PCCI conditions. Characteristic for pool-fire is a steady increase in smoke and simultaneous decrease in UHC emissions. The latter can be explained by the relatively high temperature in the characteristic diffusion-like flames [2]. NO_x emissions should reportedly suffer as well due to the aforementioned higher flame temperature [2]. NO_x emissions, however, as mentioned earlier, appear to be left unaffected by the narrower cone angle in the experiments presented in this work. This discrepancy may be explained by the marginally higher EGR (i.e. 75 vs. 70 wt-%) used in the narrow cone angle experiments, which counteracts (and might balance) the above mentioned effect.

The results at retarded SoA timings show similar distinctions between the two nozzle types. For this columns 5 thru 7 (nozzle 2, Table 6.13) have to be compared to columns 5 thru 7 (nozzle 3, Table 6.14). IMEP and ISFC are slightly improved, while NO_x remains more or less unchanged. Smoke emissions are substantially higher, while UHC emissions are significantly lower. Accordingly, the results suggest that the pool-fire phenomenon is present in a wide range of injection timings. As was the case for the previous nozzles, CA50 and SoA appear to be coupled in the investigated SoA range. More detailed information on these measurements is presented in Appendix G.

Table 6.14: Cumulative (cum.) software measures optimization with smaller nozzle holes and narrow cone angle (nozzle 3). Values in brackets are relative to the normal DI baseline case (see Appendix G).

Parameter	Unit	Normal DI baseline	EDI PCCI baseline	SoA 1 cum.	SoA 2 cum.	SoA 3 cum.
nozzle	-	2	2	3	3	3
SoA	°CA	-15	-55	-50	-30	-15
	aTDC					
EGR	wt-%	0	40	75	75	75
T _{in}	K	303	303	353	353	353
T _{fuel}	K	303	303	373	373	373
λ	-	4.2	3.1	1.7	1.7	1.7
CA ₅₀	°CA	-0.7	-6.7	-10.5	-7.5	-0.5 (-0.2)
	aTDC					
IMEP	Bar	4	3.3	3.73	4.06	4.13 (+3%)
ISFC	g/kWh	214	260	235	215	211 (-1%)
NO _x	g/kWh	15.1	0.2	0.95	0.45	0.46 (-97%)
UHC	g/kWh	0.12	4.76	0.75	0.46	0.38 (+217%)
Smoke	FSN	0.03	1.44	1.76	0.19	0.20 (+533%)

6.7 Results & discussion: part 4 of 4

It is evident from the previous sections that UHC emissions are reduced for all investigated measures aimed at curbing well-wetting. In order to make a theoretical assessment of the hypothesis that a certain measure actually reduces wall-wetting, an estimate of the degree of wall-wetting has to be made. This is realized by implementing a well-established model for wall-wetting, namely the Liquid Length (LL) engineering correlation developed by Siebers and co-workers [10, 11] in the late nineties. n-Dodecane is selected as model fuel as its boiling point corresponds to the lower limit of the diesel boiling range. Accordingly, for given operating conditions, the modeled liquid phase penetration of this compound is indicative of the minimum liquid phase penetration of diesel fuel. The properties for n-dodecane are retrieved from the DIPPR database [13].

From Table 6.15 it becomes clear that most investigated measures (i.e. intake temperature, intake pressure, fuel temperature and nozzle diameter) also result in a lower predicted LL value, suggesting that UHC emissions may be a good indicator for the degree of wall-wetting in the investigated EDI PCCI regime.

As acknowledged by the authors [10], the model is insensitive to a change in fuel injection pressure as this parameter does not influence liquid phase penetration

Table 6.15: Modeled liquid phase penetration for various operating conditions in EDI PCCI regime (SoA = -50 °CA aTDC).

Reduction method	Tin		Pin		Pf		Tf	
	303 K	353 K	1 bar	2 bar	770 bar	1490 bar	303 K	373 K
Pin [bar]	770	770	800	800	770	1490	1100	1100
Tf [K]	303	303	303	303	303	303	303	373
Tcyl [K]	505.8	584.7	505.8	507.3	505.9	505.9	505.9	505.9
pcyl [bar]	7.71	7.65	6.2	12.4	9.25	9.25	9.25	9.25
ρ_{cyl} [kg/m ³]	5.27	4.52	4.24	8.48	6.32	6.32	6.32	6.32
LL ($\varnothing = 0.190$ mm)	335	131.2	380	241.7	300.4	300.4	300.4	263.1
LL ($\varnothing = 0.161$ mm)	283.9	111.2	322	204.8	254.6	254.6	254.6	223

in the mixing-limited vaporization regime [10]. In the experiments, however, the measured decline in UHC emissions suggests a decrease in LL with increasing injection pressure (Table 6.9). A possible explanation for this discrepancy could be related to the relatively low gas temperature used in the experiments. As the gas temperature approaches the boiling range of a fuel, the assumption of mixing-limited vaporization is no longer valid and is replaced (gradually) by a regime wherein vaporization is limited by interphase transport [11]. The importance of fuel injection pressure, and in particular its impact on droplet size, in this regime is subject of current research.

6.8 Conclusions

In order to reduce the occurrence of wall-wetting under early direct injection (EDI) PCCI conditions, a number of measures have been investigated:

- Higher intake temperature (via hot EGR)
- Higher intake pressure (via external boosting)
- Higher fuel pressure (via external fuel pump)
- Higher fuel temperature (via heated commonrail)
- Smaller nozzle holes
- Smaller nozzle holes + narrower cone angle

All experiments have been performed at low load (~ 3 -4 bar IMEP) and at an engine speed of 1200 RPM, using a modified 6-cylinder 12.6 liter heavy-duty DI DAF XE 355C engine. Experiments are conducted in one dedicated cylinder, which is

Table 6.16: Best results. Note that parameters relative to engine power (i.e. g/kWh) are indicated not brake specific, as they are based on IMEP.

Parameter	Unit	Normal DI baseline	EDI PCCI baseline	EDI PCCI best	LDI PCCI best
nozzle	-	2	2	3	2
SoA	°CA aTDC	-15	-55	-30	-15
SoI	°CA aTDC	-11	-	-	-11
EoI	°CA aTDC	-1	-	-	-6
EGR	wt-%	0	40	75	70
Pin	bar	1.25	1.25	1.25	1.25
Pfuel	bar	750	750	1600	1600
Tin	K	303	303	353	353
Tfuel	K	303	303	373	360
λ	-	4.2	3.1	1.7	1.7
SoC/CA10	°CA aTDC	-2.9	-	-	-3.4
CA50	°CA aTDC	-0.7	-6.7	-7.5	-1
IMEP	bar	4	3.3	4.06	4.1
ISFC	g/kWh	214	260	215	217
NOx	g/kWh	15.1	0.2	0.45	0.65
UHC	g/kWh	0.12	4.76	0.46	0.66
Smoke	FSN	0.03	1.44	0.19	0.03

equipped with a stand-alone fuel injection system, EGR circuit and air compressor, fueled with commercial diesel fuel (EN590).

In the EDI PCCI regime, measured UHC emissions, an indicator of wall-wetting, suggest that wall-wetting is indeed (partially) suppressed for all investigated measures. Spray modeling results retrieved from the Siebers LL engineering correlation show that for most measures the LL, a measure for wall-wetting, is indeed reduced. Fuel injection pressure appears to be an exception. Not accounted for in the utilized model, higher fuel pressures obviously reduce UHC emissions in the engine experiments. Other (CFD) models which do take the fuel pressure into account are currently subject of investigation. The best overall results achieved in the EDI PCCI regime are presented in Table 6.16 (column 5).

In this workpoint the fuel and intake temperature, as well as the fuel pressure, are set to their respective maximum values. In addition, a narrow cone angle nozzle with smaller holes (nozzle 3) is used. By comparing column 4 (baseline EDI PCCI) and 5 (best EDI PCCI) in Table 6.16, the significant improvement in UHC emissions and engine performance becomes evident, indicating that wall-wetting is indeed suppressed to a large extent. Although UHC emissions can originate from other sources than solely wall-wetting, the extreme values and the observed correlation with various wall-wetting measures suggest that wall-wetting is responsible for the bulk of the UHC emissions.

Compared to conventional diesel combustion (Table 6.16, column 5 vs. 3), NOx emissions are reduced to extremely low values without a penalty in fuel economy.

Unfortunately both smoke and UHC emissions are significantly higher. The relatively high smoke values may be (partially) attributed to a phenomenon known as pool-fire (i.e. diffusion-like combustion on the piston surface) which is a direct consequence of injection via a narrow cone angle nozzle [2], while the high UHC emissions are likely the result of a remaining wall-wetting effect.

In an attempt to curb wall-wetting and retard CA50 more towards TDC, the injection timing was retarded further from -30 to -15 °CA aTDC and the nozzle was replaced by a conventional cone angle variant (nozzle 2). In doing so, a transition was made from an EDI PCCI (Table 6.16, column 5) to a late direct injection (LDI) PCCI timing (Table 6.16, column 6).

To confirm that the LDI PCCI work point in Table 6.16 indeed qualifies as PCCI, a final brief heat-release analysis is made. Herein, CA10 is taken as the start of combustion (SoC). From Table 6.16 becomes clear that, contrary to the normal DI baseline case, the CA10 occurs several crank angles later than of the end of injection (EOI). As discussed in the Introduction, the main qualifier for PCCI is that the fuel injection and heat release events are separated in time. Accordingly, the investigated LDI work point in Table 6.16 may be referred to as LDI PCCI.

Under the utilized conditions of a low compression ratio of 12 and heavy EGR (70 wt-%), retarding the injection timing and replacing the nozzle resulted in a further reduction of smoke, with an acceptable increase in UHC and NO_x emissions. Fuel economy and IMEP are comparable. The available data suggests that while acceptable PCCI operation is possible in the EDI regime, comparable fuel economy and near-EURO VI-like smoke and NO_x emissions can be realized without smoke/NO_x aftertreatment in LDI PCCI mode. UHC emissions are too high, but could be dealt with by mounting an oxidation catalyst in the exhaust system. Overall it seems that when a conventional diesel fuel is considered, LDI PCCI appears to be more promising than EDI PCCI.

Lastly, it should be noted from a control perspective that the combustion phasing is sensitive to the injection timing and other operating conditions even in the EDI PCCI regime. For LDI PCCI, this sensitivity is even stronger.

Nomenclature

Abbreviations

AFR	Air Fuel Ratio
aBDC	After Bottom Dead Center
aTDC	After Top Dead Center
bBDC	Before Bottom Dead Center
bTDC	Before Top Dead Center
CA10	Crank Angle at which 10% of the fuel is burnt
CA50	Crank Angle at which 50% of the fuel is burnt
cDPF	Catalytic Diesel Particulate Filter
CA	Crank Angle
CI	Compression Ignition
d	diameter
EDI	Early Direct Injection
EGR	Exhaust Gas Recirculation
EN590	Baseline commercial diesel fuel
EOI	End of injection (fuel delivery)
FIE	Fuel Injection Equipment
FSN	Filter Smoke Number
HDDI	Heavy Duty Direct Injection
IMEP	Indicated Mean Effective Pressure
ISFC	Indicated Specific Fuel Consumption
LDI	Late Direct Injection
LL	Liquid Length
p	Pressure
PAH	Poly Aromatic Hydrocarbons
PCCI	Premixed Charge Compression Ignition
P _{fuel}	Fuel injection pressure
P _{in}	Intake pressure
SI	Spark Ignition
SoA	Start of Injection (actuation)
SoC	Start of combustion
SOI	Start of Injection (fuel delivery)
T	Temperature
T _{fuel}	Fuel temperature
T _{in}	Intake temperature
TDC	Top Dead Center
UHC	Unburned Hydrocarbons

Greek symbols

°	Degree (i.e. Crank Angle)
∅	Diameter
φ	Equivalence ratio
θ	Cone angle

Bibliography

- [1] M.D. Boot, C.C.M. Luijten, L.M.T. Somers, U. Eguz, D.D.T.M. van Erp, B.A. Albrecht, and R.S.G. Baert. Uncooled EGR as a means of limiting wall-wetting under early direct injection conditions. *SAE Paper*, 2009-01-0665, 2009.
- [2] G.C. Martin, C.J. Mueller, D.M. Milam, M.S. Radovanovich, and C.R. Gehrke. Early directinjection, low-temperature combustion of diesel fuel in an optical engine utilizing a 15-hole, dual-row, narrow-included-angle nozzle. *SAE Paper*, 2008-01-2400, 2008.
- [3] P. Risberg, G. Kalghatgi, H-E. Ångstrom, and F. Wåhlin. Auto-ignition quality of diesel-like fuels in hcci engines. *SAE Paper*, 2005-01-2127, 2005.
- [4] H. Ogawa, S. Kimura, M. Koike, and Y. Enomoto. A study of heat rejection and combustion characteristics of a low-temperature and pre-mixed combustion concept based on measurement of instantaneous heat flux in a direct-injection diesel engine. *SAE Paper*, 2000-01-2792, 2000.
- [5] S. Kimura, O. Aoki, Y. Kitahara, and E. Aiyoshizawa. New combustion concept for ultra clean and high efficiency small DI diesel engines. *SAE Paper*, 1999-01-3681, 1999.
- [6] M.D. Boot, P.J.M. Frijters, R.J.H. Klein-Douwel, and R.S.G. Baert. Oxygenated fuel composition impact on heavy-duty diesel engine emissions. *SAE Paper*, 2007-01-2018, 2007.
- [7] M.D. Boot, P.J.M. Frijters, C.C.M. Luijten, L.M.T. Somers, R.S.G. Baert, A.J. Donkerbroek, R.J.H. Klein-Douwel, and N.J. Dam. Cyclic oxygenates: A new class of second-generation biofuels for diesel engines? *Energy Fuels*, 23:1808 – 1817, 2009.
- [8] G. Kalghatgi. Auto-ignition quality of practical fuels and implications for fuel requirements of future SI and HCCI engines. *SAE Paper*, 2005-01-0239, 2005.
- [9] N.A. Henein, A. Kastury, K. Natti, and W. Bryzik. Advanced low temperature combustion (ALTC): diesel engine performance, fuel economy and emissions. *SAE Paper*, 2008-01-0652, 2008.
- [10] B.S. Higgins, C.J. Mueller, and D.L. Siebers. Measurements of fuel effects on liquid-phase penetration in di sprays. *SAE Paper*, 1999-01-0519, 1999.
- [11] D.L. Siebers. Scaling liquid-phase fuel penetration in diesel sprays based on mixing-limited vaporization. *SAE Paper*, 1999-01-0528, 1999.
- [12] T. Kanda, T. Hakoziaki, T. Uchimoto, J. Hatano, N. Kitayama, and H. Sono. PCCI operation with early injection of conventional diesel fuel. *SAE Paper*, 2005-01-0378, 2005.
- [13] Brigham Young University. *DIPPR Database*. <http://dippr.byu.edu/>.

Appendix A: Intake Temperature (Table 6.7)

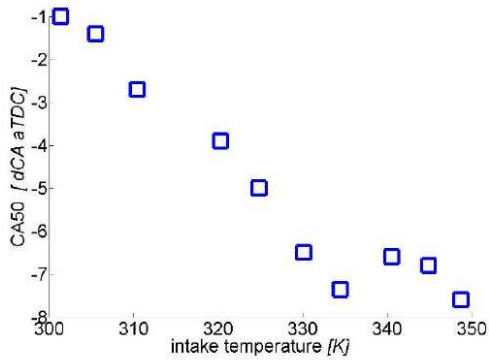


Figure 8 Impact intake temperature on CA50

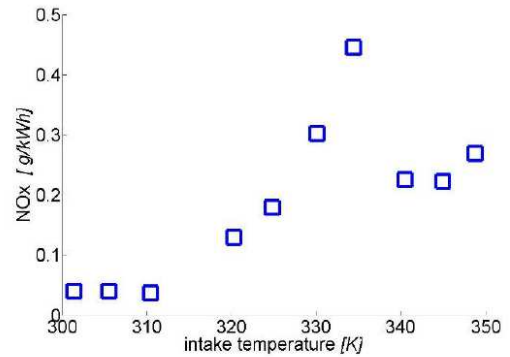


Figure 11 Impact intake temperature on NOx

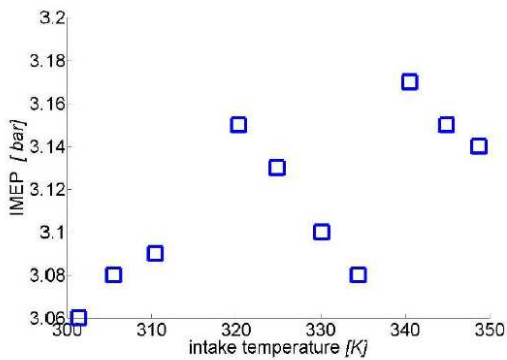


Figure 9 Impact intake temperature on IMEP¹

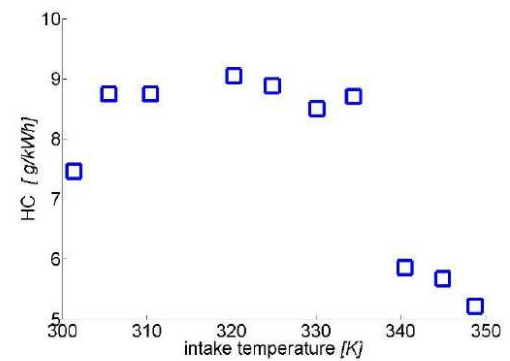


Figure 12 Impact intake temperature on HC

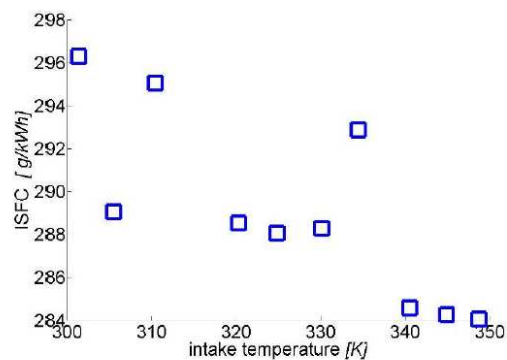


Figure 10 Impact intake temperature on ISFC

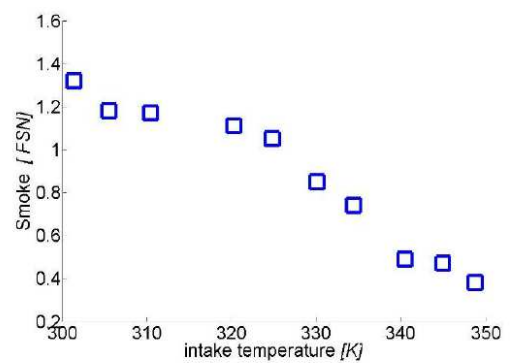


Figure 13 Impact intake temperature on smoke

¹ Odd trend is the result of a slight adjustment in EGR level made between two workpoints to correct for a small drift in EGR level.

Appendix B: Intake Pressure (Table 6.8)

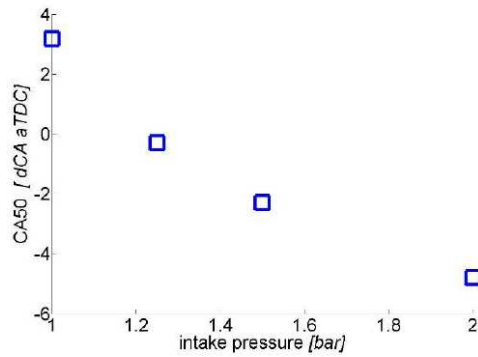


Figure 14 Impact intake pressure on CA50

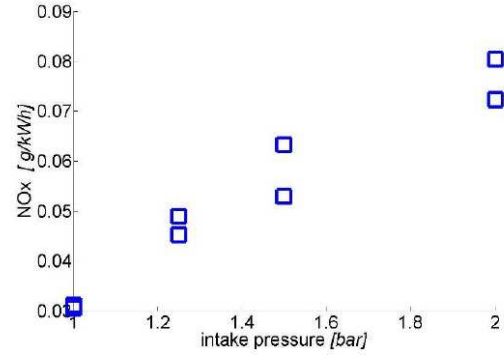


Figure 17 Impact intake pressure on NOx

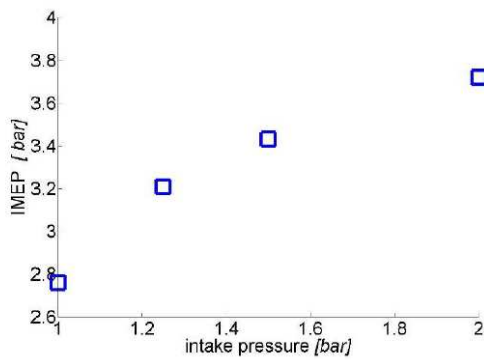


Figure 15 Impact intake pressure on IMEP

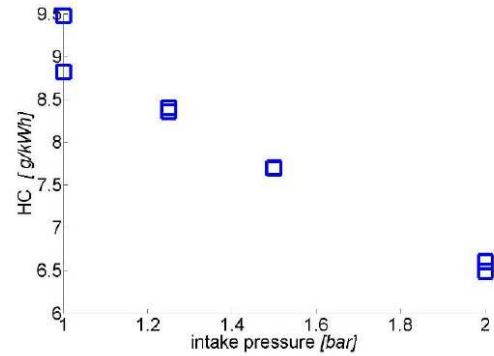


Figure 18 Impact intake pressure on HC

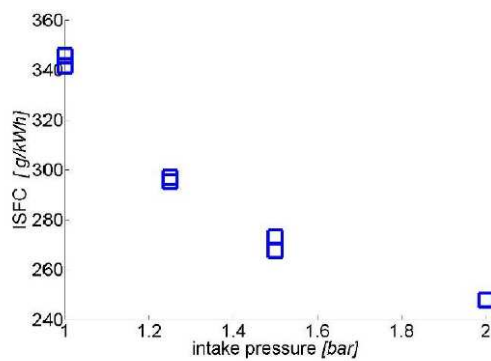


Figure 16 Impact intake pressure on ISFC¹

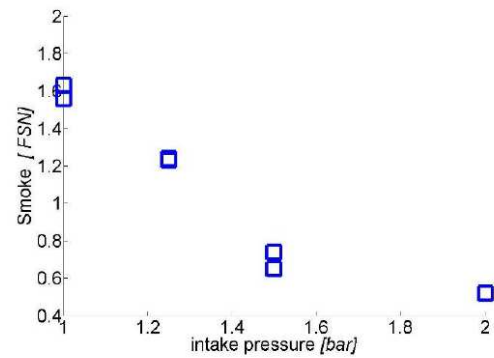


Figure 19 Impact intake pressure on smoke

¹ In Appendices B, C and D the two measuring points at a given condition are repetitions.

Appendix C: Fuel Pressure (Table 6.9)

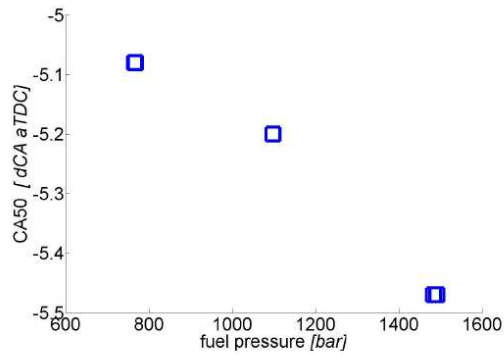


Figure 20 Impact fuel pressure on CA50

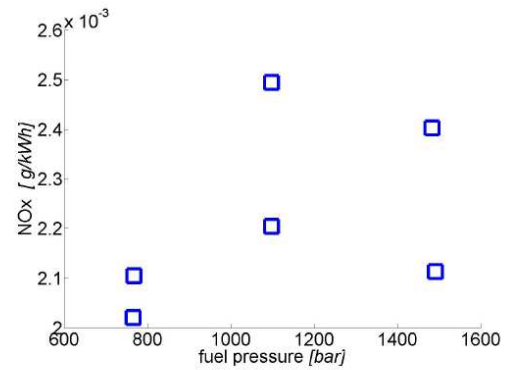


Figure 23 Impact fuel pressure on NOx

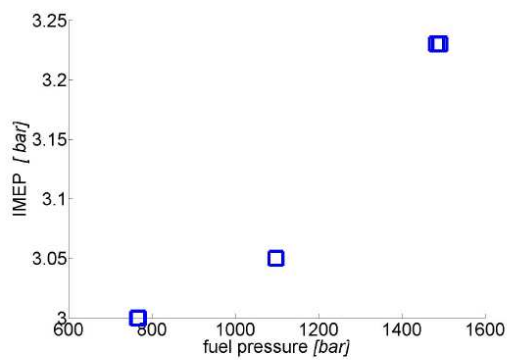


Figure 21 Impact fuel pressure on IMEP

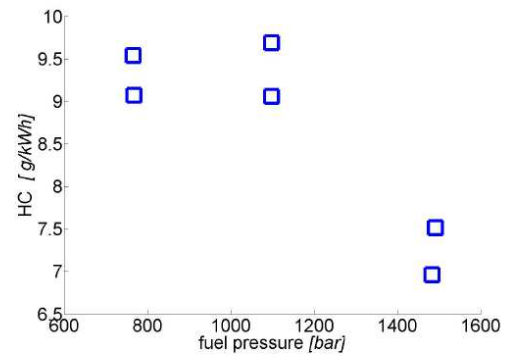


Figure 24 Impact fuel pressure on HC

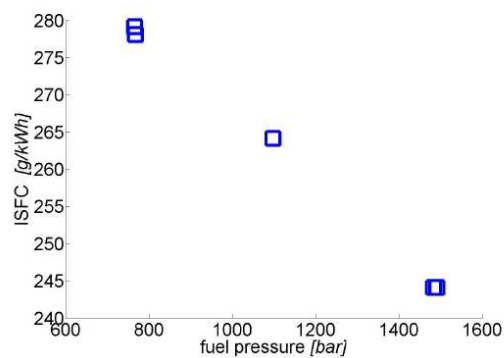


Figure 22 Impact fuel pressure on ISFC

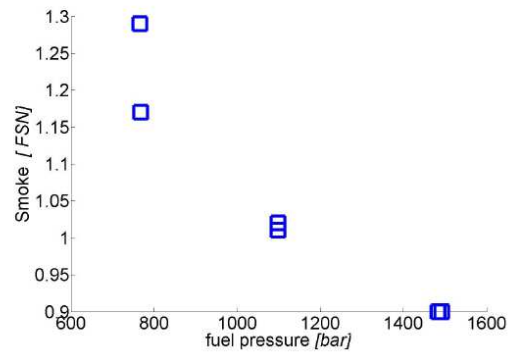


Figure 25 Impact fuel pressure on smoke

Appendix D: Fuel Temperature (Table 6.10)

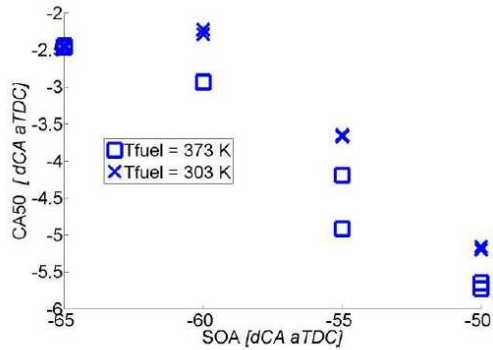


Figure 26 Impact fuel temperature on CA50

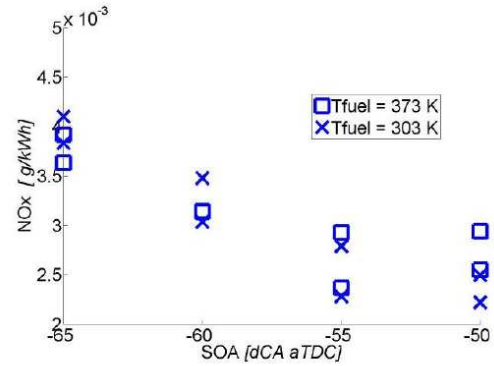


Figure 29 Impact fuel temperature on NOx

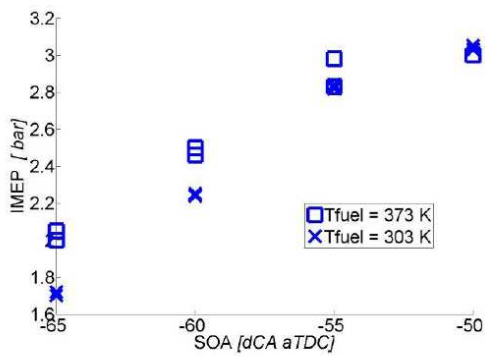


Figure 27 Impact fuel temperature on IMEP

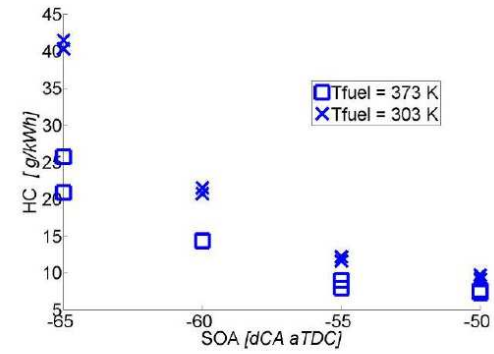


Figure 30 Impact fuel temperature on HC

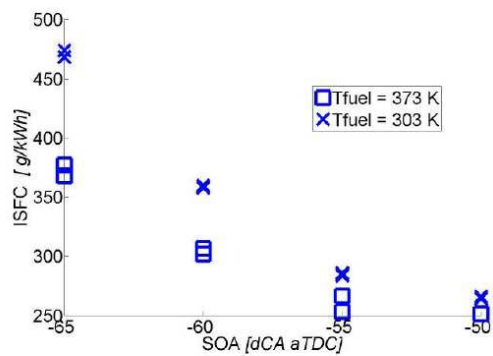


Figure 28 Impact fuel temperature on ISFC

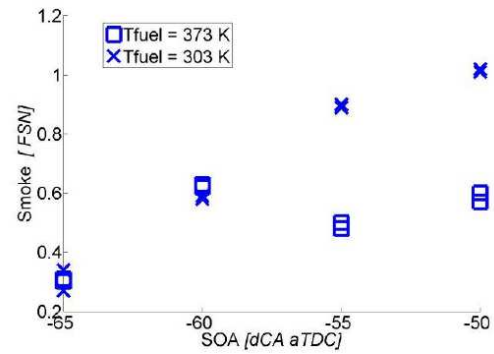


Figure 31 Impact fuel temperature on smoke

Appendix E: Cumulative Software Measures (left figures) (Table 6.12)

Appendix F1: Intake Temperature (right figures)(Table 6.13)

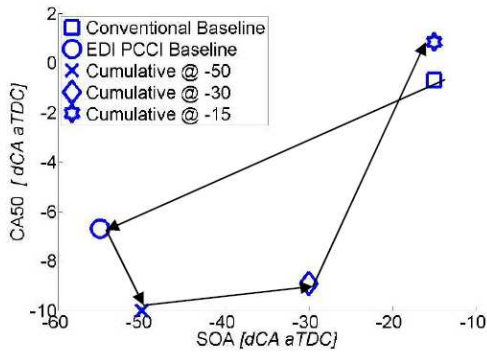


Figure 32 Impact of operation conditions on CA50

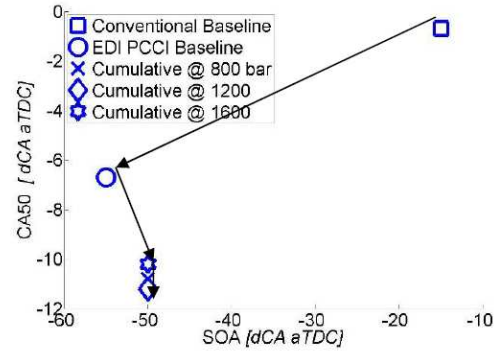


Figure 35 Impact of operation conditions on CA50

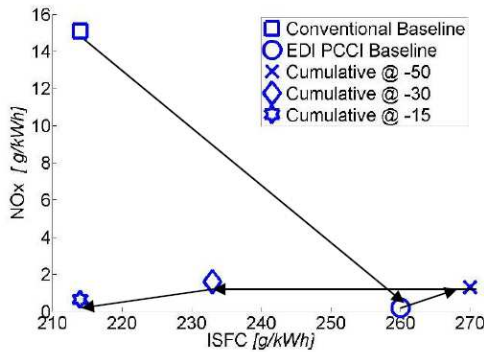


Figure 33 Impact of operation conditions on ISFC and NOx

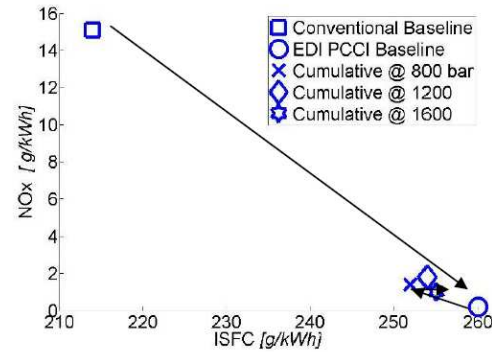


Figure 36 Impact of operation conditions on ISFC and NOx

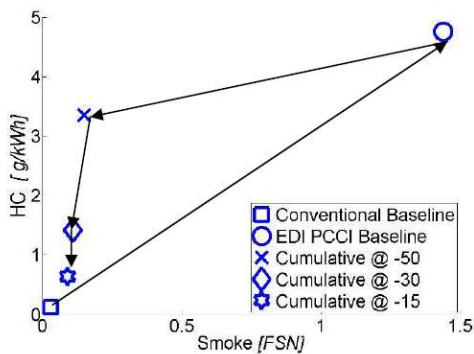


Figure 34 Impact of operation conditions on smoke and HC

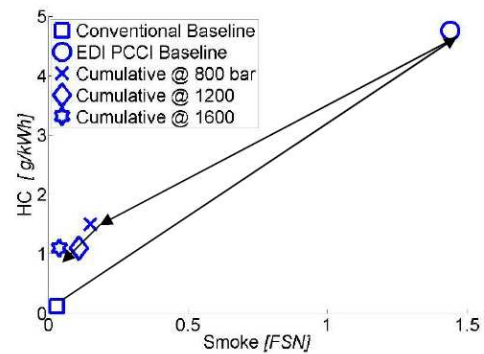


Figure 37 Impact of operation conditions on smoke and HC

Appendix F2: Nozzle Diameter (left figures) (Table 6.13)

Appendix G: Cone Angle (right figures)(Table 6.13)

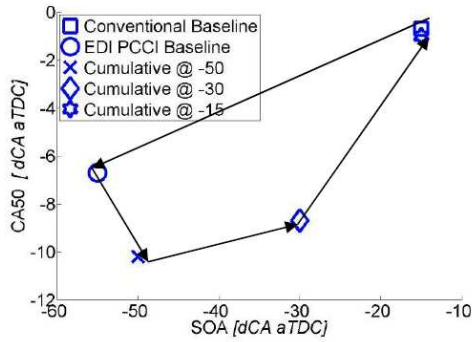


Figure 38 Impact of operation conditions on CA50

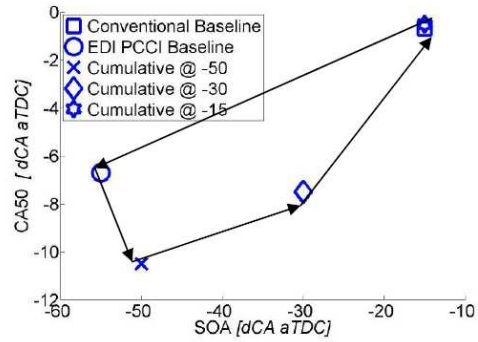


Figure 41 Impact of operation conditions on CA50

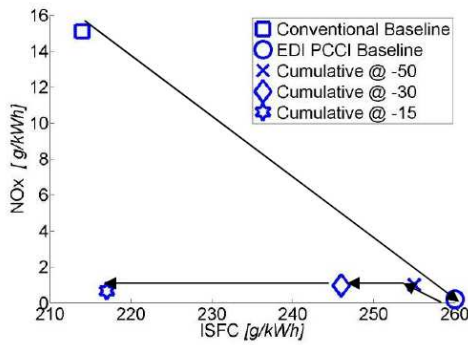


Figure 39 Impact of operation conditions on ISFC and NOx

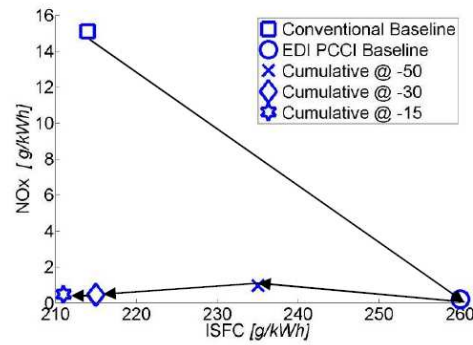


Figure 42 Impact of operation conditions on ISFC and NOx

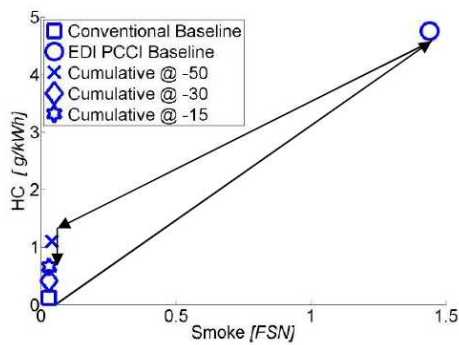


Figure 40 Impact of operation conditions on smoke and HC

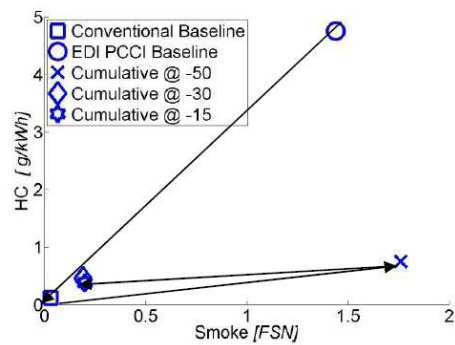


Figure 43 Impact of operation conditions on smoke and HC

Spray Impingement in the Early Direct Injection Premixed Charge Compression Ignition Regime

The main goal of this paper is to acquire more insight into the relationship between wall and piston impingement of liquid fuel and UHC emissions, under early direct injection (EDI) premixed charge compression ignition (PCCI) operating conditions. To this end, the vaporization process is modeled for various operating conditions using a commercial CFD code (StarCD). Predicted values for liquid core penetration, or liquid length (LL), have been successfully checked against experimental data from literature over a wide range of operating conditions. Next, the correlation between the CFD results for wall and piston impingement and measured UHC emissions is studied. The diesel fuel used in the experiments is modeled as n-dodecane and n-heptadecane, representing the low and high end of the diesel boiling range, respectively. A distinction is made between liquid spray impingement on the piston surface and cylinder liner. For a conventional DI diesel nozzle, the high UHC emissions in the EDI PCCI regime correlate well with modeled cylinder wall impingement. Conversely, piston impingement is negligible in this regime. Accordingly, it may be assumed that the primary cause for high UHC emissions in the EDI PCCI regime, using conventional DI nozzles, is caused by liquid spray impingement against the cylinder liner. In this regime it was found that a higher intake and fuel temperature, as well as an elevated intake pressure have a positive effect on both UHC emissions and the spray impingement against the cylinder wall. This provides additional evidence that the two parameters (i.e. UHC and wall impingement) are linked. Lastly, the impact of nozzle cone angle is investigated. When adopting a narrow cone angle nozzle in the EDI PCCI regime, wall impingement is negligible and piston wetting becomes the dominant source of UHC emissions.

The content of this chapter has been taken from:

M.D. Boot, E.P. Rijk, C.C.M. Luijten, L.M.T. Somers and R.S.G. Baert. Modeling of Liquid Phase Penetration in the Early Direct Injection Regime. *Submitted to SAE*, January 2010.

Minor edits have been made to streamline the layout of the thesis chapters. Experiments were carried out in the engine lab of the Eindhoven University of Technology.

7.1 Introduction

Combustion in compression ignition engines is highly efficient, but unfortunately results in soot emissions. By allowing a (partially) premixed bulk charge to auto-ignite rather than several poorly mixed spray cones, as is conventionally the case, the soot formation process can be substantially suppressed [1–3]. This former combustion concept, referred to as Premixed Charge Compression Ignition (PCCI), is characterized by a separation in time of the fuel injection and heat-release events. In practice this entails prolonging the ignition delay, which can be realized via various methods. For example, one can inject a less reactive fuel with a lower Cetane Number [4–6] or inject the fuel relatively late (i.e. near or slightly after top-dead-center) in the cycle, thereby exploiting the cooling effect of the expansion stroke (mostly in combination with high levels of EGR and or lower compression ratio). A third approach under investigation involves a relatively early (i.e. at roughly two-thirds of the compression stroke) fuel injection. At such early direct injection (EDI) timings, the gas temperatures and pressures are typically too low to support auto-ignition, but ideally do facilitate fuel vaporization. Unfortunately, complete vaporization is often not possible [1, 7, 8], resulting in impingement of liquid fuel on the cylinder liner (wall-wetting) and/or piston surface (piston-wetting). Wetting, in turn, is known to lead to reduced fuel economy, lubricant oil dilution and high emissions of unburnt hydrocarbons (UHC) [8].

The main goal of this paper is to acquire more insight into the relationship between wall and piston impingement of liquid fuel and UHC emissions under early direct injection (EDI) premixed charge compression ignition (PCCI) operating conditions. To this end, the vaporization process is modeled for various operating conditions using a commercial CFD code (StarCD). Predicted values for liquid core penetration (LL) are successfully checked against experimental data from literature over a wide range of operating conditions. Next, the correlation between the CFD results and measured UHC emissions is studied. The diesel fuel used in the experiments is modeled by n-dodecane and n-heptadecane, representing the low and high end of the diesel boiling curve, respectively. Furthermore, a distinction is made between liquid spray impingement on the piston surface and cylinder liner.

7.2 Background

Earlier work [8, 9] has shown that under EDI PCCI conditions the emissions of UHC are unacceptably high. Accordingly, a number of parameters, listed below, were optimized on a dedicated DAF heavy-duty diesel engine in an attempt to reduce UHC emissions.

- start of injection (SOI)
- intake temperature (T_{in})
- intake pressure (p_{in})
- fuel pressure (p_f)
- fuel temperature (T_f)

- (injector nozzle) cone angle

The working hypothesis behind this optimization was that UHC emissions result primarily from wall-wetting and so the operating conditions should be made more conducive for fuel evaporation (e.g. higher T_{in} , p_{in} , p_f and T_f). While engine results [8] clearly demonstrated that all investigated strategies yielded considerably lower UHC emissions, it was unclear how these results correlated with the actual spray behavior. A semi-empirical engineering correlation [10] was used to predict the effect of the various measures on the so-called liquid length (LL , i.e. penetration of the liquid core of the fuel jet). Although this (0D) model clearly demonstrated [8] that in most cases a reduction in measured UHC emissions coincided with a shorter predicted LL , it remained unclear which fraction of the injected diesel fuel mass collides with what part of the combustion chamber periphery (piston and/or wall). To arrive at a better understanding of the spray evolution and interaction with the wall, a 3D model of the injection process was implemented in a commercial CFD code (StarCD), to be discussed in the following section.

7.3 Modeling

7.3.1 Fuel selection

As diesel fuel is a mixture of thousands of different chemical compounds, so-called surrogate fuels are used in the modeling process to capture generic physical behavior of a multi-component fuel. Two single component fuels are selected, with boiling points corresponding to the 5%- (n-dodecane) and 90%- (n-heptadecane) boiling point of commercial diesel fuel. Requisite fuel properties are retrieved from the DIPPR database [11]. Effectively, a lower and upper limit for fuel volatility effects on diesel impingement can be predicted via this approach.

To clarify this statement, a schematic example of two different mixtures of n-dodecane and n-heptadecane is presented in figure 7.1. Here, the fraction of fuel which is in the liquid state is plotted against the axial distance a in the spray, where fuel is injected from left to right. If the spray is modeled as droplets, they have to be heated before they can be vaporized. Due to the presence of n-heptadecane in both cases, the LL will most likely be similar as it is found that the higher boiling point component is controlling the LL [12]. The liquid fuel fraction that reaches the cylinder or piston surface at distance a , however, will differ significantly due to the different fuel composition. Accordingly, when the fuel is a mixture of compounds with varying boiling points, the actual amount of liquid fuel impingement is no longer directly related to LL . The inability to predict the fraction of liquid diesel fuel that impinges with the piston and/or wall surface is a major drawback of LL models. In a later section, which treats the utilized CFD model, it will be explained how this drawback is addressed.

7.3.2 Engine and nozzle specifications

The CFD results are compared with measured engine data from an earlier study [8]. Engine and nozzle data can be found in Tables 7.1 and 7.2.

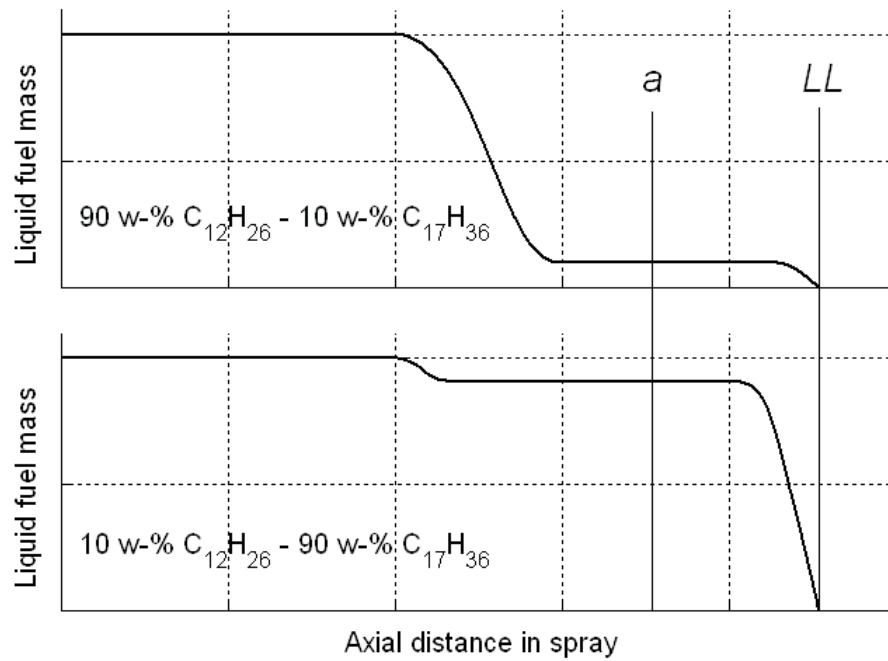


Figure 7.1: Schematic illustration of the influence of fuel composition on the LL and liquid fuel mass fraction at an arbitrary distance a

Table 7.1: Cyclops [8] Engine specifications.

engine type	six-cyl. 4-str. DI diesel
bore, stroke	130 mm, 158 mm
displacement	2.1 ℓ (per cylinder)
compression ratio	12
Intake valve open	16 $^{\circ}$ CA bTDC
Intake valve close	27 $^{\circ}$ CA aBDC
Exhaust valve open	52 $^{\circ}$ CA bBDC
Exhaust valve close	14 $^{\circ}$ CA aTDC

7.3.3 Operating conditions

The investigated strategies with their respective variation, corresponding to the bold values in table 7.3, are itemized below. Note that the fueling level (approx. 0.5 g/s or 4 bar IMEP) was kept constant during each variation. More details can be found in reference [8].

- SOI sweep from -5 to -60 $^{\circ}$ CA aTDC (table 7.3: cases 1-7).
- increase in T_{in} from 303 to 353 K (8-9).
- increase in p_{in} from 1.0 to 2.0 bar (absolute) (10-11).
- increase in p_f from roughly 800 to 1500 bar (12-13).

Table 7.2: Nozzle specifications.

nozzle #	nozzle diameter d_{noz} μm	cone angle θ $^\circ$
1	190	154
2	161	150
3	161	100

- increase in T_f from 303 to 373 K (14-15).
- narrow cone angle experiments with θ of 100° instead of 150° (16-18).

Table 7.3: Operating conditions.

case #	nozzle #	SOI $^\circ\text{CA}$	DOI $^\circ\text{CA}$	T_{in} K	p_{in} bar	p_f bar	T_f K
1	2	-5	9	303	1.25	830	303
2	2	-10	9	303	1.25	830	303
3	2	-20	9	303	1.25	830	303
4	2	-30	9	303	1.25	830	303
5	2	-40	9	303	1.25	830	303
6	2	-50	9	303	1.25	830	303
7	2	-60	9	303	1.25	830	303
8	1	-50	9	303	1.25	770	303
9	1	-50	9	353	1.25	770	303
10	1	-50	10	303	1.0	800	303
11	1	-50	10	303	2.0	800	303
12	1	-50	9	303	1.5	770	303
13	1	-50	6	303	1.5	1490	303
14	1	-50	7	303	1.5	1100	303
15	1	-50	7	303	1.5	1100	373
16	3	-50	6	360	1.25	1490	358
17	3	-30	6	360	1.25	1490	358
18	3	-10	6	360	1.25	1490	358

7.3.4 CFD model

The CFD code used in this study is Star-CD. A moving computational mesh is created, that represents a 1/7th (for each of the 7 nozzle holes) slice of the combustion chamber, to limit the amount of cells and consequently keeping computational times as small as possible. Intake- and exhaust manifolds and moving valves are not explicitly modeled, significantly reducing the complexity of the mesh. As the piston moves

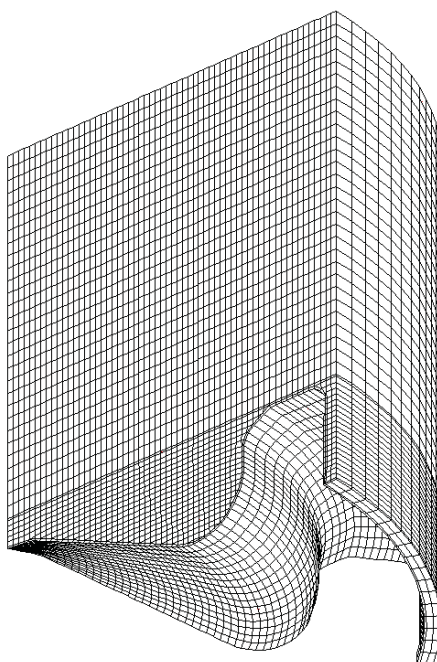


Figure 7.2: CFD mesh

up and compresses air, fuel is injected at different points in time, according to the injection timing used in the experiments.

The turbulent gas flow is based on an Eulerian description of the gas phase. Turbulence is modeled by means of a standard $k-\epsilon$ model [13], suitable for fully isotropic turbulent flows. The droplets are modeled in a Lagrangian framework. The interaction between the continuous and the dispersed phase is described by source terms for the exchange of heat, momentum and mass.

When fuel is injected through an injector, the fluid reaches a certain velocity creating a turbulent spray. To model the phenomena which occur inside the nozzle, the modified Max-Planck-Institut (MPI) nozzle model [14] has been applied. This model recognizes the creation of a cavitation region inside the nozzle and distinguishes three flow regimes in the nozzle hole. These three regimes are a non-cavitating flow, a cavitating flow where cavitation ends inside the nozzle and a cavitating flow where cavitation reaches the downstream end of the nozzle. These regimes depend on the pressure in the chamber relative to the critical pressure in the chamber at which cavitation commences, based on mass and momentum conservation equations.

After flowing through the injector, the liquid fuel jet exits the nozzle and breaks up. To describe primary and secondary break-up, the Reitz-Diwakar model [15] is applied. Depending on the ratio of inertial and surface forces (Weber number), breakup will occur in a certain mode and the model calculates a decrease in droplet diameter in time, depending on the timescale corresponding to the mode of droplet break-up.

Given the high droplet densities and velocity differences inside the spray, inter-droplet collisions can occur. Depending on the conditions, collisions can result in droplet separation, coalescence or bouncing. In the CFD model, these modes are described by the collision model of O'Rourke [16]. Here, the droplets are assumed to be uniformly distributed throughout the cell and the probability of a collision is

calculated using a Poisson distribution. If a collision occurs, the type of collision is determined using dimensionless numbers based on droplet velocities, diameter and physical properties [16].

When droplets hit a solid wall, different phenomena can occur. Examples are sticking, rebounding or splashing. In Star CD, it is possible to predict these different modes of wall interaction using the Bai [17] impingement model. In [18], three different wall impingement models have been reviewed. These models, the Bai model included, have been implemented into a KIVA-3V code and validated by experimental data from recent literature. From this research, it has been concluded that all three models should be further improved for the simulation of spray-wall interaction under EDI PCCI conditions. Main cause for the poor accuracy of the models is that they are derived from experiments performed under atmospheric conditions by injecting a single water drop onto a flat wall. These conditions are obviously not representative for in-cylinder conditions in the EDI PCCI regime. Therefore, in the present study, it has been decided not to use this model, but rather to model droplet-wall interaction via perfectly bouncing droplets. In that case, if a droplets hits a wall, its velocity-vector is reversed and the droplet returns with the same velocity magnitude. The change in vector-sign makes it possible to detect all liquid fuel impinging on either the cylinder wall or piston surface. Combustion will certainly influence the evaporation behavior as well, as the increasing temperature causes more fuel to evaporate. Considering that the injection and combustion event are by definition decoupled in time in the (EDI) PCCI combustion regime, no combustion model is used in this work to analyze spray vaporization and impingement process.

7.3.5 Validation

In order to perform a preliminary check of the CFD model, modeled LL values are compared to experimental data from literature [19–21], obtained for vaporizing sprays over a wide range of fuels and operating conditions (figure 7.3(a)). A similar procedure is executed for the semi-empirical engineering correlation discussed earlier (figure 7.3(b)). Accordingly, the performance of both models can be evaluated.

Considering experimental values, it is clear from the literature [19–21] that there is no unambiguous method to define the liquid penetration based on the recorded MIE scattering. In part this is caused by the fact that, towards the end of the liquid core, a spray tends to break up into clusters of droplets, shedding of discrete droplet clouds prior to fully evaporating [20]. In reference [19], an approach is proposed in which analysis of the Mie-scattered light images involves determining the maximum axial distance in the spray where the light intensity is above a threshold, equal to 3% of the light intensity range measurable with the camera [12]. It is stressed, however, that many definitions are found in literature, none of which are fully proven and therefore all reported LL values should be interpreted carefully.

To be able to determine the liquid length from the CFD model objectively, a suitable droplet post-processing method had to be developed. In the experimental Mie approach, the scattered intensity is a function of the product of the number of droplets and the square of the droplet diameter. Accordingly, the value of this same product is used to evaluate the LL in the CFD model. More specifically, the position of the LL is defined as the point on the spray axis where the derivative of

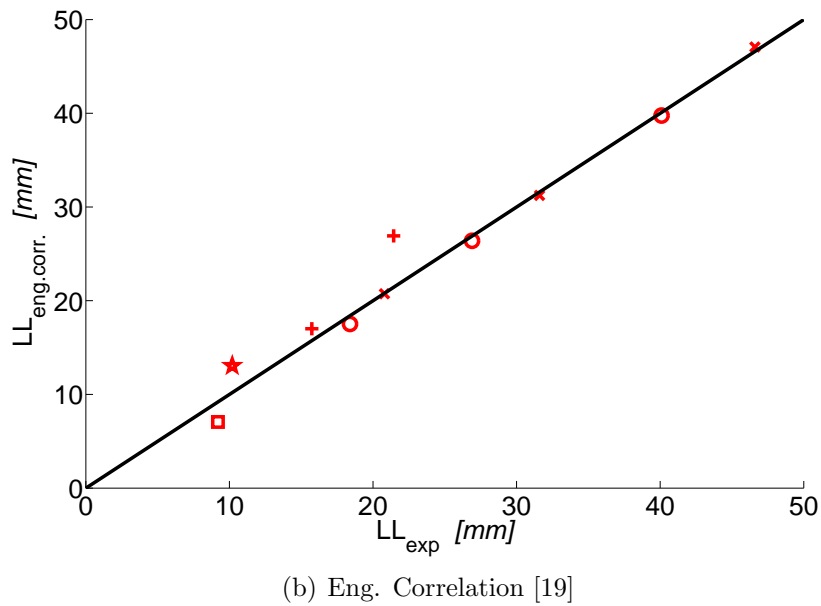
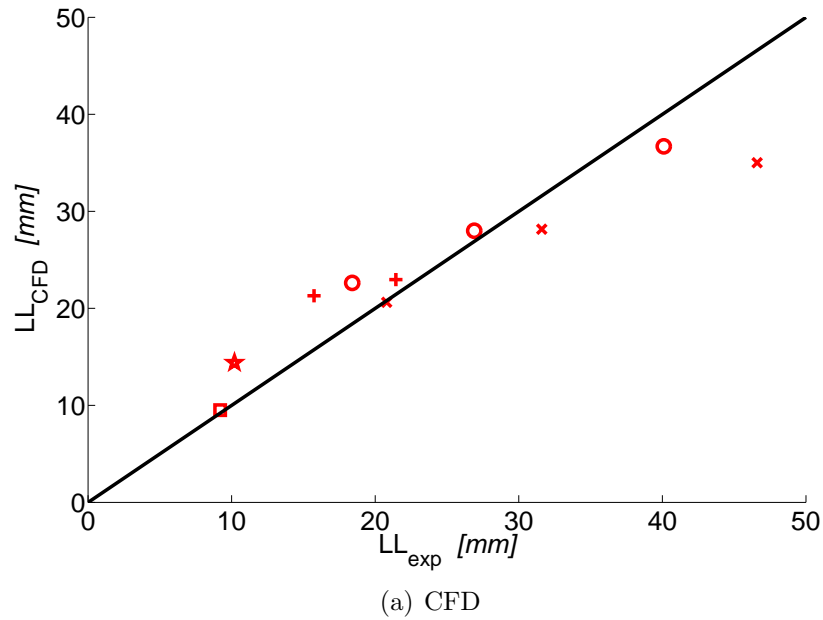


Figure 7.3: LL computed with CFD (a) and Siebers' engineering correlation [19] (b) versus experimental values for various operating conditions obtained from references [19]: n-heptane (\square), 2,2,4,4,6,8,8 heptamethyl-nonane (O), n-cetane (X). [20]: n-heptane (\star). [21]: n-heptadecane ($+$)

the aforementioned product is at its minimum, or in other words, where the drop in "predicted intensity" is at its maximum. In literature [20, 21], analogous approaches are utilized with respect to recorded scattering intensity.

From the validation it becomes clear that both models perform reasonably well for the investigated cases. For reasons not yet well understood, however, there is some indication that at higher LL values the CFD model tends to under-predict the LL . Furthermore, it is stressed that, although the models have been validated for a wide range of operating conditions and fuels, no experimental LL data could be found for relevant EDI PCCI operating conditions (i.e. for gas temperatures below 600 K). From in-house experience in this field it was found that at such low temperatures, the liquid core is no longer distinct, but segmented (likely resulting from internal spray dynamics such as vortex shedding [22]) and signal-to-noise ratios become unacceptably low [23].

Under conventional (non-premixed) diesel combustion, the combustion process will certainly influence the evaporation behavior as well, as the increasing temperature causes more fuel to evaporate. However, in the EDI PCCI combustion, since injection and combustion events are decoupled in time, the expected effect of combustion on vaporization is much less significant. Therefore, no combustion model is used in this work to analyze spray vaporization and impingement process.

7.4 Results and Discussion

7.4.1 Liquid fuel impingement

Illustrated in the figures below, two types of fuel impingements can be discerned: piston (figure (a))- and wall (figure (b)) impingement. Impingement against the cylinder head does not occur with the utilized injector setup and will therefore not be discussed.

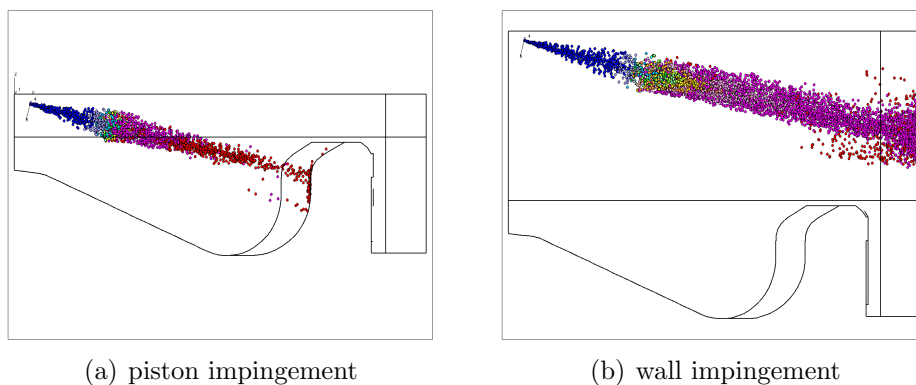


Figure 7.4: Illustrative CFD results for piston (a)- and wall- (b) impingement

In the schematic cross-section of the piston and cylinder geometry drawn in figure 7.5, the non-constant distance s defines the distance between piston and cylinder head. a is a constant value determining the axial distance between the injector and the cylinder wall and b is the distance between this point on the cylinder wall and the cylinder head.

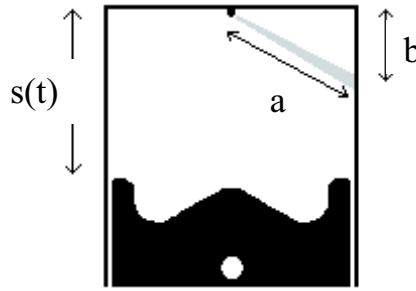


Figure 7.5: Schematic cross-section of piston and cylinder geometry

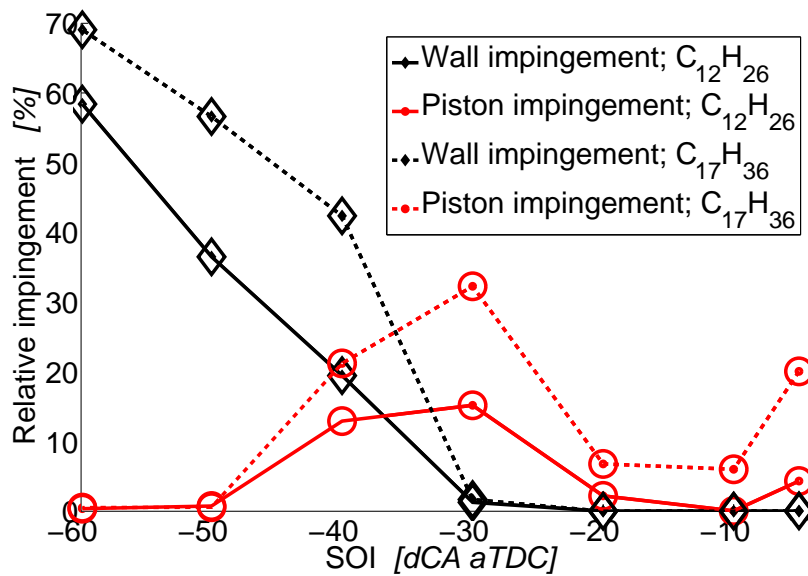


Figure 7.6: Relative impingement as a function of SOI (cases 1 thru 7 in table 7.3)

In figure 7.6, the relative impingement of fuel, as calculated with the CFD model, is plotted as a function of SOI. The relative impingement is defined as the ratio between the liquid fuel mass impinging on a surface and the total injected fuel mass during one cycle in one cylinder. The results are plotted for both n-dodecane and n-heptadecane, indicating predicted minimum and maximum levels of impingement respectively. As a result, the areas encapsulated by the solid (—) and dashed (---) lines in figure 7.6 represent more or less the entire boiling range of commercial diesel fuel. A distinction is made between piston- (○) and wall- (◇) wetting.

As the SOI is advanced, the amount of mass impinging on both the cylinder wall and piston increases, most likely due to the decreased in-cylinder temperature and pressure. Wall impingement, however, only occurs at timings earlier than -30 °CA aTDC. This is likely caused by geometrical effects. In the range -30 °CA aTDC to 30 °CA aTDC, the distance s between piston and cylinder head is smaller than b and fuel is injected onto the piston (bowl) instead of the cylinder wall. Between an SOI of -30 and -40 °CA aTDC, the distance s has approximately become the same size as distance b , so that fuel is injected on both the piston and wall. Accordingly, both wall- and piston impingement is observed in figure 7.6. At even earlier timings,

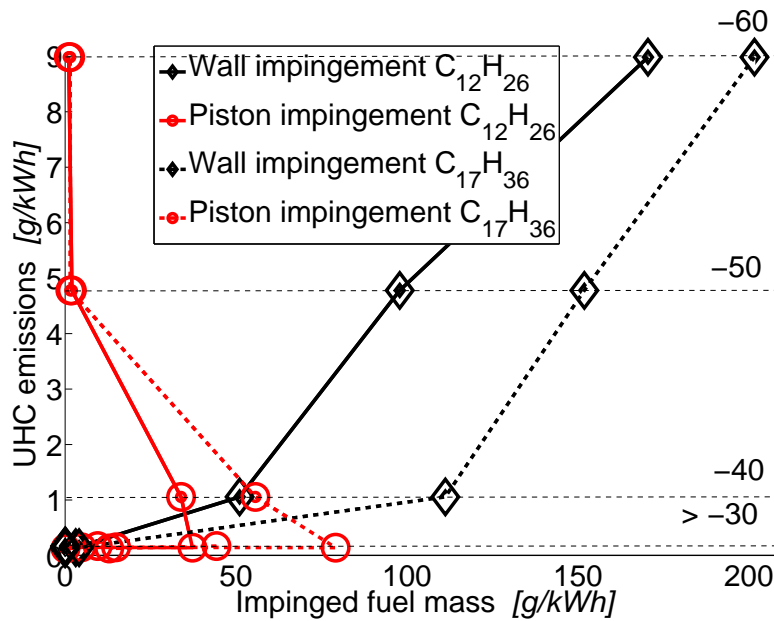


Figure 7.7: Measured UHC emissions as a function of calculated impinged fuel mass. The horizontal dashed (---) lines correspond to a constant SOI in °CA aTDC (cases 1 thru 7 in table 7.3)

the distance s becomes larger than b and piston impingement eventually no longer occurs. Finally, delaying SOI further than -10 °CA aTDC -40 °CA aTDC leads to increased piston impingement once again, because of the piston proximity to the injector coupled with the falling of in-cylinder temperature and pressure as the piston is already moving down during injection. These results suggest that, when using a conventional cone angle nozzle in the EDI PCCI regime, UHC emissions arising from liquid fuel impingement will be caused by primarily wall-wetting.

7.4.2 Sources of UHC emissions

Impingement

In figure 7.7, the measured UHC emissions [8] are plotted as a function of the calculated impinged mass against the cylinder wall (\diamond) and piston (\circ). Once again, the modeled results are presented for both n-dodecane (—) and n-heptadecane (---). When this figure is considered, there seems to be a good correlation, especially at higher UHC emission levels, between the amount of modeled wall-impingement and measured UHC emissions.

Moreover, at timings of -30 °CA and later, a significant amount of predicted piston wetting notwithstanding, measured UHC emissions drop to near-zero levels as is common for conventional DI diesel operating conditions. These results, in-line with the work of others [24, 25], suggests that liquid fuel impingement against the cylinder wall is the main source of UHC emissions under EDI PCCI operating conditions and that piston impingement, while predicted by the CFD model, does not appear to contribute to engine out UHC emissions. It is stressed that the above pertains to conventional cone angle nozzles and conventional DI injection timings.

Other potential sources

Apart from wall-wetting, other sources of UHC emissions under EDI PCCI (i.e. low temperature) operating conditions can be found in the literature [26–29]:

- Under-mixing: under-mixing can occur as a result of poor mixing rates during the fuel injection process at the tail of the combustion process [28] or due to fuel dripping from the nozzle sac after the EOI [27].
- Over-mixing: over-mixing may arise when, after the EOI, mixtures near the injector become too lean to facilitate auto-ignition [26] or due to turbulent diffusion during the ignition delay [27].
- Quenching zones: quenching of the oxidation reaction can occur due to either excessively low temperature zones and/or significant variations in the local equivalence ratio [29]. This is especially the case in crevices between the piston and cylinder wall.

Unfortunately, without optical in-cylinder measurements it is difficult to assess which of, and to what degree, the above phenomena might also contribute to the measured UHC emissions. Nonetheless, a correlation over a wide range of injection timings has been presented in the previous section between UHC emissions and wall impingement, suggesting that wall impingement at least significantly contributes to UHC emissions. Furthermore, the influence of piston impingement on UHC emissions appears to be negligible or, at most, of secondary importance.

7.4.3 Wall-wetting reduction strategies: alternative operating conditions

As can be seen in figure 7.6, advancing the SOI leads to an increase in wall-wetting. Wall-wetting, in turn, correlates well with UHC emissions (figure 7.7). In an attempt to curb UHC emissions, various strategies have been investigated in a previous study [8], as discussed earlier in section 7.3.3. In this section, experimental results (UHC emissions) are compared with CFD calculations (fraction of liquid fuel impingement on cylinder wall) in order to investigate the effectiveness of the various reduction methods. The respective operating conditions can be found in table 7.3, case #8 thru #15. In table 7.4, the reduction with respect to the baseline case, in terms of UHC emissions and wall impingement, are presented for the investigated strategies. While, the SOI was constant at -50 °CA aTDC for all EDI PCCI baseline cases, not all other operating conditions were kept constant due to technical considerations, resulting in slightly different baseline work points for the different strategies (turn to table 7.3 for details).

The following observations can be made from table 7.4:

Table 7.4: Effects of wall-wetting reduction strategies on measured UHC emissions and calculated impingement.

	$T_{in} \uparrow$ K		$p_{in} \uparrow$ bar		$p_f \uparrow$ bar		$T_f \uparrow$ K	
	303	353	1	2	770	1490	303	373
UHC (g/kWh)	7.5	5.2 (-31%)	9.1	6.5 (-29%)	9.1	7.3 (-20%)	9.4	7.5 (-20%)
impingement	47%	28% (-40%)	51%	45% (-12%)	50%	49% (-2%)	44%	34% (-23%)

- $T_{in} \uparrow$: an increasing intake temperature leads to a comparable relative reduction in both UHC emissions and impingement. Both reductions are likely the result of a higher gas temperature during the injection process.
- $T_f \uparrow$: an increasing fuel temperature leads to a similar relative reduction in both UHC emissions and impingement. Both reductions could be attributable to both smaller droplets (e.g. lower surface tension) and a higher initial droplet temperature, facilitating evaporation.
- $p_{in} \uparrow$: an increasing intake pressure leads to higher relative reduction in UHC emissions than in impingement. Both reductions are expected to be the result of a higher gas density during the injection process. It is not fully clear why the reduction in impingement is comparably lower. One possibility is that the higher density also reduces UHC emissions via other mechanisms, such as reduced under-mixing. This is in line with the observation that the reduction in UHC emission is larger than the reduction in wall impingement.
- $p_f \uparrow$: an increasing fuel pressure leads to a far higher relative reduction in UHC emissions than in calculated impingement.

The discrepancy in relative reduction in impingement and UHC observed for a higher p_f requires some more discussion. Considering the role of fuel pressure on the vaporization process, the literature [10, 12] suggests that the *position* of the *LL* does not depend on p_f . However, the *amount* of liquid fuel which reaches the *LL* could still depend on p_f (for example via smaller droplets or a larger spray angle...). Alternatively, it is possible that an increased injection pressure would reduce UHC emissions via other mechanisms than wall impingement; this may explain that UHC emissions decrease, while wall-wetting is hardly affected by an increase in p_f .

Two competing effects have to be taken into account pertaining to the liquid core penetration. On the one hand, one can expect smaller droplets, which results in a larger heat-transfer area. Conversely, the droplets are moving faster, which for a given droplet size and conditions, results in a longer traversed distance before evaporating

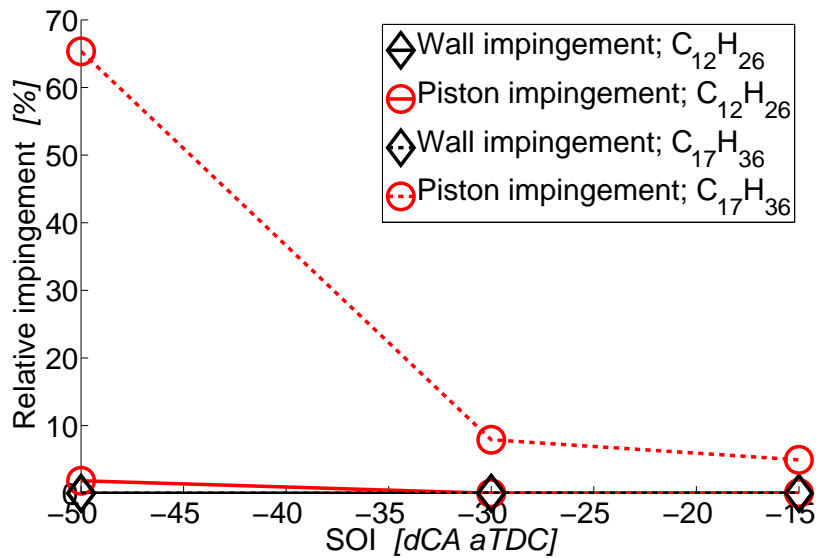


Figure 7.8: Relative impingement as a function of SOI for a narrow cone angle nozzle (cases 16 thru 18 in table 7.3)

completely. The former phenomenon in particular may not be well modeled in the CFD code, as the utilized empirical correlation for the initial droplet diameter has been developed for conventional DI diesel combustion and not yet been validated at the low gas temperatures typical for EDI PCCI combustion [15]. Therefore, more detailed (in-cylinder) spray analysis is required to adequately address this issue.

7.4.4 Wall-wetting reduction strategies: narrow cone angle nozzle

The measures discussed in the previous section can be regarded as "operating conditions"-based, in the sense that the same hardware was used in the experiments and only the engine settings were varied. It is clear from table 7.4 that UHC emissions formed under EDI PCCI operating conditions can be reduced significantly in this manner. An alternate approach is to modify the hardware such that it is tailored specifically for the EDI PCCI regime. An example discussed in this section is the use of a narrow cone angle nozzle (i.e. nozzle 3 in table 7.2). It is known from literature [30] that a narrower cone angle can reduce the occurrence of wall-wetting, for the spray is directed more downwards (rather than sideways, as is typically the case for conventional diesel nozzles). In an earlier work, lower UHC emissions were indeed recorded when operating with a narrower cone angle [8] (table 7.5). To assess the relation between cone angle and spray impingement, CFD simulations are performed with the narrow cone angle for various operating conditions (table 7.3: case 16-18)^a. From the CFD results it can be concluded that the impingement of liquid fuel on the cylinder wall is negligible irrespective of the SOI. This is in-line with the work of others [30], who report that wall-wetting can be suppressed significantly by narrowing the nozzle cone angle.

^anote that the intake temperature was 60 K higher for the narrow cone angle nozzle

In figure 7.8, however, in which the relative impingement on the piston surface is plotted as function of SOI for both n-dodecane (—) and n-heptadecane (---), it can be seen that piston-wetting becomes an issue for the narrow cone angle nozzle, especially at EDI PCCI (earlier than -30 °CA aTDC) injection timings. Note that, contrary to the conventional cone angle nozzle (figure 7.7), predicted impingement against the cylinder wall is now very low (figure 7.8).

From table 7.5 becomes clear that UHC emissions are still relatively high during EDI PCCI operation, negligible wall-wetting (figure 7.8) notwithstanding. Accordingly, it may be assumed that piston impingement can be an important source of UHC emissions in the EDI PCCI regime when a narrow cone angle is considered.

Table 7.5: Effect of cone angle on measured UHC emissions [8].

cone angle °	SOI °CA	UHC g/kWh
150	-50	1.17
	-30	0.42
	-15	0.66
100	-50	0.75
	-30	0.46
	-15	0.38

7.4.5 Discussion

By combining the information in table 7.5 and figures 7.6 and 7.8 an interesting observation can be made. Considering the -50 °CA aTDC injection timing, 1.17 and 0.75 g/kWh UHC are emitted for the conventional and narrow cone angle nozzle, respectively (table 7.5). Model results suggest that these values correspond to an average (i.e. of n-dodecane and n-heptadecane) impingement of 46 (wall-wetting) and 33 (piston-wetting) wt-%, respectively. Accordingly, roughly 0.025 g/kWh UHC are formed per wt-% fuel impingement against the cylinder wall under EDI PCCI conditions using a conventional cone angle nozzle. A similar value (0.022) is found for the narrow cone angle nozzle. These results suggest that, under EDI PCCI conditions, wall- and piston-wetting have a similar impact on UHC emissions.

By combining the information in table 7.5 and figures 7.6 and 7.8, an interesting observation can be made. Considering the -50 °CA aTDC injection timing, 1.17 and 0.75 g/kWh UHC are emitted for the conventional and narrow cone angle nozzle, respectively (table 7.5). Model results suggest that these values correspond to an average (i.e. of n-dodecane and n-heptadecane) total (i.e. wall + piston) impingement fraction of approximately 46 and 33. In the case of the conventional cone angle at an SOI of -50 °CA, piston-wetting is negligible (figure 7.6) and the aforementioned fraction can be attributed to wall-wetting. Accordingly, roughly 0.025 g/kWh UHC are measured per modeled percent of wall impingement. For the narrow cone angle nozzle at an SOI of -50 °CA, wall-wetting is negligible (figure 7.8) and the impingement fraction of 33 can be ascribed wholly to piston-wetting. Given the measured

UHC emissions in this workpoint of 0.75 g/kWh, 0.022 g/kWh of UHC are formed per percent of modeled piston impingement. Although this quantitative approach is subject to discussion, it illustrates that, at least in the investigated EDI PCCI workpoint, modeled wall- and piston-wetting have a comparable impact on measured UHC emissions for a given fraction of fuel impingement.

7.5 Conclusions

The main goal of this paper has been to acquire more insight into the relationship between spray evaporation and UHC emissions under EDI PCCI operating conditions. To this end, the vaporization process was modeled for various operating conditions using a commercial CFD code (StarCD). Next, the correlation between the CFD results and measured UHC emissions were studied. Predicted liquid core penetrations (LL) by CFD code have been successfully checked against experimental data from literature over a wide range of operating conditions. The diesel fuel used in the experiments was modeled by n-dodecane and n-heptadecane, representing the low and high end of the diesel boiling curve, respectively. A distinction has been made between liquid spray impingement on the piston surface and cylinder liner. From the presented results the following conclusions can be drawn:

- For a conventional DI diesel nozzle, the high UHC emissions in the EDI PCCI regime correlate well with modeled cylinder wall impingement. Piston impingement is far lower in magnitude under these conditions and eventually becomes negligible as the piston is positioned further down from TDC at earlier EDI PCCI injection timings (i.e. at -50 °CA aTDC and earlier). Accordingly, it may be assumed that the primary cause for high UHC emissions in the EDI PCCI regime using conventional DI nozzles is liquid fuel impingement against the cylinder wall.
- The positive effect of a higher intake and fuel temperature, as well as elevated intake pressure, on UHC emissions in the EDI PCCI regime [8] is also observed for the spray impingement against the cylinder wall, providing additional evidence that the two parameters (i.e. UHC and wall impingement) are linked.
- A higher fuel pressure, though effective at reducing the UHC emissions in the EDI PCCI regime, does not lead to a reduction in wall impingement. Either one or more phenomena - most likely initial droplet formation/size - are not well captured by the model or other (mixing) effects play a role. Alternatively, other mechanisms may be at work that reduce UHC emissions via injection pressure, leaving wall impingement unaffected. More research is required to arrive at a satisfactory explanation.
- For a narrow cone angle nozzle, the UHC emissions in the EDI PCCI regime are still relatively high. UHC emission correlate well with modeled piston impingement, while wall-wetting is now negligible irrespective of injection timing. Accordingly, the model results suggest that the primary cause for UHC emissions in the EDI PCCI regime using narrow cone nozzles is liquid spray impingement against the piston.

- Combining model results with measurement data from an earlier study suggest that, for a typical EDI PCCI injection timing of -50°CA aTDC, wall- and piston-wetting have a similar impact on UHC emissions per percent of impinged fuel. More detailed modeling of the impingement process is currently subject of research.

Bibliography

- [1] H. Kim, Y. Kim, and K. Lee. A study of the characteristics of mixture formation and combustion in a PCCI engine using an early multiple injection strategy. *Energy Fuels*, 22(3):1542–1548, 2008.
- [2] G.K. Lilik, J.M. Herreros, and A.L. Boehman. advanced combustion operation in a compression ignition engine. *Energy Fuels*, 23(1):143–150, 2009.
- [3] C. Chartier, R. Egnell, M. Alden, R. Collin, O. Andersson, M. Richter, H. Seyfried, and U. Aronsson. Analysis of smokeless spray combustion in a heavy-duty diesel engine by combined simultaneous optical diagnostics. *SAE Paper 2009-01-1353*, 2009.
- [4] G.T. Kalghatgi, P. Risberg, and Hans-Erik Ångström. Partially pre-mixed auto-ignition of gasoline to attain low smoke and low NO_x at high load in a compression ignition engine and comparison with a diesel fuel. *SAE Paper 2007-01-0006*, 2006.
- [5] M.D. Boot, P.J.M. Frijters, C.C.M Luijten, L.M.T. Somers, R.S.G. Baert, A.J. Donkerbroek, R.J.H Klein-Douwel, and N.J. Dam. Cyclic oxygenates: A new class of second-generation biofuels for diesel engines? *Energy Fuels*, 23:1808 – 1817, 2009.
- [6] M.D Boot, P.J.M. Frijters, R.J.H. Klein-Douwel, and R.S.G. Baert. Oxygenated fuel composition impact on heavy-duty diesel engine emissions. *SAE Paper 2007-01-2018*, 2007.
- [7] M.Y. Kim, J.W. Kim, C.S. Lee, and J.H. Lee. Effect of compression ratio and spray injection angle on HCCI combustion in a small DI diesel engine. *Energy Fuels*, 20(1):69–76, 2006.
- [8] M.D. Boot, C.C.M. Luijten, E.P. Rijk, B.A. Albrecht, and R.S.G. Baert. Optimization of operating conditions in the early direct injection premixed charge compression ignition regime. *SAE Paper 2009-24-0048*, 2009.
- [9] M.D. Boot, C.C.M. Luijten, L.M.T. Somers, U. Eguz, D.D.T.M. van Erp, A. Albrecht, and R.S.G. Baert. Uncooled EGR as a means of limiting wall-wetting under early direct injection conditions. *SAE Paper 2009-01-0665*, 2009.
- [10] B.S. Higgins, C.J. Mueller, and D.L. Siebers. Measurements of fuel effects on liquid-phase penetration in DI sprays. *SAE Paper 1999-01-0519*, 1999.
- [11] Brigham Young University. DIPPR database. <http://dippr.byu.edu/>.

-
- [12] D.L. Siebers. Liquid-phase fuel penetration in diesel sprays. *SAE Paper 980809*, 1998.
- [13] S.H. El Tahry. k - ϵ equation for compressible reciprocating engine flows. *J. Energy*, 7(4):345–353, 1983.
- [14] F. Obermeier. MPI für Strömungsforschung. Technical report, Model development within the CEC programme JRC-IDEA, Göttingen, 1993.
- [15] R.D. Reitz and R. Diwakar. Effect of drop breakup on fuel sprays. *SAE Paper 860469*, 1986.
- [16] P.J. O'Rourke. *Collective Drop Effects on Vaporising Liquid Sprays*. PhD thesis, University of Princeton, 1981.
- [17] C. Bai and A.D. Gosman. Development of methodology for spray impingement simulation. *SAE Paper 950283*, 1995.
- [18] M. Jia, Z. Peng, M. Xie, and R. Stobart. Evaluation of spray/wall interaction models under the conditions related to diesel HCCI engines. *SAE Paper 2008-01-1632*, 2008.
- [19] L. Pickett. Sandia experimental data. Technical report, Engine combustion network, 2007.
- [20] D. Verhoeven, J.L. Vanhemelryck, and T. Baritaud. Macroscopic and ignition characteristics of high-pressure sprays of single-component fuels. *SAE Paper 981069*, 1998.
- [21] M.D. Boot, D.D.T.M. van Erp, P.J.M. Frijters, C.C.M. Luijten, and R.S.G. Baert. Modeling of spray behavior of a diesel fuel surrogate. In *Proc. of the 8th World Congress on Computational Mechanics*, Venice, Italy, 2009.
- [22] R.S.G. Baert, P.J.M. Frijters, L.M.T. Somers, C.C.M. Luijten, and W.A. de Boer. Design and operation of a high pressure, high temperature cell for HD diesel spray diagnostics: Guidelines and results. *SAE Paper 2009-01-0649*, 2009.
- [23] D.D.T.M van Erp. Examining methods to reduce wall-wetting under HCCI conditions, MSc thesis. Technical report, Technical University of Eindhoven, 2008.
- [24] C.P. Koci, Y. Ra, R. Krieger, M. Andrie, D.E. Foster, R.M. Siewert, R.P. Durrett, I. Ekoto, and P.C. Miles. Detailed unburned hydrocarbon investigations in a highly-dilute diesel low temperature combustion regime. *SAE Paper 2009-01-0928*, 2009.
- [25] R. Opat, Y. Ra, A. Manuel, D. Gonzalez, R. Krieger, R.D. Reitz, D.E. Foster, R.P. Durrett, and R.M. Siewert. Investigation of mixing and temperature effects on HC/CO emissions for highly dilute low temperature combustion in a light duty diesel engine. *SAE Paper 2007-01-0193*, 2007.

-
- [26] M.P.B. Musculus, T. Lachaux, L.M. Pickett, and C.A. Idicheria. End-of-injection over-mixing and unburned hydrocarbon emissions in low-temperature-combustion diesel engines. *SAE Paper 2007-01-0907*, 2007.
- [27] D. Kim, I. Ekoto, W.F. Colban, and P.C. Miles. In-cylinder CO and UHC imaging in a light-duty diesel engine during PCCI low-temperature combustion. *SAE Paper 2008-01-1602*, 2008.
- [28] W.F. Colban, P.C. Miles, and S. Oh. Effect of intake pressure on performance and emissions in an automotive diesel engine operating in low temperature combustion regimes. *SAE Paper 2007-01-4063*, 2007.
- [29] J.T. Kashdan, S. Mendez, and G. Bruneaux. On the origin of unburned hydrocarbon emissions in a wall guided, low NOx diesel combustion system. *SAE Paper 2007-01-1836*, 2007.
- [30] G.C. Martin, C.J. Mueller, D.M. Milam, M.S. Radovanovich, and C.R. Gehrke. Early direct injection, low-temperature combustion of diesel fuel in an optical engine utilizing a 15-hole, dual-row, narrow-included-angle nozzle. *SAE Paper 2008-01-2400*, 2008.

Part III
Engine Hardware

PFAMEN: Porous Fuel Air Mixing Enhancing Nozzle

One of the challenges with conventional diesel engines is the emission of soot. To reduce soot emission whilst maintaining fuel efficiency, an important pathway is to improve the fuel-air mixing process. This can be achieved by creating small droplets in order to enhance evaporation. Furthermore, the distribution of the droplets in the combustion chamber should be optimized, making optimal use of in-cylinder air. To deal with these requirements a new type of injector is proposed, which has a porous nozzle tip with pore diameters between 1 and 50 μm . First, because of the small pore diameters the droplets will also be small. From literature it is known that (almost) no soot is formed when orifice diameters are smaller than 50 μm . Second, the configuration of the nozzle can be chosen such that the whole cylinder can be filled with fine droplets (i.e., spray angle nearly 180°). However, injecting through a porous nozzle is not the same as an infinite number of very small holes, due to the difference in nozzle internal flow. Therefore, the nozzle tip is modeled in COMSOL Multiphysics in order to predict the outflow direction and velocity of the fuel. The Darcy-Forchheimer equation, which follows from the Navier-Stokes equation, is used for this purpose. To validate the model, experiments have been performed in the Eindhoven High Pressure Cell (EHPC) where (for vaporizing sprays) the spray is visually analyzed and (for reacting sprays) the ignition delay has been measured.

The content of this Chapter has been taken from:

J.J.E. Reijnders, **M.D. Boot**, C.C.M. Luijten, P.J.M. Frijters and L.P.H. de Goey. Porous Fuel Air Mixing Enhancing Nozzle (PFAMEN). *SAE Paper*, 2009-24-0028, 2009.

Minor edits have been made to streamline the layout of the thesis chapters. Experiments were carried out in the engine lab of the Eindhoven University of Technology.

8.1 Introduction

Increasingly stringent emission legislation has led to an intensified research on HD diesel engines to keep and improve their fuel consumption, whilst still meeting the emission legislation. Many developments such as aftertreatment, EGR and increasingly higher fuel injection pressures were introduced to the market. Modern Heavy Duty (HD) diesel engines always have Direct Injection (DI). A high pressure pump delivers fuel at 100-250 MPa to an injector with 6-8 holes with a diameter typically around 150-200 μm . After the start of injection, the fuel forms a spray where the liquid fuel breaks up into smaller droplets. In the meantime the diesel is heated up and evaporates via entrainment of high temperature gas.

As a result of the above developments, engines have already become much cleaner. However, in order to meet EPA 10/EURO VI-like emission standards, new techniques might be required or become more interesting as costs tend to further increase. Looking at results from literature [1] and [2] there is a trend that the smaller the diameter of the injection holes gets, the less soot is formed throughout the combustion process. If the diameter of the holes becomes smaller, the total outflow area decreases, resulting in a lower volume flow. By applying more holes this issue could be overcome. However, the maximum number of holes and the minimum diameter of the holes is limited. For these reasons new solutions have to be found. One possible solution would be to inject the fuel through a porous material. The porous material contains many small pores over a large surface of the injector tip, and in this respect principally differs from injection through a conventional nozzle with straight-drilled injector holes.

To assess the technical viability of such a nozzle, a numerical model was built (using COMSOL Multiphysics) and the flow through the material and its strength were investigated. The flow through the porous material is described by the coupled Darcy-Forchheimer equation [3]. The Darcy and Forchheimer equations are derived from the Navier-Stokes equation by Neuman [4] and Chen et.al. [5], respectively.

Besides the numerical investigation, some experimental measurements with the porous injector were performed. To test the porous injector concept, prototype nozzles were produced and the original injector tip was replaced by a porous tip. The injector was connected to two different common-rail setups, one at atmospheric conditions and one at engine-like conditions in a constant volume spray bomb. The atmospheric tests are quickly and relatively easily performed and the engine-like measurements are closer to real engine circumstances. With the atmospheric measurements the spray is analyzed visually, the volume flow of the injector is evaluated and durability tests are performed. With the engine-like tests, which are performed in the Eindhoven High Pressure Cell (EHPC, for details see [6]), again the spray is analyzed, ignition delay is determined and the combustion process is qualitatively analyzed.

In Figure 8.1 a typical fuel distribution is illustrated for conventional injectors and an ideal fuel distribution for porous injectors, respectively. It is expected that the quantity of oxygen that potentially takes part in the combustion process, is much larger with the porous injector since the occupied volume is larger. However, whether this is really the case will also depend on time scales (a.o. governed by exit velocity, which will be smaller due to the internal geometry of and resulting flow friction in the porous nozzle).

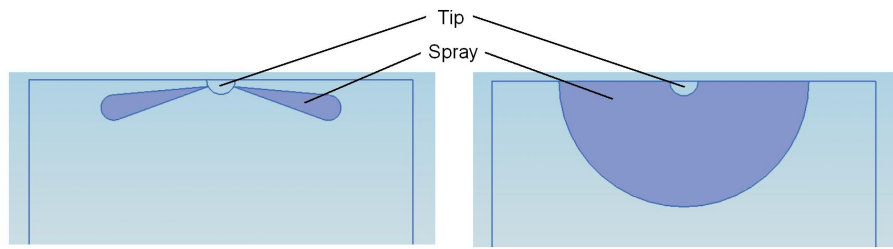


Figure 8.1: Fuel distribution of a conventional (left) and porous (right) injector.

As is shown in Figure 8.1, it is the intention to acquire a spray with a roughly hemispherical shape. Details of the optimal spray shape will depend on the combustion concept and the shape of the piston bowl. In the next section we will briefly discuss how this can be achieved.

The outline of this paper is as follows. In the first section, some preliminary work with regard to the porous nozzle concept is reported. The second section deals with modeling of the porous injector. In the third and fourth sections the experimental setup and experimental results. This is one of the subjects investigated in this work. are discussed, respectively. Finally, a discussion of the results and some conclusions are presented.

8.2 Preliminary work

In this section some preliminary work on the topic of injection through porous material is briefly discussed. To successfully inject via porous material, the properties of the material must be known. The most important are porosity and permeability. Both will be discussed here.

Porous material can be produced via sintering. With sintering, grains are pressed together at high pressure and are afterwards melted together at temperatures just beneath the melting temperature of the material. There are grains in many sizes, forms, types and materials, for example ceramics, metals, plastics, etc. The size of the grains and the pressure of the process determines for a large part the porosity and permeability of the sintered material. The porosity is defined as the volume fraction of holes in the material in relation to the total volume. The definition of permeability is the rate of flow of a liquid or gas through a porous material divided by the pressure difference that is driving the flow. In this study, stainless steel is chosen because of the favorable properties of this material in an engine environment (easy machining and high temperature resistance).

In Figure 8.2, examples are shown of different porosities and permeabilities. As becomes clear from the figure, a porous material is not by definition permeable, but a permeable material is by definition porous. In this study material is used that is closest to the lower left figure. Permeability and porosity depend on the internal structure of the material.

Darcy's Law [7] is a well known (empirical) relation to describe the flow through a porous material. It can be derived from the Navier-Stokes equations under certain

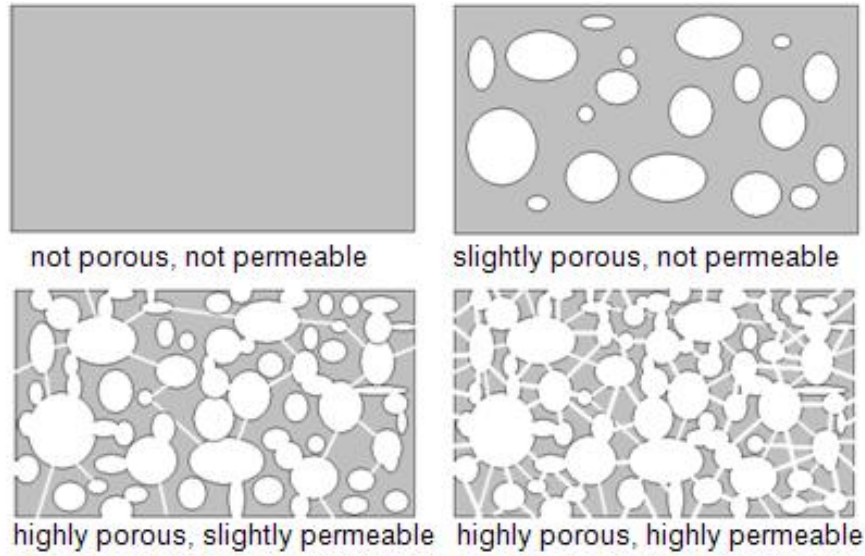


Figure 8.2: Four configurations with different porosities and permeabilities.

conditions [4] and it is defined as:

$$\nabla \cdot \left(-\frac{\kappa_d}{\eta} \nabla p \right) = 0 \quad (8.1)$$

Here, κ_d is the permeability as defined by Darcy, η the dynamic viscosity of the fuel and p is the pressure. The equation above was implemented in COMSOL Multiphysics in order to model the internal flow in the porous injector and calculate the Reynolds number. In this way, the optimal geometry of the porous nozzle is examined and Darcy's Law can be validated. Criteria in the optimization of the porous injector are: the fuel mass flux (which should be at least equal to that of conventional injectors); the spray shape (which should resemble the hemispherical shape presented in Figure 8.1; and the tensile strength (which should be larger than the tensile stresses in the nozzle, multiplied with a safety factor).

The geometries shown in Figure 8.3 were investigated to ascertain the influence of the length of the fuel channel. The sizes in the figures are in mm. The size of the outer diameter is chosen equal to the size of the conventional injector tip. To determine the size of the inner diameter, a few prototypes are made in which the inner diameter as shown in the figure, best agrees with the criteria mentioned above.

First, geometry *A* was investigated. On the inner edge the fuel pressure was prescribed, and on the outer edge a typical cylinder pressure at the time of injection. The flow through the porous tip is calculated with equation 1 where κ_d is reported by the manufacturer and η is a typical value of the dynamic viscosity for diesel. The values for these quantities are reported in Table 1. The "space dimension", which is used in COMSOL Multiphysics, is 2D axial symmetry. The calculations are performed for steady-state and the influence of the flow through the channel is neglected. Whether this is justified is investigated in the next section.

From Figure 8.4, showing the internal velocity profile in the nozzle, it follows that there is a uniform spray velocity at the outer edge which should result in the spray shape as shown in Figure 8.1. However, experiments reveal a spray shape as is

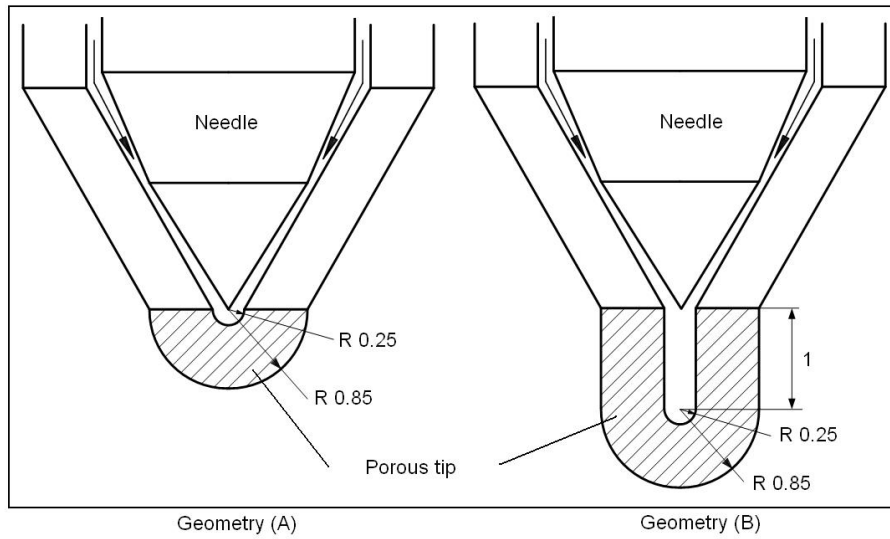


Figure 8.3: Technical drawing of porous nozzle concept.

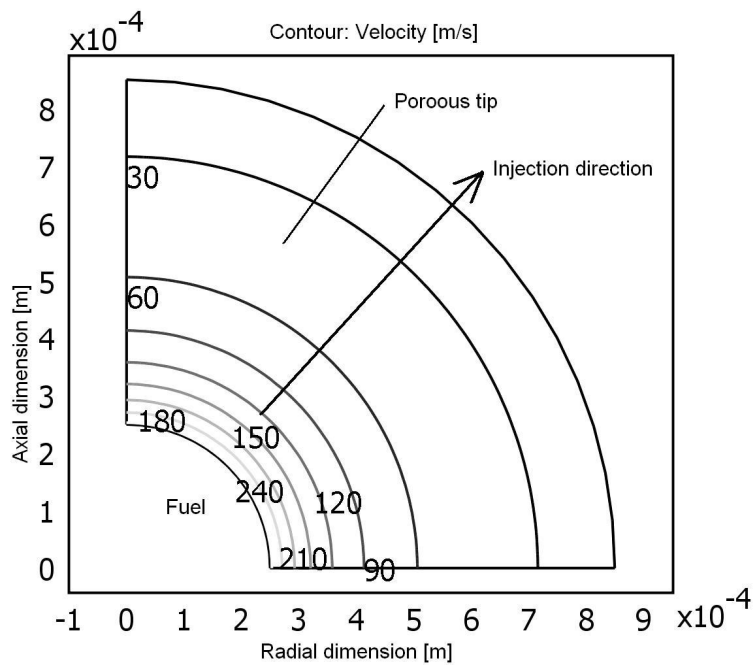


Figure 8.4: Simulation of prototype with geometry (A); isolines of the internal velocity in the nozzle. Exit velocity is approximately 21 m/s.

Table 8.1: Input parameters for simulations

Quantity	Value
Fuel Pressure Geometry (A)	60 MPa
Fuel Pressure Geometry (B)	25 MPa
Cylinder Pressure	5 MPa
Density ρ [8]	850 kg/m ³
Dynamic viscosity η [8]	3.810 ⁻³ Pa·s
Permeability κ_d [9]	310-12 m ²
Mass flow	0.8 kg/s

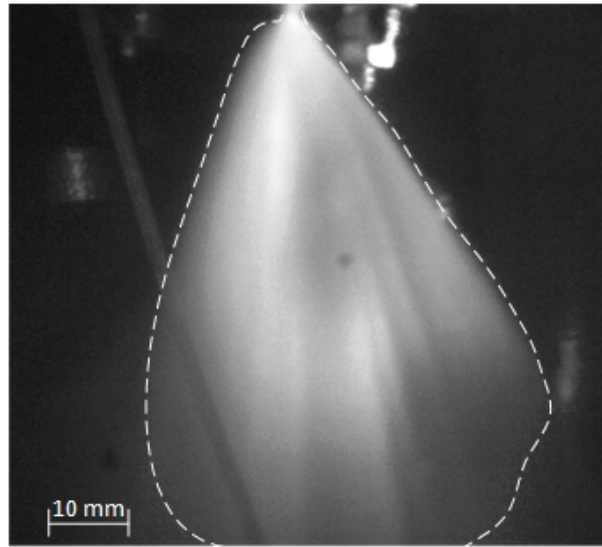


Figure 8.5: Experimental spray shape of injector with geometry (A). Atmospheric conditions, spray illuminated with high power light and captured with a high speed camera and experimental properties as listed in Table 2.

shown in Figure 8.5. The experiments are performed with a Dedotec COOLH light source (illuminating the spray) and Dedotec COOLT3 power supply combined with a Phantom 7.1 high speed camera.

From Figure 8.5 it appears that the fuel spray is finely atomized, but the desired homogeneous hemispherical distribution is not realized. The fuel spray has a preferential axial direction, which means that geometry *A* does not have the desired fuel distribution of Figure 8.1. Next, geometry *B* with the longer fuel channel was investigated. The pressure on the inner edge was lowered to reach the same mass flow as in the previous case. The other parameters were not changed. From Figure 8.6 it was concluded that again the velocity on the outer edge was almost uniform. Experiments yield the spray shape as shown in Figure 8.7.

Here, by changing the nozzle geometry, the spray shape is closer to the desired hemisphere bowl shape (Figure 8.1). Of course the figure shows that the distribution locally still seems to be quite non-uniform. However, in the near future the porous material could be tuned to result in a more homogeneous distribution. This will be done by optimizing the production process. The numerical results do not (fully)

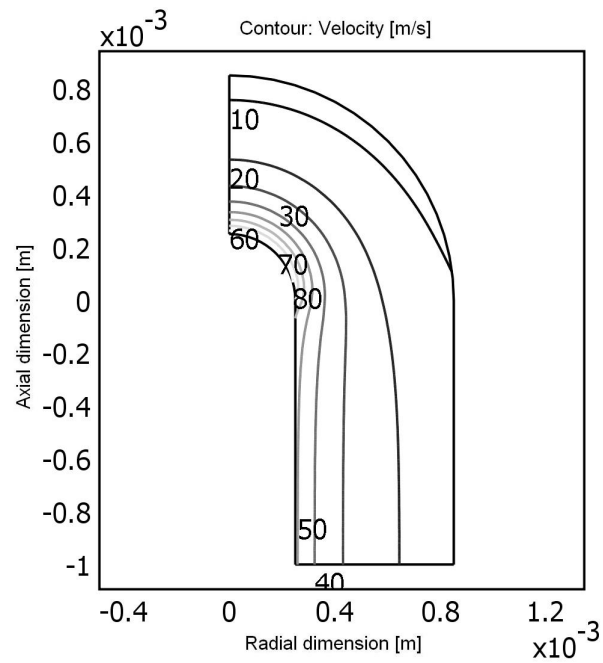


Figure 8.6: Simulation of prototype with geometry (B); isolines of the internal velocity in the nozzle. Exiting velocity on the tip is 8 m/s.

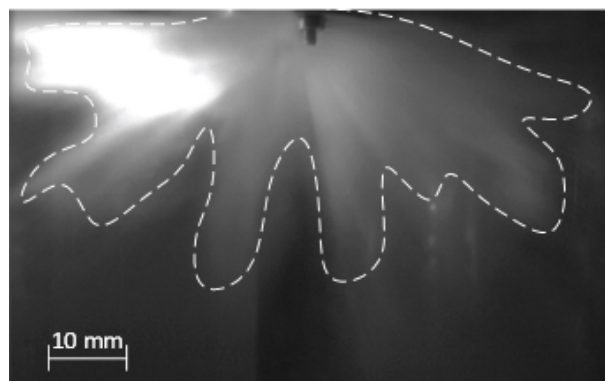
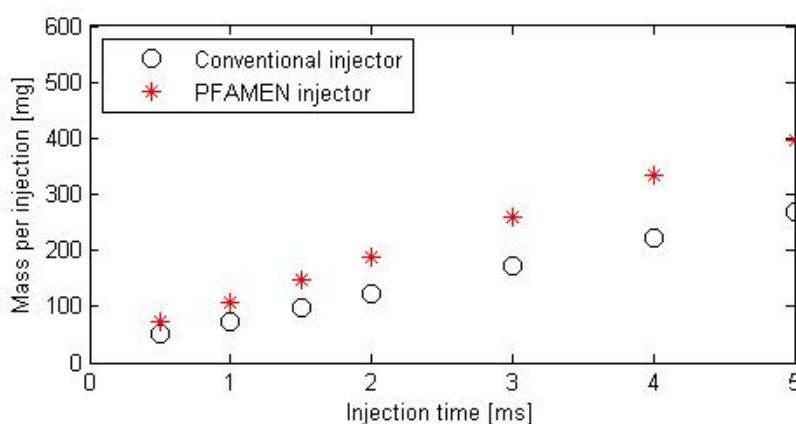


Figure 8.7: Experimental spray shape of injector with geometry (B); Same conditions as Figure 8.5.

Table 8.2: Properties used for experiments

Quantity	Value
Material	Stainless steel
Mean pore size	10 μm
Porosity	32%
Injection pressure	100 MPa
Injection time	5 ms
Shot time	4 ms

**Figure 8.8:** Injected mass versus opening time for the conventional and porous injector; injection pressure = 100 MPa, injector specification see text.

correspond with the experimental results. In order to improve the numerical results, the model is adapted as will be explained in the next section.

8.2.1 Stresses

The stresses in the material are also calculated. The maximum stress (Von Mises) that appears in the model with geometry B is 30 N/mm². The maximum allowable stress of the porous stainless steel is 90 N/mm² (from manufacturer), which indicates a safety factor of 3. This is a relatively low safety factor and experiments have demonstrated that it is not sufficient. In the Section "Experimental setup" another configuration is proposed to extend the lifetime of the porous injector.

8.2.2 Mass flow

The delivered power in diesel engines is controlled by the quantity of injected fuel. To ensure that the mass flow through the porous injector is the same as that of the conventional injector, mass flux measurements were performed by applying a high injection rate into a closed reservoir. The mass of the injected fuel is weighed and divided by the number of injections.

In Figure 8.8, the results of the mass flow measurements of a conventional and porous injector are plotted. The injection time referred to is the energizing time.

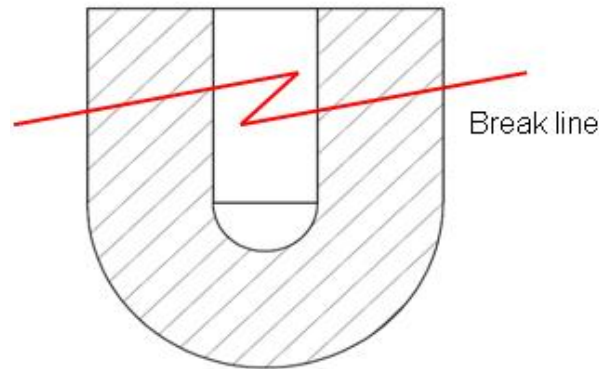


Figure 8.9: Porous injector tip with indication of break line location.

The specifications of the conventional injector are listed in Table 3. Under equal conditions, the mass flow of the porous injector is higher than the mass flow of the conventional one. Of course this is determined by the geometric details of the porous nozzle area.

Table 8.3: Specifications of the conventional injector

Quantity	Value
Number of holes	8
orifice diameter	178 μm
Injection rate	1.6 l/min @ 10 MPa
cone angle	154°

8.2.3 Lifetime

To examine the lifetime of the porous injector, durability tests were performed. From experiments it is found that the injector tip breaks down repeatedly, at a location that is roughly indicated in Figure 8.9, after about 100.000 injections. This is probably due to fatigue. This value depends on the geometry, size and thickness of the porous material. To extend the lifetime more research has to be performed.

8.3 Extended modeling of the porous injector

It is clear from the previous section that the initial model is not in-line with the experimental results. A more extensive model is therefore proposed in this section. This model gives a better understanding of the fluid flow through the porous material and therefore the distribution of the spray can be predicted better. In the previous section, the flow through the porous material was obtained using Darcy's Law. From literature, it is known that Darcy's Law only holds for small Reynolds numbers. The Reynolds number Re expresses the ratio between inertial and viscous forces, in this case given by

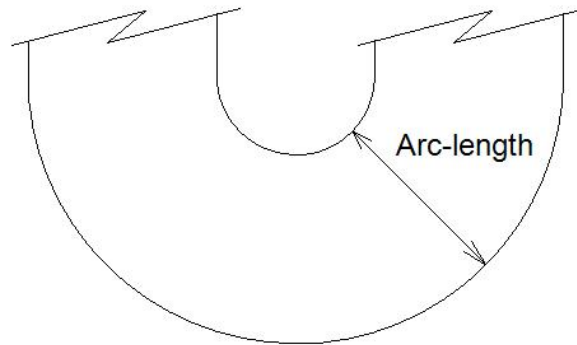


Figure 8.10: Configuration to calculate the Re number within the nozzle.

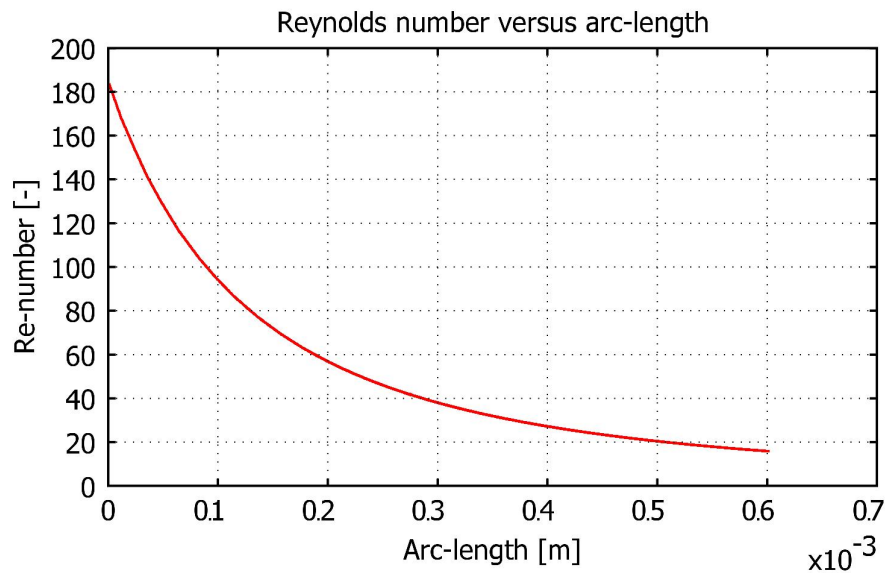


Figure 8.11: Reynolds numbers obtained from the COMSOL model as a function of arc-length.

$$Re = vd\rho/\eta, \quad (8.2)$$

where v is the velocity through the material, d the channel diameter ($10 \mu\text{m}$ [9]), ρ the density of the fluid (850 kg/m^3 [8]) and η the dynamic viscosity of the fluid ($3.8 \cdot 10^3 \text{ pa}\cdot\text{s}$ [8]).

First, the Re -number will be checked in the model as a function of the arc-length within the porous material of the nozzle, as shown in Figure 8.10. The resulting Re -number, as predicted by the COMSOL Multiphysics model, is plotted in Figure 8.11. Figure 8.11 shows that Re is in the range of 15 to 190. From Figure 8.12, taken from Reference [3], it appears that Darcy's Law is not valid anymore in this range. In Figure 8.12 the validation of Darcy's Law is shown in terms of Forchheimer variables Fanning friction factor f and the Re -number). The Fanning friction factor is a dimensionless number:

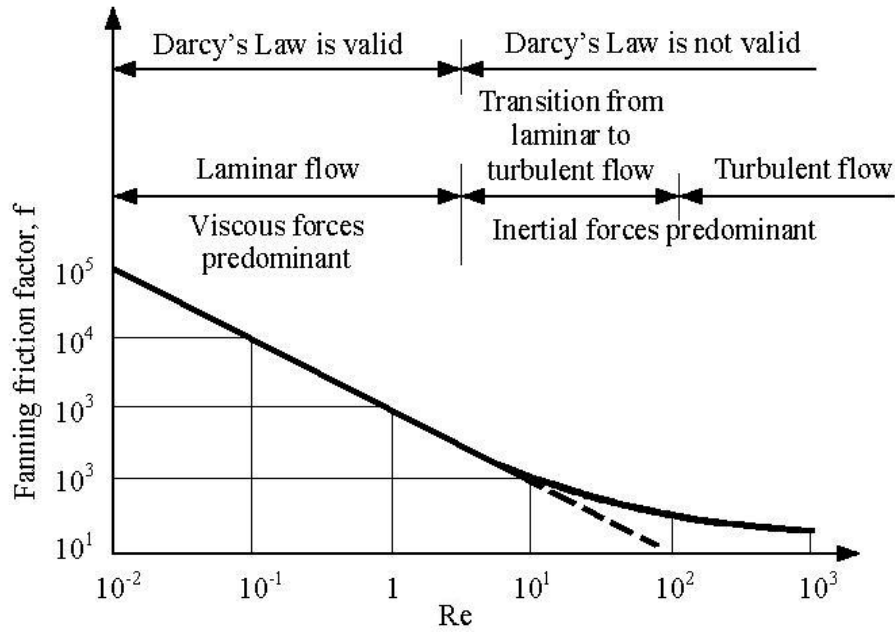


Figure 8.12: Validity range of Darcys Law [3].

$$f = \Delta p \cdot d/2 \cdot l \cdot \rho \cdot v^2, \quad (8.3)$$

where l is the mean channel length. The figure shows a transition from linear (Darcy's law) to nonlinear flow at Re values between 5 and 10. Physically, this means that inertial forces can no longer be neglected with respect to viscous forces. Forchheimer (1901) proposed a non-linear relation (Forchheimer's Law), which can also be derived from the Navier-Stokes equation [5]. Assuming stationary flow, incompressible fluid and neglecting gravity this leads to the following reduced NS-equation:

$$\nabla p = \eta \nabla^2 \mathbf{v} - \rho (\mathbf{v} \cdot \nabla) \mathbf{v}. \quad (8.4)$$

Via homogenization (Chen in [5]) the following expression can be derived:

$$\nabla p = -\frac{\eta}{\kappa_d} \mathbf{v} - \frac{\rho}{\kappa_f} |\mathbf{v}| \mathbf{v}. \quad (8.5)$$

In COMSOL Multiphysics this relation can be implemented in the Incompressible Navier-Stokes application in the following form:

$$0 = \nabla \cdot \mathbf{I} + \frac{\eta}{\kappa_d} \mathbf{v} + \frac{\rho}{\kappa_f} |\mathbf{v}| \mathbf{v}, \quad (8.6)$$

where p is the pressure, η is the dynamic viscosity, \mathbf{v} the velocity vector, ρ is the density of the fluid and $|\mathbf{v}|$ is the absolute value of the velocity vector. κ_d is the permeability defined by Darcy and κ_f is the permeability defined by Forchheimer.

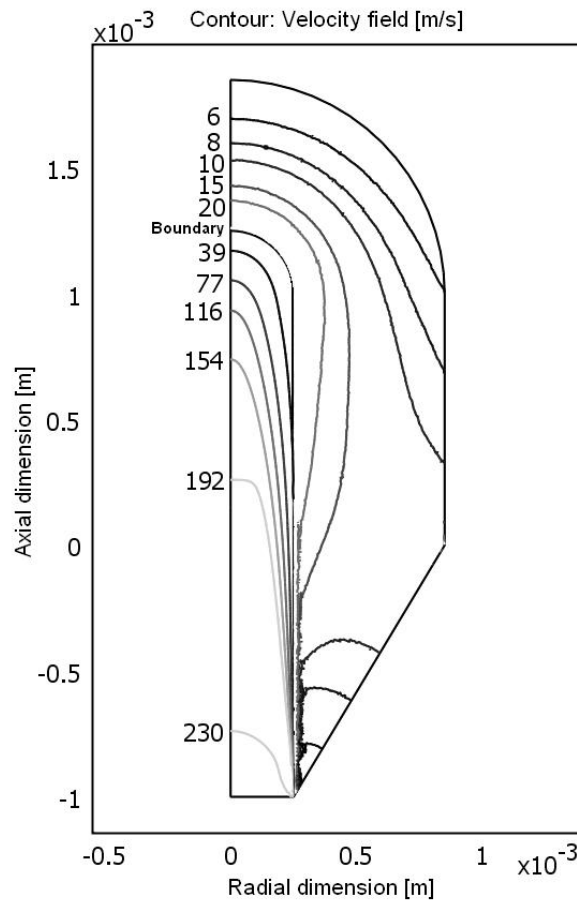


Figure 8.13: Simulation of prototype with geometry B with use of Darcy-Forchheimer equation. Fuel pressure = 100 MPa.

Geometry B is again modeled in COMSOL Multiphysics but now using Equation (4) instead of (1). Also the fuel channel is modeled with a standard $k-\epsilon$ turbulence model [10] instead of a boundary condition on the inlet side. Also, the porous material is modeled in greater detail as shown in Figure 8.13.

Figure 8.13 shows the velocity profile after Forchheimer's term is added. To reach the same overall mass flow, the fuel pressure is increased to 100 MPa. For other properties see Table 1. Now, by adding Forchheimer and more details, the velocity difference in outflow velocity between the tip and the side is larger. The exit velocity, the surface area and the porosity are known, so the model results can be qualitatively compared with the experimental results. After the model updates, the results now correspond to the experimental results, which will help to improve the quality of the prototypes.

From previous experiments it is known that the lifetime of the porous nozzle does not satisfy the required 400 million injections. To extend the lifetime and optimize the spray shape of the porous injector the geometry is modified. The external radius was changed from 0.85 mm to 2.5 mm. The wall thickness was intended to be uniform (at 2 mm), but because of a production problem the fuel channel was drilled too deep and therefore the wall thickness on the tip is smaller than on the sides. This geometry (Figure 8.15(a)) was simulated in COMSOL, resulting in the velocity contours shown

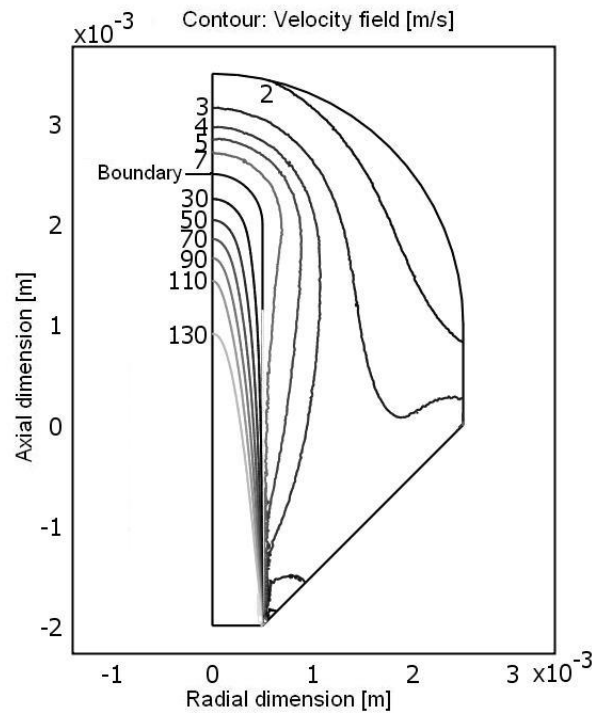


Figure 8.14: Simulation of the porous injector which is used for the experiments. The injection pressure = 100 MPa.

in Figure 8.14.

From Figure 8.14 it is expected that the spray shape has a preference in the axial direction. In the next sections, this porous nozzle will be tested experimentally.

8.4 Experimental setup

The Eindhoven High Pressure Cell (EHPC) [6] is a high pressure, constant volume vessel with optical access in which engine like conditions can be created, regarding oxygen level, temperature and pressure (up to 30 MPa). For all measurements in the EHPC the nozzle geometry corresponds to Figure 8.15(a). As discussed in the previous section, the depth of the hole is not in-line with Figure 8.3 because of a manufacturing error. A picture of the EHPC is shown in Figure 8.16.

The engine-like conditions can be obtained by a pre-combustion method [6]. As will be discussed later in this paper, a pre-combustion increases the temperature and pressure inside the EHPC, as shown in Figure 8.18. In-cylinder pressure and temperature can be chosen independently from each other. The pressure is controlled (indirectly) by the amount of filling gases and the gas temperature by the moment of injecting the test fuel. Both non-reacting (vaporizing) and reacting sprays are analyzed in the next sections.

8.4.1 non-reacting sprays

To analyze the vaporization of the spray produced by the porous injector, a reaction between the fuel and oxygen is undesirable. A simple way to realize this is to put

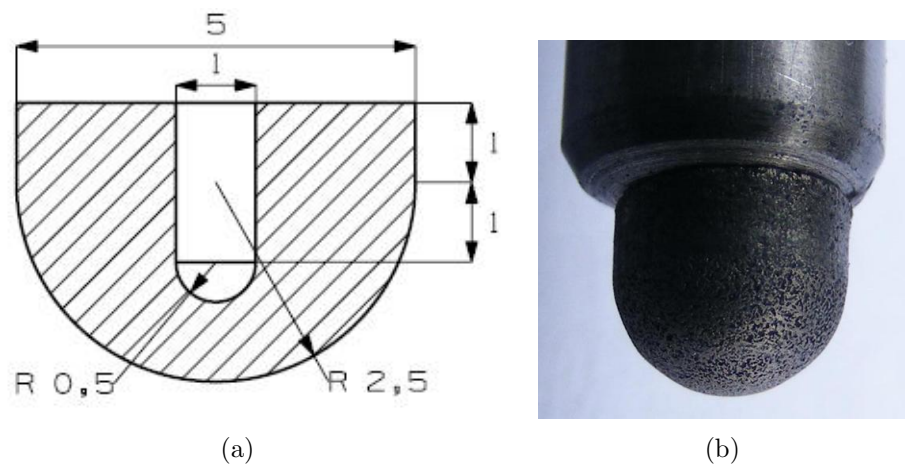


Figure 8.15: Left: Technical drawing of the porous nozzle which is tested in the EHPC; dimensions in *mm*. Right: picture of porous injector prototype.

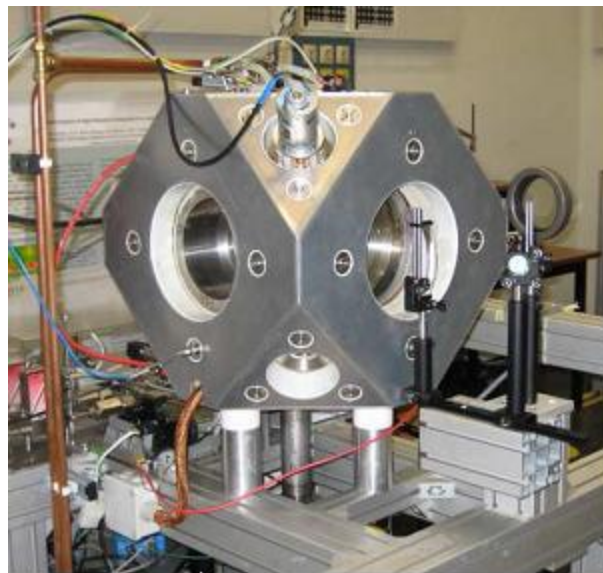


Figure 8.16: Eindhoven High Pressure Cell [11].

exactly the stoichiometric amount of oxygen in the burner vessel needed for the pre-combustion. After the pre-combustion no oxygen is left and the injected fuel will not burn. These vaporizing sprays are analyzed with the Schlieren technique [12].

The Schlieren method uses the difference in index of refraction between fuel vapor and air. In Figure 8.17, a schematic drawing of the method is shown. A powerful light (point) source generates a beam in the direction of the EHPC. With a lens, the source is collimated to form a broad parallel beam. After passing through the test vessel another lens focuses the light onto a pinhole and a high speed camera (Phantom 7.1) captures the light. In the presence of density gradients the beam is diverted onto a Schlieren stop, causing the density gradients to appear as darker regions on the camera lens.

Due to the pre-combustion, density gradients are created in the EHPC before the fuel is injected. When analyzing the recordings, one sees disturbances in the back-

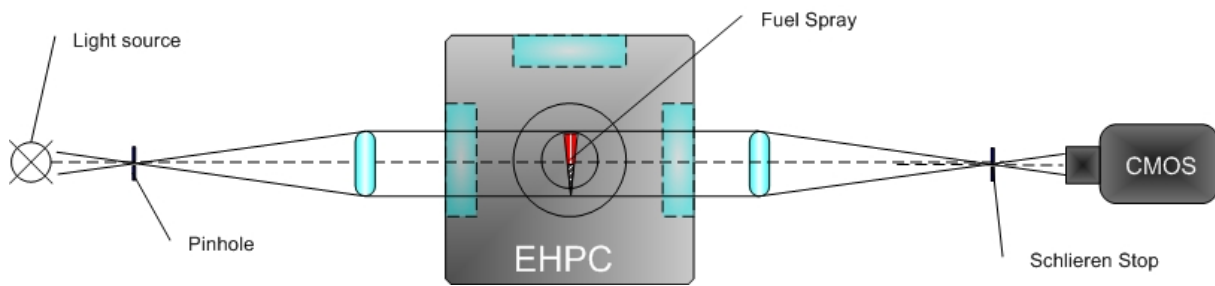


Figure 8.17: Schematic overview of the Schlieren method [12].

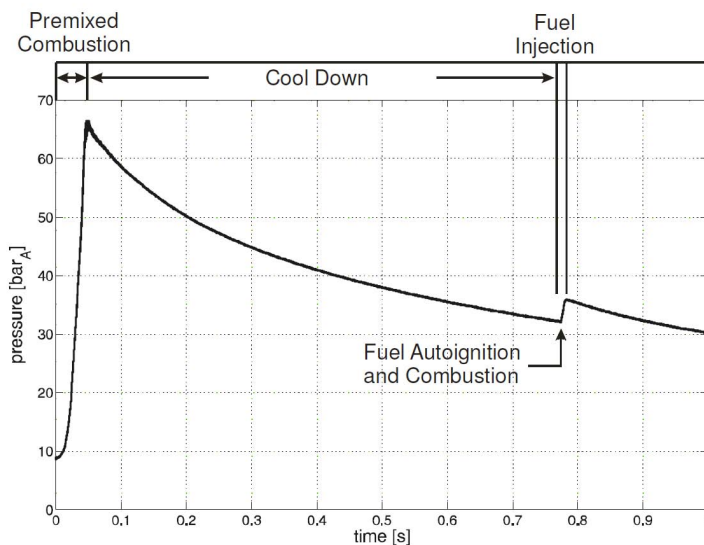


Figure 8.18: Typical pressure trace of a reacting diesel spray experiment in the EHPC.

ground of the spray. For low density conditions the disturbances are smaller compared to high ambient density conditions. However, the spray can still be distinguished from the background. To clarify the spray, a boundary line is drawn in the Figure 8.19.

8.4.2 Reacting sprays

In the previous section, it is explained how vaporizing fuel sprays are analyzed. Now we will discuss reacting sprays. To induce auto-ignition, excess oxygen is added to the EHPC. The engine conditions are realized in the same way as with non-reacting sprays. The density is governed by the filling conditions (and is constant because of constant volume vessel), temperature and pressure are controlled by the moment of injection. In Figure 8.18 an example is given of a pressure curve with a reacting spray.

First, a pre-combustion takes place to achieve the high temperature and pressure. After that, the mixture cools down and at a certain point, when the temperature has the desired value, the diesel injection is performed. Depending on the ignition delay at the experimental conditions chosen, the fuel reacts with the oxygen and the temperature as well as the pressure rise again, as can be clearly seen in Figure 8.18 at $t = 0.775$ s.

To test the functionality of the injector, the ignition delay is examined. Ignition

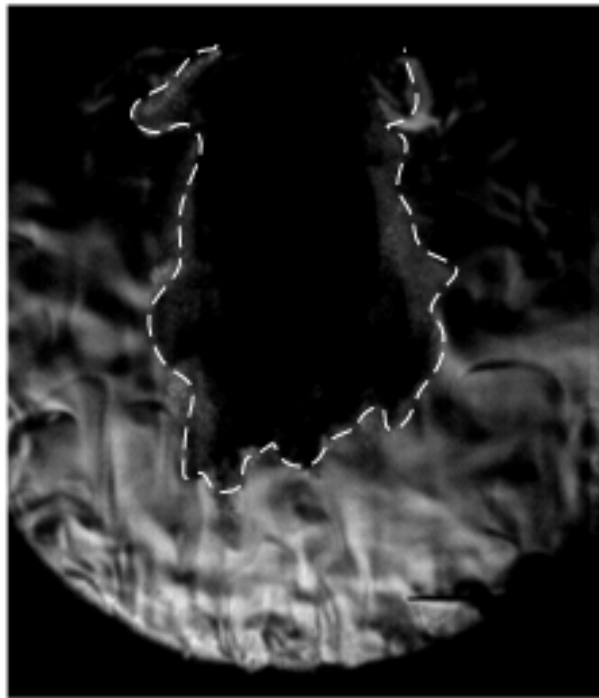


Figure 8.19: Non-reacting spray of the porous injector measured with the Schlieren technique. Conditions at the moment of fuel injection: $p_g = 1.44$ MPa, $T_g = 671$ K.

delay is defined as the time between the start of injection and the Start of Combustion (SOC). The measurements are performed as discussed in [13]. The moment of start of injection is known and the start of pressure rise in Figure 8.18 (minimum pressure) is taken as the SOC, since the experiments are performed in a constant volume vessel.

8.5 Experimental results

Figure 8.19 shows a Schlieren image of a spray from the porous injector. The spray does not have the desired homogeneous hemispherical distribution as shown in Figure 8.1. The fuel spray, still has a preferential axial direction, however, there is a wider distribution than is the case in Figure 8.5.

To predict the SOC the ignition delay is measured. In Figure 8.20 ignition delay versus temperature is plotted.

Figure 8.20 shows that the ignition delay is shorter for the porous injector (*) compared to a conventional injector (\square), especially at lower temperatures. At higher temperatures the differences are smaller. The combustion process is also observed. Figure 8.21 shows the combustion with the porous injector. In this case, the combustion spreads out over a large region in space. This suggests that better use is made of the available oxygen, which is expected to result in an overall leaner combustion. However, this can not yet be substantiated with quantitative results. Analysis of soot luminosity is subject of current investigation.

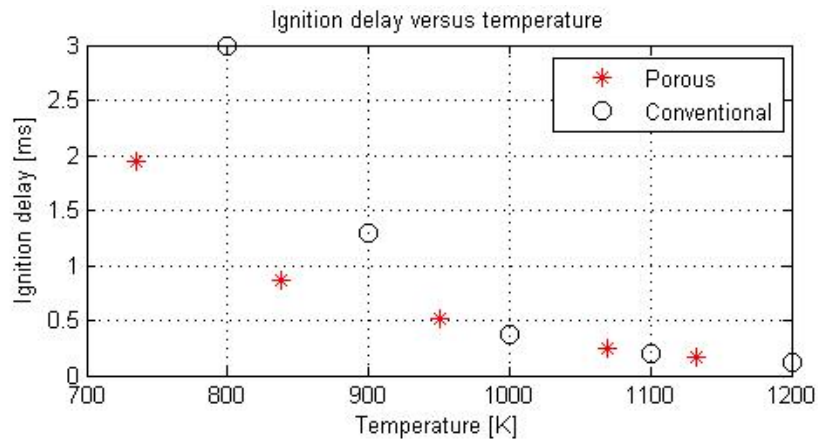


Figure 8.20: Ignition delay: $\rho_g = 16 \text{ kg/m}^3$, $\text{O}_2 \text{ Vol-\%} = 21$, fuel = EN590, $T_{inj} = 5 \text{ ms}$.

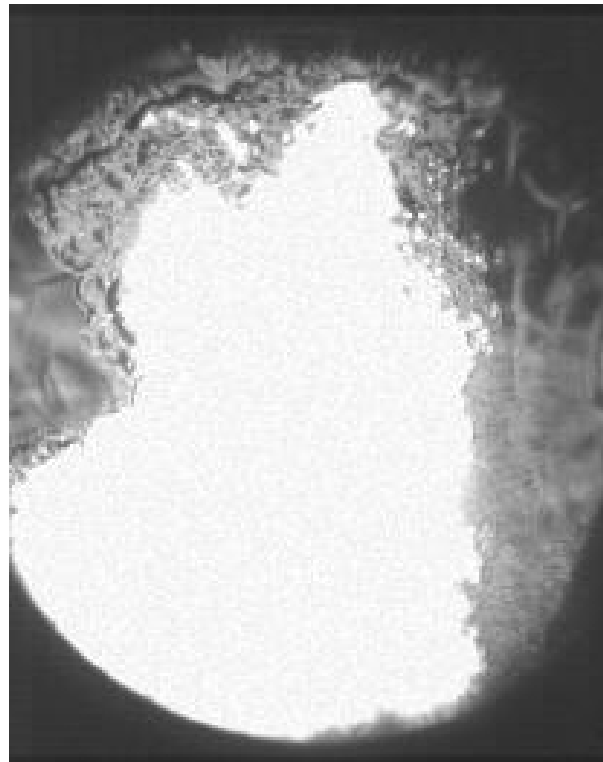


Figure 8.21: Reacting spray of porous injector; $p_{inj} = 100 \text{ MPa}$, $\rho_g = 16 \text{ kg/m}^3$, $T_g = 1000 \text{ K}$, fuel = EN590, $\text{O}_2 \text{ Vol-\%} = 21$, $T_{inj} = 5 \text{ ms}$.

8.6 Discussion

During preliminary research [14] two different geometries of porous injectors were investigated numerically and experimentally and compared with a conventional injector. First, the spray shapes of the numerical models were compared with experiments. From this comparison it became clear that the results did not match. In the model, geometry *A* shows a homogeneous distribution over the exit edge. In the experiments the spray has a preference in the axial direction. The results of geometry *B* are slightly better. The deviation in the experiments is due to oversimplifications in the model. First, the momentum of the fuel is not taken into account because the fuel channel is not modeled. Furthermore, the velocities in the porous material are such that the *Re*-number exceeds 5. The flow through porous material, however, can only be described well by Darcy's Law up to *Re* numbers of 5. In this study, a non-linear term (Forchheimer term) [3] is added and more details (fuel channel) are modeled. Now the models show a reasonable level of agreement with experiments.

The mass flow (at a given fuel pressure) through the porous injector is higher than is the case for the conventional injector (Figure 8.8), at least for the nozzle material and geometry used in this preliminary study. These results indicate that the desired mass flow can be realized with the investigated porous injector.

The desired lifetime of the injector is typically 1.000.000 km, the average speed over the whole life being 80 km/h at an engine speed of 1200 rpm. In this case, the injector has to inject approximately 400 million times during its lifetime. From the experiments we found that the injectors broke down after about one hundred thousand injections. This means that the lifetime of the injector is far too short. To extend the lifetime, the geometry has to be optimized, other materials have to be investigated and the production process has to be improved. This will be investigated in a later phase of the project.

As mentioned earlier, a better mixing of fuel with air leads to a decrease in soot emissions. It is likely that an adequate (i.e. to facilitate auto-ignition) fuel-air mixture is obtained faster and this leads to a shorter ignition delay. For a given fuel, the ignition delay is thus assumed to be a (local) measure for mixing quality. From the experimental results it is known that the ignition delay is much shorter for the porous nozzle, which suggests that the mixing quality of the spray process is improved.

8.7 Conclusions

A new fuel injector concept, based on a layer of sintered steel, was investigated numerically and experimentally. A common-rail setup has been adapted to test the porous injector. To analyze the spray at atmospheric conditions, images of the spray were captured with a high speed camera. The spray of the first prototype had a preferential axial direction instead of the desired homogeneous hemispherical distribution, which does not correspond with first simulations. After modifying the model, a new prototype was made with a larger outer diameter. The spray shape of this prototype was tested in the EHPC (constant volume chamber). It was found that the spray was not hemispherical because of a production problem.

The sprays from the simulations are compared with the experimental findings.

First simulations, with Darcy's Law did not (fully) correspond to experiments. Afterwards, when a Forchheimer term was added and more details were modeled, the results of the simulations corresponded better to the experiments.

The mass flow through the porous injector has to be at least the same as a conventional injector. From the experiments it becomes clear that the mass flow of the porous injector was higher at an equal fuel pressure. However, since this was just a prototype, this does not prove that this is generally the case for porous nozzles.

The durability of the porous injector was tested. First results indicated that normal lifetime requirements are not yet met. More research has to be performed to extend the lifetime of the injector.

Non-reacting, vaporizing sprays have been observed to estimate the spray shape. In this case the spray does not have the fully hemispherical shape due to the fact that at the moment the manufacturing process does not have the right accuracy. New prototypes have to be produced and will be tested in the future. However, the spray from the porous nozzle does have a more homogeneous distribution, based on preliminary spray visualization experiments.

Ignition delays have been measured and are found to be shorter for the porous injector than for the conventional one, especially at lower temperatures. It is very difficult to explain this right away. On the one hand air entrainment could be larger compared to the conventional. On the other hand the entrainment is expected to be very slow as the droplet speed is low. The volume of air taking part in the combustion of the porous spray may be much larger compared to conventional injectors. However, based on current experimental evidence, a firm conclusion can not yet be drawn, so that interpretation remains speculative. Further research is currently being conducted into several aspects of the porous injector nozzle.

Nomenclature

Abbreviations

DI	Direct Injection
d	Channel diameter
EHPC	Eindhoven High Pressure Cell
HCCI	Homogeneous Charge Compression Ignition
HD	Heavy Duty
ICE	Internal Combustion Engine
K	Kelvin
PCCI	Premixed Charge Compression Ignition
p	Pressure
Re	Reynolds
SOC	Start of combustion
T	Temperature
TDC	Top Dead Center
v	Velocity

Greek symbols

μ	micro
κ	Permeability
η	Dynamic viscosity
ρ	Density

Subscripts

d	Darcy
f	Forchheimer
g	Gas
inj	Injection
$conv$	Conventional
por	Porous

Bibliography

- [1] L.M Pickett and D.L Siebers. Orifice diameter effects on diesel fuel jet flame structure. *Journal of Engineering for Gas Turbines and Power*, 27:187–196, 2005.
- [2] L.G. Dodge, S. Simescu, G.D. Neely, M.J. Maymar, D.W. Dickey, and C.L. Savonen. Effect of small holes and high injection pressures on diesel engine combustion. *SAE Paper*, 2002-01-0494, 2004.
- [3] J. Bear. *Dynamics of fluids in porous media*. American elsevier publishing company Inc., New York, 1972.
- [4] S.P. Neuman. Theoretical derivation of darcy’s law. *Acta Mechanica*, 25:153–170, 1977.
- [5] G. Qin Z. Chen, S.L. Lyons. Derivation of the forchheimer law via homogenization. *Transport in porous media*, 44:325–335, 2001.
- [6] R.S.G. Baert, P.J.M. Frijters, L.M.T. Somers, C.C.M. Luijten, and W.A. de Boer. Design and operation of a high pressure, high temperature cell for HD diesel spray diagnostics: guidelines and results. *SAE Paper*, 2009-01-0649, 2009.
- [7] J. Dvorkin G. Mavko, T. Mukerji. *The Rock Physics Handbook*. 1st Edition. Cambridge University Press, 1998.
- [8] L.M. Rodriguez-Anton, J. Casanova-Kindelan, and G. Tardajos. High pressure physical properties of fluids used in diesel injection systems. *SAE Paper*, 2000-01-2046, 2000.
- [9] Firma Tridelta Siper m GmbH. Technische daten für poröse siper mwerkstoffe. 2009.
- [10] COMSOL Multiphysics. User’s guide chemical engineering module. 2006.

-
- [11] R. Peters. Penetration and dispersion research of non-reacting evaporating diesel sprays. *MSc report, Eindhoven University of Technology*, WVT 2007.11, 2007.
- [12] D.D.T.M. van Erp. Examining methods to reduce wall-wetting under HCCI conditions. *MSc report, Eindhoven University of Technology*, WVT 2009.03, 2009.
- [13] T.W. Ryan and B. Stapper. Diesel fuel ignition quality as determined in a constant volume combustion bomb. *SAE Paper*, 870586, 1987.
- [14] J.J.E. Reijnders, M.D. Boot, C.C.M. Luijten, and L.P.H. de Goey. Investigation of direct-injection via micro-porous injector nozzle. In *Proc. of the 4th European Combustion Meeting*, Austria, Vienna, April 2009. ECM 2009.

Concluding Remarks

In this thesis, three strategies aimed at improving the fuel/air mixing process, and therefore at lowering soot emissions, have been presented and grouped into three distinct categories:

- use of alternative fuels with different chemical properties (part 1),
- switching to an alternative combustion concept (part 2),
- utilization of new engine hardware (part 3).

Part 1: fuel chemistry

The molecular structure of oxygenated fuels is known to have a profound impact on the soot emissions. Contrary to literature findings, however, the carbon sequestration potential of the compound does not appear to be the primary underlying mechanism. A possible alternative mechanism, promotion of curvature in soot nanostructure, is proposed. A fuel of which is thought that it will promote such curvature, cyclohexanone, is added to the fuel matrix. Interesting enough, cyclohexanone, lead to considerably lower soot emissions than was the case for more linear oxygenates, such as TPGME and DBM. In some (high exhaust gas recirculation) cases, this the difference in soot performance was over two orders of magnitude.

From a closer look at the data in chapter 1, it becomes clear that the ignition delay for cyclohexanone is considerably longer. It is well-known from literature that longer delays can have a favorable effect on soot (via more available time for mixing). In chapter 2, relevant oxygenates are tested in an optically accessible engine. Soot luminosity was found to be considerably lower for cyclohexanone than for TPGME and DBM. The absence of soot luminosity is indicative of better suppression of soot, rather than of enhanced oxidation, therefore suggesting that the ignition delay rather than promotion of curvature is of primary importance.

Chapter 2 suggests that indeed the ignition delay of an oxygenate is important with respect to soot. Accordingly, the data in chapter 1 is replotted, but now from a cetane number (which is a measure for auto-ignition behavior) perspective. It is

found that soot emissions scale well with oxygenate CN, underlining the significance of this fuel property.

In the literature study of chapter 3 some indication is found that, apart from the ignition delay, the flame lift-off length could be an important parameter when comparing fuels with different cetane number. A longer length allows for more air to be entrained upstream of the diffusion flame. In the study presented in chapter 4, various oxygenates with different cetane numbers have been tested in a stationary burner. Use of a burner rules out the impact of ignition delay, as combustion is now continuous and stationary. Once again, the ability of an oxygenate to abate soot emissions is clearly linked to its respective CN, with lower CN's manifesting in markedly lower soot emissions. This is found to hold irrespective of oxygenate molecular structure. Apparently, fuel reactivity impacts the soot formation process via (an)other mechanism(s) than solely the incurred ignition delay.

In the final chapter of the first part, the flame lift-off length is measured in the same optical engine as utilized in chapter 2. This length, but also the ignition delay, is found to correlate reasonably well with oxygenate cetane number. On average, lower cetane numbers lead to longer lift-off lengths, which are more favorable with respect to soot.

The overall conclusion of the first part is that low reactive oxygenates yield considerably lower soot emissions than more highly reactive (higher cetane number) oxygenates. This observation holds for various experimental setups and over a wide range of operating conditions. The data suggests two underlying mechanisms are at work here:

- Longer ignition delay: more time for (pre)mixing
- Longer flame lift-off length: more time for air entrainment once a diffusion flame has settled

Part 2: Combustion Concept Approach

In the second part of this thesis, it is investigated if it is possible to suppress the soot formation process by adopting an alternative combustion concept with conventional diesel fuel. Fuel is injected early in the compression stroke, thereby creating a physically-, instead a chemically-induced longer ignition delay and lower soot emissions. The advantages of this have been discussed above. Challenges, however, exist when injecting the fuel early in the cycle. Due to the relatively low prevailing gas temperature and pressure, fuel impingement against the combustion chamber walls can occur, leading to high unburned hydrocarbon emissions and poor fuel economy. To mitigate impingement, several engine settings were varied. Of these variations, a higher intake temperature and higher intake pressure appear to be the most promising.

Although the measures in the previous chapter lead lower unburned hydrocarbons emissions, it is unclear whether or not this is attributable to reduced impingement. In this chapter, a spray model is made in a commercial CFD code to investigate the role of engine settings on spray impingement. From the model it becomes clear that modeled spray impingement correlates well with measured unburned hydrocarbon

emissions. Accordingly, it can be assumed that impingement is responsible for these emissions in the investigated combustion mode.

Part 3: Hardware Approach

In this final part, an alternative injector nozzle is proposed. Instead of the conventional nozzle with 6-10 holes of typically 100-200 microns, a sintered, porous nozzle is designed and tested with several hundreds pores of 10-50 micron. For given operating conditions, measurements conducted in the Eindhoven High Pressure Cell show that this nozzle type leads to on average shorter ignition delays and more efficient use of the available oxygen in the combustion chamber. The latter is achieved by the hemispherical, rather than conical spray shape. Both phenomena suggest that the mixing process is improved. Durability of the material, however, has to be addressed to improve the life-time of the nozzle. Ultimately, engine and/or vehicle tests will have to be performed to establish whether or not the soot emissions are really decreased by adopting the new design. Several possible reasons can be identified why this may not be the case, such as fouling of the pores, relatively low nozzle exit velocity/momentum and others.

Curriculum Vitae

Michael Boot was born in Aurora, Illinois (USA) on February 9th 1980. He attended the Kruisheren Kollege in Uden and received his VWO degree there in 1998. He started his study of Mechanical Engineering at the Eindhoven University of Technology (TU/e) in the same year. In 2004 he worked on his internship at DAF Trucks NV on the subject of nitric oxide formation. Later that year, he started his graduation project that was conducted in the Engine Labs of the TU/e Combustion Technology Group. During this period, he studied the impact of (oxygenated) fuel composition on engine performance and emissions. In May 2005, he received his MSc degree and started his PhD work in the same research group. The research topic, financed in part by DAF Trucks NV, was to investigate new combustion concepts, such as Homogeneous Charge Compression Ignition, in a DAF heavy-duty diesel research engine. In June 2009, Michael Boot co-founded a spin-off company, Progression-Industry BV, which aims to valorize the knowledge and intellectual property accumulated during his PhD period. Progression-Industry BV is currently embedded in the Faculty of Mechanical Engineering at the TU/e. Michael Boot remains closely tied to the TU/e Combustion Technology Group and will continue to supervise students, give lectures in the Fuels & Lubricants course and conduct fundamental research for the technologies Progression-Industry is trying to commercialize.

Dankwoord

Het resultaat wat hier ligt had ik zonder de hulp en steun uit academische, technische en sociale hoek niet voor elkaar kunnen krijgen. Om te beginnen wil ik mijn (co)promotoren Rik, Philip en Carlo bedanken. Zij hadden geen gemakkelijke taak mijn focus te houden op mijn onderzoekslijn. Enorme dank gaat ook uit naar Gerard van Hout, Wout de Boer, Gerard van Hattum, Bart van Pinxten, Theo de Groot, Hans van Griensven en Marc Willekens. Zonder hen was er geen motor opstelling geweest om aan te meten. Ten derde wil ik mijn voormalige (Martin) en huidige (Ron en Jos) kamergenoten bedanken voor alle gezelligheid (ook al was ik niet altijd even aanspreekbaar). Bijzondere dank gaat uit naar Marjan, de spin in het web van onze groep. Ten laatste wil ik mijn verloofde Cleontine, broertje Eric, zusje Nicole en ouders bedanken voor al hun geloof en support voor, tijdens en na mijn promotieperiode.

